MATHEMATICAL THEORY AND NUMERICAL METHODS FOR BOSE-EINSTEIN CONDENSATION WITH HIGHER ORDER INTERACTIONS

RUAN XINRAN

NATIONAL UNIVERSITY OF SINGAPORE

2017

MATHEMATICAL THEORY AND NUMERICAL METHODS FOR BOSE-EINSTEIN CONDENSATION WITH HIGHER ORDER INTERACTIONS

RUAN XINRAN

(B.Sc., Peking University)

A THESIS SUBMITTED
FOR THE DEGREE OF DOCTOR OF PHILOSOPHY
DEPARTMENT OF MATHEMATICS
NATIONAL UNIVERSITY OF SINGAPORE
2017

Supervisor:

Professor Bao Weizhu

Examiners:

Professor Ren Weiqing

Dr. Liu Jie

Professor Christophe Besse, Université Toulouse 3 Paul Sabatier

DECLARATION

I hereby declare that the thesis is my original work and it has been written by me in its entirety. I have duly acknowledged all the sources of information which have been used in the thesis.

This thesis has also not been submitted for any degree in any university previously.

RUAN XINRAN

11 Jan 2017

Acknowledgements

It is my great honor here to thank those who made this thesis possible.

First and foremost, I would express my most sincere gratitude to my supervisor Prof. Bao Weizhu, who introduced me to this exciting and interesting research area, for his continuous guidance, meticulous suggestions and astute criticism during my PhD study. I sincerely appreciate his ample knowledge and time spent despite his busy schedule in providing me with many ideas and advice, not only in research, but also in life.

I would like to express my sincere appreciation to Dr. Cai Yongyong for his invaluable help in my project and inexhaustible patience in clarifying every doubt of mine.

I heartfeltly thank all my friends, especially Li Yunzhi, Lu Hengfei, Hu Fei, Zeng Yishu, Wei Ran, Guo Han, and sincerely thank all the former colleagues and fellow graduates in my group, especially Zhao Xiaofei, Wang Yan, Zhang Yong, Tang Qinglin, for all the encouragement, technical advices in research, emotional support, comradeship and entertainment they offered.

I would like to thank all my lecturers for teaching me. Their excellent courses not only introduced me to various research topics and improved my knowledge and skills, but also reaffirmed my resolute passion in my quest for knowledge. I would also like to thank NUS for awarding me the Research Scholarship during my Ph.D candidature, and for the financial assistance during the conference leaves.

Last but not least, thank my family for their encouragement and unconditional support. Without them, I would never have arrived at this stage of my life.

Ruan Xinran

December 2016

Contents

Summary

The Gross-Pitaevskii equation (GPE), which is a particular mean field theory and approximates the binary interactions between particles by a Dirac function, has gained considerable research interest due to its simplicity and effectiveness in describing the Bose-Einstein condensation (BEC). However, the validity of the theory is limited to the low energy and low density assumption. For improvement, higher order interaction (HOI) (or effective range expansion) as a correction to the Dirac function has to be taken into account, resulting in a modified Gross-Pitaveskii equation (MGPE). Though the MGPE has been used in many physical problems, there have been only a few mathematical analysis and numerical studies for it. And that's where my work comes in.

The main purpose of this thesis is to study the MGPE mathematically and numerically. Besides, the fundamental gap problem and the energy asymptotics of the nonlinear Schrödinger equation will be considered as two minor problems in the end.

The thesis mainly contains three parts. The first part is to investigate the MGPE systematically both in theory and in practical computation. The dimension reduction problem for MGPE, especially the comparison with the problem for the GPE case, will be shown first. A new phenomenon is discovered which is totally different

from the GPE case and anti-intuitive because of the HOI term. Convergence of the dimension reduction will be established. For ground states, we will prove the existence and uniqueness as well as non-existence, which is a direct generalization of the problem for the GPE case. And the limiting behavior of the ground states for problem with box or harmonic potential in different parameter regimes will be classified in details. The HOI term introduces new Thomas-Fermi (TF) approximations, and different Thomas-Fermi approximations are proposed, theoretically analyzed and numerically tested. Besides, different schemes for computing the ground state, including the methods generalized from the GPE case and a novel method proposed by us, will be written explicitly. In particular, convergence and accuracy of our new method will be analyzed and numerically tested. For the dynamics of the MGPE, we will analyze the well-posedness, the dynamics of quantities in describing BEC and possible finite time blow-up. Finally, the time-splitting method is adopted for the computation of the dynamics.

The second part is to consider the fundamental gap problem for the GPE. Both the whole space problem with a harmonic potential and the bounded domain problem with a box potential will be studied in details. Asymptotic results as well as the numerical tests will be proposed. Problems with periodic boundary conditions (BCs) and Neumann BCs will also be considered. We discover that the dependence of the fundamental gaps on the interaction strength for the bounded domain problem and the whole space problem are completely different. Besides, the dimension of the eigenspace corresponding to second lowest eigenvalue for the linear problem will affect the fundamental gaps for the nonlinear problem significantly. Based on the asymptotic results for special cases and some numerical tests, we will propose a gap conjecture for the GPE under a more general external potential.

The third part is to study the ground state approximations and energy asymptotics of the nonlinear Schrödinger equation in three limiting regimes of the parameters. We try to write out the approximate ground state and corresponding energy as explicitly as possible. One major finding is that for the 1D problem, a bifurcation

in the ground states is observed under either a box potential or a harmonic potential when the power of the nonlinearity goes to ∞.

List of Tables

List of Figures

List of Symbols and Abbreviations

$\hbar$	reduced Planck constant
$i = \sqrt{-1}$	imaginary unit
t	time
$\mathbf{x}$	Cartesian coordinate
(r, θ)	polar coordinate
∇	gradient
$\Delta = \nabla \cdot \nabla$	Laplacian
$\psi(\mathbf{x}, t)$	wave function
$\phi(\mathbf{x})$	stationary state
$\rho(\mathbf{x}, t) = \lvert\phi(\mathbf{x}, t)\rvert^2$	position density
μ	chemical potential
E	energy
ω_x, ω_y, ω_z	trapping frequencies in x-, y-, and z- direction
γ_x, γ_y, γ_z	dimensionless trapping frequencies
τ	time step size
h	space mesh size
$\hat{f}$	Fourier transform of function f
$\bar{f}$	conjugate of of a complex function f

$\mathrm{Re}(f)$	real part of a complex function f
$\mathrm{Im}(f)$	imaginary part of a complex function f
$L_z = -i(x\partial_y - y\partial_x)$	z-component of angular momentum
$\langle L_z \rangle(t)$	angular momentum expectation
$\mathbf{x}_c(t)$	center of mass of a condensate
$\sigma_\alpha(t)$ $(\alpha = x, y, \text{or } z)$	condensate width in α-direction
BEC	Bose-Einstein condensate
HOI	higher order interaction
GPE	Gross-Pitaevskii equation
MGPE	modified Gross-Pitaevskii equation
NLSE	nonlinear Schrödinger equation
TF	Thomas-Fermi
BC	boundary condition
1D	one dimension
2D	two dimensions
3D	three dimensions
Fig.	figure
BESP	backward Euler sine pseudospectral
TSSP	time-splitting sine pseudospectral

Chapter 1

Introduction

1.1 Bose-Einstein condensation (BEC)

Bose-Einstein condensation (BEC) is a state of matter of a dilute and ultra-cold gas of bosons with temperature close to 0K or $-273.15\,^{\circ}\mathrm{C}$. In such situation, a large fraction of bosons occupy the lowest quantum state, obeying the Bose-Einstein statistics, which makes macroscopic quantum phenomena apparent. The state was predicted by Albert Einstein [58,59] in 1924-1925 by adapting Satyendra Nath Bose's statistics [38] ,and was first realized in laboratory in 1995 for ^{87}Rb, by E. Cornell and C. Wieman's group in JILA by combining the laser cooling and the evaporative cooling techniques together [4]. In the same year, another two experimental achievements were reported by the Ketterle's group in MIT for ^{23}Na [57] and Hulet's group in Rice University for ^{7}Li [39]. The breakthrough in experiments greatly inspired researchers in atomic physics community and condensed matter physics community because one can now measure the microscopic quantum mechanical properties in a macroscopic scale by optical means with the help of BEC. Besides, certain BEC system exhibits superfluidity and superconductivity [74,84], which implies the close relation between superfluidity and BEC. Since then, numerous efforts have been devoted to the area, and the numerical simulation has been playing an important role in understanding the theories and the experiments.

Mathematically, the most natural way to describe BEC is via the many body Hamiltonian. In the typical experiments of BEC, the ultra-cold bosonic gases trapped in an external potential are dilute and weakly interacting, and therefore the major properties are governed by the weak two-body interactions [54, 90, 93]. The N-body Hamiltonian can be written as [76, 79]

$$H_N = \sum_{j=1}^{N} \left(-\frac{\hbar^2}{2m} \Delta_j + V(\mathbf{x}_j) \right) + \sum_{1 \le j < k \le N} V_{\text{int}}(\mathbf{x}_j - \mathbf{x}_k), \tag{1.1.1}$$

where $\mathbf{x}_j \in \mathbb{R}^3$ $(j = 1, \ldots, N)$ are the positions of the particles, m is the mass of a boson, Δ_j is the Laplace operator with respect to $\mathbf{x}_j$, $V(\mathbf{x})$ is the external trapping potential, $V_{\text{int}}(\mathbf{x}_j - \mathbf{x}_k)$ denotes the binary interaction between particles, and $\Psi_N(\mathbf{x}_1, \ldots, \mathbf{x}_N, t)$ is the wave function for the BEC, satisfying

$$\int_{\mathbb{R}^{3N}} |\Psi_N(\mathbf{x}_1, \ldots, \mathbf{x}_N, t)|^2 \, d\mathbf{x} = 1, \tag{1.1.2}$$

where $\mathbf{X} := (\mathbf{x_1}, \ldots, \mathbf{x_N}) \in \mathbb{R}^{\mathbf{3N}}$. The dynamic of the system is then governed by the Schrödinger equation

$$i\hbar \partial_t \Psi_N(\mathbf{x}_1, \ldots, \mathbf{x}_N, t) = H_N \Psi_N(\mathbf{x}_1, ..., \mathbf{x}_N, t), \tag{1.1.3}$$

where $\hbar$ is the reduced Plank constant and $i = \sqrt{-1}$ is the complex unit.

1.2 The Gross-Pitaevskii equation (GPE)

The N-body system (1.1.3) is solvable, but is usually extremely computational expensive due to the large number of particles in the system, and therefore inappropriate for practical use. Simplification of the model will be needed, and one choice widely used is the Gross-Pitaevskii (GP) theory.

For the trapped BEC system, the GP theory, which is a special case of the mean field approximation/theory and was proposed in the 1960s by Pitaevskii [92] and Gross [67] independently, is quite popular in the computation due to its effectiveness and simplicity. The main idea of mean field theory (MFT) is to replace all

interactions to one body by an average or effective interaction, sometimes called a molecular field. This reduces a multi-body problem into an effective one-body problem, which significantly reduces the computational cost. In the GP theory, we approximate the binary interaction as the two-body Fermi contact interaction, where the interaction kernel is taken as the Dirac delta function with a single parameter, i.e.

$$V_{\text{int}}(\mathbf{x}_j - \mathbf{x}_k) = g_0 \delta(\mathbf{x}_j - \mathbf{x}_k), \tag{1.2.1}$$

where $\delta(\cdot)$ is the Dirac distribution and $g_0 = \frac{4\pi\hbar^2 a_s}{m}$ with a_s to be the zero energy s-wave scattering length [79]. This is the heart of the mean field GP theory for BEC [79, 80, 93], and the approximation is valid only when the temperature is low and the gas is dilute. For BEC, all particles are in the same quantum state and we can formally take the Hartree ansatz for the many body wave function as

$$\Psi_N(\mathbf{x}_1, \ldots, \mathbf{x}_N, t) = \prod_{j=1}^{N} \psi(\mathbf{x}_j, t), \tag{1.2.2}$$

with the normalization condition for the single-particle wave function as $\|\psi(\mathbf{x}, t)\|_2^2 = \int_{\mathbb{R}^3} |\psi(\mathbf{x}, t)|^2 \, d\mathbf{x} = 1$. Based on (1.2.1) and taking the Hartree ansatz (1.2.2), the energy of the BEC system can be written as

$$E(\Psi_N) = N \int_{\mathbb{R}^3} \left[\frac{\hbar^2}{2m} |\nabla \psi(\mathbf{x}, t)|^2 + V(\mathbf{x}) |\psi(\mathbf{x}, t)|^2 + \frac{N-1}{2} g_0 |\psi(\mathbf{x}, t)|^4 \right] d\mathbf{x} \approx N E(\psi),$$

where $E(\psi)$ is the energy per particle which approximates $\frac{N-1}{2}$ by $\frac{N}{2}$ for large N and is defined as

$$E(\psi) = \int_{\mathbb{R}^3} \left[\frac{\hbar^2}{2m} |\nabla \psi(\mathbf{x}, t)|^2 + V(\mathbf{x}) |\psi(\mathbf{x}, t)|^2 + \frac{N}{2} g_0 |\psi(\mathbf{x}, t)|^4 \right] d\mathbf{x}. \tag{1.2.3}$$

And then the **Gross-Pitaevskii equation (GPE)** is derived by the variation of $E(\psi)$

$$i\hbar \partial_t \psi(\mathbf{x}, t) = \frac{\delta E(\psi)}{\delta \bar{\psi}} = \left[-\frac{\hbar^2}{2m} \nabla^2 + V(\mathbf{x}) + N g_0 |\psi(\mathbf{x}, t)|^2 \right] \psi(\mathbf{x}, t), \tag{1.2.4}$$

where $\hbar, m, g_0$ have been defined before, and $\|\psi(\mathbf{x}, t)\|_2 = 1$.

When the trapping potentials are strongly anisotropic, we can perform the dimension reduction of the GPE for BEC as shown in [10,14,36,93] and the GPE (1.2.4) in 3D can be formally reduced to two dimensions (2D) or one dimension (1D) for the disk-shaped or cigar-shaped BEC [108], respectively. In fact, after nondimensionalization [14], the resulting GPE can be written in a unified form in d-dimensions ($d = 1, 2, 3$) with $\mathbf{x} \in \mathbb{R}^d$ (denoted as $\mathbf{x} = x \in \mathbb{R}$ for $d = 1$, $\mathbf{x} = (x, y)^T \in \mathbb{R}^2$ for $d = 2$ and $\mathbf{x} = (x, y, z)^T \in \mathbb{R}^3$ for $d = 3$) as

$$i\partial_t \psi = \left[-\frac{1}{2}\nabla^2 + V(\mathbf{x}) + \beta|\psi|^2\right]\psi, \quad t \geq 0, \quad \mathbf{x} \in \mathbb{R}^d, \tag{1.2.5}$$

where $\psi := \psi(\mathbf{x}, t)$ is a dimensionless complex-valued wave function, $V(\mathbf{x})$ is a dimensionless real-valued potential, β is a dimensionless constant describing the interaction strength.

It can be shown that the dimensionless GPE (1.2.5) conserves the total mass, i.e.

$$N(t) := \int_{\mathbb{R}^d} |\psi(\mathbf{x}, t)|^2 d\mathbf{x} \equiv N(0) = 1, \quad t \geq 0, \tag{1.2.6}$$

and the energy per particle

$$E(\psi(\cdot, t)) := \int_{\mathbb{R}^d} \left[\frac{1}{2}|\nabla\psi|^2 + V(\mathbf{x})|\psi|^2 + \frac{\beta}{2}|\psi|^4\right] d\mathbf{x} \equiv E(\psi(\cdot, 0)). \tag{1.2.7}$$

The ground state $\phi_g := \phi_g(\mathbf{x})$ of the GPE (1.2.5) is defined as the minimizer of the energy functional (1.2.7) under the constraint (1.2.6), i.e. find $\phi_g \in S$, such that

$$E_g := E(\phi_g) = \min_{\phi \in S} E(\phi), \tag{1.2.8}$$

where S is defined as

$$S := \{\phi \,|\, \|\phi\|_2 = 1, \quad E(\phi) < \infty\}. \tag{1.2.9}$$

In addition, the ground state ϕ_g can also be characterized as a solution to the following nonlinear eigenvalue problem, i.e. Euler-Lagrange equation of the problem (1.2.8),

$$\mu\phi = \left[-\frac{1}{2}\nabla^2 + V(\mathbf{x}) + \beta|\phi|^2\right]\phi, \tag{1.2.10}$$

under the normalization constraint that $\phi \in S$, where the corresponding eigenvalue (or chemical potential) $\mu := \mu(\phi)$ can be computed as

$$\mu = E(\phi) + \frac{\beta}{2}\int_{\mathbb{R}^d} |\phi|^4 \, d\mathbf{x}. \tag{1.2.11}$$

It is obvious from the definition that the ground state is an eigenfunction (or stationary state) of (1.2.10) with the least energy, while it is possible that there are other eigenfunctions of (1.2.10) with energies larger than that of the ground state. Any other eigenfunctions of the GPE (1.2.10) under the constraint (1.2.6) whose energies are larger than that of the ground state are usually called the excited states in physics literatures [14, 54, 93]. Specifically, the excited state with the least energy among all excited states is usually called the first excited state, which is denoted as ϕ_1.

One thing worth mentioning here is that, in the repulsive interaction regime, the eigenfunction of (1.2.10) with the least energy is also the eigenfunction with the least chemical potential. In other words, if the eigenstates of the GPE (1.2.5) with $\beta \geq 0$, $\lim_{|\mathbf{x}|\to+\infty} V(\mathbf{x}) = +\infty$ and the constraint (1.2.6) can be ordered according to their energies as ϕ_g^β, ϕ_1^β, $\phi_2^\beta, \ldots$ satisfying $E_g(\beta) := E(\phi_g^\beta) < E_1(\beta) := E(\phi_1^\beta) \leq E(\phi_2^\beta) \leq \ldots$, it can be shown that $\mu_g(\beta) := \mu(\phi_g^\beta) < \mu_1(\beta) := \mu(\phi_1^\beta)$ [43]. We apply the super-index β here to indicate the first excited state ϕ_1^β depends on the value of β. Therefore, the fundamental gap for chemical potential is well defined as long as the fundamental gap for energy is well defined.

The GP theory has been verified to predict many properties of BEC quite well, and it has been the fundamental mathematical model to understand BEC up till now. Numerous efforts have been devoted to studying the GPE both theoretically and numerically. For the GPE itself, two problems are mostly studied mathematically, the ground state and the dynamics.

For ground states, Lieb et al. [77] proved the existence and uniqueness of the ground state in 3D and a more general result for 1D, 2D and 3D was shown in [14]. As for the computation, various numerical methods have been proposed. One of the most popular method for computing the ground state is the gradient flow with

discrete normalization (GFDN), which is also known as the imaginary time method in physical literatures [9,18,51]. Numerous numerical tests have verified the accuracy and efficiency of the method. Other schemes include a Runge-Kutta spectral method with spectral discretization in space and Runge-Kutta type integration in time by Adhikari et al. in [88], Gauss-Seidel-type methods in [49] by Lin et al., a finite element method by directly minimizing the energy functional in [29] by Bao and Tang, a feasible gradient type method and a regularized newton method by Wu, Wen and Bao in [32], and so on.

For the dynamical part, the well-posedness, dynamical properties, finite time blow-up and solitons of the GPE have been studied in [14, 44, 103] and references therein. For the computation, a lot of numerical methods have been proposed and an overview can be found in [14]. Several commonly used methods that are accurate and effecient include the time-splitting sine pseudospectral method [21–23, 33], time-splitting finite difference method [30, 111], time-splitting Laguerre-Hermite pseudospectral method [28], conservative Crank-Nicolson finite difference method [12, 13, 49], semi-implicit finite difference method [12, 13], etc. The comparisons between different numerical methods can be refered to [6, 14, 31, 48, 86, 105] and references therein.

1.3 Problems to study

In this section, I will briefly introduce the three problems to be studied.

- The first problem, which is also the main problem, to be studied in this thesis is to analyse the modified Gross-Pitaevskii equation (MGPE),

$$i\partial_t\psi = \left[-\frac{1}{2}\nabla^2 + V(\mathbf{x}) + \beta|\psi|^2 - \delta\nabla^2(|\psi|^2)\right]\psi, \quad t \geq 0,\ \mathbf{x} \in \mathbb{R}^d, \quad (1.3.1)$$

  where $\psi := \psi(\mathbf{x}, t)$ is a complex-valued wave function, $V(\mathbf{x})$ is a given real-valued potential, β and δ are dimensionless constants describing the interaction

between particles and $d = 1, 2, 3$. The details for the derivation of the equation can be referred to Chapter 2

We aim to lay a theoretical foundation of the MGPE (1.3.1) and propose efficient and accurate numerical methods for the computation. Chapter 2, Chapter 3, Chapter 4 and Chapter 5 study the MGPE (1.3.1) from different aspects, including the dimension reduction problem, theory and computation of the ground state and dynamics.

- The second problem is to study the fundamental gaps of the GPE (1.2.5) which are defined as

$$\delta_E(\beta) := E(\phi_1^\beta) - E(\phi_g^\beta) > 0, \quad \delta_\mu(\beta) := \mu(\phi_1^\beta) - \mu(\phi_g^\beta) > 0, \tag{1.3.2}$$

where ϕ_g^β and ϕ_1^β are the ground state and the first excited state of the GPE (1.2.5) for a given β. We are interested in finding a uniform lower bound with respect to all $\beta \geq 0$, i.e.

$$\delta_E^\infty := \inf_{\beta \geq 0} \delta_E(\beta), \qquad \delta_\mu^\infty := \inf_{\beta \geq 0} \delta_\mu(\beta). \tag{1.3.3}$$

We aim to study $\delta_E(\beta)$ and $\delta_\mu(\beta)$ asymptotically and numerically for two special cases, i.e. the GPE (1.2.5) with a box potential or a harmonic potential, to shed light on the fundamental gap problem under a more general external potential. The effect of the interaction strength β under a fixed external potential will be focused on and new gap conjectures will be proposed.

- The third problem considered in the thesis is the ground state approximations and energy asymptotics of the dimensionless time-independent nonlinear Schrödinger equation (NLSE) in d-dimensions ($d = 1, 2, 3$) [10,14,21,54,93,103]

$$\left[-\frac{1}{2}\Delta + V(\mathbf{x}) + \beta|\phi(\mathbf{x})|^{2\sigma}\right]\phi(\mathbf{x}) = \mu\phi(\mathbf{x}), \qquad \mathbf{x} \in \Omega \subseteq \mathbb{R}^d, \tag{1.3.4}$$

where $\phi := \phi(\mathbf{x})$ is a complex-valued wave function satisfying $\|\phi\|_2 = 1$, $V(\mathbf{x})$ is a given real-valued potential, $\beta \geq 0$ and $\sigma \geq 0$ are dimensionless constants describing the interaction strength and nonlinearity, respectively. The eigenvalue $\mu := \mu(\phi)$, also named as the chemical potential, is defined as [10, 14, 54, 93]

$$\mu(\phi) = E(\phi) + \frac{\sigma\beta}{\sigma+1}\int_\Omega |\phi(\mathbf{x})|^{2\sigma+2} d\mathbf{x}, \tag{1.3.5}$$

where $E := E(\phi)$ is usually called the energy and defined as [14, 103]

$$E(\phi) = \int_\Omega \left[\frac{1}{2}|\nabla\phi(\mathbf{x})|^2 + V(\mathbf{x})|\phi(\mathbf{x})|^2 + \frac{\beta}{\sigma+1}|\phi(\mathbf{x})|^{2\sigma+2}\right] d\mathbf{x}. \tag{1.3.6}$$

The ground state can be defined in the same way as in (1.2.8). We aim to find the energy asymptotics for two cases, either letting $\beta \to 0$ or ∞ with fixed $\sigma > 0$, or letting $\sigma \to \infty$ with fixed $\beta > 0$.

1.4 Scope of the thesis

As shown in the previous section, we will build a theoretical foundation of the MGPE (1.3.1), considering both its ground state and dynamics, and propose numerical schemes suitable for the computation. The fundamental gap problem for the GPE and the energy asymptotics for the NLSE will also be studied in this thesis.

The thesis is organized as follows. Chapter 2 is devoted to the dimension reduction problem for the MGPE. We will introduce the dimensionless MGPE in 3D under a harmonic potential. Then we derive rigorously one- and two-dimensional mean-field equations for cigar- and pancake-shaped BECs with higher-order interactions (HOIs), respectively. We show how the HOI modifies the contact interaction of the strongly confined particles. Numerical results will be provided to show the accuracy of our results.

Chapter 3 is devoted to characterizing the ground states of BEC with HOI, modeled by the MGPE (1.3.1). In fact, due to the appearance of HOI, the ground state structures become very complicated. We establish the existence, uniqueness and non-existence results under different parameter regimes, and obtain their limiting

behaviors and/or structures with different pairs of HOI and contact interactions. Both the whole space case and the bounded domain case are considered, where different structures of the ground states are identified. In addition, for both box and harmonic traps in 1D, 2D and 3D, we obtain explicitly the analytical Thomas-Fermi (TF) densities and corresponding energies, together with numerical validation.

In Chapter 4, we propose and compare several numerical schemes for computing the ground state. We will firstly review the widely used methods for the GPE, i.e. the gradient flow method and a gradient-type method by directly minimizing the discretized energy, and generalize them to the MGPE case. And then a new scheme, which minimizes the discretized energy via density formulation, will be proposed. One obvious benefit by using density formulation is that we change the original nonconvex problem to be a convex optimization problem. But we will also have a disadvantage that the nonlinear term is not well defined in the region where density is almost zero. As a result, regularization is needed. The convergence problem and the efficiency of our new scheme will be studied in details. We will write out each scheme explicitly and analyze the basic properties of the schemes. Numerical tests will also be performed to test the efficiency and accuracy of our schemes.

In Chapter 5, we analyze the dynamical properties of the MGPE both theoretically and numerically. In particular, we would like to see how the HOI affects the dynamics. In theory, we show the dynamics of the quantities like momentum and center of mass. For a problem with a harmonic potential, a special type of the exact solution will be constructed. We will also show conditions of possible finite time blow-up. As for the computation, we adopt the time-splitting method to the MGPE, and numerical tests will be provided.

Chapter 6 mainly focuses on a special problem, i.e. the fundamental gap problem for the GPE. We study both asymptotically and numerically the fundamental gaps in energy and chemical potential of the GPE with repulsive interactions under different trapping potentials including box potential and harmonic potential. Based

on our asymptotic and numerical results, we formulate gap conjectures on the fundamental gaps in energy and chemical potential of the GPE in bounded domains with the homogeneous Dirichlet boundary condition, and in the whole space with a convex trapping potential growing at least quadratically in the far field. We then extend these results to the GPE on bounded domains with either the homogeneous Neumann boundary condition or periodic boundary condition.

Chapter 7 is about the ground state approximations and energy asymptotics of the NLSE (1.3.4). One limiting case is to let $\beta \to 0$ or ∞ with $\sigma > 0$ fixed, and the other limiting case is to let $\sigma \to \infty$ with $\beta > 0$ fixed. Two special external potentials are considered, the box potential and the harmonic potential. Though most results are just generalizations of the GPE case, it is worth noticing that a bifurcation is observed in the ground state when the power of the nonlinearity goes to ∞ for both choices of the external potentials.

In Chapter 8, conclusions are drawn and some possible future studies are discussed.

Chapter 2

BEC with Higher Order Interactions

2.1 Introduction

The treatment of effective two-body contact interactions has been proven to be successful, but it is limited due to the low energy or low density assumption [60]. In the case of high particle densities or strong confinement, there will be a wider range of possible momentum states and correction terms should be included in the GPE for better description [3, 63]. In [53, 60], a higher order interaction (HOI) correction to the pseudopotential approximation has been analyzed, and gives the new form of the binary interaction between atoms as

$$V_{\text{int}}(\mathbf{z}) = g_0 \left[\delta(\mathbf{z}) + \frac{g_1}{2}\left(\delta(\mathbf{z})\nabla_{\mathbf{z}}^2 + \nabla_{\mathbf{z}}^2\delta(\mathbf{z})\right)\right], \tag{2.1.1}$$

where $\mathbf{z} = \mathbf{x}_1 - \mathbf{x}_2$ and $g_0 = \frac{4\pi\hbar^2 a_s}{m}$ is the contact interaction strength with a_s being the s-wave scattering length. HOI correction is given by the parameter $g_1 = \frac{a_s^2}{3} - \frac{a_s r_e}{2}$ with r_e being the effective range of the two-body interaction. When $r_e = \frac{2}{3}a_s$, it is for the hard sphere potential.

2.2 The modified Gross-Pitaevskii equation (MGPE)

In this section, we derive the MGPE and get its dimensionless form in 3D. Analogous to the derivation of the GPE (1.2.5), we show briefly how the HOI correction

to the pseudopotential approximation modifies the GPE by following the procedure in [63]. It is obvious that we only need to study the term for the HOI correction. For simplicity, we introduce

$$\hat{H}_{\text{mod}} = \frac{g_0 g_1}{2}\left[\delta(\mathbf{x}_1-\mathbf{x}_2)\nabla^2_{\mathbf{x}_1-\mathbf{x}_2} + \nabla^2_{\mathbf{x}_1-\mathbf{x}_2}\delta(\mathbf{x}_1-\mathbf{x}_2)\right]. \tag{2.2.1}$$

By changing $\mathbf{x}_1, \mathbf{x}_2$ to be $\mathbf{R} = (\mathbf{x}_1+\mathbf{x}_2)/2, \mathbf{r} = \mathbf{x}_1-\mathbf{x}_2$, integrating over $\mathbf{r}$ and doing integration by parts when necessary, we get

$$\begin{aligned}
&\iint_{\mathbb{R}^3\times\mathbb{R}^3} \bar{\psi}(\mathbf{x}_1,t)\bar{\psi}(\mathbf{x}_2,t)\hat{H}_{\text{mod}}\psi(\mathbf{x}_1,t)\psi(\mathbf{x}_2,t)\,d\mathbf{x}_1 d\mathbf{x}_2\\
&= \frac{g_0 g_1}{2}\iint_{\mathbb{R}^3\times\mathbb{R}^3} \bar{\psi}(\mathbf{R}+\frac{\mathbf{r}}{2},t)\bar{\psi}(\mathbf{R}-\frac{\mathbf{r}}{2},t)\left[\delta(\mathbf{r})\nabla^2_{\mathbf{r}} + \nabla^2_{\mathbf{r}}\delta(\mathbf{r})\right]\\
&\qquad \psi(\mathbf{R}+\frac{\mathbf{r}}{2},t)\psi(\mathbf{R}-\frac{\mathbf{r}}{2},t)\,d\mathbf{r}d\mathbf{R}\\
&= \frac{g_0 g_1}{4}\int_{\mathbb{R}^3}\left[\bar{\psi}^2\psi\nabla^2\psi - \bar{\psi}^2(\nabla\psi)^2 + \psi^2\bar{\psi}\nabla^2\bar{\psi} - \psi^2(\nabla\bar{\psi})^2\right]d\mathbf{R}\\
&= \frac{g_0 g_1}{2}\int_{\mathbb{R}^3}|\psi|^2\nabla^2(|\psi|^2)\,d\mathbf{R}.
\end{aligned}$$

Now substituting (2.1.1) into the N-body Schrödinger equation (1.1.3) with the N-body Hamiltonian defined in (1.1.1), and then taking the Hartree ansatz (1.2.2) and applying the results computed above, we can rewrite the energy of the BEC with HOI as

$$\begin{aligned}
E(\Psi_N) = N\int_{\mathbb{R}^3}\Bigg[&\frac{\hbar^2}{2m}|\nabla\psi(\mathbf{x},t)|^2 + V(\mathbf{x})|\psi(\mathbf{x},t)|^2 + \frac{N-1}{2}g_0|\psi(\mathbf{x},t)|^4\\
&+\frac{N-1}{4}g_0 g_1|\psi(\mathbf{x},t)|^2\nabla^2(|\psi(\mathbf{x},t)|^2)\Bigg]\,d\mathbf{x} \approx NE(\psi),
\end{aligned}$$

where $E(\psi)$ is the energy per particle which approximates $N-1$ by N for large N and is defined as

$$\begin{aligned}
E(\psi) = \int_{\mathbb{R}^3}\Bigg[&\frac{\hbar^2}{2m}|\nabla\psi(\mathbf{x},t)|^2 + V(\mathbf{x})|\psi(\mathbf{x},t)|^2\\
&+\frac{N}{2}g_0\left(|\psi(\mathbf{x},t)|^4 + \frac{g_1}{2}|\psi(\mathbf{x},t)|^2\nabla^2(|\psi(\mathbf{x},t)|^2)\right)\Bigg]\,d\mathbf{x}.
\end{aligned}$$

And then the modified Gross-Pitaveskii equation (MGPE) [53,63,64,108], is derived by the variation of $E(\psi)$ as

$$i\hbar\partial_t\psi = \left[-\frac{\hbar^2}{2m}\nabla^2 + V(\mathbf{x}) + Ng_0\left(|\psi|^2 + \frac{g_1}{2}\nabla^2|\psi|^2\right)\right]\psi, \quad t\geq 0,\ \mathbf{x}\in\mathbb{R}^3, \tag{2.2.2}$$

where $\mathbf{x} \in \mathbb{R}^3$ is the Cartesian coordinate vector, $\hbar$ is the reduced Planck constant, m is the mass of the particle, $V(\mathbf{x})$ is a real-valued external trapping potential, g_0, g_1 have been defined before and $\|\psi(\mathbf{x}, t)\|_2 = 1$.

To nondimensionalize the MGPE (2.2.2), we consider a special but commonly used external potential, i.e. the harmonic potential which is defined as

$$V_{\text{ho}}(\mathbf{x}) = \frac{m}{2}(\omega_x^2 x^2 + \omega_y^2 y^2 + \omega_z^2 z^2), \tag{2.2.3}$$

where $\omega_x, \omega_y, \omega_z$ are trapping frequencies in x-, y-, and z- direction.

In order to nondimensionalize the 3D MGPE (2.2.2), we introduce [10, 14]

$$\tilde{t} = \frac{t}{t_s}, \quad \tilde{\mathbf{x}} = \frac{\mathbf{x}}{x_s}, \quad \tilde{\psi}(\tilde{\mathbf{x}}, \tilde{t}) = x_s^{3/2}\psi(\mathbf{x}, t), \quad \tilde{V}(\tilde{\mathbf{x}}) = \frac{t_s^2}{m x_s^2} V(\mathbf{x}), \tag{2.2.4}$$

where t_s, x_s are the scaling parameters of dimensionless time and length units, respectively, satisfying $\hbar = m x_s^2/t_s$. Plugging (2.2.4) into (2.2.2), multiplying by $t_s^2/(m x_s^2)$, and then removing all $\tilde{}$, we obtain the following dimensionless MGPE in 3D,

$$i\partial_t \psi = -\frac{1}{2}\nabla^2\psi + V(\mathbf{x})\psi + \beta|\psi|^2\psi - \delta\nabla^2|\psi|^2\psi, \tag{2.2.5}$$

where $\beta = \frac{4\pi N a_s}{x_s}$, $\delta = -\frac{4\pi N}{x_s^3}\left(\frac{a_s^3}{3} - \frac{a_s^2 r_e}{2}\right)$.

For the 3D harmonic potential (2.2.3), we may choose $t_s = \frac{1}{\omega_0}$, $x_s = \sqrt{\frac{\hbar}{m\omega_0}}$ with $\omega_0 = \min\{\omega_x, \omega_y, \omega_z\}$. Introducing $\gamma_x = \frac{\omega_x}{\omega_0}$, $\gamma_y = \frac{\omega_y}{\omega_0}$ and $\gamma_z = \frac{\omega_z}{\omega_0}$, and the dimensionless trapping potential is given by

$$V(\mathbf{x}) = \frac{1}{2}\left(\gamma_x^2 x^2 + \gamma_y^2 y^2 + \gamma_z^2 z^2\right), \quad \mathbf{x} \in \mathbb{R}^3. \tag{2.2.6}$$

2.3 Dimension reduction

In this section, we study dimension reduction problem for the MGPE (2.2.5). In many experiments, a strong harmonic trap is applied along one or two directions to confine (or suppress) the condensate into pancake or cigar shape, respectively. In such cases, the usual Thomas-Fermi (TF) approximation for the full

three-dimensional (3D) case becomes invalid. It is then desirable to derive the effective one- (1D) and two-dimensional (2D) models, which offers compelling advantage for numerical computations compared to the 3D case.

We present effective mean-field equations for trapped BECs with HOI in one and two dimensions. Our equations are based on a mathematically rigorous dimension reduction of the 3D MGPE (2.2.5) to lower dimensions. Such dimension reduction has been formally derived in [14,20,26,42,99,115] and rigorously analyzed in [24,36], for the conventional GPE, i.e. without HOI. While for the MGPE, to our knowledge, this result has not been obtained, except for some preliminary works [108, 110], where the Gaussian profile is assumed in the strongly confining direction following the conventional GPE case. Surprisingly, our findings suggest that the Gaussian profile assumption is inappropriate for the quasi-1D BEC with HOI.

In the derivation of the quasi-1D (2D) model for the BEC with HOI, we assume that the leading order (in terms of aspect ratio) of the full 3D energy is from the radial (longitudinal) wave function, such that the BEC can only be excited in the non-confining directions, resulting in effective 1D (2D) condensates. Based on this principle, we show that the longitudinal wave function can be taken as the ground state of the longitudinal harmonic trap in quasi-2D BEC, and the radial wave function has to be taken as the Thomas-Fermi (TF) type (see (2.3.2)) in quasi-1D BEC, which is totally different from the conventional GPE case [108, 110]. We compare the ground states of the quasi-1D and quasi-2D BEC with the ground states of the full 3D BEC and find good agreement. In particular, our ground states are good approximations to those of the full 3D MGPE in regimes where the TF approximation fails.

For simplicity, we only consider the cylinder symmetric case in this section where we introduce $\omega_r := \omega_x = \omega_y$ and define the aspect ratio of the harmonic trap as

$$\gamma = \omega_r/\omega_z. \tag{2.3.1}$$

2.3.1 From 3D to 1D

Intuitively, the energy separation between stationary states is much larger in the radial direction than in the axial direction, and it is possible to freeze the radial motion of BEC [66]. As a consequence, the wave function of the system is in the variable separated form, i.e. it is the multiplication of the axial direction function and the radial direction function.

First, we present an effective mean-field equation for the axial wave function of the BEC with HOI, by assuming a strong radial confinement. In order to derive the mean-field equation for the axial wave function, we start with with the dimensionless 3D equation (2.2.5). In the quasi-1D BEC with HOI, the 3D wave function can be factorized as

$$\psi(\mathbf{x}, t) = e^{-i\mu_{2D}t}\chi_{2D}(x, y)\psi_{1D}(z, t), \tag{2.3.2}$$

with appropriate radial state function χ_{2D} and $\mu_{2D} \in \mathbb{R}$. Once the radial state χ_{2D} is known, we could project the MGPE (2.2.5) onto the axial direction to derive the quasi-1D equation. The key to find such χ_{2D} is the criterion that, the energy separation between stationary states should be much larger in the radial direction than in the axial direction, i.e. there is an energy scale separation between the radial state χ_{2D} and the axial wave function.

For the conventional GPE, i.e. $\delta = 0$, a good choice for χ_{2D} is the Gaussian function [14], which is the ground state of the radial harmonic trap, as $\chi_{2D}(r) = \sqrt{\frac{\gamma}{\pi}}e^{-\frac{\gamma r^2}{2}}$. The reason is that the order of the energy separation between states of the conventional BEC is dominated in the radial direction by the radial harmonic oscillator part, which is $O(\gamma)$, much larger than the interaction energy part if $\beta = O(1)$. Alternatively, it would be possible to use variational Gaussian profile approach to find $\chi_{2D}(r)$ [99]. In a similar dimension reduction problem for cold fermion gases [2], the profile χ_{2D} is chosen based on comparison between energy levels of the harmonic oscillator and Fermi energy. For BEC with HOI, the extra HOI term contributes to the energy. Thus, a more careful comparison between the kinetic

energy part and the HOI energy part is needed.

Substitute (2.3.2) into Eq. (2.2.5), we can get the equations for ψ_{1D} for appropriate μ_{2D} as

$$i\partial_t\psi_{1D}(z,t) = \left[-\frac{1}{2}\partial_{zz} + V_{1D}(z) + \beta_1|\psi_{1D}|^2 - \delta_1(\partial_{zz}|\psi_{1D}|^2)\right]\psi_{1D}, \tag{2.3.3}$$

where $V_{1D}(z) = \frac{1}{2}z^2$,

$$\beta_1 = \beta\iint|\chi_{2D}|^4dxdy + \delta\iint|\nabla_\perp|\chi_{2D}|^2|^2dxdy, \tag{2.3.4a}$$

$$\delta_1 = \delta\iint|\chi_{2D}|^4dxdy, \tag{2.3.4b}$$

and $\nabla_\perp = (\partial_x, \partial_y)^T$. It remains to determine χ_{2D} and we are going to use the criteria that the energy separation scales are different in different directions. In order to do this, we need calculate the energy scale in z direction. Hence, we take the stationary states (ground states) of (2.3.3) as

$$\psi_{1D}(z,t) = e^{-i\mu_{1D}t}\phi_{1D}(z). \tag{2.3.5}$$

Combining Eqs. (2.3.2) and (2.3.5), following the way to find Eq. (2.3.3), we can derive the equations for $\chi_{2D}(x,y)$ as

$$\mu_{2D}\chi_{2D} = -\frac{1}{2}\nabla_\perp^2\chi_{2D} + V_{2D}(r)\chi_{2D} + \beta_2|\chi_{2D}|^2\chi_{2D} - \delta_2(\nabla_\perp^2|\chi_{2D}|^2)\chi_{2D}, \tag{2.3.6}$$

where $\nabla_\perp^2 = \partial_{xx} + \partial_{yy}$, the radially symmetric potential $V_{2D} = \frac{\gamma^2}{2}(x^2+y^2)$,

$$\beta_2 = \beta\int|\phi_{1D}|^4dz + \delta\int|\partial_z|\phi_{1D}|^2|^2dz, \tag{2.3.7a}$$

$$\delta_2 = \delta\int|\phi_{1D}|^4dz. \tag{2.3.7b}$$

To determine the frozen state χ_{2D}, we need minimize the energy of Eq. (2.3.6), while parameters β_2 and δ_2 depends on ϕ_{1D}. So actually, we need solve a coupled system simultaneously for χ_{2D} and ϕ_{1D}. To this purpose, we will consider the problem in the quasi-1D limit as $\gamma \to \infty$. Intuitively, transverse direction is almost compressed to a Dirac delta function as $\gamma \to \infty$, so that a proper scaling is needed to obtain the correct form of χ_{2D}.

We will determine χ_{2D} via a self consistent iteration as follows: given some β_2 and δ_2, under proper scaling as $\gamma \to \infty$, (i) drop the less important part to get approximate χ_{2D}, (ii) put χ_{2D} into Eq. (2.3.3) to determine the longitudinal ground state ϕ_{1D}, (iii) use ϕ_{1D} to compute β_2 and δ_2, and then (iv) check if it is consistent.

In the quasi-1D regime, $\gamma \to \infty$, similar to the conventional GPE case, due to the strong confinement in transverse direction, the ground state solution ϕ_{1D} is very flat in z direction, as both nonlinear terms exhibit repulsive interactions. It is easy to get the scalings of $\int |\partial_z|\phi_{1D}|^2|^2 dz = O(L^{-3})$, $\int |\phi_{1D}|^4 dz = O(L^{-1})$, where L indicates the correct length scale of ϕ_{1D}. Therefore β_2 and δ_2 are of the same order by definition, since $L \to \infty$ in the quasi-1D limit.

For mathematical convenience, we introduce $\varepsilon = 1/\sqrt{\gamma}$ such that $\varepsilon \to 0^+$. In the radial variable, introduce the new scale $\tilde{r} = r/\varepsilon^\alpha$ and $\tilde{w}(\tilde{r}) = \varepsilon^\alpha \chi_{2D}(r)$ such that $\tilde{r} \sim O(1)$ and $\|\tilde{w}\| = 1$, then (2.3.6) becomes

$$\mu_{2D}\tilde{w} = -\frac{\nabla_\perp^2 \tilde{w}}{2\varepsilon^{2\alpha}} + \frac{\tilde{r}^2 \tilde{w}}{2\varepsilon^{4-2\alpha}} + \frac{\beta_2}{\varepsilon^{2\alpha}}\tilde{w}^3 - \frac{\delta_2}{\varepsilon^{4\alpha}}\nabla_\perp^2(|\tilde{w}|^2)\tilde{w}. \tag{2.3.8}$$

Notice that the term $\beta_2/\varepsilon^{2\alpha}\tilde{w}^3$ can be always neglected compared to the last term since $\beta_2 \sim \delta_2$ and $\varepsilon^{-\alpha} \ll \varepsilon^{-3\alpha}$ as $\varepsilon \to 0^+$. On the other hand, β_2 and δ_2 are both repulsive interactions while only the potential term confines the condensate. Thus, the correct leading effects (HOI or kinetic term) should be balanced with the potential term. Now, we are only left with two possibilities:

Case I, $-\frac{1}{2\varepsilon^{2\alpha}}\tilde{\nabla}^2{}_\perp \tilde{w}$ is balanced with term $\frac{\tilde{r}^2}{2\varepsilon^{4-2\alpha}}\tilde{w}$, and $\frac{\delta_2}{\varepsilon^{4\alpha}}\tilde{\nabla}^2{}_\perp(|\tilde{w}|^2)\tilde{\psi}$ is smaller. In this case, $\varepsilon^{2\alpha} \sim \varepsilon^{4-2\alpha}$. So we get $\alpha = 1$. Besides, we also need $\varepsilon^{-2\alpha} \gg \frac{\delta_2}{\varepsilon^{4\alpha}}$, i.e. $\delta_2 \ll \varepsilon^2$.

Case II, $\frac{\delta_2}{\varepsilon^{4\alpha}}\tilde{\nabla}^2{}_\perp(|\tilde{w}|^2)\tilde{w}$ is balanced with term $\frac{\tilde{r}^2}{2\varepsilon^{4-2\alpha}}\tilde{w}$, and $-\frac{1}{2\varepsilon^{2\alpha}}\tilde{\nabla}^2{}_\perp \tilde{w}$ is much smaller. In this case, $\frac{\delta_2}{\varepsilon^{4\alpha}} \sim \frac{1}{\varepsilon^{4-2\alpha}}$ and $\varepsilon^{-2\alpha} \ll \frac{1}{\varepsilon^{4-2\alpha}}$, i.e. $\alpha < 1$ and $\delta_2 \sim \varepsilon^{6\alpha-4}$.

We will check if the scaling is consistent for each case.

Case I. Since $\alpha = 1$, we have χ_{2D} as the ground state of the radial harmonic oscillator,

$$\chi_{2D}(r) = \frac{1}{\sqrt{\pi\varepsilon^2}} e^{-\frac{r^2}{2\varepsilon^2}}, \tag{2.3.9}$$

and

$$\iint |\chi_{2D}|^4 dxdy = \frac{1}{2\pi\varepsilon^2}, \iint |\nabla_\perp(|\chi_{2D}|^2)|^2 dxdy = \frac{1}{\pi\varepsilon^4}.$$

Recalling β_1 and δ_1 in Eq. (2.3.4), the parameters are in TF regime I (cf. section 3.3.2), so in z direction we can get the approximate solution from section 3.3.2 as:

$$\phi_{1D} \approx \sqrt{\frac{((z^*)^2 - z^2)_+}{2\beta_1}}, \quad z^* = \left(\frac{3\beta_1}{2}\right)^{\frac{1}{3}}, \tag{2.3.10}$$

By definition of δ_2 (2.3.7b), we obtain

$$\delta_2 = \delta \int |\phi_{1D}|^4 dz = \frac{3\delta}{5}\left(\frac{2}{3\beta_1}\right)^{\frac{1}{3}}, \tag{2.3.11}$$

while

$$\beta_1 \sim \delta \iint |\nabla_\perp(|\chi_{2D}|^2)|^2 dxdy = \frac{\delta}{\pi\varepsilon^4}. \tag{2.3.12}$$

Combining (2.3.11) and (2.3.12), we get $\delta_2 = O(\varepsilon^{\frac{4}{3}})$. But this contradicts the requirement that $\delta_2 \ll \varepsilon^2$. Thus *Case I* is inconsistent.

Case II. As δ_2 term is more significant than the kinetic term, we solve $\mu_{2D} = r^2/2\varepsilon^4 - \delta_2\nabla_\perp^2|\chi_{2D}|^2$ within the support of $\chi_{2D}(r)$ and get

$$\chi_{2D}(r) = \frac{(R^2 - r^2)_+}{\sqrt{32\varepsilon^4\delta_2}}, \; R = 2a\varepsilon, \; a = \left(\frac{3\delta_2}{2\pi\varepsilon^2}\right)^{\frac{1}{6}}. \tag{2.3.13}$$

Hence, we know

$$\iint |\chi_{2D}|^4 dxdy = \frac{3}{10\delta_2}\left(\frac{3\delta_2}{2\pi\varepsilon^2}\right)^{\frac{2}{3}}, \tag{2.3.14}$$

$$\iint |\nabla_\perp|\chi_{2D}|^2|^2 dxdy = \frac{1}{2\delta_2\varepsilon^2}\left(\frac{3\delta_2}{2\pi\varepsilon^2}\right)^{\frac{1}{3}}. \tag{2.3.15}$$

Again, recalling β_1 and δ_1 in Eq. (2.3.4), the parameters are in TF regime I (cf. Sec. 3.3.2), so in z direction we can get the approximate solution from Sec. 3.3.2 as Eq. (2.3.10). Using $\phi_{1D}(z)$ in Eq. (2.3.10), we can compute

$$\delta_2 = \delta \int |\phi_{1D}|^4 dz = \frac{3\delta}{5}\left(\frac{2}{3\beta_1}\right)^{\frac{1}{3}}, \tag{2.3.16}$$

while

$$\beta_1 \sim \delta \int |\nabla_\perp|\chi_{2D}|^2|^2 dxdy = \left(\frac{3}{2\pi}\right)^{\frac{1}{3}} \frac{\delta}{2\varepsilon^{\frac{8}{3}}\delta_2^{\frac{2}{3}}}. \tag{2.3.17}$$

Combining (2.3.16) and (2.3.17), we find $\delta_2 = \frac{2\cdot 3^{\frac{5}{7}}\pi^{\frac{1}{7}}\delta^{\frac{6}{7}}\varepsilon^{\frac{8}{7}}}{5^{\frac{9}{7}}}$, $\beta_1 \sim \frac{5^{\frac{6}{7}}}{3^{\frac{1}{7}}\cdot 4\pi^{\frac{3}{7}}}\delta^{\frac{3}{7}}\gamma^{\frac{12}{7}}$. Noticing the requirement that $\delta_2 \sim \varepsilon^{6\alpha-4}$, we get $\alpha = 6/7$, and it satisfies the other constraint $\alpha < 1$. Thus, *Case II* is self consistent, and it is the case that we should choose to derive the mean field equation for the quasi-1D BEC. β_1, δ_1 can be obtained as in Eq. (2.3.20).

To summarize, we identify that the energy contribution from the HOI term (2.3.6) in transverse direction is dominant when $\gamma \gg 1$. It shows a completely different scenario compared to the conventional GPE, in which the transverse harmonic oscillator terms are dominant. The explicit form for the transverse radial state function $\chi_{2D}(r)$ for the quasi-1D BEC with HOI is determined as

$$\chi_{2D}(x,y) \approx \frac{\gamma(R^2 - r^2)_+}{4\sqrt{2\delta_r}}, \quad r = \sqrt{x^2+y^2}, \tag{2.3.18}$$

where $R = 2\left(\frac{3\delta_r}{2\pi\gamma^2}\right)^{\frac{1}{6}}$, $\delta_r = \frac{2\cdot 3^{\frac{5}{7}}\pi^{\frac{1}{7}}\delta^{\frac{6}{7}}}{5^{\frac{9}{7}}\gamma^{\frac{4}{7}}}$, $\mu_{2D} \approx \frac{3^{\frac{4}{7}}\delta^{\frac{2}{7}}\gamma^{\frac{8}{7}}}{\pi^{\frac{2}{7}}5^{\frac{3}{7}}}$ and $(f)_+ = \max\{f, 0\}$.

With this explicit form of the approximate solutions, we can further get the leading order approximations of chemical potential and energy for the original 3D problem. It turns out that $\mu_g^{3D} \approx \frac{9}{8}\mu_{2D}$ and $E_g^{3D} \approx \frac{7}{8}\mu_{2D}$, where μ_{2D} is computed approximately as before.

It is worth pointing out that the determination of the radial state $\chi_{2D}(r)$ is coupled with the axial direction state (see (2.3.4)). Therefore, a coupled system of the radial and axial states is necessary to get more refined approximate density profiles for ground states, as compared to the above approximation $\chi_{2D}(r)$.

In the axial z direction, multiplying (2.2.5) by χ_{2D} and integrating the x, y variables, we obtain the mean-field equation for the quasi-1D BEC with HOI as

$$i\partial_t\psi_{1D}(z,t) = -\frac{1}{2}\partial_{zz}\psi_{1D} + V_{1D}(z)\psi_{1D} + \beta_1|\psi_{1D}|^2\psi_{1D} - \delta_1(\partial_{zz}|\psi_{1D}|^2)\psi_{1D}, \tag{2.3.19}$$

where $V_{1D}(z) = \frac{1}{2}\gamma_z^2 z^2 = \frac{1}{2}z^2$, and

$$\beta_1 = \frac{5^{\frac{6}{7}}}{3^{\frac{1}{7}} \cdot 4\pi^{\frac{3}{7}}} \delta^{\frac{3}{7}} \gamma^{\frac{12}{7}} + \frac{3^{\frac{10}{7}}}{4 \cdot 5^{\frac{4}{7}} \pi^{\frac{5}{7}}} \frac{\beta \gamma^{\frac{6}{7}}}{\delta^{\frac{2}{7}}}, \tag{2.3.20a}$$

$$\delta_1 = \frac{3^{\frac{10}{7}}}{4 \cdot 5^{\frac{4}{7}} \pi^{\frac{5}{7}}} \delta^{\frac{5}{7}} \gamma^{\frac{6}{7}}. \tag{2.3.20b}$$

From Eq. (2.3.19), it is observed that the HOI provides extra repulsive contact interactions in the quasi-1D BEC. More interestingly, the first term in β_1 suggests that the contact interaction is dominated by the HOI part.

If the repulsive contact interaction dominates the dynamics in (2.3.19), we could neglect the kinetic and HOI parts to obtain an analytical expression for the quasi-1D BEC with HOI. This agrees with the usual Thomas-Fermi approximation for the conventional quasi-1D BEC, and its validity is shown in Sec. 3.3.2 (referred as region I). In such situation, the approximate density profile is given as:

$$n_{1D}(z) = |\psi_{1D}|^2 = \frac{((z^*)^2 - z^2)_+}{2\beta_1}, \tag{2.3.21}$$

where $z^* = \left(\frac{3\beta_1}{2}\right)^{\frac{1}{3}}$.

In Fig. 2.1, we compare the ground state densities of quasi-1D BEC with HOI determined via (2.3.19) and the numerical results from 3D MGPE in (2.2.5) by integrating over the transversal directions. As shown in the figure, our proposed 1D equation, Eq. (2.3.19), and (2.3.18) describes the BEC accurately in axial and radical direction separately, while the traditional Gauss approximation totally fails.

2.3.2 From 3D to 2D

In this section, we consider the BEC being strongly confined in the axial direction, which corresponds to the case $0 < \gamma \ll 1$. Accordingly, we choose rescaling parameters used in (2.2.5) as $\omega_0 = \omega_r$, $x_s = \sqrt{\hbar/m\omega_r}$, and we work with the dimensionless equation (2.2.5).

Similar to the case of quasi-1D BEC, we assume that the wave function can be factorized in the quasi-2D case as

$$\psi(\mathbf{x}, t) = e^{-i\mu_{1D}t} \psi_{2D}(x, y, t) \chi_{1D}(z), \tag{2.3.22}$$

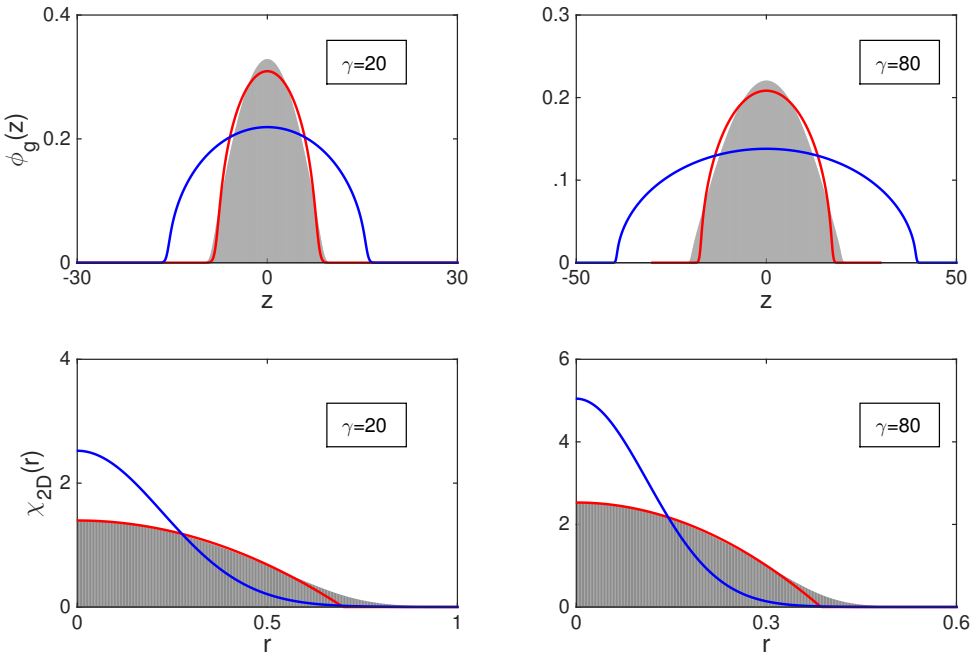

Figure 2.1: (quasi-1D ground state) Red line: approximation (2.3.18) in radical direction and numerical solution of (2.3.19) in axial direction. Blue line: traditional Gauss approximation in radical direction and corresponding numerical solution in axial direction. Shaded area: numerical solution from the original 3D model (1.3.1). The corresponding γ's are given in the plots. For other parameters, we choose $\beta = 1, \delta = 20$.

for appropriate longitudinal state $\chi_{1D}(z)$ and $\mu_{1D} \in \mathbb{R}$.

Plugging Eq. (2.3.22) into Eq. (2.2.5), we can get the equations for ψ_{2D} with appropriate μ_{1D} as

$$i\partial_t \psi_{2D}(x,y,t) = \left[-\frac{1}{2}\nabla_\perp^2 + V_{2D}(x,y) + \beta_2|\psi_{2D}|^2 - \delta_2(\nabla_\perp^2|\psi_{2D}|^2)\right]\psi_{2D}, \quad (2.3.23)$$

where the radially symmetric potential $V_{2D}(r) = \frac{1}{2}r^2$ and

$$\beta_2 = \beta\int |\chi_{1D}|^4 dxdy + \delta\int |\partial_z|\chi_{1D}|^2|^2 dz, \quad (2.3.24a)$$

$$\delta_2 = \delta\int |\chi_{1D}|^4 dxdy. \quad (2.3.24b)$$

It remains to determine χ_{1D} and we are going to use the same idea as that in the quasi-1D BEC. In order to do this, we need calculate the energy scale in the r direction. Hence, we take the stationary states (ground states) of Eq. (2.3.23) as

$$\psi_{2D}(r,t) = e^{-i\mu_{2D}t}\phi_{2D}(r). \quad (2.3.25)$$

Combining Eq. (2.3.22) with Eq. (2.3.25), we can derive the equations for $\chi_{1D}(z)$ as

$$\mu_{1D}\chi_{1D} = -\frac{1}{2}\partial_{zz}\chi_{1D} + V_{1D}(z)\chi_{1D} + \beta_1|\chi_{1D}|^2\chi_{1D} - \delta_1(\partial_{zz}|\chi_{1D}|^2)\chi_{1D}, \quad (2.3.26)$$

where $V_{1D}(z) = \frac{z^2}{2\gamma^2}$,

$$\beta_1 = \beta\int |\phi_{2D}|^4 dz + \delta\int |\nabla_\perp|\phi_{2D}|^2|^2 dz, \quad (2.3.27a)$$

$$\delta_1 = \delta\int |\phi_{2D}|^4 dz. \quad (2.3.27b)$$

We proceed similarly to the quasi-1D case. For mathematical convenience, denote $\varepsilon = \sqrt{\gamma}$ such that $\varepsilon \to 0^+$. Rescale z variable as $\tilde{z} = z/\varepsilon^\alpha$, $\tilde{w}(\tilde{z}) = \varepsilon^{\frac{\alpha}{2}}\chi_{1D}(z)$ for some $\alpha > 0$. By removing the tildes, Eq. (2.3.26) becomes

$$\mu_{1D}w = -\frac{1}{2\varepsilon^{2\alpha}}\partial_{zz}w + \frac{z^2}{2\varepsilon^{4-2\alpha}}w + \frac{\beta_1}{\varepsilon^\alpha}w^3 - \frac{\delta_1}{\varepsilon^{3\alpha}}(\partial_{zz}|w|^2)w. \quad (2.3.28)$$

Assuming that the scale is correct, then w will be a regular function, independent of ε so that its norm will be $O(1)$. Now, we will determine the scale. Intuitively, by

the same reason shown in the quasi-1D case, the term $\frac{\beta_1}{\varepsilon^\alpha}w^3$ can always be neglected compared to the HOI term. In addition, the potential term is the only effect that confines the condensate, and can not be neglected. As a result, there are only two possibilities:

Case I. $-\frac{1}{2\varepsilon^{2\alpha}}\partial_{zz}w$ is balanced with term $\frac{z^2}{2\varepsilon^{4-2\alpha}}w$, and $\frac{\delta_1}{\varepsilon^{3\alpha}}(\partial_{zz}|w|^2)w$ is much smaller. In this case, $\varepsilon^{2\alpha} \sim \varepsilon^{4-2\alpha}$. So we get $\alpha = 1$. Besides, we also need $\varepsilon^{-2\alpha} \gg \frac{\delta_1}{\varepsilon^{3\alpha}}$, i.e. $\delta_1 \ll \varepsilon$.

Case II. $\frac{\delta_1}{\varepsilon^{3\alpha}}(\partial_{zz}|w|^2)w$ is balanced with term $\frac{z^2}{2\varepsilon^{4-2\alpha}}w$, and $-\frac{1}{2\varepsilon^{2\alpha}}\partial_{zz}w$ is much smaller. In this case, $\frac{\delta_1}{\varepsilon^{3\alpha}} \sim \frac{1}{\varepsilon^{4-2\alpha}}$ and $\varepsilon^{-2\alpha} \ll \frac{1}{\varepsilon^{4-2\alpha}}$, i.e. $\alpha < 1$ and $\delta_1 \sim \varepsilon^{5\alpha-4}$.

Now, we check the consistency of each case.

Case I. Since $\alpha = 1$, we can obtain $\chi_{1D}(z)$ as the ground state of the longitudinal harmonic oscillator as

$$\chi_{1D}(z) = \left(\frac{1}{\pi\varepsilon^2}\right)^{\frac{1}{4}} e^{-\frac{z^2}{2\varepsilon^2}}, \tag{2.3.29}$$

and the following quantities can be calculated:

$$\int |\chi_{1D}|^4 dz = \frac{1}{\sqrt{2\pi}\varepsilon} \ , \ \int |(|\chi_{1D}|^2)'|^2 dz = \frac{1}{\sqrt{2\pi}\varepsilon^3}. \tag{2.3.30}$$

By examining β_2 and δ_2 in Eq. (2.3.23), we find β_2 is dominant as $\varepsilon \to 0^+$ and the ground state $\phi_{2D}(r)$ can be obtained as TF approximation in the parameter regime I as shown in section 3.3.2,

$$\phi_{2D}(r) = \sqrt{\frac{(R^2 - r^2)_+}{2\beta_2}}, \text{ where } R = \left(\frac{4\beta_2}{\pi}\right)^{\frac{1}{4}}. \tag{2.3.31}$$

Then we can compute

$$\iint |\phi_{2D}|^4 dxdy = \frac{2}{3\sqrt{\pi\beta_2}}, \tag{2.3.32}$$

$$\iint |\nabla_\perp(|\phi_{2D}|^2)|^2 dxdy = \frac{2}{\beta_2}. \tag{2.3.33}$$

Having ϕ_{2D}, we can check the consistency of *Case I.* By the definition of δ_1 in Eq. (2.3.27), we get

$$\delta_1 = \delta \iint |\phi_{2D}|^4 dxdy = \frac{2\delta}{3\sqrt{\pi\beta_2}}, \tag{2.3.34}$$

while it follows from the definition of β_2 in Eq. (2.3.24),

$$\beta_2 \sim \delta \int |(|\chi_{1D}|^2)'|^2 dz = \frac{\delta}{\sqrt{2\pi}\varepsilon^3}. \tag{2.3.35}$$

Combining Eqs. (2.3.34) and (2.3.35), we obtain $\delta_1 = \frac{2}{3}\sqrt{\frac{\delta}{\pi}}\,(2\pi)^{\frac{1}{4}}\,\varepsilon^{\frac{3}{2}} = O(\varepsilon^{\frac{3}{2}}) = o(\varepsilon)$, which satisfies the requirement for δ_1. Thus, *Case I* is self consistent.

Case II. In this case, we solve equation $\mu_{1D} = \frac{z^2}{2\varepsilon^4} - \delta_1 \partial_{zz}|\chi_{1D}|^2$ within the support of χ_{1D} and get

$$\chi_{1D}(z) = \frac{((z^*)^2 - z^2)_+}{2\varepsilon^2\sqrt{6\delta_1}}, \quad z^* = \left(\frac{45\delta_1\varepsilon^4}{2}\right)^{\frac{1}{5}}.$$

Then we have the identities as

$$\int |\chi_{1D}|^4 dz = \frac{2}{63}\left(\frac{45}{2}\right)^{\frac{4}{5}} \left(\varepsilon^4\delta_1\right)^{-\frac{1}{5}}, \tag{2.3.36}$$

$$\int |(|\chi_{1D}|^2)'|^2 dz = \frac{2}{21}\left(\frac{45}{2}\right)^{\frac{2}{5}} \left(\varepsilon^4\delta_1\right)^{-\frac{3}{5}}. \tag{2.3.37}$$

In the quasi-2D limit regime, i.e. $0 < \varepsilon \ll 1$, by the definitions of β_2 and δ_2 in Eq. (2.3.24), we find β_2 is dominant and ϕ_{2D} can be obtained as the TF density in parameter regime I shown in section 3.3.2, which is exactly the same as Eq. (2.3.31).

Similar to the previous case, we can calculate

$$\delta_1 = \delta \iint |\phi_{2D}|^4 dxdy = \frac{2\delta}{3\sqrt{\pi\beta_2}}, \tag{2.3.38}$$

where

$$\beta_2 \sim \delta \int |(|\chi_{1D}|^2)'|^2 dz = \frac{2\delta}{21}\left(\frac{45}{2}\right)^{\frac{2}{5}} \left(\varepsilon^4\delta_1\right)^{-\frac{3}{5}}. \tag{2.3.39}$$

Combining Eqs. (2.3.38) and (2.3.39), we can get $\delta_1 \approx \frac{2}{45}\left(\frac{105\delta}{\pi}\right)^{\frac{5}{7}}\varepsilon^{\frac{12}{7}}$. But the requirement is $\delta_1 \sim \varepsilon^{5\alpha-4}$, so we get $\alpha = 8/7$. This contradicts the other requirement that $\alpha < 1$. In other words, *Case II* is inconsistent.

In summary, only *Case I* is consistent and χ_{1D} should be chosen as Eq. (2.3.29). Thus, mean-field equation for quasi-2D BEC is derived in Eq. (2.3.41) with given

constants in Eq. (2.3.42). In this way, we find that the leading order energy separation in z direction is due to the longitudinal harmonic oscillator, while the cubic interaction and HOI parts are less important. This fact suggests that the ground mode of the longitudinal harmonic oscillator, i.e. a Gaussian type function, is a suitable choice for $\chi_{1D}(z)$. To be more specific,

$$\chi_{1D}(z) \approx \left(\frac{1}{\pi\gamma}\right)^{\frac{1}{4}} e^{-\frac{z^2}{2\gamma}}, \tag{2.3.40}$$

and $\mu_{1D} \approx 1/2\gamma$.

Substituting (2.3.22) with (2.3.40) into the MGPE (1.3.1), then multiplying (1.3.1) by χ_{1D} and integrating the longitudinal z out, we obtain the mean-field equation for the quasi-2D BEC with HOI as

$$i\partial_t\psi_{2D} = -\frac{1}{2}\nabla^2\psi_{2D} + V_{2D}(x,y)\psi_{2D} + \beta_2|\psi_{2D}|^2\psi_{2D} - \delta_2(\nabla^2|\psi_{2D}|^2)\psi_{2D}, \tag{2.3.41}$$

where $V_{2D}(x,y) = \frac{1}{2}(x^2+y^2)$ and

$$\beta_2 = \frac{\beta}{\sqrt{2\pi\gamma}} + \frac{\delta}{\sqrt{2\pi\gamma^3}}, \quad \delta_2 = \frac{\delta}{\sqrt{2\pi\gamma}}. \tag{2.3.42}$$

Similar to the quasi-1D BEC case, HOI induces effective contact interaction in the quasi-2D regime, which dominates the contact interaction (β part). We then conclude that even for small HOI δ, the contribution of HOI could be significant in the high particle density regime of quasi-2D BEC.

Analogous to the quasi-1D BEC case, we can derive the usual Thomas-Fermi (TF) approximation when the repulsive interaction β_2 dominates the dynamics, and the analytical density for the quasi-2D BEC with HOI reads as

$$n_{2D}(r) = |\psi_{2D}|^2 = \frac{(R^2-r^2)_+}{2\beta_2}, \quad r = \sqrt{x^2+y^2}, \tag{2.3.43}$$

where $R = \left(\frac{4\beta_2}{\pi}\right)^{\frac{1}{4}}$.

In order to verify our findings in this section, we compare the quasi-2D ground state densities obtained via Eq. (2.3.41), TF density (2.3.43) and the numerical results from 3D MGPE (2.2.5) by integrating z out. The results are displayed in

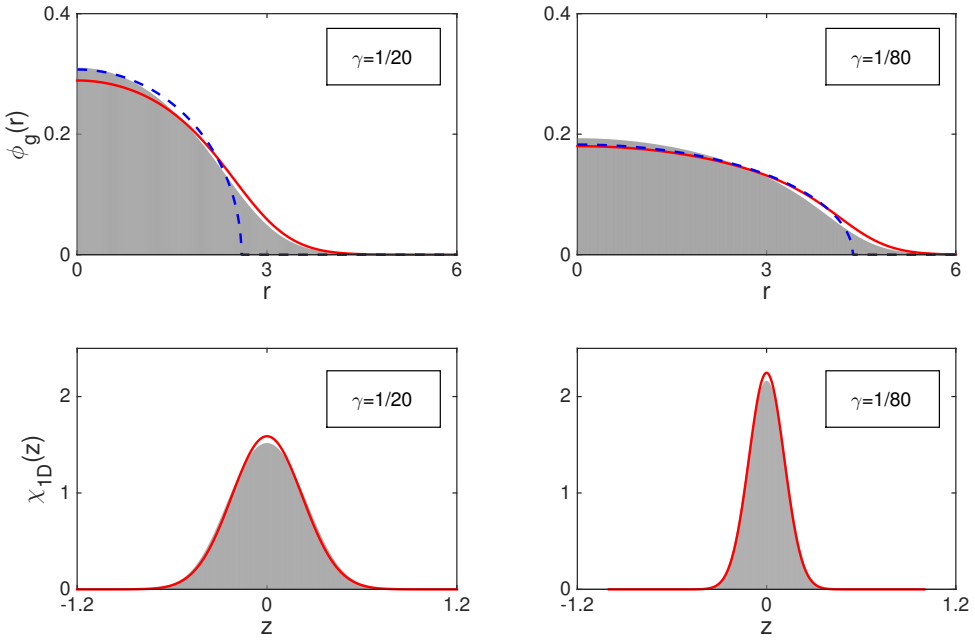

Figure 2.2: (quasi-2D ground state) Red line: approximation (2.3.40) in axial direction and numerical solution of (2.3.41) in radical direction. Blue dash line: Thomas-Fermi approximation of (2.3.43) in radical direction. Shaded area: numerical solution from the original 3D model (1.3.1). The corresponding γ's are given in the plots. For other parameters, we choose $\beta = 5, \delta = 1$.

Fig. 2.2. The BEC is broadened compared to the analytically predicated profile because of the effective repulsive interaction from the HOI. Thus, in the regime of small or moderate interaction energy β_2, the usual approach to BECs with HOI via conventional Thomas-Fermi approximation fails. On the other hand, it turns out that our proposed 2D equation, Eq. (2.3.41), is accurate for quasi-2D BEC in the mean-field regime at experimentally relevant trap aspect ratios γ.

2.4 The d-dimensional MGPE

As shown in the previous section, we might need the MGPE in 1D and 2D as well in practice. In fact, the MGPE (2.2.5) under a harmonic potential can be written

in a unified form in d-dimensions ($d = 1, 2, 3$) with $\mathbf{x} \in \mathbb{R}^d$ (denoted as $\mathbf{x} = x \in \mathbb{R}$ for $d = 1$, $\mathbf{x} = (x, y)^T \in \mathbb{R}^2$ for $d = 2$ and $\mathbf{x} = (x, y, z)^T \in \mathbb{R}^3$ for $d = 3$) as

$$i\partial_t \psi = \left[-\frac{1}{2}\nabla^2 + V(\mathbf{x}) + \beta|\psi|^2 - \delta\nabla^2|\psi|^2 \right] \psi, \quad t \geq 0, \, \mathbf{x} \in \mathbb{R}^d, \tag{2.4.1}$$

where

$$V(\mathbf{x}) = \begin{cases} \frac{1}{2}(\gamma_1^2 x^2 + \gamma_2^2 y^2 + \gamma_3^2 z^2), & d = 3, \\ \frac{1}{2}(\gamma_1^2 x^2 + \gamma_2^2 y^2), & d = 2, \\ \frac{1}{2}\gamma_1^2 x^2, & d = 1, \end{cases} \tag{2.4.2}$$

where $\gamma_1, \gamma_2, \gamma_3$ are dimensionless trapping frequencies in x-, y-, and z- direction, β and δ are two dimensionless real constants for describing the contact interaction and HOI strengths, respectively.

Another commonly seen potential is the box potential, which is defined as

$$V(\mathbf{x}) = \begin{cases} 0, & \mathbf{x} \in \Omega. \\ \infty, & \mathbf{x} \notin \Omega, \end{cases} \tag{2.4.3}$$

where $\Omega \subset \mathbb{R}^d$ ($d = 1, 2, 3$) is a bounded domain. In this case, the MGPE can be written as the following equation defined in the bounded domain Ω,

$$i\partial_t \psi = \left[-\frac{1}{2}\nabla^2 + \beta|\psi|^2 - \delta\nabla^2|\psi|^2 \right] \psi, \quad t \geq 0, \, \mathbf{x} \in \Omega, \quad \psi|_{\partial\Omega} = 0. \tag{2.4.4}$$

We can change $V(\mathbf{x})$ to be some other potentials such as optical lattice potential and double-well potential as well. We refer to [11, 14, 93] and references therein. For the rest of this paper, we assume that $V(\mathbf{x})$ is a general given real-valued function, and without loss of generality, we assume $V(\mathbf{x}) \geq 0$ for external potentials that are bounded from below.

For the d-dimensional MGPE (2.4.1), we can show that it conserves the total mass , i.e.

$$N(t) := \int_{\mathbb{R}^d} |\psi(\mathbf{x}, t)|^2 d\mathbf{x} \equiv N(0) = 1, \quad t \geq 0, \tag{2.4.5}$$

and the energy per particle, i.e.

$$E(\psi(\cdot,t)) = \int_{\mathbb{R}^d} \left[\frac{1}{2}|\nabla\psi|^2 + V(\mathbf{x})|\psi|^2 + \frac{\beta}{2}|\psi|^4 + \frac{\delta}{2}|\nabla|\psi|^2|^2\right] d\mathbf{x} \equiv E(\psi(\cdot,0)). \quad (2.4.6)$$

The proofs can be referred to section 5.1.

The ground state $\phi_g := \phi_g(\mathbf{x})$ of the MGPE (2.4.1) is defined as the minimizer of the energy functional (2.4.6) under the constraint (2.4.5), i.e.

$$\phi_g := \arg\min_{\phi\in S} E(\phi), \quad (2.4.7)$$

where S is defined as

$$S := \{\phi \,|\, \|\phi\|_2 = 1, \quad E(\phi) < \infty\}, \quad (2.4.8)$$

and $E_g = E(\phi_g)$ is call the ground state energy. The existence, uniqueness and nonexistence of the ground state will be shown in Chapter 3.

The ground state ϕ_g can also be characterized as a solution to the following nonlinear eigenvalue problem, i.e. Euler-Lagrange equation of the problem (2.4.7)

$$\mu\phi = \left[-\frac{1}{2}\nabla^2 + V(\mathbf{x}) + \beta|\phi|^2 - \delta\nabla^2(|\phi|^2)\right]\phi, \quad (2.4.9)$$

under the normalization constraint $\phi \in S$, where the energy and the corresponding eigenvalue (or chemical potential) $\mu := \mu(\phi)$ can be computed as

$$E(\phi) = \int_{\mathbb{R}^d} \left[\frac{1}{2}|\nabla\phi|^2 + V(\mathbf{x})|\phi|^2 + \frac{\beta}{2}|\phi|^4 + \frac{\delta}{2}\left|\nabla|\phi|^2\right|^2\right] d\mathbf{x}, \quad (2.4.10)$$

$$\mu = E(\phi) + \int_{\mathbb{R}^d} \left(\frac{\beta}{2}|\phi|^4 + \frac{\delta}{2}\left|\nabla|\phi|^2\right|^2\right) d\mathbf{x}. \quad (2.4.11)$$

Later, we will start from the d-dimensional ($d = 1, 2, 3$) MGPE (2.4.1). In Chapter 3 and Chapter 4, I will focus on the theory and computation of the ground state, respectively. In Chapter 5, the dynamics will be focused on.

Chapter 3

Mathematical Theory for Ground States

3.1 Introduction

In this chapter, we aim to build a theoretical foundation of the ground state of the modified Gross-Pitaevskii equation (MGPE) (2.4.1). For ground state, instead of considering the MGPE (2.4.1), we usually consider the time-independent nonlinear eigenvalue problem (2.4.9) via the normalized time-independent wave function $\phi(\mathbf{x})$ satisfying

$$\|\phi(\mathbf{x})\|_2 = 1, \tag{3.1.1}$$

with energy and chemical potential defined as before in (2.4.10) and (2.4.11).

The MGPE (2.4.1) has been found in many applications and the MGPE (2.4.1) with $\delta = 0$ has been thoroughly studied in literatures and we refer the readers to [10,14,93] and reference therein. However, there have been only a few mathematical results for MGPE (2.4.1), including the local well-posedness of the Cauchy problem [87,94], existence of solutions to the time independent version of (2.4.1) [81,82], the stability of standing waves [52], spectral method for (2.4.1) [85], etc. To the best of our knowledge, all the known mathematical results for the MGPE (2.4.1) are not based on the application in BEC and thus have different setups in the trapping potentials and/or parameter regimes. On the contrary, some physical studies for

the MGPE (2.4.1) have been carried out with the application in BEC, such as the ground state properties [63, 106], the dynamical instabilities [95, 96], etc. Very recently, we have studied the dimension reduction of the MGPE from 3D to lower dimensions [98].

In this Chapter, we will present our mathematical results [15] on ground states of BEC based on the MGPE (2.4.1), including the conditions for exsitence, uniqueness and nonexistence of the ground state, classifying the limiting behaviors of the ground state in different parameter regimes and prove them rigorously in mathematics.

3.2 Existence, uniqueness and nonexistence

For simplicity, we introduce the function space

$$X = \left\{ \phi \in H^1(\mathbb{R}^d) \,\middle|\, \|\phi\|_X^2 = \|\phi\|^2 + \|\nabla\phi\|^2 + \int_{\mathbb{R}^d} V(\mathbf{x})|\phi(\mathbf{x})|^2 \, d\mathbf{x} < \infty \right\}.$$

The ground state $\phi_g := \phi_g(\mathbf{x})$ of a BEC modelled by MGPE (2.4.9) is defined as the minimizer of the energy functional (2.4.10) under the constraint (3.1.1), i.e.

$$\phi_g := \arg\min_{\phi \in S} E(\phi), \tag{3.2.1}$$

where S is defined as

$$S := \{\phi \in X | \, \|\phi\| = 1, \quad E(\phi) < \infty\}. \tag{3.2.2}$$

Since S is a nonconvex set, the problem (2.4.7) is a nonconvex minimization problem.

The following embedding results hold [14].

Lemma 3.2.1. *Under the assumption that $V(\mathbf{x}) \geq 0$ for $\mathbf{x} \in \mathbb{R}^d$ is confining potentials, i.e. $\lim_{R\to\infty} \operatorname{ess\,inf}_{|\mathbf{x}|<R} V(\mathbf{x}) = \infty$, we have that the embedding $X \hookrightarrow L^p(\mathbb{R}^d)$ is compact provided that exponent p satisfies*

$$\begin{cases} p \in [2, 6), & d = 3, \\ p \in [2, \infty), & d = 2, \\ p \in [2, \infty], & d = 1. \end{cases} \tag{3.2.3}$$

In 2D, i.e. $d = 2$, let C_b be the best constant in the following inequality [112]

$$C_b := \inf_{0\neq f\in H^1(\mathbb{R}^2)} \frac{\|\nabla f\|^2_{L^2(\mathbb{R}^2)}\|f\|^2_{L^2(\mathbb{R}^2)}}{\|f\|^4_{L^4(\mathbb{R}^2)}} = \pi\cdot(1.86225\ldots). \tag{3.2.4}$$

Then for the existence and uniqueness of the ground states (2.4.7), we have

Theorem 3.2.1. *(Existence and uniqueness) Suppose $V(\mathbf{x}) \geq 0$ satisfying the confining condition, i.e. $\lim_{|\mathbf{x}|\to\infty} V(\mathbf{x}) = +\infty$, then there exists a minimizer $\phi_g \in S$ of (2.4.7) if one of the following conditions holds*

(i) $\delta > 0$ when $d = 1, 2, 3$ for all $\beta \in \mathbb{R}$;

(ii) $\delta = 0$ when $d = 1$ for all $\beta \in \mathbb{R}$, when $d = 3$ for $\beta \geq 0$, and when $d = 2$ for $\beta > -C_b$.

Furthermore, $e^{i\theta}\phi_g$ is also a ground state of (2.4.7) for any $\theta \in [0, 2\pi)$. In particular, the ground state can be chosen as positive and the positive ground state is unique if $\delta \geq 0$ and $\beta \geq 0$. In contrast, there exists no ground state of (2.4.7) if one of the following holds

(i') $\delta < 0$;

(ii') $\delta = 0$ and $\beta < 0$ when $d = 3$; and $\delta = 0$ and $\beta < -C_b$ when $d = 2$.

The results also apply to the bounded connected open domain $\Omega \subset \mathbb{R}^d$ case, i.e. $V(\mathbf{x}) = +\infty$ when $\mathbf{x} \notin \Omega$. In such case, for any $\delta > 0$, there exists $C_\Omega > 0$ (depending on Ω) such that when $\beta \geq -\delta/C_\Omega$, the positive ground state ϕ_g of (2.4.7) is unique.

Proof. The case with $\delta = 0$ is well-known [14, 80] and thus is omitted here.

(i) In order to prove the existence, we assume $\delta > 0$. By the inequality [78]

$$|\nabla|\phi(\mathbf{x})|| \leq |\nabla\phi(\mathbf{x})|, \quad \text{a.e.} \quad \mathbf{x} \in \mathbb{R}^d, \tag{3.2.5}$$

we deduce

$$E(\phi) \geq E(|\phi|), \tag{3.2.6}$$

where equality holds iff $\phi = e^{i\theta}|\phi|$ for some constant $\theta \in [0, 2\pi)$. It suffices to consider the real non-negative minimizers of (2.4.7). On the other hand, for any

$\phi \in S$ and denote $\rho = |\phi|^2$, Nash inequality and Young inequality imply that

$$\int_{\mathbb{R}^d} |\phi|^4 \, d\mathbf{x} \leq \left[C \int_{\mathbb{R}^d} \rho(\mathbf{x}) \, d\mathbf{x} \right]^{\frac{4}{d+2}} \|\nabla |\phi|^2\|^{\frac{2d}{d+2}} \leq \frac{C}{\varepsilon} + \varepsilon \|\nabla \rho\|^2, \quad \forall \varepsilon > 0.$$

Thus we can conclude that $E(\phi)$ ($\phi \in S$) is bounded from below

$$E(\phi) \geq \int_{\mathbb{R}^d} \left(\frac{1}{2} |\nabla \phi|^2 + V(\mathbf{x}) |\phi|^2 + \frac{\delta}{4} \left| \nabla |\phi|^2 \right|^2 \right) d\mathbf{x} - C.$$

Taking a nonnegative minimizing sequence $\{\phi_n\}_{n=1}^{\infty} \subset S$, we find the ϕ_n is uniformly bounded in X and there exists $\phi_\infty \in X$ and a subsequence (denote as the original sequence for simplicity) such that

$$\phi_n \hookrightarrow \phi_\infty \quad \text{in} \quad X. \tag{3.2.7}$$

Lemma 3.2.1 ensures that $\phi_n \to \phi_\infty$ in L^p with p given in the lemma. We also have $\nabla |\phi_n|^2 \hookrightarrow \nabla |\phi_\infty|^2$ in L^2. Hence we know $\phi_\infty \in S$ with ϕ_∞ being nonnegative. Under the condition $\delta > 0$, we get

$$E(\phi_\infty) \leq \liminf_{n \to \infty} E(\phi_n) = \min_{\phi \in S} E(\phi), \tag{3.2.8}$$

which shows that ϕ_∞ is a ground state.

For the case $\beta \geq 0$ and $\delta \geq 0$, we can prove the uniqueness of the nonnegative ground state. In order to do so, denote $\rho = |\phi|^2$, then for $\phi = \sqrt{\rho} \in S$, the energy is

$$E(\sqrt{\rho}) = \int_{\mathbb{R}^d} \left[\frac{1}{2} |\nabla \sqrt{\rho}|^2 + V(\mathbf{x}) \rho + \frac{\beta}{2} \rho^2 + \frac{\delta}{2} |\nabla \rho|^2 \right] d\mathbf{x}. \tag{3.2.9}$$

The sum of first three terms in the energy $E(\sqrt{\rho})$ is strictly convex in ρ [14, 80], and the last term is also convex because it is quadratic in ρ and $\delta \geq 0$. Hence, we know $E(\sqrt{\rho})$ is strictly convex in ρ and the uniqueness of the nonnegative ground state follows [14, 80]. In addition, from regularity results (see details in Theorem 3.2.2 below) and maximal principle [78, 80], we can deduce that the nonnegative ground state is strictly positive.

(ii) Secondly, we prove the nonexistence when $\delta < 0$. Choosing a non-negative smooth function $\varphi(\mathbf{x}) \in S$ with compact support and denoting $\varphi_\varepsilon(\mathbf{x}) = \varepsilon^{-d/2}\varphi(\mathbf{x}/\varepsilon) \in S$, we have

$$E(\varphi_\varepsilon) = \int_{\mathbb{R}^d} \left[\frac{1}{2\varepsilon^2}|\nabla\varphi|^2 + V(\varepsilon\mathbf{x})|\varphi|^2 + \frac{\beta}{2\varepsilon^d}|\varphi|^4 + \frac{\delta}{2\varepsilon^{2+d}}\left|\nabla|\varphi|^2\right|^2 \right] d\mathbf{x}. \quad (3.2.10)$$

From the above equation, we see that $\lim_{\varepsilon\to 0^+} E(\varphi_\varepsilon) \to -\infty$ if $\delta < 0$ and there exists no ground state.

(iii) In the case with $V(\mathbf{x}) = \infty$ for $\mathbf{x} \notin \Omega$, we know $\phi_g \in H_0^1(\Omega)$. Using Sobolev inequality, there exists $C_\Omega > 0$ such that

$$\|f\|_{L^2(\Omega)} \le C_\Omega \|\nabla f\|_{L^2(\Omega)}. \quad (3.2.11)$$

Denote $\rho = |\phi|^2$, then for $\phi = \sqrt{\rho} \in S$, and we claim the energy $E(\sqrt{\rho})$ is convex in ρ for $\beta \ge -\delta/C_\Omega$. To see this, we only need examine the case $\beta \in (-C_\Omega\delta, 0)$. For any $\sqrt{\rho_j} \in S$ with $\rho_j \in H_0^1(\Omega)$ and $\theta \in [0,1]$, we have

$$\begin{aligned}
&\theta E(\sqrt{\rho_1}) + (1-\theta)E(\sqrt{\rho_2}) - E(\sqrt{\theta\rho_1 + (1-\theta)\rho_2}) \\
&\ge \frac{1}{2}\theta(1-\theta)\left(\beta\|\rho_1-\rho_2\|^2 + \delta\|\nabla(\rho_1-\rho_2)\|^2\right) \\
&\ge \frac{1}{2}\theta(1-\theta)\left(-\delta\|\nabla(\rho_1-\rho_2)\|^2 + \delta\|\nabla(\rho_1-\rho_2)\|^2\right) = 0,
\end{aligned}$$

where we used the fact $\|\nabla\sqrt{\rho}\|^2$ is convex in ρ. This shows $E(\sqrt{\rho})$ is convex when $\beta > -\frac{\delta}{C_\Omega}$. The uniqueness follows. In the general whole space case, the energy functional $E(\sqrt{\rho})$ is no longer convex and the uniqueness when $\beta < 0$ is not clear (see recent results obtained by Guo et al. in [68] about the uniqueness when $\delta = 0$ with small $|\beta|$). □

Concerning the ground state of (2.4.7), we have the following properties.

Theorem 3.2.2. *Let $\delta > 0$ and $\phi_g \in S$ be the nonnegative ground state of (2.4.7), we have the following properties:*

(i) There exists $\alpha > 0$ and $C > 0$ such that $|\phi_g(\mathbf{x})| \le Ce^{-\alpha|\mathbf{x}|}$, $\mathbf{x} \in \mathbb{R}^d$.

(ii) If $V(\mathbf{x}) \in L^\infty_{\mathrm{loc}}(\mathbb{R}^d)$, we have ϕ_g is once continuously differentiable and $\nabla\phi_g$ is Hölder continuous with order 1. In particular, if $V(\mathbf{x}) \in C^\infty$, ϕ_g is smooth.

Proof. (i) We show the L^∞ bound of ϕ_g by a Moser's iteration and De Giorgi's iteration following [82]. From the fact that $\phi_g \in S$ minimizes the energy (2.4.10), it is easy to check that ϕ_g satisfies the Euler-Lagrange equation (2.4.9), which shows that for any test function $\varphi \in C_0^\infty(\mathbb{R}^d)$, the following holds for $\phi = \phi_g$ and $\mu = \mu(\phi_g)$

$$\int_{\mathbb{R}^d} \left[\frac{1}{2}\nabla\phi\cdot\nabla\varphi + V(\mathbf{x})\phi\varphi + 2\delta\phi\nabla\phi\cdot\nabla(\phi\varphi)\right] d\mathbf{x} = \int_{\mathbb{R}^d} \left[-\beta|\phi|^2\phi\varphi + \mu\phi\varphi\right] d\mathbf{x}. \tag{3.2.12}$$

Using the Moser and De Giorgi iterations, we will prove that any weak solution $\phi \in X \cap \{E(\phi) < \infty\}$ of (3.2.12) is bounded and decays exponentially as $|\mathbf{x}| \to \infty$. In detail, we first observe that by an approximation argument, the test function φ can be any functions in X such that $\int_{\mathbb{R}^d} |\varphi|^2|\nabla\phi|^2\, d\mathbf{x} < \infty$ and $\int_{\mathbb{R}^d} |\phi|^2|\nabla\varphi|^2\, d\mathbf{x} < \infty$.

Firstly, we show that for all $q \geq 1$, $\int_{\mathbb{R}^d}(1+\phi^{2q})|\nabla\phi|^2\, d\mathbf{x} < \infty$. Choosing $q_0 = 12$, since $\nabla\phi^2 \in L^2$ and $\phi \in H^1$, we can get that $\phi \in L^p(\mathbb{R}^d)$ for $p \in [2, q_0]$ and $d = 1, 2, 3$. Let $M > 0$ and

$$\phi_M(\mathbf{x}) = \begin{cases} M, & \phi(\mathbf{x}) > M, \\ \phi(\mathbf{x}), & |\phi(\mathbf{x})| \leq M, \\ -M, & \phi(\mathbf{x}) < -M, \end{cases} \qquad \mathbf{x} \in \mathbb{R}^d,$$

and take $\varphi = |\phi_M|^{q_0-4}\phi_M$ as the test function. Plugging $\varphi = |\phi_M|^{q_0-4}\phi_M$ into (3.2.12), we obtain

$$\begin{aligned}&(q_0-3)\int_{\mathbb{R}^d}\left(\frac{1}{2}+2\delta\phi^2\right)|\phi_M|^{q_0-4}\nabla\phi\cdot\nabla\phi_M\, d\mathbf{x} + 2\delta\int_{\mathbb{R}^d}\phi\phi_M|\phi_M|^{q_0-4}|\nabla\phi|^2\, d\mathbf{x}\\ &+\int_{\mathbb{R}^d} V(\mathbf{x})\phi\phi_M|\phi_M|^{q_0-4}\, d\mathbf{x} = \int_{\mathbb{R}^d}\left(-\beta|\phi|^2\phi+\mu\phi\right)|\phi_M|^{q_0-4}\phi_M\, d\mathbf{x}.\end{aligned}$$

Letting $M \to \infty$, we get

$$2(q_0-2)\delta\int_{\mathbb{R}^d}|\phi|^{2\tilde{q}}|\nabla\phi|^2\, d\mathbf{x} + \int_{\mathbb{R}^d} V(\mathbf{x})|\phi|^{2\tilde{q}}\, d\mathbf{x} \leq \int_{\mathbb{R}^d}\left(|\beta||\phi|^{q_0} + |\mu||\phi|^{q_0-2}\right) d\mathbf{x}, \tag{3.2.13}$$

which shows $\int_{\mathbb{R}^d}|\phi|^{\tilde{q}}|\nabla\phi|^2\, d\mathbf{x} < \infty$ with $\tilde{q} = \frac{q_0}{2} - 1$. So $\nabla\phi^{\tilde{q}+1} \in L^2$ and for $q_1 = 6\tilde{q} = 3q_0 = 36$, $\phi \in L^p(\mathbb{R}^d)$ for $p \in [2, q_1]$ and $d = 1, 2, 3$. Then, the Moser iteration

can continue with $q_j = 3^j q_0$, and $\phi \in L^{q_j}(\mathbb{R}^d)$ (it is obvious when $d = 1, 2$) which verifies our claim. In particular $\phi \in L^p$ for any $p \in [2, \infty)$.

Secondly, we show that $\phi \in L^\infty(\mathbb{R}^d)$ and $\lim_{|\mathbf{x}|\to\infty} \phi(\mathbf{x}) = 0$ by De Giorgi's iteration. Denoting $f = -\beta|\phi|^2\phi + \mu\phi$ and choosing the test function $\varphi(\mathbf{x}) = (\xi(\mathbf{x}))^2(\phi(\mathbf{x}) - k)_+$ with $k \geq 0$ in (3.2.12), where $(g(\mathbf{x}))_+ = \max\{g(\mathbf{x}), 0\}$ and $\xi(\mathbf{x})$ is a smooth cutoff function, we have

$$\begin{aligned}
&\int_{\mathbb{R}^d} \left[\left(\frac{1}{2} + 2\delta\phi^2 + 2\delta\phi(\phi - k)_+ \right) |\xi|^2 |\nabla(\phi - k)_+|^2 + V(\mathbf{x})|\xi|^2\phi(\phi - k)_+ \right] d\mathbf{x} \\
&= \int_{\mathbb{R}^d} \left[-(1 + 4\delta\phi^2)(\phi - k)_+ \xi \nabla(\phi - k)_+ \cdot \nabla\xi + f\xi^2(\phi - k)_+ \right] d\mathbf{x}.
\end{aligned}$$

Cauchy inequality gives that

$$\begin{aligned}
&\int_{\mathbb{R}^d} -(1 + 4\delta\phi^2)(\phi - k)_+ \xi \nabla(\phi - k)_+ \cdot \nabla\xi \, d\mathbf{x} \\
&\leq \varepsilon \int_{\mathbb{R}^d} (1 + \phi^2)|\nabla(\phi - k)_+|^2 \, d\mathbf{x} + C_\varepsilon \int_{\mathbb{R}^d} (1 + \phi^2)|\nabla\xi|^2(\phi - k)_+^2 \, d\mathbf{x}.
\end{aligned}$$

Now choosing sufficiently small $\varepsilon > 0$ and defining the function $\Phi_k(\mathbf{x}) = (1+\phi)(\phi - k)_+$, we can get

$$\int_{\mathbb{R}^d} |\nabla\Phi_k|^2|\xi|^2 \, d\mathbf{x} \leq C \int_{\mathbb{R}^d} |\nabla\xi|^2\Phi_k^2 \, d\mathbf{x} + C \int_{\mathbb{R}^d} |f|(\phi - k)_+\xi^2 \, d\mathbf{x}, \tag{3.2.14}$$

and

$$\int_{\mathbb{R}^d} |\nabla(\xi\Phi_k)|^2 \, d\mathbf{x} \leq C \int_{\mathbb{R}^d} |\nabla\xi|^2\Phi_k^2 \, d\mathbf{x} + C \int_{\mathbb{R}^d} |f|(\phi - k)_+\xi^2 \, d\mathbf{x}. \tag{3.2.15}$$

Since $f = -\beta|\phi|^2\phi + \mu\phi \in L^q(\mathbb{R}^d)$ for any $2 \leq q < \infty$, we can proceed to obtain L^∞ bound of ϕ by De Giorgi's iteration. Let $B_r(\mathbf{x})$ be the ball centered at $\mathbf{x}$ with radius $r > 0$, and we use B_r for short to denote the ball centered at the origin. For $0 < r < R \leq 1$, we choose C_0^∞ nonnegative cutoff function $\xi(\mathbf{x}) = 1$ for $\mathbf{x} \in B_r(\mathbf{x}_0)$ and $\xi(\mathbf{x}) = 0$ for $\mathbf{x} \notin B_R(\mathbf{x}_0)$ such that $|\nabla\xi(\mathbf{x})| \leq \frac{2}{R-r}$. Since for large q,

$$\int_{\mathbb{R}^d} |f|(\phi - k)_+\xi^2 \, d\mathbf{x} \leq \|\xi f\|_{L^q} \|(\phi - k)_+\xi\|_{L^6} |\{\Phi_k\xi > 0\}|^{\frac{5}{6} - \frac{1}{q}}, \tag{3.2.16}$$

where $|A|$ denotes the Lebesgue measure of the set A, for any $\varepsilon > 0$, we have by

Hölder inequality and Sobolev inequality in 2D and 3D

$$\begin{aligned}
&\int_{\mathbb{R}^d} |f|(\phi-k)_+\xi^2\,d\mathbf{x}\\
&\le C\|\xi f\|_{L^q}\|\nabla((\phi-k)_+\xi)\||\{\Phi_k\xi>0\}|^{\frac{5}{6}-\frac{1}{q}}\\
&\le \varepsilon\|\nabla((\phi-k)_+\xi)\|^2 + C_\varepsilon\|\xi f\|^2_{L^q}|\{\Phi_k\xi>0\}|^{\frac{5}{3}-\frac{2}{q}}\\
&\le 4\varepsilon(\|\nabla(\Phi_k\xi)\|^2 + 2\|\Phi_k\nabla\xi\|^2) + C_\varepsilon\|\xi f\|^2_{L^q}|\{\Phi_k\xi>0\}|^{\frac{5}{3}-\frac{2}{q}}.
\end{aligned}$$

Thus, from the above inequality and (3.2.15), we arrive at

$$\|\nabla(\xi\Phi_k)\|^2 \le C\left(\|\Phi_k\nabla\xi\|^2 + \|\xi f\|^2_{L^q}|\{\Phi_k\xi>0\}|^{\frac{5}{3}-\frac{2}{q}}\right). \tag{3.2.17}$$

Since $\xi\Phi_k \in H^1_0(B_1(\mathbf{x}_0))$, we conclude by Sobolev inequality that,

$$\|\xi\Phi_k\|^2 \le \|\xi\Phi_k\|^2_{L^6}|\{\Phi_k\xi>0\}|^{1-\frac{2}{6}} \le C(d)\|\nabla(\xi\Phi_k)\|^2|\{\Phi_k\xi>0\}|^{\frac{2}{3}}. \tag{3.2.18}$$

By choosing $q=3$, (3.2.17) and (3.2.18) imply that

$$\|\xi\Phi_k\|^2 \le C\left(\|\Phi_k\nabla\xi\|^2|\{\Phi_k\xi>0\}|^{\frac{2}{3}} + \|f\|^2_{L^3(B_1(\mathbf{x}_0))}|\{\Phi_k\xi>0\}|^{\frac{5}{3}}\right). \tag{3.2.19}$$

Denote

$$A(k,r) = \{\mathbf{x}|\mathbf{x}\in B_r(\mathbf{x}_0), \quad \phi(\mathbf{x})>k\}. \tag{3.2.20}$$

For $k>0$ and $0<r<R\le 1$, we have

$$\int_{A(k,r)}\Phi_k^2 d\mathbf{x} \le C\left[\frac{|A(k,R)|^{\frac{2}{3}}}{(R-r)^2}\int_{A(k,R)}\Phi_k^2 d\mathbf{x} + |A(k,R)|^{\frac{5}{3}}\|f\|^2_{L^3(B_1(\mathbf{x}_0))}\right]. \tag{3.2.21}$$

We claim that there exists $\tilde{C}>0$, such that for $k=\tilde{C}\Big[\|f\|_{L^3(B_1(\mathbf{x}_0))} + \|(1+\phi)\phi\|_{L^2(B_1(\mathbf{x}_0))}\Big]$,

$$\int_{A(k,\frac{1}{2})}\Phi_k^2\,d\mathbf{x} = 0. \tag{3.2.22}$$

Taking $h>k>k_0$ and $0<r<1$, we find $A(h,r)\subset A(k,r)$ with

$$\int_{A(h,r)}\Phi_h^2\,d\mathbf{x} \le \int_{A(k,r)}\Phi_k^2\,d\mathbf{x}. \tag{3.2.23}$$

In addition, since $\Phi_k = (1+\phi)(\phi-k)_+$, we have

$$|A(h,r)| = |B_r(\mathbf{x}_0) \cap \{\phi - k \geq h - k\}| \leq \frac{1}{(h-k)^2} \int_{A(k,r)} \Phi_k^2 \, d\mathbf{x}. \tag{3.2.24}$$

Choosing $\frac{1}{2} \leq r < R \leq 1$, from (3.2.21), we get

$$\begin{aligned}
&\int_{A(h,r)} \Phi_h^2 \, d\mathbf{x} \\
&\leq C \left(\frac{1}{(R-r)^2} \int_{A(h,R)} \Phi_h^2 \, d\mathbf{x} + \|f\|^2_{L^3(B_1(\mathbf{x}_0))} |A(h,R)| \right) |A(h,R)|^{\frac{2}{3}} \\
&\leq \frac{C}{(h-k)^{\frac{4}{3}}} \left(\frac{1}{(R-r)^2} + \frac{\|f\|^2_{L^3(B_1(\mathbf{x}_0))}}{(h-k)^2} \right) \left(\int_{A(k,R)} \Phi_k^2 \, d\mathbf{x} \right)^{\frac{5}{3}},
\end{aligned}$$

and

$$\|\Phi_h\|_{L^2(B_r(\mathbf{x}_0))} \leq \frac{C}{(h-k)^{\frac{2}{3}}} \left(\frac{1}{R-r} + \frac{\|f\|_{L^3(B_1(\mathbf{x}_0))}}{h-k} \right) \|\Phi_k\|^{\frac{5}{3}}_{L^2(B_R(\mathbf{x}_0))}. \tag{3.2.25}$$

Denote the function

$$\chi(k,r) = \|\Phi_k\|_{L^2(B_r(\mathbf{x}_0))}. \tag{3.2.26}$$

For some value of $k > 0$ to be determined later, we define

$$k_l = \left(1 - \frac{1}{2^l}\right) k, \quad r_l = \frac{1}{2} + \frac{1}{2^{l+1}}, \qquad l = 0, 1, 2, \ldots, \tag{3.2.27}$$

then $k_l - k_{l-1} = \frac{k}{2^l}$ and $r_{l-1} - r_l = \frac{1}{2^{l+1}}$. From (3.2.25), we find

$$\begin{aligned}
\chi(k_l, r_l) \leq & C \left(2^{l+1} + \frac{2^l \|f\|_{L^3(B_1(\mathbf{x}_0))}}{k} \right) \frac{2^{\frac{2l}{3}}}{k^{\frac{2}{3}}} (\chi(k_{l-1}, r_{l-1}))^{\frac{5}{3}} \\
\leq & 2C \frac{\|f\|_{L^3(B_1(\mathbf{x}_0))} + k}{k^{\frac{5}{3}}} 2^{\frac{5l}{3}} (\chi(k_{l-1}, r_{l-1}))^{\frac{5}{3}}.
\end{aligned}$$

Then, we prove that there exists $\gamma > 1$ such that

$$\chi(k_l, r_l) \leq \frac{\chi(k_0, r_0)}{\gamma^l}, \quad l = 0, 1, 2, \ldots \tag{3.2.28}$$

We will argue by induction. When $l = 0$, it is obvious true. Suppose (3.2.28) is true for $l-1$ with $l \geq 1$, i.e.

$$\chi(k_{l-1}, r_{l-1}) \leq \frac{\chi(k_0, r_0)}{\gamma^{l-1}} \Rightarrow (\chi(k_{l-1}, r_{l-1}))^{\frac{5}{3}} \leq \frac{\gamma^{\frac{5}{3}} (\chi(k_0, r_0))^{\frac{2}{3}}}{\gamma^{\frac{2l}{3}}} \cdot \frac{\chi(k_0, r_0)}{\gamma^l}.$$

Then, we have

$$\begin{aligned}\chi(k_l, r_l) \leq & 2C\frac{\|f\|_{L^3(B_1(\mathbf{x}_0))}+k}{k^{\frac{5}{3}}}2^{\frac{5l}{3}}(\chi(k_l,r_l))^{\frac{5}{3}}\\ \leq & 2C\gamma^{\frac{5}{3}}(\chi(k_0,r_0))^{\frac{2}{3}}\frac{\|f\|_{L^3(B_1(\mathbf{x}_0))}+k}{k^{\frac{5}{3}}}\cdot\frac{2^{\frac{5l}{3}}}{\gamma^{\frac{2l}{3}}}\cdot\frac{\chi(k_0,r_0)}{\gamma^l}.\end{aligned}$$

Let us choose $\gamma > 1$ such that $\gamma^{\frac{2}{3}} = 2^{\frac{5}{3}}$. Now we want to pick k sufficiently large such that

$$2C\gamma^{\frac{5}{3}}\frac{\|f\|_{L^3(B_1(\mathbf{x}_0))}+k}{k}\left(\frac{\chi(k_0,r_0)}{k}\right)^{\frac{2}{3}} \leq 1. \tag{3.2.29}$$

Choosing $k = \tilde{C}(\|f\|_{L^3(B_1(\mathbf{x}_0))} + \chi(k_0, r_0))$ for sufficiently large $\tilde{C}$, we get the desired inequality (3.2.29). This gives that (3.2.28) is true for l and hence the induction is done. Letting $l \to \infty$ in (3.2.28), we find $\chi(k, \frac{1}{2}) = 0$, which implies that

$$\Phi_k(\mathbf{x}) = 0, \quad \forall \mathbf{x} \in B_{\frac{1}{2}}(\mathbf{x}_0), \tag{3.2.30}$$

i.e.,

$$\begin{aligned}\sup_{B_{\frac{1}{2}}(\mathbf{x}_0)}\phi_+ \leq & \tilde{C}\left[\|f\|_{L^3(B_1(\mathbf{x}_0))}+\chi(k_0,r_0)\right]\\ \leq & \tilde{C}\left[\|f\|_{L^3(B_1(\mathbf{x}_0))}+\|\Phi_0\|_{L^2(B_1(\mathbf{x}_0))}\right]\\ \leq & \tilde{C}\left[\|f\|_{L^3(B_1(\mathbf{x}_0))}+\|\phi\|_{L^2(B_1(\mathbf{x}_0))}+\|\phi\|_{L^4(B_1(\mathbf{x}_0))}\right].\end{aligned}$$

The same estimates applies for $-\phi$ and we can conclude that

$$\|\phi\|_{L^\infty(B_{\frac{1}{2}}(\mathbf{x}_0))} \leq \tilde{C}\left[\|f\|_{L^3(B_1(\mathbf{x}_0))}+\|\phi\|_{L^2(B_1(\mathbf{x}_0))}+\|\phi\|_{L^4(B_1(\mathbf{x}_0))}\right].$$

This shows ϕ is bounded and $\lim_{|\mathbf{x}|\to 0}\phi(\mathbf{x}) = 0$.

Thirdly, we prove that $\int_{\mathbb{R}^d\setminus B_R}(|\nabla\phi|^2 + |\phi|^2)\,d\mathbf{x}$ decays exponentially as $R \to \infty$. Choose the test function $\varphi = \eta^2(\mathbf{x})\phi$ in (3.2.12) with $\eta(\mathbf{x})$ being a smooth nonnegative cutoff function such that $\eta(\mathbf{x}) = 0$ for $\mathbf{x} \in B_R$ and $\eta(\mathbf{x}) = 1$ for $\mathbf{x} \in \mathbb{R}^d\setminus B_{R+1}$, then the following holds

$$\begin{aligned}&\int_{\mathbb{R}^d\setminus B_R}\left[\left(\frac{1}{2}+4\delta\phi^2\right)|\nabla\phi|^2\eta^2 + V(\mathbf{x})|\phi|^2\eta^2 + \beta\phi^4\eta^2 - \mu\phi^2\eta^2\right]d\mathbf{x}\\ &= -\int_{B_{R+1}\setminus B_R}\left(1+4\delta\phi^2\right)\eta\phi\nabla\phi\cdot\nabla\eta\,d\mathbf{x}.\end{aligned}$$

Since $\lim_{|\mathbf{x}|\to\infty} V(\mathbf{x}) = \infty$ and ϕ is bounded, we find that for large R,

$$\int_{\mathbb{R}^d\setminus B_R} (|\phi|^2 + |\nabla\phi|^2)\, d\mathbf{x} \le C \int_{B_{R+1}\setminus B_R} (|\phi|^2 + |\nabla\phi|^2)\, d\mathbf{x}. \tag{3.2.31}$$

Let $a_n = \int_{\mathbb{R}^d\setminus B_{R_n}} (|\phi|^2 + |\nabla\phi|^2)\, d\mathbf{x}$ with $R_n = R + n$ $(n = 0, 1, 2, \ldots)$, then $a_n \le C(a_{n+1-a_n})$ and $a_{n+1} \le \alpha a_n$ with $\alpha = \frac{C}{1+C}$. Hence $a_{n+1} \le \alpha^n a_0$ which would imply the exponential decay of a_n as well as $\int_{\mathbb{R}^d\setminus B_R} (|\nabla\phi|^2 + |\phi|^2)\, d\mathbf{x}$.

Lastly, combining the exponential decay of $\int_{\mathbb{R}^d\setminus B_R} (|\nabla\phi|^2+|\phi|^2)\, d\mathbf{x}$ and De Giorgi's iteration shown above, we can derive the exponential fall-off of $\phi(\mathbf{x})$.

(ii) The regularity of the ground state ϕ_g can be proved by a change of variable method [52, 81]. Let $v = F(t)$ be the solution to the ODE $F'(t) = \sqrt{\frac{1}{2} + \frac{\delta}{2}t^2}$ with $F(0) = 0$, then $F(t)$ is strictly increasing, and its inverse exists (denoted as $t = G(v)$). Let $u = F(\phi)$, then $\phi = G(u)$ and the energy functional $E(\cdot)$ in (2.4.10) becomes

$$E(\phi) = \int_{\mathbb{R}^d} \left(|\nabla u|^2 + V(\mathbf{x})G^2(u) + \frac{\beta}{2}G^4(u) \right) d\mathbf{x} := \hat{E}(u). \tag{3.2.32}$$

$u_g = F(\phi_g)$ is the minimizer of $\hat{E}(u)$ under constraint $\int_{\mathbb{R}^d} G(u)^2\, d\mathbf{x} = 1$. It follows that u_g satisfies the following Euler-Lagrange equation (for C_0^∞ test function)

$$-\nabla^2 u + V(\mathbf{x})G(u)G'(u) + \beta|G(u)|^2 G(u)G'(u) = \lambda G(u)G'(u). \tag{3.2.33}$$

Since ϕ_g is bounded, we know u_g is bounded, hence $G(u_g)$ and $G'(u_g)$ are bounded with $\nabla^2 u_g \in L^\infty_{\text{loc}}$. We conclude that u_g is once continuously differentiable and ∇u_g is Hölder continuous with exponent 1. Noticing that $\nabla^2\phi_g = G'(u_g)\nabla^2 u_g + G''(u_g)|\nabla u_g|^2$, we find that ϕ_g is once continuously differentiable and $\nabla\phi_g$ is Hölder continuous with exponent 1. In addition, if $V \in C^\infty$, we can obtain $\phi_g \in C^\infty$ by a bootstrap argument using the L^∞ bound of ϕ_g. □

3.3 Approximations under a harmonic potential

3.3.1 Approximation in weak interaction regime

In this section, we consider the general harmonic potential (2.4.2) with parameters in the weak interaction regime, i.e. $|\beta| \ll 1, 0 \leq \delta \ll 1$.

We start with the linear case when $\beta = 0$ and $\delta = 0$, i.e. the interaction between particle is neglected. In this scenario, all the eigenfunctions can be obtained via the Hermite functions [25, 26]. Thus the ground state $\phi_g^0(\mathbf{x})$ can be given explicitly as [25, 26]

$$\phi_g^0(\mathbf{x}) = \prod_{j=1}^{d} \left(\frac{\gamma_j}{\pi}\right)^{\frac{1}{4}} e^{-\frac{\gamma_j x_j^2}{2}}. \tag{3.3.1}$$

When $|\beta| \ll 1, 0 \leq \delta \ll 1$, i.e. weakly repulsive interaction regime, we can approximate the ground state $\phi_g(\mathbf{x})$ by $\phi_g^0(\mathbf{x})$. Thus we have

Lemma 3.3.1. *In the weakly repulsive interaction regime, i.e. $|\beta| \ll 1, 0 \leq \delta \ll 1$, we have*

$$\phi_g(\mathbf{x}) \approx \prod_{j=1}^{d} \left(\frac{\gamma_j}{\pi}\right)^{\frac{1}{4}} e^{-\frac{\gamma_j x_j^2}{2}}, \tag{3.3.2}$$

In addition, the energy and chemical potential of the ground and first excited states can be approximated as

$$E_g(\beta, \delta) = B_1 + \frac{B_0}{2}\beta + B_0 B_1 \delta + o(\beta + \delta), \tag{3.3.3}$$

$$\mu_g(\beta, \delta) = B_1 + B_0\beta + 2B_0 B_1 \delta + o(\beta + \delta), \tag{3.3.4}$$

where

$$B_0 = \prod_{j=1}^{d} \sqrt{\frac{\gamma_j}{2\pi}}, \qquad B_1 = \frac{1}{2}\sum_{j=1}^{d} \gamma_j. \tag{3.3.5}$$

The proof is just computation and is omitted here for brevity.

3.3.2 Thomas-Fermi approximation

In this section, we take $V(\mathbf{x})$ to be a radially symmetric harmonic potential as

$$V(\mathbf{x}) = \frac{1}{2}\gamma_0^2 r^2, \qquad r = |\mathbf{x}|, \tag{3.3.6}$$

where $\gamma_0 > 0$ is a dimensionless constant. Analogous to the conventional BEC case, a dominant repulsive contact interaction will lead to an analytical Thomas-Fermi (TF) densities. However, with HOI (2.4.1), the system is characterized by two interactions, contact interaction strength β and HOI strength δ, which is totally different from the classical GPE theory where the BEC is purely characterized by the contact interaction β. Hence, for BEC with HOI (2.4.1), it is possible that HOI interaction competes with contact interaction, and may be the major effect determining the properties of BEC. In this section, we will discuss how the competition between β and δ leads to different density profiles for the strong interactions ($|\beta|, \delta \gg 1$), for which we refer such analytical density approximations as the TF approximations [80].

For the general consideration of the large β and δ interactions, we show in Fig. 3.1 the phase diagram of the different parameter regimes for β and δ, in which the TF approximation are totally different. Intuitively, there are three of them: β term is more important (regime I in Fig. 3.1), δ term is more important (regime III), and β term is comparable to the δ term (regimes II & IV). The boundary lines for the regimes shown in Fig. 3.1 can be understood mathematically in the following way. In d ($d = 3, 2, 1$) dimensions, introduce $\tilde{\mathbf{x}} = \frac{\mathbf{x}}{x_s}$, and $\tilde{\psi}(\tilde{\mathbf{x}}) = x_s^{d/2}\psi(\mathbf{x})$ such that x_s is the Thomas-Fermi radius of the wave function and then the Thomas-Fermi radius in the new scaling is $O(1)$. It's easy to check that such scaling conserves the normalization condition Eq. (3.1.1). Substituting $\tilde{\mathbf{x}}$ and $\tilde{\psi}$ into the time-independent version of (2.4.9) and then removing all $\tilde{}$, we get

$$\frac{\mu}{x_s^2}\psi = -\frac{1}{2x_s^4}\nabla^2\psi + \frac{\gamma_0^2|\mathbf{x}|^2}{2}\psi + \frac{\beta}{x_s^{2+d}}\psi^3 - \frac{\delta}{x_s^{4+d}}\nabla^2(|\psi|^2)\psi.$$

x_s is the length scale and the potential term is $O(1)$. To balance the confinement with repulsive interactions, we need $\frac{\beta}{x_s^{2+d}} \sim O(1)$ and/or $\frac{\delta}{x_s^{4+d}} \sim O(1)$. For simplicity,

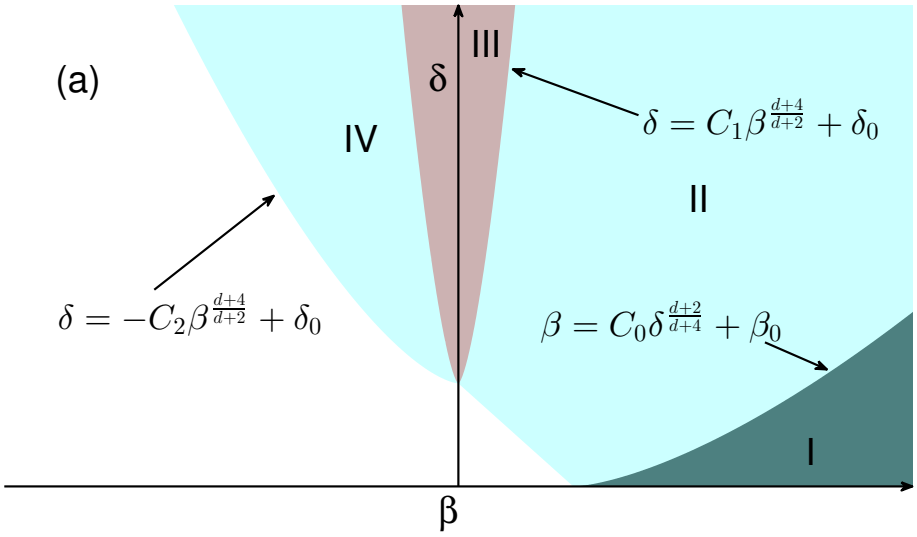

Figure 3.1: Phase diagram for extreme regimes under a harmonic potential. In the figure, we choose $\beta_0 \gg 1$ and $\delta_0 \gg 1$, and C_0, C_1 and C_2 positive constants.

we require $\frac{\delta}{x_s^{4+d}} = 1$, then $x_s = \delta^{\frac{1}{4+d}}$, and further $\beta \sim O(x_s^{2+d}) \sim O(\delta^{\frac{2+d}{4+d}})$. So the borderline case is $\beta = C_0\delta^{\frac{2+d}{4+d}}$. If $C_0 \gg 1$, β term is much more significant than the δ term; if $|C_0| \ll 1$, δ term is much more significant than the β term.

From Fig. 3.1(a), the curve $\beta = O(\delta^{\frac{d+2}{d+4}})$ divides the regimes for harmonic potential case to four parts, as shown in the figure labelled by I, II, III and IV. We'll write out the approximate ground states, i.e. Thomas-Feimi(TF) approximations, and their corresponding energies and chemical potentials explicitly and separately according to the division. The resulting analytical TF density profiles in different regimes, are listed below:

Regime I, i.e. $\beta \gg \delta^{\frac{d+2}{d+4}}$, the δ term and the kinetic energy term are dropped, and the density profile is determined as

$$n_{\mathrm{TF}}(r) = |\psi_{\mathrm{TF}}|^2 = \frac{\gamma_0^2(R^2 - r^2)_+}{2\beta}, \tag{3.3.7}$$

where $R = \left(\frac{(d+2)\tilde{C}_d\beta}{\gamma_0^2}\right)^{\frac{1}{d+2}}$, and the constant $\tilde{C}_d$ is defined as

$$\tilde{C}_d = \begin{cases} \frac{1}{2}, & d = 1, \\ \frac{1}{\pi}, & d = 2, \\ \frac{3}{4\pi}, & d = 3. \end{cases} \tag{3.3.8}$$

With the above TF densities, the leading order approximations for chemical potential μ and energy E of the ground state are: $\mu_{\rm TF} = \frac{1}{2}\left((d+2)\tilde{C}_d\beta\right)^{\frac{2}{d+2}}\gamma_0^{\frac{2d}{d+2}}$, $E_{\rm TF} = \frac{d+2}{d+4}\mu_{\rm TF}$ for d $(d = 3, 2, 1)$ dimensional case.

Regime II, i.e. $\beta = C_0\delta^{\frac{d+2}{d+4}}$ with $C_0 > 0$, neglecting the kinetic term in the time-independent MGPE, we have

$$\mu\psi = \frac{\gamma_0^2|\mathbf{x}|^2}{2}\psi + C_0\delta^{\frac{d+2}{d+4}}|\psi|^2\psi - \delta\nabla^2(|\psi|^2)\psi. \tag{3.3.9}$$

Formally, Eq. (3.3.9) degenerates at position $\mathbf{x}$ if $\psi(\mathbf{x}) = 0$ and it is indeed a free boundary problem (boundary of the zero level set of ψ), which requires careful consideration. Motivated by [106] for the 3D case, we impose $n'(R) = 0$ besides the condition that $n(R) = 0$ along the free boundary $|\mathbf{x}| = R$, and we assume $n(r) = 0$ for $r > R$.

The TF density profile in regime II is self similar under appropriate scalings. To be more specific, the analytical TF density takes the form

$$n_{\rm TF}(r) = |\psi_{\rm TF}|^2 = \delta^{-\frac{d}{d+4}}n_0(\delta^{-\frac{1}{d+4}}r), \tag{3.3.10}$$

where $n_0(r)$ is a function that can be calculated exactly as below.

Plugging (3.3.10) into (3.3.9), we obtain the equation for $n_0(r)$ by imposing the aforementioned conditions at the free boundary,

$$\tilde{\mu} = \frac{\gamma_0^2 r^2}{2} + C_0 n_0 - \partial_{rr}n_0(r) - \frac{d-1}{r}\partial_r n_0(r), \tag{3.3.11}$$

for $r \le R$ and $n_0(s) = 0$ for $s \ge R$, and $n_0(R) = 0$, $n_0'(R) = 0$, where R is the free boundary that has to be determined and $\tilde{\mu} = \delta^{-\frac{2}{d+4}}\mu$. In addition, we assign the boundary condition at $r = 0$ as $n_0'(0) = 0$, because of the symmetry.

Note that C_0 can be negative as δ term can bound the negative cubic interaction, which corresponds to Regime IV. In fact for Regime IV, we will repeat the above procedure.

Denote $a = \sqrt{C_0}$ and the ordinary differential equation (3.3.11) in d dimensions can be solved analytically. Denote

$$f_{a,d}(r) = \begin{cases} e^{ar} + e^{-ar}, & \text{for } d = 1, \\ I_0(ar), & \text{for } d = 2, \\ (e^{ar} - e^{-ar})/r, & \text{for } d = 3, \end{cases} \tag{3.3.12}$$

where $I_0(r)$ is the standard modified Bessel function I_α with $\alpha = 0$. Then the solution of Eq. (3.3.11) with prescribed Neumann boundary conditions reads as

$$n_0(r) = -\frac{\gamma_0^2 r^2}{2a^2} + \left(\frac{\tilde{\mu}}{a^2} - \frac{d\gamma_0^2}{a^4}\right) + \frac{\gamma_0^2 R}{a^2 f'_{a,d}(R)} f_{a,d}(r). \tag{3.3.13}$$

Inserting the above expression to the normalization condition that $\int_{\mathbb{R}^d} n_0(\mathbf{x})\, d\mathbf{x} = 1$, we find chemical potential,

$$\tilde{\mu} = \frac{\tilde{C}_d a^2}{R^d} + \frac{d\gamma_0^2 R^2}{2(d+2)}. \tag{3.3.14}$$

Combining (3.3.14) and (3.3.13), noticing the Dirichlet condition $n(R) = 0$, we have the equation for R,

$$\left(\frac{(aR)^2}{d+2} - \frac{\tilde{C}_d a^4}{\gamma_0^2 R^d} + d\right) f'_{a,d}(R) = a^2 R f_{a,d}(R). \tag{3.3.15}$$

Thus, the free boundary R can be calculated and $n_0(r)$ is then determined.

Regime III, i.e. $\beta \ll \delta^{\frac{d+2}{d+4}}$, the β term and the kinetic energy term are dropped, and the TF density profile is

$$n_{\mathrm{TF}}(r) = |\psi_{\mathrm{TF}}|^2 = \frac{\gamma_0^2 (R^2 - r^2)_+^2}{8(d+2)\delta}, \tag{3.3.16}$$

where $R = \left(\frac{(d+2)^2(d+4)\tilde{C}_d\delta}{\gamma_0^2}\right)^{\frac{1}{d+4}}$. Again, the leading order approximations for chemical potential and energy, with the above TF densities, are

$$\mu_{\mathrm{TF}} = \frac{d}{2(d+2)} \left((d+2)^2(d+4)\tilde{C}_d\delta\gamma_0^{d+2}\right)^{\frac{2}{d+4}}, \quad E_{\mathrm{TF}} = \frac{d+4}{d+6}\mu_{\mathrm{TF}} \tag{3.3.17}$$

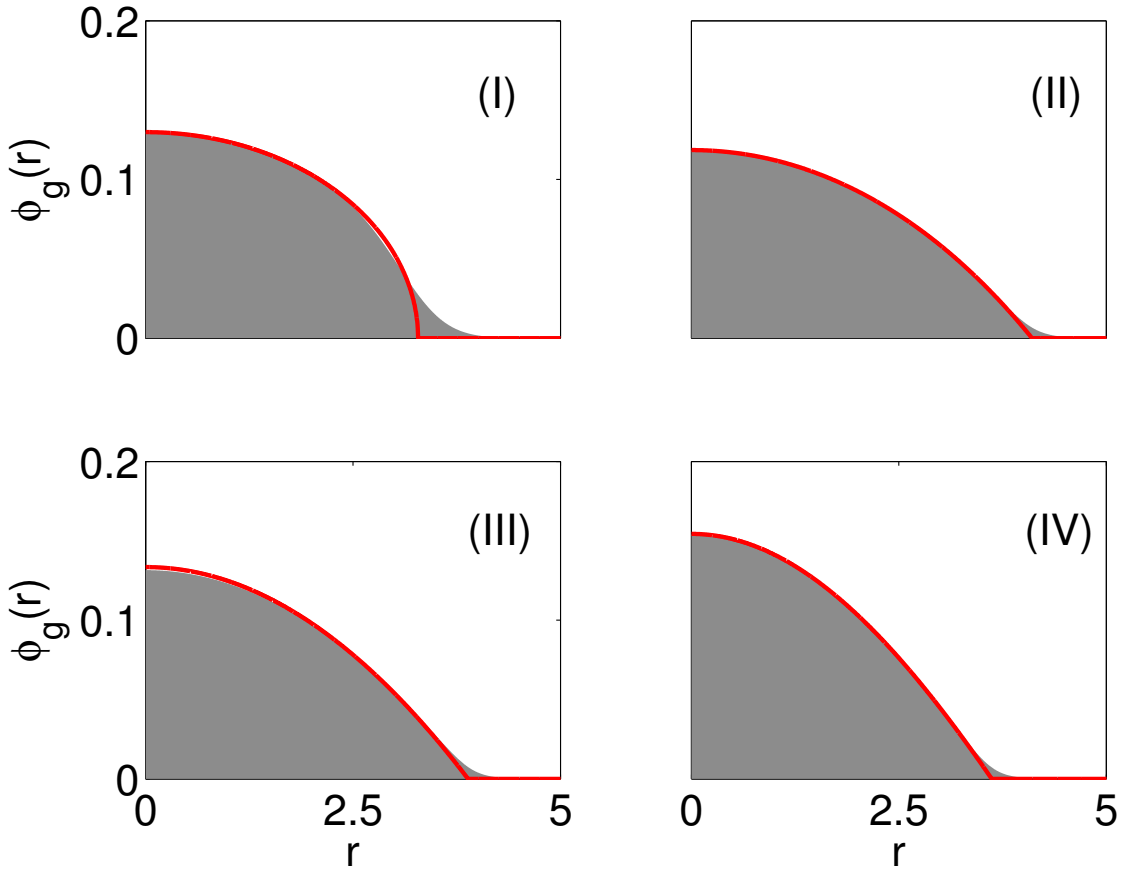

Figure 3.2: Comparisons of 3D numerical ground states with TF densities, the harmonic potential case in region I, II, III and IV, which are define in Fig. 3.1(a). Red line: Thomas-Fermi approximation, and shaded area: numerical solution from the equation (2.4.1). The parameters are chosen to be $\gamma = 2$ and (I) $\beta = 1280$, $\delta = 1$; (II) $\beta = 828.7$, $\delta = 1280$; (III) $\beta = 1$, $\delta = 1280$; (IV) $\beta = -828.7$, $\delta = 1280$; respectively.

in d dimensions.

Regime IV, i.e. $\beta = -C_0\delta^{\frac{d+2}{d+4}}$ with $C_0 > 0$. By a similar procedure as for Regime II, we can get (3.3.10) and

$$\tilde{\mu} = \frac{\gamma_0^2 r^2}{2} - C_0 n_0 - \partial_{rr} n_0(r) - \frac{d-1}{r}\partial_r n_0(r), \tag{3.3.18}$$

for $r \leq R$ and $n_0(s) = 0$ for $s \geq R$, and $n_0'(0) = 0$, $n_0(R) = 0$, $n_0'(R) = 0$, where R is the free boundary that has to be determined and $\tilde{\mu} = \delta^{-\frac{2}{d+4}}\mu$. Again, let $a = \sqrt{C_0}$ and denote

$$g_{a,d}(r) = \begin{cases} \cos(ar), & \text{for } d = 1, \\ J_0(ar), & \text{for } d = 2, \\ \sin(ar)/r, & \text{for } d = 3, \end{cases} \tag{3.3.19}$$

where $J_0(r)$ is the Bessel function of the first kind $J_\alpha(r)$ with $\alpha = 0$. The solution of Eq. (3.3.18) with the assigned Neumann boundary conditions can be written as:

$$n_0(r) = \frac{\gamma_0^2 r^2}{2a^2} - \left(\frac{\tilde{\mu}}{a^2} + \frac{d\gamma_0^2}{a^4}\right) - \frac{\gamma_0^2 R}{a^2 g_{a,d}'(R)} g_{a,d}(r). \tag{3.3.20}$$

The chemical potential is then calculated from normalization condition as

$$\tilde{\mu} = -\frac{\tilde{C}_d a^2}{R^d} + \frac{d\gamma_0^2 R^2}{2(d+2)}. \tag{3.3.21}$$

Finally, the free boundary R is determined from the Dirichlet condition $n_0(R) = 0$,

$$\left(\frac{a^2 R^2}{d+2} + \frac{\tilde{C}_d a^4}{\gamma_0^2 R^d} - d\right) g_{a,d}'(R) = a^2 R g_{a,d}(R). \tag{3.3.22}$$

After R is computed, we then find $n_0(r)$.

In Fig. 3.2, we compare the analytical TF densities (3.3.7), (3.3.16) and (3.3.10) with the numerical results computed via full equation (2.4.1) by the backward Euler finite difference (BEFD) method [18]. We observe that in all the extreme regions, the analytical TF densities agree very well with the full equation simulations. As a byproduct, we compare the corresponding chemical potentials and energies in Fig. 3.3.

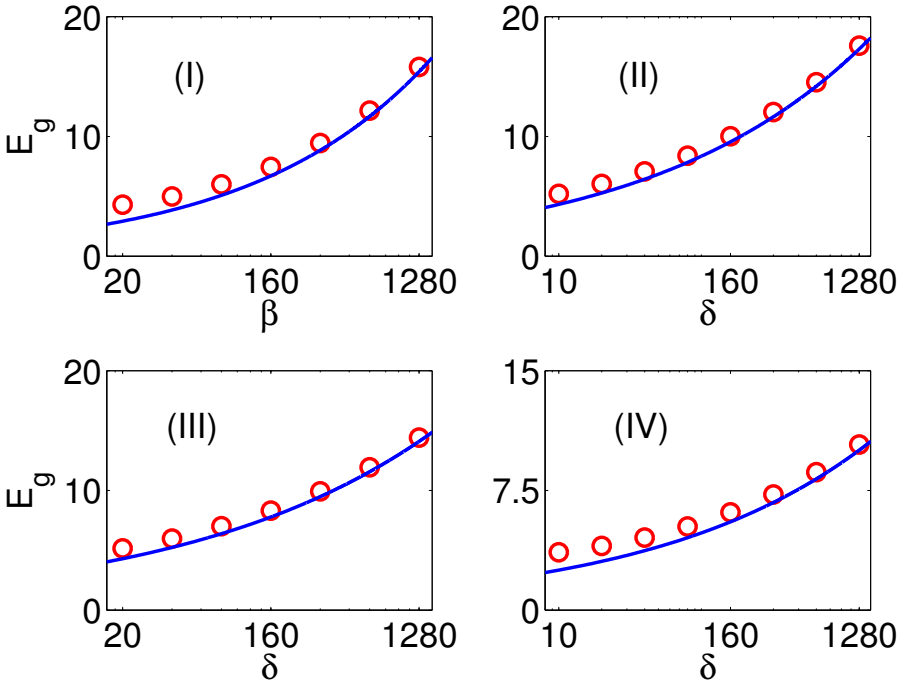

(a) comparison of energy (harmonic potential case)

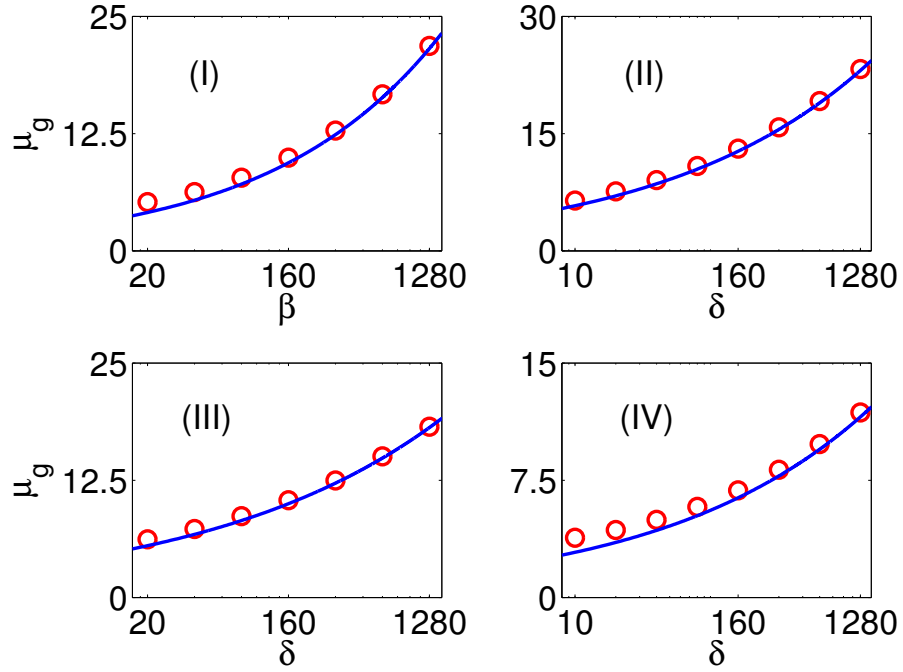

(b) comparison of chemical potential (harmonic potential case)

Figure 3.3: Comparisons of numerical energies and chemical potentials with TF approximations, the harmonic potential case. 3D problem is considered here. Blue line: Thomas-Fermi approximation, and red circles: numerical results obtained from the equation (2.4.1). The parameters are chosen to be $\gamma = 2$ and (I) $\delta = 1$, (II) $\beta = 5\delta^{\frac{5}{7}}$, (III) $\beta = 1$, (IV) $\beta = -5\delta^{\frac{5}{7}}$, respectively.

3.4 Approximations under a box potential

3.4.1 Approximation in weak interaction regime

In this section, we consider the box potential (2.4.3) with parameters in the weak interaction regime, i.e. $|\beta| \ll 1, 0 \leq \delta \ll 1$.

If $\Omega = \prod_{j=1}^{d}(0, L_j)$, then the case when $\beta = 0$ and $\delta = 0$, i.e. the interaction between particle is absent, is clear and all the eigenfunctions can be obtained via the sine series [25, 26]. Thus the ground state $\phi_g^0(\mathbf{x})$ can be given explicitly as [25, 26]

$$\phi_g^0(\mathbf{x}) = \prod_{j=1}^{d} \sqrt{\frac{2}{L_j}} \sin\left(\frac{\pi x_j}{L_j}\right), \text{ for } \mathbf{x} \in \bar{\Omega} \tag{3.4.1}$$

When $0 < \beta \ll 1$, i.e. weakly repulsive interaction regime, we can approximate the ground state $\phi_g^\beta(\mathbf{x})$. Thus we have

Lemma 3.4.1. *In the weakly repulsive interaction regime, i.e.* $|\beta| \ll 1$ *and* $0 \leq \delta \ll 1$, *we have*

$$\phi_g(\mathbf{x}) \approx \prod_{j=1}^{d} \sqrt{\frac{2}{L_j}} \sin\left(\frac{\pi x_j}{L_j}\right). \tag{3.4.2}$$

In addition, the energy and chemical potential of the ground and first excited states can be approximated as

$$E_g(\beta, \delta) = A_2 + \frac{3^d A_0^2}{2^{d+1}}\beta + \frac{3^{d-1}}{2^{d-2}} A_0^2 A_2 \delta + o(\beta + \delta), \tag{3.4.3}$$

$$\mu_g(\beta, \delta) = A_2 + \frac{3^d A_0^2}{2^d}\beta + \frac{3^{d-1}}{2^{d-3}} A_0^2 A_2 \delta + o(\beta + \delta), \tag{3.4.4}$$

where $A_0 = \frac{1}{\sqrt{\prod_{j=1}^{d} L_j}}$, $\quad A_2 = \frac{\pi^2}{2}\sum_{j=1}^{d} \frac{1}{L_j^2}$.

If $\Omega = \{|\mathbf{x}| \leq R\}$, then the ground state for the linear case, i.e. $\beta = \delta = 0$, is an eigenstate of the following problem,

$$\mu\phi = -\frac{1}{2}(\phi'' + \frac{d-1}{r}\phi'), \tag{3.4.5}$$

where $d = 1, 2, 3$ is the dimension of the problem, and the solution can be computed explicitly as

$$\phi_g^0(r) = \begin{cases} \frac{1}{\sqrt{R}} \cos\left(\frac{\pi r}{2R}\right), & d = 1, \\ A J_0(\sqrt{2\mu_{2\mathrm{D}}} r), & d = 2, \\ \frac{1}{\sqrt{2\pi R}} \frac{\sin(\frac{\pi r}{R})}{r}, & d = 3, \end{cases} \tag{3.4.6}$$

with the corresponding eigenvalues (also energies in this case)

$$\mu_g = \begin{cases} \frac{1}{2}\left(\frac{\pi}{2R}\right)^2, & d = 1, \\ \frac{1}{2}\left(\frac{\pi}{R}\right)^2, & d = 3, \end{cases} \tag{3.4.7}$$

where $J_0(r)$ is the Bessel function of the first kind $J_\alpha(r)$ with $\alpha = 0$, A is some constant that normalizes the ground state and $\mu_{2\mathrm{D}}$, which can be determined by letting $\sqrt{2\mu_{2\mathrm{D}}}R$ equals the smallest positive zeros of $J_0(r)$ (roughly 2.4048), is the eigenvalue for $d = 2$ case.

In weak interaction regime, i.e. $|\beta| \ll 1$ and $0 \le \delta \ll 1$, the ground state can be approximated by (3.4.6).

3.4.2 Thomas-Fermi approximation

In this section, we consider the special box potential (2.4.3) that confines the BEC in the bounded domain $\Omega = \{|\mathbf{x}| \le R\}$. Using a similar method for the harmonic potential case, we can obtain the analytical TF densities if the contact interaction and/or HOI dominates the ground state in Eq. (2.4.1). The analytical TF densities for different regimes which are shown in Fig. 3.4 are derived. The borderline of the three regimes is $\beta = O(\delta)$, which is different from the harmonic potential case.

Regime I, β term is dominant, i.e. $\beta \gg 1$ and $\delta = o(\beta)$. The kinetic term and the HOI term are dropped and the time independent MGPE equation in the radial variable r becomes

$$\mu\psi(r) = \beta|\psi|^2\psi, \quad 0 \le r = |\mathbf{x}| < R, \tag{3.4.8}$$

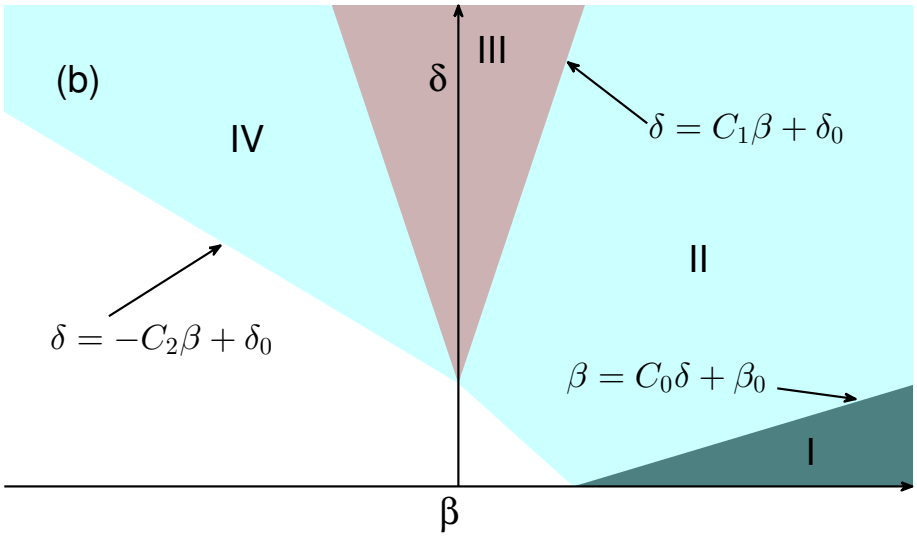

Figure 3.4: Phase diagram for extreme regimes under a harmonic potential. In the figure, we choose $\beta_0 \gg 1$ and $\delta_0 \gg 1$, and C_0, C_1 and C_2 positive constants.

with boundary condition $\psi(R) = 0$. Thus, the TF density is a constant, which can be uniquely determined by the normalization condition $\|\psi\| = 1$. Explicitly, TF density is given by $n_{\rm TF}(r) = |\psi|^2 = \frac{\tilde{C}_d}{R^d}$, and $\mu_{\rm TF} = \frac{\tilde{C}_d \beta}{R^d}$, where $\tilde{C}_d$ is defined in previous subsection.

It is obvious that the TF density is inconsistent with zero boundary condition, thus a boundary layer appears in the ground state density profile [26]. In fact, as shown in [26], for the case $d = 1$, an asymptotic analysis to match the boundary layers at $x = \pm R$ leads to the following matched density for $0 \le r = |x| \le R$ when $\beta \gg 1$ and $\delta \sim o(1)$,

$$n_{\rm as}(r) = |\psi_{\rm as}|^2 = \frac{1}{2R}\left(\tanh(\sqrt{\mu_{\rm as}}(R - r))\right)^2, \tag{3.4.9}$$

with the chemical potential $\mu_{\rm as} = \frac{1}{2R}\beta + \frac{1}{R}\sqrt{\frac{\beta}{2R}}$, and the energy $E_{\rm as} = \frac{1}{4R}\beta + \frac{2}{3R}\sqrt{\frac{\beta}{2R}}$. Similar matched densities can be derived for $d = 2, 3$.

From our numerical experience, the matched asymptotic density $n_{\rm as}$ provides much more accurate approximation to the ground state of Eq. (2.4.1), than the TF density $n_{\rm TF}$, in the parameter regime $\beta \gg 1$ and $\delta = O(1)$.

Regime II, both β and δ are important, i.e. $\beta = O(\delta)$ as $\delta \to \infty$. We assume that $\beta = C_0\delta$, with $\delta \gg 1$ for some constant $C_0 > 0$.

Omitting the less important kinetic part, the radially symmetric time independent MGPE reads

$$\mu\psi(r) = C_0\delta|\psi|^2\psi - \delta\nabla^2(|\psi|^2)\psi, \quad r < R, \tag{3.4.10}$$

with $\psi(R) = 0$. The above equation can be simplified for density $n(r) = |\psi|^2$ in d dimensions as

$$\frac{\mu}{\delta} = C_0 n(r) - \partial_{rr} n - \frac{d-1}{r}\partial_r n, \tag{3.4.11}$$

with $n(R) = 0$, and at $r = 0$ with $n'(0) = 0$. Eq. (3.4.11) can be solved analytically.

The TF density, or solution of the boundary value problem (3.4.11), is given explicitly as

$$n_{\rm TF}(r) = |\psi_{\rm TF}|^2 = \frac{\mu_{\rm TF}}{a^2\delta}\left[1 - \frac{f_{a,d}(r)}{f_{a,d}(R)}\right], \tag{3.4.12}$$

where $a = \sqrt{C_0}$, $f_{a,d}(r)$ is defined in Eq. (3.3.12) and $\mu_{\rm TF} = \tilde{C}_d a^2\delta/(R^d - d\frac{\int_0^R f_{a,d}(r)r^{d-1}dr}{f_{a,d}(R)})$ with $\tilde{C}_d$ defined in Eq. (3.3.8). Further, we have $E_{\rm TF} = \mu_{\rm TF}/2$,

Regime III, δ term is dominant, i.e. $\delta \gg 1$, $\beta = o(\delta)$. The kinetic term and the β term are dropped. The corresponding stationary MGPE for the ground state reads

$$\mu\psi = -\delta\nabla^2(|\psi|^2)\psi, \tag{3.4.13}$$

with boundary condition $\psi(R) = 0$.

Solving the equation and using the normalization condition, we obtain the TF density as

$$n_{\rm TF}(r) = |\psi_{\rm TF}|^2 = \frac{(d+2)\tilde{C}_d(R^2 - r^2)}{2R^{d+2}}, \tag{3.4.14}$$

with chemical potential $\mu_{\rm TF} = \tilde{C}_d d(d+2)\delta/R^{d+2}$ and energy $E_{\rm TF} = \mu_{\rm TF}/2$.

Regime IV, i.e. $\beta = -C_0\delta$, with $\delta \gg 1$ for some constant $C_0 > 0$.

Intuitively, if C_0 is small, the repulsive HOI δ term is dominant and the particle density will still occupy the entire domain. If C_0 is sufficiently large, the attractive β interaction becomes the major effect, where the particles will be self trapped and the density profile will concentrate in a small portion of the domain. Therefore, unlike the corresponding harmonic potential case, we have two different situations here.

By a similar procedure as for Regime II, we get

$$\frac{\mu}{\delta} = -C_0 n(r) - \partial_{rr} n - \frac{d-1}{r}\partial_r n, \tag{3.4.15}$$

with $n(R') = 0$ and R' to be determined. In the first situation, the density spreads over the whole domain and thus $R' = R$; in the second situation, the density is constrained to a small region $[0, R']$, where $0 < R' < R$.

Case I, i.e. $C_0 \leq C_{\rm cr}$, where $C_{\rm cr} = \hat{R}^2/R^2$ and $\hat{R}$ is the first positive root of $g'_{a,d}(r/a) = 0$, where $g'_{a,d}(r)$ is defined in Eq. (3.3.19) with $a = \sqrt{C_0}$. As mentioned before, because of the relatively weak attractive interaction, we have the following boundary conditions at the boundary: $n(R) = 0$, $n'(0) = 0$.

The TF density, or solution of Eq. (3.4.15), can be expressed as:

$$n_{\rm TF} = |\psi_{\rm TF}|^2 = -\frac{\mu}{a^2\delta}\left[1 - \frac{g_{a,d}(r)}{g_{a,d}(R)}\right], \tag{3.4.16}$$

with $\mu_{\rm TF} = \tilde{C}_d a^2 \delta / (d\frac{\int_0^R g_{a,d}(r) r^{d-1} dr}{g_{a,d}(R)} - R^d)$ and $E_{\rm TF} = \mu_{\rm TF}/2$, where $\tilde{C}_d$ is given in (3.3.8).

In fact, the condition $C_0 \leq C_{\rm cr}$, which is equivalent to $aR \leq \hat{R}$, is necessary. A simple argument for d=2, 3 case is as follows. If $aR > \hat{R}$, we know from the property of $g_{a,d}(r)$ that the image of $g_{a,d}(r)$ for $r \in [0, \hat{R}]$ is exactly the image of $g_{a,d}(r)$ for all $r \geq 0$ and $g_{a,d}(R) \in (\min g_{a,d}(r), \max g_{a,d}(r))$. Then we can find $r_0 \in (0, \hat{R})$ such that $g_{a,d}(r_0) = g_{a,d}(R)$, and $1 - g_{a,d}(r)/g_{a,d}(R)$ changes signs for r around r_0. On the other hand, $1 - g_{a,d}(r)/g_{a,d}(R)$ can't change signs in $[0, R]$ since the density must be nonnegative. So we get a contradiction. Hence $aR \leq \hat{R}$, i.e. $C_0 \leq C_{\rm cr}$.

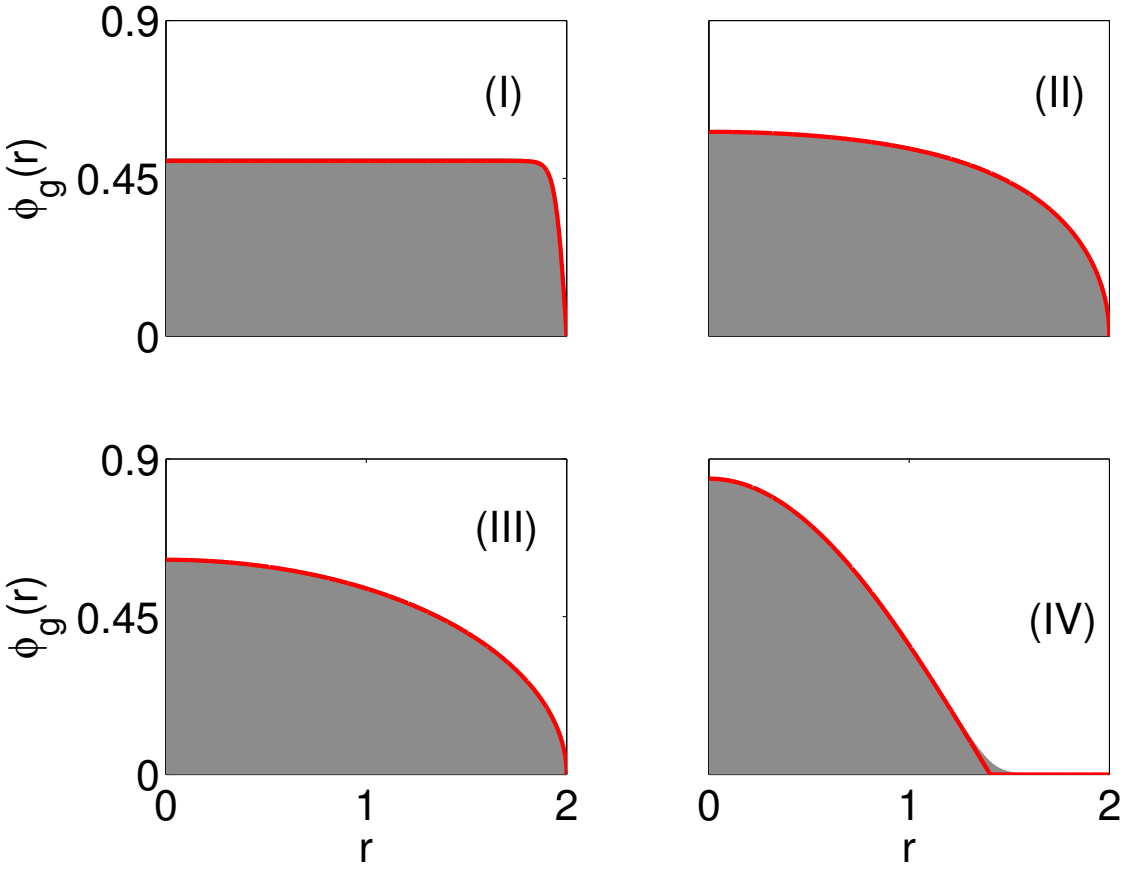

Figure 3.5: Comparisons of 1D numerical ground states with TF densities, the box potential case in region I, II, III and IV, which are defined in Fig. 3.1(b). Red line: analytical TF approximation, and shaded area: numerical solution obtained from (2.4.1). Domain is $\{r|0 \leq r < 2\}$ and the corresponding β's and δ's are (I) $\beta = 1280$, $\delta = 1$; (II) $\beta = 320$, $\delta = 160$; (III) $\beta = 1$, $\delta = 160$; (IV) $\beta = -400$, $\delta = 80$.

$g'_{a,d}$ at r/a can be computed as

$$g'_{a,d}(r/a) = \begin{cases} -a\sin(r), & d=1, \\ -aJ_1(r), & d=2, \\ a^2(r\cos(r)-\sin(r))/r^2, & d=3, \end{cases} \tag{3.4.17}$$

and we have for 1D case, $\hat{R} = \pi$; for 2D case, $\hat{R} = 3.8317\cdots$; for 3D case, $\hat{R} = 4.4934\cdots$.

Case II, $C_0 > C_{\rm cr}$. As observed above, the densities drop to 0 before reaching the boundaries. Thus, free boundary conditions should be used as $n(\tilde{R}) = 0$, $n'(\tilde{R}) = 0$, $n'(0) = 0$, where $\tilde{R} < R$ is the boundary for the TF density that we want to find.

Hence the domain $[0, R]$ in *Case I* needs to be replaced by $[0, \tilde{R}]$ with $n'(\tilde{R}) = 0$. Denoting $a = \sqrt{C_0}$ and using the solution in *Case I*, we get $g'_{a,d}(\tilde{R}) = 0$, and $a\tilde{R} \le \hat{R}$. Both conditions can only be satisfied when $a\tilde{R} = \hat{R}$. Hence $\tilde{R} = \hat{R}/a < R$.

Replacing R with $\hat{R}/a$ in the TF solution of *Case I*, we obtain the analytical TF density

$$n_{\rm TF}(r) = |\psi_{\rm TF}|^2 = \frac{\tilde{C}_d a^d}{\hat{R}^d}\left[1 - \frac{g_{a,d}(r)}{g_{a,d}(\frac{\hat{R}}{a})}\right], \tag{3.4.18}$$

where $\hat{R}$ is defined in *Case I*. Further we have $\mu_{\rm TF} = -\tilde{C}_d a^{d+2}\delta/\hat{R}^d$ and $E_{\rm TF} = \mu_{\rm TF}/2$.

In Fig. 3.5, we compare the analytical TF densities listed above with the ground state obtained from numerical results via Eq. (2.4.1) computed by the BEFD method [18] in various parameter regimes discussed above. Fig. 3.5 shows our analytical TF densities are good approximations for the ground states. Fig. 3.6 compares the chemical potentials and energies between the TF approximations and the numerical values by solving Eq. (2.4.1).

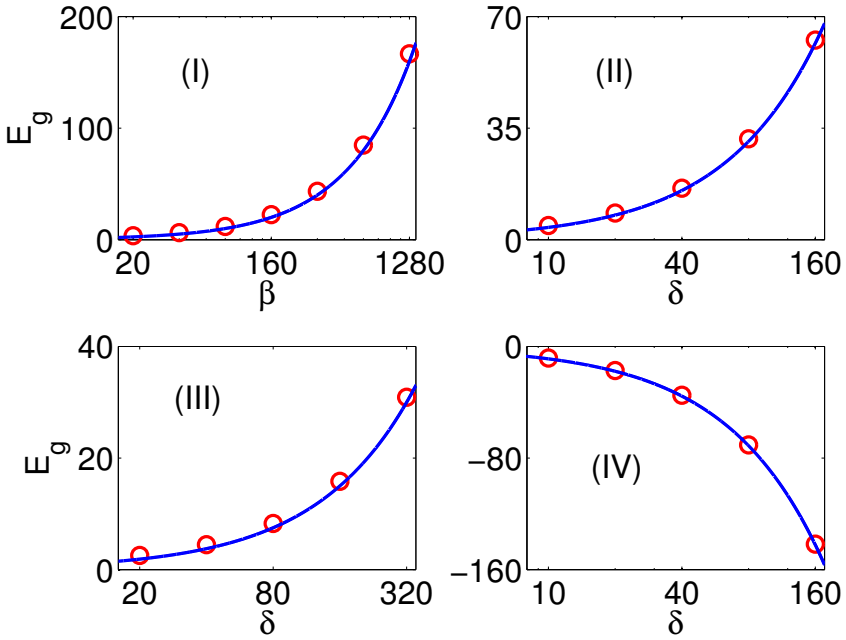

(a) comparison of energy

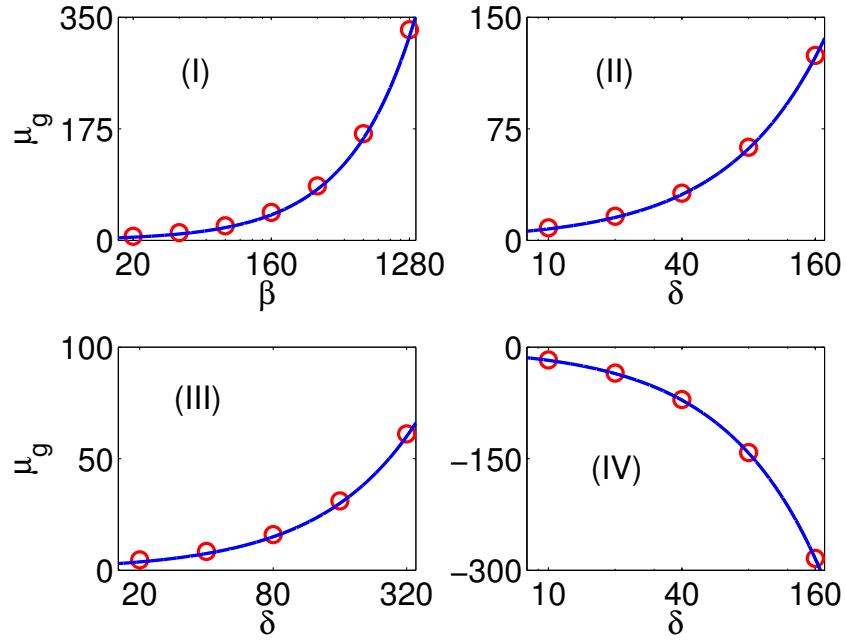

(b) comparison of chemical potential

Figure 3.6: Comparisons of numerical energies and chemical potentials with TF approximations, the box potential case. 1D problem is considered here. Blue line: analytical TF approximation, and red circles: numerical results obtained from (2.4.1). The parameters are chosen to be (I) $\delta = 1$, (II) $\beta = 2\delta$, (III) $\beta = 1$, (IV) $\beta = -5\delta$, respectively, and domain is $\{r|0 \leq r < 2\}$.

3.5 Limiting behavior under a harmonic potential

In this section, $V(\mathbf{x})$ is taken as the harmonic potential (2.4.2) and we prove rigourously the limiting profiles of ground states defined in (3.2.1) under different sets of parameters δ and β, especially for the Thomas-Fermi approxmations.

The following rescaling will be used in the proof. For any $\phi(\mathbf{x}) \in S$, choose $\phi^\varepsilon(\mathbf{x}) = \varepsilon^{-d/2}\phi(\mathbf{x}/\varepsilon) \in S$, i.e.

$$\phi(\mathbf{x}) = \varepsilon^{d/2}\phi^\varepsilon(\mathbf{x}\varepsilon), \tag{3.5.1}$$

we find the energy $E(\cdot)$ (2.4.10) can be written as

$$\begin{aligned} E(\phi) &= \int_{\mathbb{R}^d} \left[\frac{\varepsilon^2}{2}|\nabla\phi^\varepsilon|^2 + \frac{1}{\varepsilon^2}V(\mathbf{x})|\phi^\varepsilon|^2 + \frac{\beta\varepsilon^d}{2}|\phi^\varepsilon|^4 + \frac{\delta\varepsilon^{2+d}}{2}\left|\nabla|\phi^\varepsilon|^2\right|^2 \right] d\mathbf{x} \\ &:= \frac{1}{\varepsilon^2}E^\varepsilon(\phi^\varepsilon), \end{aligned} \tag{3.5.2}$$

where

$$E^\varepsilon(\phi^\varepsilon) = \int_{\mathbb{R}^d} \left[\frac{\varepsilon^4}{2}|\nabla\phi^\varepsilon|^2 + V(\mathbf{x})|\phi^\varepsilon|^2 + \frac{\beta\varepsilon^{d+2}}{2}|\phi^\varepsilon|^4 + \frac{\delta\varepsilon^{4+d}}{2}\left|\nabla|\phi^\varepsilon|^2\right|^2 \right] d\mathbf{x}, \tag{3.5.3}$$

which indicates that

$$\phi_g = \arg\min_{\phi\in S} E(\phi) \overset{\phi_g(\mathbf{x})=\varepsilon^{d/2}\phi_g^\varepsilon(\varepsilon\mathbf{x})}{\Longleftrightarrow} \phi_g^\varepsilon = \arg\min_{\phi^\varepsilon\in S} E^\varepsilon(\phi^\varepsilon). \tag{3.5.4}$$

Now, we give characterization of the ground state ϕ_g (3.2.1) when the two interactions strength are very large.

Theorem 3.5.1. *(Thomas-Fermi limit, positive β limit) Let $V(\mathbf{x})$ ($\mathbf{x} \in \mathbb{R}^d$, $d = 1, 2, 3$) be given in (2.4.2), $\delta > 0$, $\phi_g \in S$ be the positive ground state defined as (3.2.1).*

(1) If $\beta \to +\infty$ and $\delta = o(\beta^{\frac{4+d}{2+d}})$. Set $\phi_g^\varepsilon(\mathbf{x}) = \varepsilon^{-d/2}\phi_g(\mathbf{x}/\varepsilon) \in S$ with $\varepsilon = \beta^{-\frac{1}{2+d}}$. For $\beta \to +\infty$ ($\varepsilon \to 0^+$), we have $\rho^\varepsilon = |\phi_g^\varepsilon(\mathbf{x})|^2$ converges to $\rho_\infty(\mathbf{x}) := |\phi_\infty(\mathbf{x})|^2$ in L^2, where $\phi_\infty(\mathbf{x})$ is the unique nonnegative minimizer of the energy

$$E_1(\phi) = \int_{\mathbb{R}^d} \left(V(\mathbf{x})|\phi|^2 + \frac{1}{2}|\phi|^4 \right) d\mathbf{x}, \quad \|\phi\| = 1. \tag{3.5.5}$$

More precisely, $\rho_\infty = |\phi_\infty|^2 = (\mu - V(\mathbf{x}))_+$ *with* $\mu = E_1(\phi_\infty) + \frac{1}{2}\|\phi_\infty\|_{L^4}^4$ *and* $(f)_+ = \max\{f, 0\}$.

(2) If $\beta \to +\infty$ *and* $\delta = O(\beta^{\frac{4+d}{2+d}})$, *i.e.* $\lim_{\beta\to+\infty} \frac{\delta}{\beta^{\frac{4+d}{2+d}}} = \delta_\infty > 0$. *Set* $\phi_g^\varepsilon(\mathbf{x}) = \varepsilon^{-d/2}\phi_g(\mathbf{x}/\varepsilon) \in S$ *with* $\varepsilon = \beta^{-\frac{1}{2+d}}$. *For* $\delta \to +\infty$ *(*$\varepsilon \to 0^+$*), we have* $\rho_g^\varepsilon(\mathbf{x}) = |\phi_g^\varepsilon(\mathbf{x})|^2$ *converges to* $\rho_\infty(\mathbf{x})$ *in* H^1, *where* $\phi_\infty(\mathbf{x}) = \sqrt{\rho_\infty(\mathbf{x})}$ *is the unique nonnegative minimizer of the energy*

$$E_2(\phi) = \int_{\mathbb{R}^d} \left(V(\mathbf{x})|\phi|^2 + \frac{|\phi|^4}{2} + \frac{\delta_\infty}{2}|\nabla|\phi|^2|^2 \right) d\mathbf{x}, \quad \|\phi\| = 1. \tag{3.5.6}$$

The minimizer ρ_∞ *of* $E_2(\sqrt{\rho})$ *exists by a similar argument as that in Theorem 7.1.1 and is unique because* $E_2(\sqrt{\rho})$ *is convex in* ρ.

(3) If $\beta \to +\infty$ *and* $\delta/\beta^{\frac{4+d}{2+d}} \gg 1$, *i.e.* $\beta = o(\delta^{\frac{2+d}{4+d}})$ *as* $\delta \to +\infty$. *Set* $\phi_g^\varepsilon(\mathbf{x}) = \varepsilon^{-d/2}\phi_g(\mathbf{x}/\varepsilon) \in S$ *with* $\varepsilon = \delta^{-\frac{1}{4+d}}$. *For* $\delta \to +\infty$ *(*$\varepsilon \to 0^+$*), we have* $\rho_g^\varepsilon(\mathbf{x}) = |\phi_g^\varepsilon(\mathbf{x})|^2$ *converges to* $\rho_\infty(\mathbf{x})$ *in* H^1, *where* $\phi_\infty(\mathbf{x}) = \sqrt{\rho_\infty(\mathbf{x})}$ *is the unique nonnegative minimizer of the energy*

$$E_3(\phi) = \int_{\mathbb{R}^d} \left(V(\mathbf{x})|\phi|^2 + \frac{1}{2}|\nabla|\phi|^2|^2 \right) d\mathbf{x}, \quad \|\phi\| = 1. \tag{3.5.7}$$

The minimizer ρ_∞ *of* $E_3(\sqrt{\rho})$ *exists by a similar argument as that in Theorem 7.1.1 and is unique because* $E_3(\sqrt{\rho})$ *is convex in* ρ.

Proof. We separate the three cases.

(1) Using (3.5.3) and choosing $\varepsilon = \beta^{-1/d+2}$, we find $\phi_g^\varepsilon \in S$ minimizes

$$E^\varepsilon(\phi^\varepsilon) = \int_{\mathbb{R}^d} \left[\frac{\varepsilon^4}{2}|\nabla\phi^\varepsilon|^2 + V(\mathbf{x})|\phi^\varepsilon|^2 + \frac{|\phi^\varepsilon|^4}{2} + \frac{\delta\varepsilon^{4+d}}{2}\left|\nabla|\phi^\varepsilon|^2\right|^2 d\mathbf{x} \right]. \tag{3.5.8}$$

On the other hand, $E_1(\phi)$ has a unique nonnegative minimizer ϕ_∞ and by an approximation argument, we can take any smooth approximations of $\phi_\infty(\mathbf{x})$ in S and find that for any $\eta > 0$ with $\delta = o(\beta^{\frac{2}{d+2}})$

$$E_1(\phi_\infty) \le E^\varepsilon(\phi_g^\varepsilon) \le E_1(\phi_\infty) + \eta + C(\eta)(\varepsilon^4 + o(1)),$$

which implies

$$\lim_{\varepsilon\to 0^+} E_1(\phi_g^\varepsilon) = E_1(\phi_\infty). \tag{3.5.9}$$

Hence we know ϕ_g^ε ($\varepsilon \to 0^+$) is a minimizing sequence for $E_1(\cdot)$. On the other hand,

$$\begin{aligned} E_1(\phi_g^\varepsilon) - E_1(\phi_\infty) =& \int_{\mathbb{R}^d} \left[(V(\mathbf{x}) + |\phi_\infty|^2)(|\phi_g^\varepsilon|^2 - |\phi_\infty|^2) + \frac{1}{2}(|\phi_g^\varepsilon|^2 - |\phi_\infty|^2)^2 \right] d\mathbf{x} \\ =& \int_{\mathbb{R}^d} \left[\max\{V(\mathbf{x}), \mu\}(|\phi_g^\varepsilon|^2 - |\phi_\infty|^2) + \frac{1}{2}(|\phi_g^\varepsilon|^2 - |\phi_\infty|^2)^2 \right] d\mathbf{x} \\ \geq& \int_{\mathbb{R}^d} \left[\mu|\phi_g^\varepsilon|^2 - \mu|\phi_\infty|^2 + \frac{1}{2}(|\phi_g^\varepsilon|^2 - |\phi_\infty|^2)^2 \right] d\mathbf{x} \\ =& \frac{1}{2}\int_{\mathbb{R}^d} (|\phi_g^\varepsilon|^2 - |\phi_\infty|^2)^2 d\mathbf{x}, \end{aligned}$$

and the conclusion follows.

(2) The proof is similar to the case (1), where it is easy to show $\lim_{\varepsilon \to 0^+} E_2(\phi_g^\varepsilon) = E_2(\phi_\infty)$. Noticing that for any function $0 \leq \sqrt{\rho(\mathbf{x})} \in H^1$ with $\int_{\mathbb{R}^d} \rho(\mathbf{x}) = 1$, we have $E_2(\sqrt{(\rho_\infty + s\rho)/(1+s)})$ ($s \geq 0$) attains minimum at $s = 0$. By direct computation, we find

$$\begin{aligned} \frac{d}{ds} E_2\left(\sqrt{\frac{\rho_\infty + s\rho}{1+s}}\right)\Big|_{s=0} =& \int_{\mathbb{R}^d} (V(\mathbf{x})\rho(\mathbf{x}) + \rho_\infty(\mathbf{x})\rho(\mathbf{x}) + \delta_\infty \nabla\rho_\infty(\mathbf{x}) \cdot \nabla\rho(\mathbf{x}))\, d\mathbf{x} \\ & - \int_{\mathbb{R}^d} (V(\mathbf{x})\rho_\infty(\mathbf{x}) + \rho_\infty^2(\mathbf{x}) + \delta_\infty |\nabla\rho_\infty(\mathbf{x})|^2)\, d\mathbf{x} \\ \geq& 0. \end{aligned}$$

A simple calculation shows

$$\begin{aligned} & E_2(\phi_g^\varepsilon) - E_2(\phi_\infty) \\ &= \frac{d}{ds} E_2\left(\sqrt{\frac{\rho_\infty + s\rho^\varepsilon}{1+s}}\right)\Big|_{s=0} + \int_{\mathbb{R}^d} \left[\frac{1}{2}(|\phi_g^\varepsilon|^2 - |\phi_\infty|^2)^2 + \frac{\delta_\infty}{2}(\nabla|\phi_g^\varepsilon|^2 - \nabla|\phi_\infty|^2)^2 \right] d\mathbf{x} \\ &\geq \int_{\mathbb{R}^d} \left[\frac{1}{2}(|\phi_g^\varepsilon|^2 - |\phi_\infty|^2)^2 + \frac{\delta_\infty}{2}(\nabla|\phi_g^\varepsilon|^2 - \nabla|\phi_\infty|^2)^2 \right] d\mathbf{x}, \end{aligned}$$

which implies $\rho_g^\varepsilon(\mathbf{x}) = |\phi_g^\varepsilon(\mathbf{x})|^2$ converges to $\rho_\infty(\mathbf{x})$ in H^1.

(3) Using (3.5.3) and choosing $\varepsilon = \delta^{-\frac{1}{4+d}}$, we find $\phi_g^\varepsilon \in S$ minimizes

$$E^\varepsilon(\phi^\varepsilon) = \int_{\mathbb{R}^d} \left[\frac{\varepsilon^4}{2}|\nabla\phi^\varepsilon|^2 + V(\mathbf{x})|\phi^\varepsilon|^2 + \frac{\beta\varepsilon^{d+2}|\phi^\varepsilon|^4}{2} + \frac{1}{2}\left|\nabla|\phi^\varepsilon|^2\right|^2 \right] d\mathbf{x}. \quad (3.5.10)$$

Nash inequality and Young inequality imply that for $\rho^\varepsilon = |\phi^\varepsilon|^2$ ($\phi^\varepsilon \in S$),

$$\int_{\mathbb{R}^d} |\rho^\varepsilon(\mathbf{x})|^2\, d\mathbf{x} \leq C\|\rho^\varepsilon\|_{L^1}^{4/d+2}\|\nabla\rho^\varepsilon\|^{2d/d+2} \leq C + \|\nabla\rho^\varepsilon\|^2.$$

Thus, we conclude that for $\beta = o(\delta^{\frac{2+d}{4+d}})$,

$$E^\varepsilon(\phi^\varepsilon) \geq \int_{\mathbb{R}^d} \left(V(\mathbf{x})|\phi^\varepsilon|^2 + \frac{1}{2}(1 - o(1))|\nabla|\phi^\varepsilon|^2|^2 \right) d\mathbf{x} - o(1), \quad \phi^\varepsilon \in S. \tag{3.5.11}$$

For sufficient small ε, (3.5.11) gives that for the ground state ϕ_g^ε,

$$E_3(\phi_g^\varepsilon) \leq C, \tag{3.5.12}$$

and we obtain

$$E^\varepsilon(\phi_g^\varepsilon) \geq E_3(\phi_g^\varepsilon) - o(1). \tag{3.5.13}$$

Choosing smooth approximations of ϕ_∞ in S if necessary, we could get for any $\eta > 0$,

$$E^\varepsilon(\phi_g^\varepsilon) \leq E_3(\phi_\infty) + \eta + C(\eta)(\varepsilon^4 + o(1)). \tag{3.5.14}$$

Combining (3.5.13), (3.5.14) and the fact that ϕ_∞ minimizes E_3 under the constraint, we find that

$$\lim_{\varepsilon \to 0^+} E_3(\phi_g^\varepsilon) = E_3(\phi_\infty). \tag{3.5.15}$$

On the other hand, $E_3(\sqrt{(\rho_\infty + s\rho_g^\varepsilon)/(1+s)})$ $(s \geq 0)$ reach its minimum at $s = 0$, and

$$\begin{aligned} 0 &\leq \frac{d}{ds} E_3 \left(\sqrt{\frac{\rho_\infty + s\rho_g^\varepsilon}{1+s}} \right) \Big|_{s=0} \\ &= \int_{\mathbb{R}^d} \left(\rho_g^\varepsilon V(\mathbf{x}) + \nabla \rho_g^\varepsilon \cdot \nabla \rho_\infty \right) d\mathbf{x} - \int_{\mathbb{R}^d} \left(\rho_\infty V(\mathbf{x}) + \nabla \rho_\infty \cdot \nabla \rho_\infty \right) d\mathbf{x}. \end{aligned}$$

Therefore.

$$\begin{aligned} &E_1(\phi_g^\varepsilon) - E_1(\phi_\infty) \\ &= \int_{\mathbb{R}^d} \left((\rho_g^\varepsilon - \rho_\infty)V + \nabla(\rho_g^\varepsilon - \rho_\infty) \cdot \nabla \rho_\infty \right) d\mathbf{x} + \frac{1}{2}\|\nabla \rho_g^\varepsilon - \nabla \rho_\infty\|^2 \\ &\geq \frac{1}{2}\|\nabla \rho_g^\varepsilon - \nabla \rho_\infty\|^2. \end{aligned}$$

The convergence of ρ_g^ε towards ρ_∞ as $\varepsilon \to 0^+$ is then a direct consequence. □

In Theorem 3.5.1, three types limiting profiles are obtained and the usual TF density as the minimizer of energy $E_1(\cdot)$ in (3.5.5) has a compact support. We would like to show that the minimizers of energy functionals $E_2(\cdot)$ (3.5.7) and $E_3(\cdot)$ (3.5.6) are indeed solution of certain free boundary problems.

Theorem 3.5.2. *Let $V(\mathbf{x}) \geq 0$ ($\mathbf{x} \in \mathbb{R}^d$, $d = 1, 2, 3$) be given in (2.4.2), and nonnegative functions $\rho_1(\mathbf{x}) \geq 0$ and $\rho_2(\mathbf{x}) \geq 0$ be the unique minimizers of $E_2(\sqrt{\rho})$ and $E_3(\sqrt{\rho})$ under the constraints $\|\rho\|_{L^1} = 1$ and $\rho \geq 0$, respectively. Then $\rho_1, \rho_2 \in C^{1,\alpha}_{\mathrm{loc}} \subset W^{2,p}_{\mathrm{loc}}$ ($1 < p < \infty$ and $0 < \alpha < 1$) solve the free boundary value problems*

$$-\delta_\infty \Delta \rho_1 + \rho_1 = (\mu_1 - V(\mathbf{x}))\, \chi_{\{\rho_1 > 0\}}, \quad a.e. \quad \mathbf{x} \in \mathbb{R}^d, \tag{3.5.16}$$

$$-\delta_\infty \Delta \rho_2 = (\mu_2 - V(\mathbf{x}))\, \chi_{\{\rho_2 > 0\}}, \quad a.e. \quad \mathbf{x} \in \mathbb{R}^d, \tag{3.5.17}$$

where $\mu_1 = 2E_2(\sqrt{\rho_1}) - \int_{\mathbb{R}^d} V(\mathbf{x})\rho_1 d\mathbf{x}$ and $\mu_2 = 2E_3(\sqrt{\rho_2}) - \int_{\mathbb{R}^d} V(\mathbf{x})\rho_2\, d\mathbf{x}$. The conditions at the free boundaries are

$$\rho_j|_{\partial\{\rho_j > 0\}} = 0, \quad |\nabla \rho_j||_{\partial\{\rho_j > 0\}} = 0, \quad j = 1, 2. \tag{3.5.18}$$

If $V(\mathbf{x})$ is radially symmetric and non-decreasing, $\rho_j(\mathbf{x})$ ($j = 1, 2$) are radially symmetric non-increasing and compactly supported.

Proof. (i) We verify the two equations (3.5.16) and (3.5.17). The arguments are very similar, and we only prove (3.5.16) for simplicity.

We adapt an approach for the classical obstacle problem in [91]. Since $\rho_1 \geq 0$ minimizes $E_2(\sqrt{\rho})$ under the constraints $\|\rho\|_{L^1} = 1$ and $\rho \geq 0$, in addition $V(\mathbf{x}) \geq 0$, we can conclude that ρ_1 minimizes the following energy

$$\tilde{E}(\rho) = \int_{\mathbb{R}^d} \left(V(\mathbf{x})|\rho| + \frac{\rho^2}{2} + \frac{\delta_\infty}{2} |\nabla \rho|^2 \right) d\mathbf{x} \quad \text{with} \quad \int_{\mathbb{R}^d} \rho(\mathbf{x})\, d\mathbf{x} = 1, \tag{3.5.19}$$

i.e. ρ_1 is still a minimizer if we remove the nonnegative constraint with the price to have a non-smooth $V(\mathbf{x})|\rho|$ term. The reason is that if $\int_{\mathbb{R}^d} \rho(\mathbf{x})\, d\mathbf{x} = 1$, we can write $\rho_+(\mathbf{x}) = \max\{\rho(\mathbf{x}), 0\}$ and $\rho_-(\mathbf{x}) = \max\{-\rho(\mathbf{x}), 0\}$, and $\int_{\mathbb{R}^d} \rho_+(\mathbf{x}) \geq 1$. Since all the terms in the energy $\tilde{E}(\rho)$ are positive, we have $\tilde{E}(\rho_+/\|\rho_+\|_{L^1}) \leq \tilde{E}(\rho_+) \leq \tilde{E}(\rho)$.

Thus, the minimizer must be nonnegative and the unique minimizer of (3.5.19) (by convexity) is ρ_1.

Now, we would like to derive the equation for ρ_1. In order to do this, we introduce the following regularization of (3.5.19). Mollify the step function $\chi_{[0,\infty)}(s)$ ($s \in \mathbb{R}$) to get smooth function $g_\varepsilon(s) \in C^\infty(\mathbb{R})$ ($\varepsilon > 0$) such that $g_\varepsilon(s) = 1$ if $s > 0$, $g_\varepsilon(s) = 0$ if $s \le -\varepsilon$ and $g_\varepsilon'(s) \ge 0$ for all $s \in \mathbb{R}$. Moreover, $g_\varepsilon(s) \to \chi_{(0,\infty)}$ as $\varepsilon \to 0^+$. Denote $G_\varepsilon(s) = \int_{-\infty}^s g_\varepsilon(s)\,ds$ and $G_\varepsilon'' \ge 0$ indicating that G_ε is a convex function. Now, let us consider

$$\tilde{E}^\varepsilon(\rho) = \int_{\mathbb{R}^d} \left(V(\mathbf{x}) G_\varepsilon(\rho) + \frac{\rho^2}{2} + \frac{\delta_\infty}{2} |\nabla \rho|^2 \right) d\mathbf{x} \text{ with } \int_{\mathbb{R}^d} \rho(\mathbf{x})\, d\mathbf{x} = 1, \quad (3.5.20)$$

which is still a convex minimization problem and we have a unique minimizer $\rho_g^\varepsilon(\mathbf{x}) \ge 0$. Moreover, we can find the equations for $\rho_g^\varepsilon(\mathbf{x})$.

For any compactly supported smooth function $\varphi \in C_c^\infty(\mathbb{R}^d)$, consider $h(s) = \tilde{E}^\varepsilon(\rho_s(\mathbf{x}))$ where $\rho_s(\mathbf{x}) = (\rho_g^\varepsilon + s\varphi)/\int_{\mathbb{R}^d}(\rho_g^\varepsilon + s\varphi)\,d\mathbf{x}$ and $s \in (-s_0, s_0)$ with sufficiently small $s_0 > 0$ such that $\int_{\mathbb{R}^d}(\rho_g^\varepsilon + s\varphi)\,d\mathbf{x} \ge 1/2$, we then have $h(s)$ attains its minimum at $s = 0$. By standard computations and arguments [61, 78], we can get that there exists a Lagrangian multiplier μ_ε, such that ρ_g^ε solves (in the weak sense)

$$-\delta_\infty \Delta \rho_g^\varepsilon + \rho_g^\varepsilon = \mu^\varepsilon - V(\mathbf{x}) g_\varepsilon(\rho_g^\varepsilon). \quad (3.5.21)$$

It is easy to see that μ^ε is uniformly bounded and $\mu^\varepsilon - V(\mathbf{x})g_\varepsilon(\rho_g^\varepsilon) \in L^\infty_{\text{loc}}$, which implies that for any bounded smooth domain $\Omega \subset \mathbb{R}^d$, ρ_g^ε is uniformly bounded in $W^{2,p}(\Omega)$ ($p \in (1,\infty)$) by classical elliptic regularity results [61, 78]. Using Sobolev embedding, ρ_g^ε is uniformly bounded in $C^{1,\alpha}(\Omega)$ (for some $0 < \alpha < 1$) locally and hence there exist $\tilde{\rho} \in W^{2,p}(\Omega)$ such that as $\varepsilon \to 0^+$ (take a subsequence $\varepsilon_k \to 0^+$ if necessary), ρ_g^ε converges to $\tilde{\rho}$ strongly in $C^{1,\alpha}_{\text{loc}}$ and weakly in $W^{2,p}_{\text{loc}}$. Consequently, $\tilde{\rho} \ge 0$ and $\|\tilde{\rho}\|_{L^1} = 1$ ($V(\mathbf{x})$ is a confining potential). In fact, we can show $\tilde{\rho} = \rho_1$. Passing to the limit as $\varepsilon \to 0^+$ in $\tilde{E}(\rho_g^\varepsilon) \le \tilde{E}^\varepsilon(\rho_g^\varepsilon) \le \tilde{E}^\varepsilon(\rho_1)$ ($G_\varepsilon(|s|) \ge |s|$), we observe that $\tilde{E}(\tilde{\rho}) \le \limsup_{\varepsilon \to 0^+} \tilde{E}^\varepsilon(\rho_g^\varepsilon) \le \tilde{E}(\rho_1)$ and it is obvious $\tilde{\rho} = \rho_1$.

Now, we have $\rho_1 \in W^{2,p}_{\text{loc}} \cap C^{1,\alpha}_{\text{loc}}$ and we want to show that

$$-\delta_\infty \Delta \rho_1 + \rho_1 = (\mu - V(\mathbf{x}))\chi_{\{\rho_1 > 0\}}, \quad \text{a.e.} \quad \mathbf{x} \in \mathbb{R}^d. \quad (3.5.22)$$

Since $\rho_g^\varepsilon \in W^{2,p}_{\rm loc}$ is a strong solution of (3.5.21), thus (3.5.21) is valid almost everywhere. In addition, $\rho_g^\varepsilon \to \rho_1$ in $C^{1,\alpha}_{\rm loc}$, so we can pass to the limit as $\varepsilon \to 0^+$ in (3.5.21) to get

$$-\delta_\infty \Delta \rho_1 + \rho_1 = \mu - V(\mathbf{x}), \quad \text{a.e.} \quad \mathbf{x} \in \{\rho_1 > 0\}, \tag{3.5.23}$$

where μ is a limiting point of μ_ε as $\varepsilon \to 0^+$ (take a subsequence if necessary here). On the other hand, $\rho_1 \in W^{2,p}_{\rm loc}$ implies $\Delta \rho_1 = 0$ a.e. $\mathbf{x} \in \{\rho_1 = 0\}$. Together, we have shown ρ_1 is the solution of the free boundary value problem (3.5.16) and μ can be computed via multiplying both sides of (3.5.16) by ρ_1 and integrating over $\mathbb{R}^d$, which leads to $\mu = \mu_1$.

(ii) When $V(\mathbf{x}) = V(r)$ ($r = |\mathbf{x}|$) is radially symmetric and non-decreasing, it is easy to find $\rho_j(\mathbf{x})$ is radially symmetric and non-increasing by Schwarz rearrangement [78]. For simplicity, we write $\rho_j(\mathbf{x}) = \rho_j(|\mathbf{x}|) = \rho_j(r)$ ($r = |\mathbf{x}|$, $j = 1, 2$) and $\rho'(r) \le 0$. Integrating (3.5.16) over the ball $B_R = \{|\mathbf{x}| < R\}$, we get

$$\int_{B_R} \big(V(\mathbf{x})\chi_{\{\rho_1>0\}} + \rho_1(\mathbf{x})\big)\, d\mathbf{x} - \delta_\infty \int_{\partial B_R} \partial_n \rho_1(\mathbf{x}) dS = \mu \int_{B_R} \chi_{\{\rho_1>0\}}\, d\mathbf{x},$$

where $\partial_{\mathbf{n}} \rho_1(\mathbf{x})|_{\partial B_R} \le 0$ ($\rho_1(r)$ is non-increasing). On the other hand, $\lim\limits_{r\to\infty} V(r) = \infty$, choosing R_0 large enough such that $V(r) \ge 2\mu$ ($r \ge R_0$), we have

$$\int_{B_R \setminus B_{R_0}} \big[(V(\mathbf{x}) - \mu)\chi_{\{\rho_1>0\}} + \rho_1(\mathbf{x})\big]\, d\mathbf{x} \le \mu |B_{R_0}|,$$

which is true for all $R > 0$. Thus, we arrive at

$$|B^c_{R_0} \cap \chi_{\{\rho_1>0\}}| \le |B_{R_0}|, \tag{3.5.24}$$

and it implies that $|\{\rho_1 > 0\}| < \infty$. Therefore ρ_1 is compactly supported. Similarly, ρ_2 is also compactly supported under the hypothesis of $V(\mathbf{x})$. □

Next, we consider another interesting case that $\beta \to -\infty$ and/or large δ.

Theorem 3.5.3. *(Limits when $\beta \to -\infty$) Let $V(\mathbf{x})$ ($\mathbf{x} \in \mathbb{R}^d$, $d = 1, 2, 3$) be given in (2.4.2), $\beta < 0$, $\delta > 0$, $\phi_g \in S$ be a positive ground state of (2.4.7).*

(1) If $\beta \to -\infty$ and $\delta = O(|\beta|^{\frac{4+d}{2+d}})$, i.e. $\lim_{\beta\to+\infty} \frac{\delta}{|\beta|^{\frac{4+d}{2+d}}} = \delta_\infty > 0$. Set $\phi_g^\varepsilon(\mathbf{x}) = \varepsilon^{-d/2}\phi_g(\mathbf{x}/\varepsilon) \in S$ with $\varepsilon = |\beta|^{-\frac{1}{2+d}}$. For $\beta \to -\infty$ ($\varepsilon \to 0^+$), there exists a subsequence $\beta_n \to -\infty$ ($n = 1, 2, \ldots$), such that for $\varepsilon_n = |\beta_n|^{-\frac{1}{2+d}} \to 0^+$ and $\rho^{\varepsilon_n}(\mathbf{x}) = \varepsilon_n^{-d}|\phi_g^{\beta_n}(\mathbf{x}/\varepsilon_n)|^2$, we have $\rho^{\varepsilon_n}(\mathbf{x}) \to \rho_g(\mathbf{x})$ in H^1, where $\rho_g(\mathbf{x})$ is a nonnegative minimizer of the energy

$$E_{\delta_\infty}(\sqrt{\rho}) = \int_{\mathbb{R}^d} \left(V(\mathbf{x})\rho - \frac{1}{2}\rho^2 + \frac{\delta_\infty}{2}|\nabla\rho|^2 \right) d\mathbf{x}, \quad \|\rho(\mathbf{x})\|_{L^1} = 1, \quad \rho(\mathbf{x}) \geq 0. \tag{3.5.25}$$

(2) If $\beta \to -\infty$ and $\delta/|\beta|^{\frac{4+d}{2+d}} \gg 1$, i.e. $\beta = o(\delta^{\frac{2+d}{4+d}})$ as $\delta \to +\infty$. Set $\phi_g^\varepsilon(\mathbf{x}) = \varepsilon^{-d/2}\phi_g(\mathbf{x}/\varepsilon) \in S$ with $\varepsilon = \delta^{-\frac{1}{4+d}}$. For $\delta \to +\infty$ ($\varepsilon \to 0^+$), we have $\rho_g^\varepsilon(\mathbf{x}) = |\phi_g^\varepsilon(\mathbf{x})|^2$ converges to $\rho_\infty(\mathbf{x})$ in H^1, where $\phi_\infty(\mathbf{x}) = \sqrt{\rho_\infty(\mathbf{x})}$ is the unique nonnegative minimizer of the energy $E_3(\cdot)$ (3.5.7).

(3) If $\beta \to -\infty$ and $\delta = o(|\beta|^{\frac{4+d}{2+d}})$, we also assume that $V(\mathbf{x})$ is radially symmetric and the ground state $\phi_g \in S$ can be chosen as a decreasing radially symmetric function. Let $\phi_g^\varepsilon(\mathbf{x}) = \varepsilon^{-d/2}\phi_g(\mathbf{x}/\varepsilon) \in S$ with $\varepsilon = |\beta|^{1/2}/\delta^{1/2}$, and $\rho^\varepsilon = |\phi_g^\varepsilon| \to \rho_\infty$ in H^1 as $\beta \to -\infty$, where ρ_∞ is the unique non-increasing radially symmetric minimizer of the following energy

$$E_r(\sqrt{\rho}) = \int_{\mathbb{R}^d} \left(\frac{1}{2}|\nabla\rho|^2 - \frac{1}{2}|\rho|^2 \right) d\mathbf{x}, \quad \int_{\mathbb{R}^d} \rho(\mathbf{x})\, d\mathbf{x} = 1, \quad \rho(\mathbf{x}) \geq 0. \tag{3.5.26}$$

In fact, ρ_∞ solves the equation

$$-\Delta\rho_\infty - \rho_\infty = \mu\chi_{\{\rho_\infty>0\}}, \quad \mu = 2E_r(\sqrt{\rho_\infty}). \tag{3.5.27}$$

Proof. (1) The existence of the nonnegative minimizer of E_{δ_∞} can be proved similarly to Theorem 7.1.1 and we omit the details here for brevity.

Let $\varepsilon = |\beta|^{-\frac{1}{2+d}}$ and $\rho^\varepsilon(\mathbf{x}) = \varepsilon^{-d}|\phi_g(\mathbf{x}/\varepsilon)|^2$ where $\phi_g(\mathbf{x})$ is a ground state of (1.2.8), then $\sqrt{\rho^\varepsilon} \in S$ is a ground state of (3.5.3). Using Nash inequality with the fact $\sqrt{\rho^\varepsilon} \in S$, we can easily find

$$\int_{\mathbb{R}^d} V(\mathbf{x})\rho^\varepsilon(\mathbf{x})\, d\mathbf{x} + \|\nabla\rho^\varepsilon\| + \|\rho^\varepsilon\| \leq C. \tag{3.5.28}$$

We can extract a subsequence $\varepsilon_n \to 0$, such that for some $\rho_0 \in H^1$, we have

$$\rho^{\varepsilon_n} \to \rho_0, \quad \text{weakly in } H^1, \quad \text{weakly-}\star \quad \text{in } L^1_V = \{\rho | \int_{\mathbb{R}^d} V(\mathbf{x})|\rho|\, dx < +\infty\}, \tag{3.5.29}$$

and

$$\int_{\mathbb{R}^d} V(\mathbf{x})\rho_0(\mathbf{x}) + \|\nabla\rho_0\| + \|\rho_0\| \le \liminf_{\varepsilon_n \to 0^+} \left(\int_{\mathbb{R}^d} V(\mathbf{x})\rho^{\varepsilon_n}(\mathbf{x}) + \|\nabla\rho^{\varepsilon_n}\| + \|\rho^{\varepsilon_n}\| \right).$$

We then show that the convergence is strong in L^2. For any $\eta > 0$, there exists $R > 0$ such that $\int_{|\mathbf{x}|>R} \rho^{\varepsilon_n}(\mathbf{x})\, d\mathbf{x} < \eta$ (confining property of $V(\mathbf{x})$). Since $H^1(B_R) \hookrightarrow L^2(B_R)$ is compact, $\int_{|\mathbf{x}|\le R} |\rho^{\varepsilon_n}(\mathbf{x}) - \rho_0(\mathbf{x})|^2\, d\mathbf{x} \to 0$ and

$$\begin{aligned}
&\limsup_{\varepsilon_n\to 0} \|\rho^{\varepsilon_n} - \rho_0\|^2 \\
&= \limsup_{\varepsilon_n\to 0} \int_{|\mathbf{x}|\le R} |\rho^{\varepsilon_n}(\mathbf{x}) - \rho_0(\mathbf{x})|^2\, d\mathbf{x} + \limsup_{\varepsilon_n\to 0} \int_{|\mathbf{x}|>R} |\rho^{\varepsilon_n}(\mathbf{x}) - \rho_0(\mathbf{x})|^2\, d\mathbf{x} \\
&\le \limsup_{\varepsilon_n\to 0} \left(\int_{|\mathbf{x}|>R} |\rho^{\varepsilon_n}(\mathbf{x}) - \rho_0(\mathbf{x})|\, d\mathbf{x} \right)^{\frac{1}{2}} \left(\int_{|\mathbf{x}|>R} |\rho^{\varepsilon_n}(\mathbf{x}) - \rho_0(\mathbf{x})|^3\, d\mathbf{x} \right)^{\frac{1}{2}} \\
&\le C\eta^{1/2}.
\end{aligned}$$

Hence $\limsup_{\varepsilon_n\to 0} \|\rho^{\varepsilon_n} - \rho_0\|^2 = 0$ and $\rho^{\varepsilon_n} \to \rho_0$ in L^2, which implies that $\rho_0(\mathbf{x}) \ge 0$. Similarly, due to the confining property of $V(\mathbf{x})$, $\|\rho_0\|_{L^1} = 1$. In particular, regularizing the minimizers of $E_{\delta_\infty}(\cdot)$ in (3.5.25) if necessary, we have

$$E_{\delta_\infty}(\sqrt{\rho_0}) \le \liminf_{\varepsilon^n\to 0} E_{\delta_\infty}(\sqrt{\rho^{\varepsilon_n}}) \le \limsup_{\varepsilon^n\to 0} E^{\varepsilon_n}(\sqrt{\rho^{\varepsilon_n}}) \le E^{\varepsilon_n}(\sqrt{\rho_0}),$$

and $E^{\varepsilon_n}(\sqrt{\rho_0}) \le E_{\delta_\infty}(\sqrt{\rho_0}) + o(1)$, which verifies ρ_0 is a minimizer of $E_{\delta_\infty}(\cdot)$ in (3.5.25) as well as $\|\nabla\rho^{\varepsilon_n}\| \to \|\nabla\rho_0\|$. Thus, $\rho^{\varepsilon_n} \to \rho_0$ in H^1.

(2) The proof is similar to part (1) in view of the fact that the minimizer of (3.5.7) is unique, thus it is omitted here for brevity.

(3) We first show the fact that the decreasing radially symmetric minimizer ρ_∞ of (3.5.26) exists and is unique. In view of Nash inequality, $E_r(\sqrt{\rho})$ is bounded from below under constraint $\|\rho\|_{L^1} = 1$ with $\rho \ge 0$. By Schwarz rearrangement, we can take a minimizing sequence of nonincreasing radially symmetric functions

$\{\rho_n\}_{n=1}^{\infty}$ where $\|\rho_n\|_{L^1} = 1$ and $\|\rho_n\|_{H^1} \leq C$. Therefore, there exists $\rho_\infty \in H^1$ such that a subsequence (denoted as the original sequence) $\rho_n \to \rho_\infty$ weakly in H^1. Applying necessary scaling $\rho_n^\eta = \eta^{-d}\rho_n(\mathbf{x}/\eta)$ $(\eta > 0)$ in $E_r(\cdot)$, then $E_r(\sqrt{\rho_n^\eta})$ attains its minimum at some $\eta_n > 0$ and we can take $\rho_n^{\eta_n}$ as the minimizing sequence. As a consequence, we can assume $\eta_n = 1$ and have the relation $\|\rho_n\|^2 = \frac{d}{2+d}\|\nabla\rho_n\|^2$ and $E_r(\sqrt{\rho_n}) < 0$ by the optimality of $\eta_n = 1$ among all the possible scalings. In addition, for the nonincreasing radially symmetric function ρ_n,

$$|\rho_n(\mathbf{x})| \leq \frac{C}{R^d}\|\rho_n\|_{L^1} \leq \frac{C}{R^d}, \quad |\mathbf{x}| \geq R > 0, \tag{3.5.30}$$

which would imply $\rho_n \to \rho_\infty$ strongly in L^2 and so $\rho_\infty \geq 0$. In fact, we can show $\|\rho_\infty\|_{L^1} = 1$. Denote $I_\alpha = \inf_{\rho\geq 0, \|\rho\|_{L^1}=\alpha} E_r(\sqrt{\rho})$ $(\alpha > 0)$, then it is obvious $I_\alpha = \alpha^2 I_1$ and $I_1 < 0$. If $\|\rho_\infty\|_{L^1} = \alpha < 1$, by the convergence of ρ_n, we get

$$\alpha^2 I_1 = I_\alpha \leq E_r(\sqrt{\rho_\infty}) \leq \liminf_{n\to+\infty} E_r(\sqrt{\rho_n}) = I_1, \tag{3.5.31}$$

which leads to $I_1 \geq 0$ contradicting to the fact $I_1 < 0$. Thus $\|\rho_\infty\|_{L^1} = 1$ and ρ_∞ is a non-increasing radially symmetric minimizer of (3.5.26). Next, we show such a minimizer is unique. Following Theorem 3.5.2, we can get the equation for the minimizer of (3.5.26) as

$$-\Delta\rho - \rho = \mu\chi_{\{\rho>0\}}, \tag{3.5.32}$$

and a non-increasing radially symmetric minimizer ρ is compactly supported with the regularity stated in Theorem 3.5.2. If there are two non-increasing radially symmetric minimizers ρ_1 and ρ_2 to the energy (3.5.26), we have

$$-\Delta\rho_1 - \rho_1 = \mu_1\chi_{\{\rho_1>0\}}, \quad -\Delta\rho_2 - \rho_2 = \mu_2\chi_{\{\rho_2>0\}},$$

and $\mu_1 = \mu_2 = 2I_1$. Thus, by integrating the equations, we know ρ_1 and ρ_2 have the same supports (denote as the ball B_R). $\rho_1 = \rho_2$ is then a consequence of classical ODE theory by noticing that $\rho_j(R) = \partial_r\rho_j(R) = 0$. The existence and uniqueness of non-increasing radially symmetric minimizers are proved.

Next, choosing $\varepsilon = \frac{|\beta|^{1/2}}{\delta^{1/2}}$ in (3.5.3), we find ϕ_g^ε minimizes the following energy

$$E_\eta(\phi) = \int_{\mathbb{R}^d} \left[\frac{\eta_1}{2}|\nabla\phi|^2 + \eta_2 V(\mathbf{x})|\phi|^2 - \frac{1}{2}|\phi|^4 + \frac{1}{2}\left|\nabla|\phi|^2\right|^2 \right] d\mathbf{x}, \quad \phi \in S, \tag{3.5.33}$$

with $\eta_1 = \frac{\delta^{\frac{d-2}{2}}}{|\beta|^{d/2}} = o(1)$ and $\eta_2 = \frac{\delta^{\frac{d+2}{2}}}{|\beta|^{\frac{4+d}{2}}} = o(1)$ when $\beta \to -\infty$ and $\delta = o(|\beta|^{\frac{4+d}{2+d}})$. Intuitively, only the leading $O(1)$ terms in (3.5.33) are important in the limit as $\beta \to -\infty$. Under the hypothesis of a radially symmetric increasing potential $V(\mathbf{x})$, we have (regularize $\phi_\infty = \sqrt{\rho_\infty}$ such that $\phi_\infty \in H^1$ if necessary)

$$E_r(\sqrt{\rho_\infty}) \le E_r(\sqrt{\rho_g^\varepsilon}) \le E_\eta(\phi_g^\varepsilon) \le E_\eta(\sqrt{\rho_\infty}) \le o(1) + E_r(\sqrt{\rho_\infty}), \tag{3.5.34}$$

which shows $\lim\limits_{\beta\to-\infty} E_r(\sqrt{\rho_g^\varepsilon}) = E_r(\sqrt{\rho_\infty}) = I_1$. Repeating the previous arguments, we will have $\rho_g^\varepsilon \to \rho_\infty$ in H^1. □

Next, we consider the effects as $\delta \to 0^+$, i.e. the vanishing higher order effects. It is worth noticing that the ground state profiles will have certain blow-up phenomenon as $\delta \to 0^+$ in the classical regimes where the ground state does not exist when $\delta = 0$.

Theorem 3.5.4. *(Limits when $\delta \to 0^+$) Let $V(\mathbf{x})$ ($\mathbf{x} \in \mathbb{R}^d$, $d = 1, 2, 3$) be given in (2.4.2), $\delta > 0$, $\phi_g^\delta \in S$ be a nonnegative ground state of (1.2.8).*

(1) Suppose $\beta > 0$ when $d = 3$, $\beta > -C_b$ when $d = 2$, and $\beta \in \mathbb{R}$ when $d = 1$, where C_b is given in (3.2.4). There exists a subsequence $\delta_n \to 0$ ($n = 1, 2, \ldots$), such that $\phi_g^{\delta_n}(\mathbf{x}) \to \phi_g(\mathbf{x})$ in H^1, where $\phi_g(\mathbf{x})$ is a nonnegative minimizer of the energy

$$E_{\mathrm{GP}}(\phi) = \int_{\mathbb{R}^d} \left[\frac{1}{2}|\nabla\phi|^2 + V(\mathbf{x})|\phi|^2 + \frac{\beta}{2}|\phi|^4 \right] d\mathbf{x} \quad \textit{with} \quad \|\phi\| = 1. \tag{3.5.35}$$

Moreover, when $\beta \ge 0$, the nonnegative minimizer ϕ_g of (3.5.35) is unique and $\phi_g^\delta \to \phi_g$ in H^1 as $\delta \to 0^+$.

(2) When $d = 2$ and $\beta < -C_b$, denote $\tilde{\phi}_\delta(\mathbf{x}) = \sqrt{\delta}\phi_g^\delta(\sqrt{\delta}\mathbf{x})$ and we have for a subsequence $\delta_n \to 0$, $\tilde{\phi}_{\delta_n}(\mathbf{x}) \to \phi_0(\mathbf{x})$ in H^1, where $\phi_0(\mathbf{x})$ is a nonnegative minimizer of the energy

$$E_\beta(\phi) = \int_{\mathbb{R}^d} \left[\frac{1}{2}|\nabla\phi|^2 + \frac{\beta}{2}|\phi|^4 + \frac{1}{2}|\nabla|\phi|^2|^2 \right] d\mathbf{x} \quad \textit{with} \quad \|\phi\| = 1. \tag{3.5.36}$$

(3) When $d = 3$ and $\beta < 0$, we also assume that $V(\mathbf{x})$ is radially symmetric and it is sufficient to consider the ground state $\phi_g^\delta(\mathbf{x})$ as decreasing radially symmetric functions. Let $\tilde{\rho}_\delta(\mathbf{x}) = |\tilde{\phi}_\delta(\mathbf{x})|^2$, where $\tilde{\phi}_\delta(\mathbf{x}) = \delta^{3/4}\phi_g^\delta(\sqrt{\delta}\mathbf{x})$. There exists $0 \le \rho_0(\mathbf{x}) \in H^1$ such that $\tilde{\rho}_\delta \to \rho_0$ in H^1 as $\delta \to 0$, where ρ_0 is the unique decreasing radially symmetric nonnegative minimizer of the energy

$$E_r^\beta(\sqrt{\rho}) = \int_{\mathbb{R}^d} \left[\frac{\beta}{2}|\rho|^2 + \frac{1}{2}|\nabla\rho|^2\right] d\mathbf{x}, \quad \rho \ge 0, \quad \int_{\mathbb{R}^d} \rho(\mathbf{x})\, d\mathbf{x} = 1. \tag{3.5.37}$$

More precisely, $\rho_0 \ge 0$ satisfies the free boundary problem

$$\beta\rho - \Delta\rho = \mu\chi_{\{\rho>0\}}, \quad \rho|_{\partial\{\rho>0\}} = |\nabla\rho|\Big|_{\partial\{\rho>0\}} = 0, \tag{3.5.38}$$

where $\mu = 2E_r^\beta(\sqrt{\rho_0})$.

Proof. (1) The proof is similar to that presented in Theorem 3.5.3 and is omitted here for brevity.

(2) The existence of the nonnegative minimizer of $E_\beta(\cdot)$ can be proved by a similar argument in Theorem 3.5.3 for the energy $E_r(\cdot)$ and the detail is omitted here. We denote the minimum energy of $E_\beta(\cdot)$ as E_0.

Letting $\varepsilon = \delta^{-1/2}$ in (3.5.3), it is obvious that $\tilde{\phi}_\delta(\mathbf{x}) \in S$ minimizes the energy

$$\tilde{E}_\delta(\phi) = \int_{\mathbb{R}^d} \left[\frac{1}{2}|\nabla\phi|^2 + \delta^2 V(\mathbf{x})|\phi|^2 + \frac{\beta}{2}|\phi|^4 + \frac{1}{2}|\nabla|\phi|^2|^2\right] d\mathbf{x}, \quad \phi \in S. \tag{3.5.39}$$

Now, choosing a ground state $\phi_g \in S$ of (3.5.36) as a testing state (using a C_0^∞ approximation if necessary for the potential term), we have

$$\delta^2 \int_{\mathbb{R}^d} V(\mathbf{x})|\tilde{\phi}_\delta(\mathbf{x})|^2\, d\mathbf{x} + E_\beta(\tilde{\phi}_\delta) = \tilde{E}_\delta(\tilde{\phi}_\delta) \le \tilde{E}_\delta(\phi_g) \le E_0 + C\delta^2,$$

which implies $\int_{\mathbb{R}^d} V(\mathbf{x})|\tilde{\phi}_\delta(\mathbf{x})|^2\, d\mathbf{x} \le C$. Therefore, we have

$$\int_{\mathbb{R}^d} V(\mathbf{x})|\tilde{\phi}_\delta(\mathbf{x})|^2\, d\mathbf{x} + \|\tilde{\phi}_\delta\|_{H^1} + \|\nabla|\tilde{\phi}_\delta|^2\| \le C.$$

Following the proof in Theorem 7.1.1, there exists $\phi_0 \in H^1$ with $\|\phi_0\| = 1$ and a subsequence $\delta_n \to 0$ such that $\phi_{\delta_n} \to \phi_0$ strongly in L^2 and weakly in H^1,

$$E_\beta(\phi_0) \le \liminf_{n\to\infty} E_\beta(\tilde{\phi}_{\delta_n}) \le \liminf_{n\to\infty} \tilde{E}_\delta(\tilde{\phi}_{\delta_n}) \le E_0,$$

and ϕ_0 is a minimizer of (3.5.36). From the above inequality, it is easy to find that $\phi_{\delta_n} \to \phi_0$ strongly in H^1.

(3) The proof is essentially presented in part (3) of Theorem 3.5.3. □

3.6 Limiting behavior under a box potential

Now we consider (2.4.9) defined in a bounded domain $\Omega \subset \mathbb{R}^d$, the limiting profile of ground states (3.2.1) are considered under different sets of parameters δ and β. To simplify the discussion, we choose the external potential as box potential (2.4.3). The energy $E(\cdot)$ (2.4.10) reduces to

$$E_\Omega(\phi) = \int_\Omega \left[\frac{1}{2}|\nabla\phi|^2 + \frac{\beta}{2}|\phi|^4 + \frac{\delta}{2}\left|\nabla|\phi|^2\right|^2\right] d\mathbf{x}, \tag{3.6.1}$$

and the ground state ϕ_g is then the minimizer of the energy E_Ω under the constraint $\|\phi\|_{L^2(\Omega)} = 1$. The characterization of the ground state ϕ_g for (3.6.1) in some limiting case is listed in the following lemma. The major difference between whole space case (section 3.5) and bounded domain case is that the scalings are very different.

Theorem 3.6.1. *(Thomas-Fermi limit) Let $V(\mathbf{x})$ be the box potential (2.4.3), $\delta > 0$, and $\phi_g \in S$ be the positive ground state of (1.2.8).*

(1) If $\beta \to +\infty$ and $\delta = o(\beta)$, we have $\rho_g^\beta = |\phi_g(\mathbf{x})|^2$ converge to $\rho_\infty(\mathbf{x}) := |\phi_\infty(\mathbf{x})|^2$ in L^2, where $\phi_\infty(\mathbf{x})$ is the unique nonnegative minimizer of the energy

$$E_b(\phi) = \int_\Omega \frac{1}{2}|\phi|^4\, d\mathbf{x} \quad \text{with} \quad \|\phi\|^2 = 1. \tag{3.6.2}$$

More precisely, $\rho_\infty = \frac{1}{|\Omega|}$ with $\mu = \frac{\beta}{2|\Omega|}$, where $|\Omega|$ is the the volume of the domain Ω.

(2) If $\beta \to +\infty$ and $\lim\limits_{\beta\to+\infty} \frac{\delta}{\beta} = \delta_0 > 0$ for some $\delta_0 > 0$, we have $\rho_g^{\beta,\delta} = |\phi_g(\mathbf{x})|^2$ converge to $\rho_\infty(\mathbf{x})$ in H^1, where $\rho_\infty(\mathbf{x})$ is the unique nonnegative minimizer of the energy

$$E_{\rm bd}^+(\sqrt{\rho}) = \int_\Omega \left[\frac{1}{2}|\rho|^2 + \frac{\delta_0}{2}|\nabla\rho|^2\right] d\mathbf{x}, \quad \rho \geq 0, \quad \int_\Omega \rho(\mathbf{x})\, d\mathbf{x} = 1. \tag{3.6.3}$$

More precisely, $\rho_\infty(\mathbf{x}) \geq 0$ *satisfies the equation*

$$\rho_\infty(\mathbf{x}) - \delta_0 \Delta \rho_\infty(\mathbf{x}) = \mu, \quad \mathbf{x} \in \Omega, \quad \rho_\infty(\mathbf{x})|_{\partial\Omega} = 0, \tag{3.6.4}$$

where $\mu = 2E^+_{\rm bd}(\sqrt{\rho_\infty})$.

(3) If $\delta \to +\infty$ *and* $\beta = o(\delta)$, *we have* $\rho_g^\delta = |\phi_g(\mathbf{x})|^2$ *converge to* $\rho_\infty(\mathbf{x})$ *in* H^1, *where* $\rho_\infty(\mathbf{x})$ *is the unique nonnegative minimizer of the energy*

$$E_d(\sqrt{\rho}) = \int_\Omega \frac{1}{2}|\nabla \rho|^2 \, d\mathbf{x}, \quad \rho \geq 0, \quad \int_\Omega \rho(\mathbf{x}) \, d\mathbf{x} = 1. \tag{3.6.5}$$

More precisely, $\rho_\infty(\mathbf{x}) \geq 0$ *satisfies the equation*

$$-\Delta \rho_\infty(\mathbf{x}) = \mu, \quad \mathbf{x} \in \Omega, \quad \rho_\infty(\mathbf{x})|_{\partial\Omega} = 0, \tag{3.6.6}$$

where $\mu = 2E_d(\sqrt{\rho_\infty})$.

Proof. The proof is similar to those in Theorem 3.5.1 for the whole space case. □

Remark 3.6.1. *In the Theorem 3.6.1, case (3) holds true in the case* $\beta \to -\infty$ *and* $\delta \gg |\beta|$, *i.e.* $\beta = o(\delta)$.

Remark 3.6.2. *For case (2), when* $\beta \to -\infty$ *and* $\lim_{\beta\to-\infty} \frac{\delta}{|\beta|} = \delta_0 > 0$ *for some* $\delta_0 > 0$, *we have there exists a subsequence of* $\beta_n \to -\infty$ *and* δ_n, *such that* $\rho_g^{\beta_n,\delta_n} = |\phi_g^{\beta_n,\delta_n}(\mathbf{x})|^2$ *converges to* $\rho_\infty(\mathbf{x})$ *in* H^1, *and* $\rho_\infty(\mathbf{x})$ *is a nonnegative minimizer of the energy*

$$E^-_{bd}(\sqrt{\rho}) = \int_\Omega \left[-\frac{1}{2}|\rho|^2 + \frac{\delta_0}{2}|\nabla \rho|^2\right] d\mathbf{x}, \quad \rho \geq 0, \quad \int_\Omega \rho(\mathbf{x}) \, d\mathbf{x} = 1. \tag{3.6.7}$$

It remains to consider the last case in the Theorem 3.6.1 as $\beta \to -\infty$ and $\delta = o(|\beta|)$. For simplicity, we assume Ω is a ball in $\mathbb{R}^d$.

Theorem 3.6.2. *Let* $\Omega = B_R = \{|\mathbf{x}| < R\}$ *in the box potential given in (2.4.3),* $\beta < 0$ *and* $\delta > 0$, $\phi_g^\beta \in H^1(\Omega)$ *be a non-increasing radially symmetric ground state of (3.6.1). Define* $\tilde{\phi}_g^\beta \in H^1(\mathbb{R}^d)$ *such that* $\tilde{\phi}_g^\beta(\mathbf{x}) = 0$ *when* $\mathbf{x} \notin \Omega$, *and* $\tilde{\phi}_g^\beta(\mathbf{x}) = \phi_g^\beta(\mathbf{x})$ *when* $\mathbf{x} \in \Omega$. *Let* $\tilde{\phi}_g^\varepsilon(\mathbf{x}) = \varepsilon^{d/2}\tilde{\phi}_g^\beta(\mathbf{x}\varepsilon) \in S$ *with* $\varepsilon = \delta^{1/2}/|\beta|^{1/2}$, *thus* $\varepsilon \to 0^+$ *as* $\beta \to -\infty$. *We have* $\tilde{\rho}^\varepsilon = |\tilde{\phi}_g^\varepsilon|^2 \to \rho_\infty$ *in* H^1 *as* $\varepsilon \to 0^+$, *where* ρ_∞ *is the unique non-increasing radially symmetric minimizer of energy* $E_r(\cdot)$ *in (3.5.26).*

Proof. Let $\Omega^\varepsilon = \{\mathbf{x}/\varepsilon, \mathbf{x} \in \Omega\}$. Since ρ_∞ is compactly supported as shown in Theorem 3.5.3, for sufficiently small $\varepsilon > 0$, we have $\mathrm{supp}(\rho_\infty) \subset \Omega^\varepsilon$. On the other hand, $\tilde{\phi}_g^\varepsilon$ minimizes the energy

$$E^\eta_{\mathrm{box}}(\phi) = \int_{\mathbb{R}^d} \left[\frac{\eta}{2} |\nabla \phi|^2 - \frac{1}{2}|\phi|^4 + \frac{1}{2} \left| \nabla |\phi|^2 \right|^2 \right] d\mathbf{x}, \quad \phi \in H_0^1(\Omega^\varepsilon), \quad \|\phi\| = 1, \tag{3.6.8}$$

where $\eta = \frac{\delta^{\frac{d-2}{2}}}{|\beta|^{\frac{d}{2}}} = o(1)$ as $\varepsilon \to 0^+$. We can then proceed as that in Theorem 3.5.3 and the limit of $\tilde{\rho}^\varepsilon$ as $\beta \to -\infty$ ($\varepsilon \to 0^+$) follows. □

Similarly, we could extend the $\delta \to 0^+$ limiting results in Theorem 3.5.4 to the bounded domain case too. Since no different scaling is involved, the extension is straightforward and we omit it here for brevity.

Chapter 4

Numerical Methods for Computing Ground States

In this chapter, we aim to propose three methods for computing the ground state of the MGPE (2.4.1). The first two methods, namely the normalized gradient flow method and the method of directly minimizing the discretized energy formulated via the wave function, are direct generalizations of the methods commonly used for the traditional GPE (1.2.5). The last method, which minimizes the discretized energy formulated via the density function, is seldomly used for the traditional GPE (1.2.5) but might have advantage for the MGPE (2.4.1) due to the fact that the HOI term is now changed to a quadratic term. For each method, the detailed description of the scheme and some numerical analysis as well as numerical tests will be provided.

4.1 The normalized gradient flow method

In this section, we will extend the normalized gradient flow method, which is a widely used method for the GPE, to the MGPE problem. For completeness, we

start from the continuous normalized gradient flow,

$$\phi_t = \frac{1}{2}\Delta\phi - V(\mathbf{x})\phi - \beta|\phi|^2\phi + \delta\Delta(|\phi|^2)\phi + \mu_\phi(t)\phi, \quad \mathbf{x} \in \Omega,\ t \geq 0, \tag{4.1.1}$$

$$\phi(\mathbf{x}, t) = 0, \quad \mathbf{x} \in \partial\Omega, \tag{4.1.2}$$

$$\phi(\mathbf{x}, 0) = \phi_0(\mathbf{x}), \quad \mathbf{x} \in \Omega, \tag{4.1.3}$$

where Ω is the domain where MGPE is defined and $\mu_\phi(t)$ depending on $\phi = \phi(\mathbf{x}, t)$ is defined as

$$\mu_\phi(t) = \frac{1}{\|\phi(\cdot, t)\|} \int_\Omega \left[\frac{1}{2}|\nabla\phi|^2 + V(\mathbf{x})|\phi|^2 + \beta|\phi|^4 + \delta|\nabla(|\phi|^2)|^2\right] d\mathbf{x}. \tag{4.1.4}$$

Following a procedure that is almost the same as in [18], we can establish the following energy diminishing property. The proof is omitted here for brevity.

Theorem 4.1.1. *Suppose $V(\mathbf{x}) \geq 0$ for all $\mathbf{x} \in \Omega, \beta \geq 0$ and $\|\phi_0\|_2 = 1$. Then the normalized gradient flow (4.1.1)-(4.1.3) is normalization conservation and energy diminishing, i.e.*

$$\|\phi(\cdot, t)\|_2^2 = \|\phi_0\|_2 = 1, \quad t \geq 0, \tag{4.1.5}$$

$$\frac{d}{dt}E(\phi) = -2\|\phi_t(\cdot, t)\|_2^2, \quad t \geq 0, \tag{4.1.6}$$

which implies that

$$E(\phi(\cdot, t_1)) \geq E(\phi(\cdot, t_2)), \quad 0 \leq t_1 \leq t_2 < \infty. \tag{4.1.7}$$

In practice, we can discretise the continuous normalized gradient flow in time in the following way: choose a sequence $0 = t_0 < t_1 < \cdots < t_n < \ldots$ with $\Delta t_n = t_{n+1} - t_n > 0$ and compute the following semi-discrete scheme, i.e. the normalized gradient flow,

$$\phi_t = \frac{1}{2}\Delta\phi - V(\mathbf{x})\phi - \beta|\phi|^2\phi + \delta\Delta(|\phi|^2)\phi, \quad \mathbf{x} \in \Omega,\ t_n < t < t_{n+1}, \tag{4.1.8}$$

$$\phi(\mathbf{x}, t) = 0, \quad \mathbf{x} \in \partial\Omega, \tag{4.1.9}$$

$$\phi(\mathbf{x}, t_{n+1}) := \phi(\mathbf{x}, t_{n+1}^+) = \frac{\phi(\mathbf{x}, t_{n+1}^-)}{\|\phi(\mathbf{x}, t_{n+1}^-)\|_2}, \quad \mathbf{x} \in \Omega, \tag{4.1.10}$$

$$\phi(\mathbf{x}, 0) = \phi_0(\mathbf{x}), \quad \mathbf{x} \in \Omega. \tag{4.1.11}$$

Easy to see that the semi-discrete scheme for the normalized gradient flow (4.1.8)-(4.1.11) collapses to the continuous scheme (4.1.1)-(4.1.3) as $\max\{\Delta t_n\} \to 0$. For simplicity, we consider the simplest case where we discretize uniformly in time, i.e.

$$t_n = n\Delta t, \quad \text{with } \Delta t > 0 \text{ and } n = 0, 1, 2, \dots. \tag{4.1.12}$$

In space, we discretize (4.1.8)-(4.1.11) via the finite difference method and get the following semi-implicit scheme. Only 1D problem is considered here for simplicity, and the extension to 2D or 3D is straightforward. An equivalent form of the normalized gradient flow scheme (4.1.8) is studied due to some technical reasons,

$$\partial_t \phi = \frac{1}{2}\partial_{xx}\phi - V\phi - \beta|\phi|^2\phi + \delta\partial_{xx}|\phi|^2\phi \tag{4.1.13}$$

$$= (\frac{1}{2} + 2\delta|\phi|^2)\partial_{xx}\phi - V\phi - \beta|\phi|^2\phi + 2\delta(\partial_x\phi)^2\phi \tag{4.1.14}$$

Take $U = (a, b)$ to be an interval in 1D and denote the grid points as

$$x_j = a + jh, \text{ for } j = 0, 1, \dots N, \tag{4.1.15}$$

where $h = (b-a)/N$ is the mesh size. It's obvious that the $N+1$ points are evenly distributed, i.e. $a = x_0 < x_1 < \cdots < x_{N-1} < x_N = b$ is the equidistant partition of U. Let ϕ_j be the numerical approximation of $\phi(x_j)$ for $j = 0, 1, \dots, N$ and denote

$$\Phi = (\phi_1, \dots, \phi_{N-1})^T \in \mathbb{R}^{N-1}. \tag{4.1.16}$$

By the homogenous Dirichlet BC, we have $\phi_0 = \phi(a) = \phi_N = \phi(b) = 0$. And we use the super-index to denote time, i.e. Φ^n is the numerical solution after n steps. Then we can get the following backward Euler finite difference (BEFD) scheme depending on the sign of β:

if $\beta < 0$, the scheme is

$$\frac{\phi_j^{n+1} - \phi_j^n}{\Delta t} = \left(\frac{1}{2} + 2\delta|\phi_j^n|^2\right)\delta_x^2\phi_j^{n+1} - V\phi_j^{n+1} - \beta|\phi_j^n|^2\phi_j^n + 2\delta(\delta_x\phi_j^n)^2\phi_j^n, \tag{4.1.17}$$

if $\beta > 0$, the scheme is

$$\frac{\phi_j^{n+1} - \phi_j^n}{\Delta t} = \left(\frac{1}{2} + 2\delta|\phi_j^n|^2\right)\delta_x^2\phi_j^{n+1} - V\phi_j^{n+1} - \beta|\phi_j^n|^2\phi_j^{n+1} + 2\delta(\delta_x\phi_j^n)^2\phi_j^n, \tag{4.1.18}$$

where δ_x and δ_x^2 are the finite difference operators approximating ∂_x and ∂_{xx} and $j = 0, 1, \ldots, N$. The only difference between (4.1.17) and (4.1.18) is that for $\beta < 0$, we treat the term $\beta|\phi|^2\phi$ explicitly while for $\beta > 0$, $\beta|\phi|^2\phi$ is treated semi-implicitly. Notice that if we write the scheme (4.1.17) and (4.1.18) in a matrix form, i.e. $\Phi^{n+1} = A\Phi^n + d_n$, then the matrix A will be sparse and strictly diagonal dominant, which enables us to apply iterative solvers, for example the Gauss-Seidel method, for the efficient computation in each time step and the convergence is guaranteed.

Remark 4.1.1. *The schemes (4.1.17) and (4.1.18) introduced above are semi-implicit. We may also consider a fully implicit scheme. Although an iteration is needed for each step, the total computation cost may be not so large since a larger time step can be applied. The update from $t = t_n$ to $t = t_{n+1}$ can be computed as*

$$\frac{\phi^{(m+1)} - \phi^n}{\Delta t} = \left(\frac{1}{2} + \delta|\phi^{(m)}|^2\right)\partial_{xx}\phi^{(m+1)} - V\phi^{(m+1)} - \beta|\phi^{(m)}|^2\phi^{(m+1)} + 2\delta(\partial_x\phi^{(m)})^2\phi^{(m+1)},$$

until $\phi^{(m)}$ converge. Then ϕ^{n+1} is chosen as $\phi^{n+1} = \lim_{m\to\infty}\phi^{(m)}$.

Next, we will do the numerical tests to check the accuracy of the BEFD method with $\beta > 0$ (4.1.18). Because we will test the accuracy for the method proposed in Section 4.2 and 4.3 as well, the setup of the numerical test is summarized as below.

Example 4.1.1. *We take $d = 1$ and choose the external potential to be the harmonic potential $V(x) = x^2/2$ with $x \in (-16, 16)$. The Dirichlet BC is applied and two cases are tested.*

Case I: $\beta = 400$ and $\delta = 0$.

Case II: $\beta = 1$ and $\delta = 100$.

The initial conditions are chosen to be the proper Thomas-Fermi (TF) approximations as proposed in Section 3.3.2, i.e. the TF approximation for large β (Regime I) for case I and the TF approximation for large δ (Regime III) for case II. The accurate solutions are chosen to be the results computed with a sufficiently small mesh size $h = \frac{1}{256}$. We denote the computed 'exact' ground state as ϕ_g with energy $E_g = E(\phi_g)$ and chemical potential $\mu_g = \mu(\phi_g)$. It can be computed that for Case I, $E_g = 21.360$ and $\mu_g = 35.577$, and for Case II, $E_g = 2.737$ and $\mu_g = 3.823$.

Error	$h = 1/2$	$h/2$	$h/2^2$	$h/2^3$
$\lvert E(\phi_{g,h}^{\mathrm{FD}}) - E(\phi_g)\rvert$	9.65E-4	2.54E-4	6.43E-5	1.61E-5
rate	-	1.92	1.98	2.00
$\lVert\phi_{g,h}^{\mathrm{FD}} - \phi_g\rVert_{l_2}$	1.44E-3	3.13E-4	7.70E-5	1.91E-5
rate	-	2.20	2.02	2.01
$\lVert\phi_{g,h}^{\mathrm{FD}} - \phi_g\rVert_{h_1}$	4.04E-3	9.82E-4	2.48E-4	6.18E-5
rate	-	2.04	1.99	2.00
$\lVert\phi_{g,h}^{\mathrm{FD}} - \phi_g\rVert_{\infty}$	1.24E-3	2.89E-4	7.53E-5	1.87E-5
rate	-	2.10	1.94	2.01

Table 4.1: Spatial resolution of the ground state for Case I in Example 4.1.1.

We denote the numerical ground state by BEFD (4.1.18) to be $\phi_{g,h}^{\mathrm{FD}}$, then Table 4.1 listed the errors for Case I and Table 4.2 listed the errors for Case II. Fig. 4.1 plots the ground states for Case I and Case II. From Table 4.1 and Table 4.2, we can see that the BEFD method (4.1.18) is second order accurate in space.

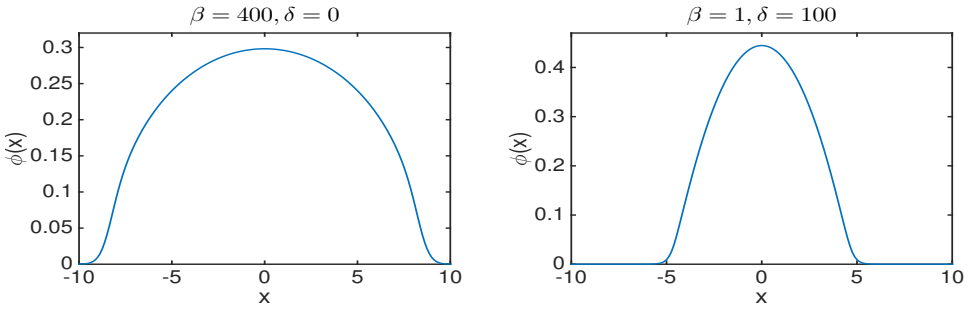

Figure 4.1: Ground states for Case I and Case II in Example 4.1.1.

Error	$h = 1/2$	$h/2$	$h/2^2$	$h/2^3$
$\lvert E(\phi_{g,h}^{\mathrm{FD}}) - E(\phi_g)\rvert$	1.02E-2	2.76E-3	6.99E-4	1.75E-4
rate	-	1.89	1.98	1.99
$\lVert\phi_{g,h}^{\mathrm{FD}} - \phi_g\rVert_{l_2}$	8.71E-3	1.67E-3	4.13E-4	1.02E-4
rate	-	2.37	2.02	2.01
$\lVert\phi_{g,h}^{\mathrm{FD}} - \phi_g\rVert_{h_1}$	1.78E-2	3.65E-3	9.21E-4	2.29E-4
rate	-	2.29	1.99	2.01
$\lVert\phi_{g,h}^{\mathrm{FD}} - \phi_g\rVert_{\infty}$	8.06E-3	1.45E-3	3.97E-4	9.79E-5
rate	-	2.48	1.87	2.02

Table 4.2: Spatial resolution of the ground state for Case II in Example 4.1.1.

4.2 A gradient method for minimizing discretized energy function

In this section, we introduce the finite difference and pseudo-spectral discretization of the energy functional (2.4.6) and constraint (2.4.5) in the constrained minimization problem (2.4.7). Then the original minimization problem is reduced to a finite dimensional problem with a spherical constraint. It's worth noticing that this is a nonconvex optimization problem because the feasible region is a unit sphere, which is not convex. As shown in Theorem 7.1.1, we may choose the ground state to be a real function. Besides, since the external trapping potential satisfies the confining condition, i.e. $\lim_{R\to\infty} \operatorname{ess\,inf}_{|\mathbf{x}|<R} V(\mathbf{x}) = \infty$, the ground state defined by (2.4.7) decays exponentially as $|x| \to \infty$ as shown in Theorem 3.2.2. Thus we can truncate the energy function and constraint from the whole space $\mathbb{R}^d$ to a bounded domain U, which is large enough such that the truncation error is negligible and the homogeneous Dirichlet BC can be applied.

4.2.1 Finite difference discretization

In this part, we consider the finite difference (FD) discretization of (2.4.6) and (2.4.5) truncated on a bounded computational domain U with homogeneous Dirichlet boundary condition. We approximate gradients by the central difference and compute the integrals using the composite trapezoidal quadrature. For simplicity, only the 1D case is shown here. Extensions to 2D and 3D are straightforward and the details are omitted here for brevity.

For $d = 1$, we adopt the notations (4.1.15) and (4.1.16) introduced in the last section. The energy functional (2.4.6) under constraint (2.4.5) with $d = 1$ can then be formulated as

$$E_h^{\mathrm{FD}}(\Phi) = h \sum_{j=0}^{N-1} \left[\frac{1}{2} \left| \frac{\phi_{j+1} - \phi_j}{h} \right|^2 + V(x_j)\phi_j^2 + \frac{\beta}{2}\phi_j^4 + \frac{\delta}{2} \left| \frac{\phi_{j+1}^2 - \phi_j^2}{h} \right|^2 \right], \quad (4.2.1)$$

subject to $h\sum_{j=0}^{N-1} |\phi_j|^2 = 1$ and $\phi_0 = \phi_N = 0$. For simplicity, we introduce $\|\Phi\|_{l_2} = \sqrt{h\sum_{j=0}^{N-1} |\phi_j|^2}$ to be the discrete l_2-norm. A simple computation implies that (4.2.1) can be rewritten in the form

$$E_h^{\mathrm{FD}}(\Phi) = h \sum_{j=1}^{N-1} \left[-\frac{1}{2}\phi_j \delta_x^2 \phi_j + V(x_j)\phi_j^2 + \frac{\beta}{2}\phi_j^4 - \frac{\delta}{2}\phi_j^2 \delta_x^2(\phi_j^2) \right], \quad (4.2.2)$$

subject to $\|\Phi\|_{l_2} = 1$, where δ_x^2 is an operator defined as

$$\delta_x^2 \phi_j = \frac{\phi_{j+1} - 2\phi_j + \phi_{j-1}}{h^2}. \quad (4.2.3)$$

Define matrix $A = (a_{jk}) \in \mathbb{R}^{(N-1)\times(N-1)}$ as

$$a_{jk} = \begin{cases} \frac{1}{h^2}, & j = k, \\ -\frac{1}{2h^2}, & |j-k| = 1, \\ 0, & \text{otherwise}, \end{cases} \quad (4.2.4)$$

then (4.2.2) can be written in a matrix form as

$$E_h^{\mathrm{FD}}(\Phi) = h \left[\Phi^T A \Phi + \Phi^T V \Phi + \frac{\beta}{2}\Phi^4 + \delta(\Phi^2)^T A \Phi^2 \right], \quad (4.2.5)$$

where Φ^2 is defined component-wisely as $(\Phi^2)_j = \phi_j^2$ and $V = \mathrm{diag}(V(x_1), \ldots, V(x_{N-1}))$. The matrix form (4.2.5) is concise and suitable for programming, and is thus used in practice.

Most methods that are widely used for an optimization problem are gradient-based. Therefore, it's necessary for us to write the gradient of (4.2.5) explicitly. Denote $G_h^{\mathrm{FD}}(\Phi) = \nabla E_h^{\mathrm{FD}}(\Phi)$, then a direct computation from (4.2.1) implies that

$$\begin{aligned} G_h^{\mathrm{FD}}(j) &= \tfrac{\partial E_h^{\mathrm{FD}}}{\partial \phi_j} = h\left[-\delta_x^2\phi_j + 2V(x_j)\phi_j + 2\beta\phi_j^3 - 2\delta\phi_j\delta_x^2(\phi_j^2)\right] \\ &= 2h(A\Phi + V\Phi + \beta\Phi^3 + 2\delta\Phi .* (A\Phi^2)), \end{aligned}$$

where, for simplicity, we introduce the operator $.*$ for componentwise multiplication between two vectors. To be more specific, for general two vectors $a = (a_j)_{j=1,\dots,N} \in \mathbb{R}^N$ and $b = (b_j)_{j=1,\dots,N} \in \mathbb{R}^N$, we define $a .* b \in \mathbb{R}^N$ as $(a .* b)_j = a_j b_j$.

Now the the original problem (2.4.7) with $d = 1$ can be approximated by the discretized minimization problem via FD discretization:

$$\Phi_g = \arg\min E_h^{\mathrm{FD}}(\Phi), \text{ subject to } \|\Phi\|_{l_2}^2 = 1,\ \Phi_0 = \Phi_N = 0,\ \Phi \in \mathbb{R}^{N+1}. \quad (4.2.6)$$

4.2.2 Sine pseudospectral discretization

In space, we can replace the FD discretization by the sine pseudospectral (SP) method when homogeneous Dirichlet boundary conditions are applied. Compared to the finite difference method, the spectral method has the advantage of high accuracy, especially for smooth problems with regular geometry. Again, only the discretization in 1D is presented here, and extensions to 2D and 3D are straightforward and the details are omitted here for brevity.

For $d = 1$, we consider the problem in $U = (a, b)$. As proposed in [14], for any function $f \in \mathbb{C}_0([a, b])$, i.e. f is continuous in $[a, b]$ and $f(a) = f(b) = 0$, we can do the interpolation of f at the grid points by sine series as

$$(I_N f)(x) = \sum_{l=1}^{N-1} \tilde{f}_l \sin(\mu_l(x - a)), \quad (4.2.7)$$

satisfying $(I_N f)(x_j) = f(x_j)$, where $\mu_l = \frac{\pi l}{b-a}$ and $\tilde{f}_l$ can be computed by

$$\tilde{f}_l = \frac{2}{N} \sum_{j=1}^{N-1} f_j \sin\left(\frac{jl\pi}{N}\right), \quad (4.2.8)$$

where $f_j = f(x_j)$. Choosing the interpolation function $(I_N f)(x)$ as the approximation of $f(x)$, we get

$$f''(x) \approx -\sum_{l=1}^{N-1} \mu_l^2 \tilde{f}_l \sin(\mu_l(x-a)), \tag{4.2.9}$$

which immediately implies that

$$f''(x_j) \approx \partial_{xx}^s f|_{x=x_j} = -\sum_{l=1}^{N-1} \mu_l^2 \tilde{f}_l \sin\left(\frac{jl\pi}{N}\right), \tag{4.2.10}$$

where ∂_{xx}^s is the pseudospectral differential operator approximating ∂_{xx}. Via a similar argument, we can approximate the first derivative by

$$f'(x_j) \approx \partial_x^s f|_{x=x_j} = \sum_{l=1}^{N-1} \mu_l \tilde{f}_l \cos\left(\frac{jl\pi}{N}\right), \tag{4.2.11}$$

where ∂_x^s is the pseudospectral differential operator approximating ∂_x.

With similar notations as the FD scheme, the energy functional (2.4.6) truncated on $U = (a, b)$ can be discretized as

$$E_h^{\mathrm{SP}}(\Phi) = h \sum_{j=0}^{N-1} \left[-\frac{1}{2}\phi_j \partial_{xx}^s \phi_j + V(x_j)\phi_j^2 + \frac{\beta}{2}\phi_j^4 + 2\delta\phi_j^2 (\partial_x^s \phi_j)^2 \right]. \tag{4.2.12}$$

By defining matrix $C = (c_{jk}) \in \mathbb{R}^{(N-1)\times(N-1)}$ with $c_{jk} = \sin\left(\frac{jk\pi}{N}\right)$, $\Lambda = \mathrm{diag}(\mu_1^2, \ldots, \mu_{N-1}^2)$, $B = (b_{jk}) \in \mathbb{R}^{(N-1)\times(N-1)}$ with $b_{jk} = \cos\left(\frac{jk\pi}{N}\right)$, and using similar notions as in the FD scheme, we can rewrite (4.2.12) in an equivalent form as

$$E_h^{\mathrm{SP}}(\Phi) = h \left[\frac{1}{N}\Phi^T C\Lambda C\Phi + \Phi^T V\Phi + \frac{\beta}{2}\Phi^4 + \frac{8\delta}{N^2}\Phi^2 .* (A\Phi)^2 \right], \tag{4.2.13}$$

where $A = B\Lambda^{\frac{1}{2}}C$. One remark here is that, in practice, instead of doing the matrix multiplication, whose computational cost is $\mathcal{O}(N^2)$, (4.2.13) can be computed efficiently by using discrete sine transform (DST) for ∂_{xx}^s and fast Fourier transform (FFT) for ∂_x^s, and the total computational cost now is $\mathcal{O}(N \log N)$.

The computation for the gradient $G_h^{\mathrm{SP}}(\Phi) = \nabla E_h^{\mathrm{SP}}(\Phi)$ is tricky. As shown in [32], for the first three terms in (4.2.12), i.e.

$$E_h^{GP} = h \sum_{j=0}^{N-1} \left[-\frac{1}{2}\phi_j \partial_{xx}^s \phi_j + V(x_j)\phi_j^2 + \frac{\beta}{2}\phi_j^4 \right], \tag{4.2.14}$$

we have

$$\nabla E_h^{GP} = 2h\left(\frac{1}{N}C\Lambda C\Phi + V\Phi + \beta\Phi^3\right). \tag{4.2.15}$$

While for the last term

$$F_h(\Phi) = 2h\delta\sum_{j=0}^{N-1}\phi_j^2(\partial_x^s\phi_j)^2, \tag{4.2.16}$$

we have

$$\nabla F_h = \frac{16\delta h}{N^2}(\Phi.*(A\Phi)^2 + A^T(\Phi^2.*A\Phi)), \tag{4.2.17}$$

which immediately gives that

$$G_h^{\mathrm{SP}}(\Phi) = \nabla E_h^{\mathrm{SP}}(\Phi) = 2h\left(\frac{1}{N}C\Lambda C\Phi + V\Phi + \beta\Phi^3\right) + \nabla F_h. \tag{4.2.18}$$

The original optimization problem (2.4.7) now is approximated by the discretized minimization problem via SP discretization which finds $\Phi_g \in \mathbb{R}^{N-1}$ such that

$$\Phi_g = \arg\min E_h^{\mathrm{SP}}(\Phi), \text{ subject to } \|\Phi\|_{l_2}^2 = 1,\ \Phi_0 = \Phi_N = 0. \tag{4.2.19}$$

4.2.3 A feasible gradient type method

In this subsection, we solve the problem (4.2.6) or (4.2.19) by following the feasible method proposed in [113]. For self-consistency, we include the description of the method here. Notice that by doing a rescaling $X = \sqrt{h}\Phi$, the constraint of (4.2.6) and (4.2.19) will become $\|X\|_2^2 = X^TX = 1$. By differentiating both sides of $X^TX = 1$, we obtain the tangent vector set of the constraints

$$T_X := \{Z \in \mathbb{R}^{N-1} : X^TZ = 0\}. \tag{4.2.20}$$

For the rest of this subsection, the problem expressed by X instead of Φ will be considered.

Consider the minimization problem,

$$\min E(X), \text{ subject to } \|X\|_2^2 = 1, X \in \mathbb{R}^{N-1}. \tag{4.2.21}$$

The Lagrangian function of (4.2.21) is

$$L(X,\theta) = E(X) - \frac{\theta}{2}\left(\|X\|_2^2 - 1\right), \tag{4.2.22}$$

and the first-order optimality condtions can be then derived as

$$G - \theta X = 0, \quad \|X\|_2^2 = X^T X = 1, \tag{4.2.23}$$

where $G = \nabla E(X)$ and θ can be computed as $\theta = X^T G = G^T X$.

Define $\mathcal{A}(X) = GX^T - XG^T$, and then we can check that

$$(I - XX^T)G = \mathcal{A}(X)X = 0, \tag{4.2.24}$$

which implies that $\mathcal{A}(X)X$ is the projection of the gradient of $E(X)$ at X to the tangent space of the constraints T_X.

The steepest descent method suggest using $Y(\tau) := X - \tau\mathcal{A}(X)X$ with some positive number τ as the step size for updating. However, there is no guarantee that $Y(\tau)$ preserves the unit l_2 norm. To get an update which automatically preserves the unit norm, we try a different type of the updating path which is implicit

$$Y(\tau) := X - \tau\mathcal{A}(X)(X + Y(\tau)) \Leftrightarrow Y(\tau) := QX \tag{4.2.25}$$

where $Q = (I + \tau\mathcal{A}(X))^{-1}(I - \tau\mathcal{A}(X))$. Easy to see that $\mathcal{A}(X)$ is skew-symmetric, i.e. $\mathcal{A}(X)^T = -\mathcal{A}(X)$. Then by a simple computation that

$$\begin{aligned} Q^T Q &= (I - \tau\mathcal{A}(X))^T (I + \tau\mathcal{A}(X))^{-T} (I + \tau\mathcal{A}(X))^{-1}(I - \tau\mathcal{A}(X)) \\ &= (I + \tau\mathcal{A}(X))(I - \tau\mathcal{A}(X))^{-1}(I + \tau\mathcal{A}(X))^{-1}(I - \tau\mathcal{A}(X)) \\ &= (I - \tau\mathcal{A}(X))^{-1}(I + \tau\mathcal{A}(X))(I + \tau\mathcal{A}(X))^{-1}(I - \tau\mathcal{A}(X)) \\ &= I, \end{aligned}$$

we can get Q is orthonormal and therefore $Y(\tau)$ preserves the l_2 norm automatically for any τ. In addition, $Y(\tau)$ can be computed explicitly and given in a closed form as [32, 113]

$$Y(\tau) = \alpha(\tau)X + \beta(\tau)G, \tag{4.2.26}$$

where

$$\alpha(\tau) = \frac{(1+\tau X^T G)^2 - \tau^2\|X\|_2^2\|G\|_2^2}{1-\tau^2(X^TG)^2+\tau^2\|X\|_2^2\|G\|_2^2}, \beta(\tau) = \frac{-2\tau\|X\|_2^2}{1-\tau^2(X^TG)^2+\tau^2\|X\|_2^2\|G\|_2^2}. \tag{4.2.27}$$

A suitable step size in the k-th step, denoted as $\tau^{(k)}$, can be chosen by applying the backtracking steps to $\tau^{k,1}$ or $\tau^{k,2}$, which are determined by the Barzilai-Borwein (BB) formula [34], to guarantee convergence. The details are omitted here for brevity and can be referred to [32]. Further the following theorem holds since the energy function $E(X)$ is differentiable and its gradient $\nabla E(X)$ is Lipschitiz continuous [32, 72].

Theorem 4.2.1. *Let $\{X^{(k)} : k \geq 0\}$ be an infinite sequence generated by the Algorithm 1. Then either $\|\mathcal{A}(X^{(k)})X^{(k)}\|_2 = 0$ for some finite k or*

$$\liminf_{k\to\infty} \|\mathcal{A}(X^{(k)})X^{(k)}\|_2 = 0. \tag{4.2.28}$$

The feasible gradient method can then be summarized in the following algorithm.

Algorithm 1 A feasible gradient method

1: Given the current solution $X^{(0)}$, $k = 0$.
2: **while** stopping conditions are not met **do**
3: Choose suitable time step $\tau^{(k)}$
4: Set $X^{(k+1)} \leftarrow Y(\tau^{(k)})$ and update other parameters if necessary
5: $k \leftarrow k + 1$
6: **end while**

4.2.4 Accuracy test

In this section, we will perform accuracy tests for the feasible gradient method, i.e. Algorithm 1, with either finite difference discretization (4.2.5) or the sine pseudospectral discretization (4.2.13).

Error	$h = 1/2$	$h/2$	$h/2^2$	$h/2^3$
$\lvert E(\phi_{g,h}^{\mathrm{FD}}) - E(\phi_g)\rvert$	2.66E-4	6.49E-5	1.62E-5	4.05E-6
rate	-	2.04	2.00	2.00
$\lVert\phi_{g,h}^{\mathrm{FD}} - \phi_g\rVert_{l_2}$	1.44E-3	3.13E-4	7.70E-5	1.92E-5
rate	-	2.20	2.02	2.01
$\lVert\phi_{g,h}^{\mathrm{FD}} - \phi_g\rVert_{\infty}$	1.24E-3	2.89E-4	7.54E-5	1.87E-5
rate	-	2.10	1.94	2.01

Table 4.3: Spatial resolution of the ground state for Case I in Example 4.1.1 via finite difference scheme.

Error	$h = 1$	$h/2$	$h/2^2$	$h/2^3$
$\lvert E(\phi_{g,h}^{\mathrm{SP}}) - E(\phi_g)\rvert$	1.84E-2	2.64E-6	8.46E-12	<1E-12
$\lVert\phi_{g,h}^{\mathrm{SP}} - \phi_g\rVert_{l_2}$	5.27E-1	7.42E-5	2.32E-8	5.85E-11
$\lVert\phi_{g,h}^{\mathrm{SP}} - \phi_g\rVert_{\infty}$	3.19E-1	7.04E-5	1.96E-8	4.60E-11

Table 4.4: Spatial resolution of the ground state for Case I in Example 4.1.1 via sine pseudospectral scheme.

Again, the setup of the numerical test is chosen to be the one in Example 4.1.1. The exact solution is chosen to be the one computed via the pseudospectral scheme with a sufficiently small step $h = 1/64$. We denote the numerical ground state via the FD method (4.2.5) to be $\phi_{g,h}^{\mathrm{FD}}$ and the one via the SP method (4.2.13) to be $\phi_{g,h}^{\mathrm{SP}}$. Table 4.3 and Table 4.4 listed the errors for Case I. Table 4.5 and Table 4.6 listed the errors for Case II. From Table 4.3, 4.4, 4.5 and 4.6, we can see that the the numerical ground state computed using (4.2.5) is second order accurate in space and the one computed using (4.2.13) is spectral accurate.

Error	$h = 1/2$	$h/2$	$h/2^2$	$h/2^3$
$\lvert E(\phi_{g,h}^{\mathrm{FD}}) - E(\phi_g)\rvert$	9.59E-3	2.38E-3	5.95E-4	1.49E-4
rate	-	2.01	2.00	2.00
$\lVert\phi_{g,h}^{\mathrm{FD}} - \phi_g\rVert_{l_2}$	6.25E-3	1.29E-3	3.21E-4	8.01E-5
rate	-	2.27	2.01	2.00
$\lVert\phi_{g,h}^{\mathrm{FD}} - \phi_g\rVert_{\infty}$	5.75E-3	1.16E-3	3.02E-4	7.49E-5
rate	-	2.31	1.94	2.01

Table 4.5: Spatial resolution of the ground state for Case II in Example 4.1.1 via finite difference scheme.

Error	$h = \frac{1}{2}$	$h/2$	$h/2^2$	$h/2^3$
$\lvert E(\phi_{g,h}^{\mathrm{SP}}) - E(\phi_g)\rvert$	2.33E-1	2.16E-4	2.81E-7	6.27E-12
$\lVert\phi_{g,h}^{\mathrm{SP}} - \phi_g\rVert_{l_2}$	2.42E-1	4.66E-3	6.75E-5	9.40E-8
$\lVert\phi_{g,h}^{\mathrm{SP}} - \phi_g\rVert_{\infty}$	1.03E-1	2.74E-3	5.45E-5	5.31E-8

Table 4.6: Spatial resolution of the ground state for Case II in Example 4.1.1 via sine pseudospectral scheme.

4.3 Minimization of the regularized energy via density formulation

In the previous section, the energy is formulated via the wave function. In this section, a new scheme for the ground state of the MGPE will be proposed. We'll compute the ground state by directly minimizing the energy using $\rho = |\psi|^2$ instead ψ. Notice that we can consider the density ρ directly for the ground state because we have proved in Theorem 7.1.1 the ground state can be chosen to be a nonnegative real function and therefore we have a 1-1 correspondence between ϕ_g and ρ_g. By considering this new form of energy, we gain benefits that, firstly, we change the problem to be a convex optimization problem, which enables to use techniques for convex optimization, and, secondly, the interaction energy terms are quadratic now, but with a cost that the kinetic energy now becomes nonlinear and it is not well defined where $\rho \approx 0$, which impies regularization is needed.

In this section, we will first show the regularized energy formulated by density and its discretization. Then the convergence problem will be analyzed theoretically and tested numerically.

4.3.1 Density function formulation and regularization

Rewriting the energy functional (2.4.6) by letting $\rho = |\phi|^2$, we get a new formulation of the energy,

$$E(\rho) = \int_{\mathbb{R}^d} \left[\frac{1}{2} |\nabla \sqrt{\rho}|^2 + V(\mathbf{x})\rho + \frac{\beta}{2}\rho^2 + \frac{\delta}{2} |\nabla \rho|^2 \right] d\mathbf{x}. \tag{4.3.1}$$

However, it's not a good idea to consider (4.3.1) directly because $|\nabla \sqrt{\rho}| \to \infty$ as $\rho \to 0$, which implies big and uncontrollable errors will be included after discretization of energy. Due to the singularity of $|\nabla \sqrt{\rho}|^2$, we regularize the term and get an approximation of the energy,

$$E^{\varepsilon}(\rho) = \int_{\Omega} \left[\frac{1}{2} |\nabla \sqrt{\rho + \varepsilon}|^2 + V(\mathbf{x})\rho + \frac{\beta}{2}\rho^2 + \frac{\delta}{2} |\nabla \rho|^2 \right] d\mathbf{x}. \tag{4.3.2}$$

After regularization, the singularity of the kinetic term will be removed because $|\nabla\sqrt{\rho+\varepsilon}|$ is bounded above by some number depending on ε, which makes the error induced by discretization controllable and enables the use of gradient-based optimization methods for the computation. We can then define the ground states,

$$\rho_g = \arg\min E(\rho), \text{ subject to } \|\rho\|_1 := \int_{\mathbb{R}^d} \rho(\mathbf{x})\, d\mathbf{x} = 1, \text{ and } \rho \geq 0, \tag{4.3.3}$$

$$\rho_g^\varepsilon = \arg\min E^\varepsilon(\rho), \text{ subject to } \|\rho\|_1 := \int_{\mathbb{R}^d} \rho(\mathbf{x})\, d\mathbf{x} = 1, \text{ and } \rho \geq 0. \tag{4.3.4}$$

But the regularization introduces new questions as we changed the energy functional. Basically, we have the following two questions:
(i) Do we have $\lim_{\varepsilon\to 0} E^\varepsilon(\rho_g^\varepsilon) = E(\rho_g)$ and $\lim_{\varepsilon\to 0} \rho_g^\varepsilon = \rho_g$ under some norm?
(ii) If we have the convergence result, what would be the convergence rate?
It turns out we do have the convergence result when $\beta > 0$ and $\delta > 0$, and the convergence rate of the ground state can be bounded by the convergence rate of the energy. In Section 4.3.3, we will show the rigorous proof of the results.

Remark 4.3.1. *There is an equivalent way of writing the regularized energy* (4.3.2) *as*

$$E^\varepsilon(\rho) = \int_\Omega \left[\frac{|\nabla\rho|^2}{8(\rho+\varepsilon)} + V(\mathbf{x})\rho + \frac{\beta}{2}\rho^2 + \frac{\delta}{2}|\nabla\rho|^2\right] d\mathbf{x}. \tag{4.3.5}$$

The two definitions are essentially the same, but will lead to different discretized energy formulations.

4.3.2 Finite difference discretization

In this section, we consider the finite difference discretization of (4.3.2) formulated via $\rho = |\phi|^2$ and truncated on a bounded domain U with homogeneous Dirichlet BC. Again the central difference is applied for approximating the derivatives and the integrals are computed by the composite trapezoidal rule. For simplicity, the 1D case is shown here. Extensions to 2D and 3D are straightforward and the details are omitted here for brevity.

For $d = 1$, we take $U = (a, b)$ to be an interval in 1D, and take the $N + 1$ grid points that are evenly distributed and defined in (4.1.15). Let ρ_j be the numerical approximation of $\rho(x_j)$ for $j = 0, 1, \ldots, N$ and denote

$$\rho = (\rho_0, \rho_1, \ldots, \rho_N)^T \in \mathbb{R}^{N+1}. \tag{4.3.6}$$

Then by the homogenous Dirichlet boundary condition, we have $\rho_0 = \rho_N = 0$. The energy functional (4.3.2) under constraint $\|\rho\|_{h_1} = 1$ can then be formulated as

$$E^{\mathrm{FD}}_{h,\varepsilon}(\rho) = h \sum_{j=0}^{N-1} \left[\frac{1}{2} |\delta_x^+ \sqrt{\rho_j + \varepsilon}|^2 + V(x_j)\rho_j + \frac{\beta}{2}\rho_j^2 + \frac{\delta}{2} |\delta_x^+ \rho_j|^2 \right], \tag{4.3.7}$$

subject to $\|\rho\|_{h_1} = 1$, $\rho_j \geq 0$ and $\rho_0 = \rho_N = 0$, where we introduce $\|\rho\|_{h_1} = h \sum_{j=0}^{N-1} \rho_j$ to be the discrete l_1-norm and the operator δ_x^+ defined as $\delta_x^+ \rho_j = \frac{\rho_{j+1} - \rho_j}{h}$ for simplicity.

Denote $G^{\mathrm{FD}}_{h,\varepsilon} = \nabla E^{\mathrm{FD}}_{h,\varepsilon}(\rho)$ to be the gradient of the discretized energy, then it can be computed as

$$G^{\mathrm{FD}}_{h,\varepsilon}(j) = \frac{\partial E^{\mathrm{FD}}_{h,\varepsilon}}{\partial \rho_j} = h \left[-\frac{\delta_x^2 \sqrt{\rho_j + \varepsilon}}{2\sqrt{\rho_j + \varepsilon}} + V(x_j) + \beta\rho_j - \delta(\delta_x^2 \rho_j) \right]. \tag{4.3.8}$$

By using the matrix A defined in (4.2.4), $G^{\mathrm{FD}}_{h,\varepsilon}$ can be written in a compact form as

$$G^{\mathrm{FD}}_{h,\varepsilon} = h \left[(A\sqrt{\rho + \varepsilon})./\sqrt{\rho + \varepsilon} + V + \beta\rho + 2\delta A\rho \right], \tag{4.3.9}$$

where ./ is an elementwise division operator between vectors.

From Theorem 4.3.2, which will be proved later, the ground state corresponds to the regularized energy (4.3.2) will converge to the ground state of (4.3.1) as $\varepsilon \to 0^+$. On the other hand, the ground state of (4.3.7) will converge to the ground state of (4.3.2) as $h \to 0^+$. As a result, the original optimization problem (2.4.7) now becomes choosing a sequence of $\varepsilon_n \to 0^+$ and for each fixed ε_n finding $\rho_g^{h,\varepsilon_n} \in \mathbb{R}^{N-1}$ such that

$$\rho_g^{h,\varepsilon_n} = \operatorname*{arg\,min}_{\rho \in \mathbb{R}^{N+1}} E^{\mathrm{FD}}_{h,\varepsilon_n}(\rho), \text{ subject to } \|\rho\|_{h_1} = 1,\ \rho \geq 0,\ \rho_0 = \rho_N = 0. \tag{4.3.10}$$

The ground state and the corresponding energy is computed by taking the limit

$$\rho_g^{h,0} = \lim_{n\to\infty} \rho_g^{h,\varepsilon_n}, \quad E_g^{h,0} = \lim_{n\to\infty} E^{\mathrm{FD}}_{h,\varepsilon_n}(\rho_g^{h,\varepsilon_n}). \tag{4.3.11}$$

Due to the zero boundary condition, we may also view $E_{h,\varepsilon}^{\mathrm{FD}}(\rho)$ as a function of

$$\rho = (\rho_1, \ldots, \rho_{N-1})^T \in \mathbb{R}^{N-1} \tag{4.3.12}$$

for simplicity. It's worth noticing that the new problem (4.3.10) we get is a convex optimization problem. To get it, we only need to show that the discretized energy is convex, which is stated in Theorem 4.3.1, because the feasible set $\{\rho \in \mathbb{R}^{N+1} \,|\, \|\rho\|_{h_1} = 1, \rho \geq 0, \rho_0 = \rho_N = 0\}$ is obviously convex.

Theorem 4.3.1. *The discretized energy function $E_{h,\varepsilon}^{\mathrm{FD}}(\rho)$ defined in (4.3.2) is convex with respect to $\rho = (\rho_1, \ldots, \rho_{N-1})^T \in \mathbb{R}^{N-1}$ for $\beta \geq 0$ and $\delta \geq 0$.*

Proof. For $\beta \geq 0$ and $\delta \geq 0$, it's easy to check the last three terms in (4.3.2), which are linear or quadratic in ρ, are convex. The details are omitted here for brevity. Therefore, we only need to check the first term in (4.3.2) is convex.

Notice that

$$|\delta_+ \sqrt{\rho_j + \varepsilon}|^2 = \frac{\rho_j + \rho_{j+1} + 2\varepsilon - 2\sqrt{\rho_{j+1} + \varepsilon}\sqrt{\rho_j + \varepsilon}}{h^2}, \tag{4.3.13}$$

it's sufficient to show $E_1(\rho) = \sum_{j=0}^{N-1} \sqrt{\rho_{j+1} + \varepsilon}\sqrt{\rho_j + \varepsilon}$ is concave with respect to ρ. This is true because, for each term $E_{1,j}(\rho) = \sqrt{\rho_{j+1} + \varepsilon}\sqrt{\rho_j + \varepsilon}$, we have

$$\begin{aligned}
&\left|\frac{E_{1,j}(a) + E_{1,j}(b)}{2}\right|^2 = \left|\frac{1}{2}(\sqrt{a_{j+1} + \varepsilon}\sqrt{a_j + \varepsilon} + \sqrt{b_{j+1} + \varepsilon}\sqrt{b_j + \varepsilon})\right|^2 \\
&\leq \left(\frac{a_{j+1} + \varepsilon}{2} + \frac{b_{j+1} + \varepsilon}{2}\right)\left(\frac{a_j + \varepsilon}{2} + \frac{b_j + \varepsilon}{2}\right) \\
&= \left|\sqrt{\frac{a_{j+1} + b_{j+1}}{2} + \varepsilon}\sqrt{\frac{a_j + b_j}{2} + \varepsilon}\right|^2 \\
&= \left|E_{1,j}\left(\frac{a+b}{2}\right)\right|^2, \quad \text{for } j = 0, 1, \ldots, N-1
\end{aligned}$$

where $a = (a_1, \ldots, a_{N-1})^T \in \mathbb{R}^{N-1}$ and $b = (b_1, \ldots, b_{N-1})^T \in \mathbb{R}^{N-1}$ with $a_0 = a_N = b_0 = b_N = 0$. □

Remark 4.3.2. *Based on the other form of the regularized energy (4.3.5), we can get another discretized energy formulation, which is slightly different from (4.3.7).*

$$\tilde{E}_{h,\varepsilon}^{\mathrm{FD}} = h \sum_{j=0}^{N-1} \left[\frac{|\delta_x^+ \rho_j|^2}{4(\rho_j + \rho_{j+1} + 2\varepsilon)} + V_j \rho_j + \frac{\beta}{2}\rho_j^2 + \frac{\delta}{2}|\delta_x^+ \rho_j|^2\right], \tag{4.3.14}$$

where $\rho = (\rho_1, \ldots, \rho_{N-1})^T \in \mathbb{R}^{N-1}$ *satisfies* $h\sum_{j=0}^{N-1}\rho_j = 1$, $\rho_j \geq 0$ *and* $\rho_0 = \rho_N = 0$. *The gradient, i.e.* $\nabla E_{h,\varepsilon}^{\mathrm{FD}}(\rho)$, *can be computed as*

$$\frac{\partial \tilde{E}_{h,\varepsilon}^{\mathrm{FD}}}{\partial \rho_j} = h\left[F_j(\rho) + V(x_j) + \beta\rho_j - \delta(\delta_x^2\rho_j)\right], \tag{4.3.15}$$

where

$$F_j(\rho) = \frac{1}{4h}\left[\frac{-2(\rho_{j+1}-\rho_j)}{\rho_j+\rho_{j+1}+2\varepsilon} - \frac{(\rho_{j+1}-\rho_j)^2}{(\rho_j+\rho_{j+1}+2\varepsilon)^2} + \frac{2(\rho_j-\rho_{j-1})}{\rho_j+\rho_{j-1}+2\varepsilon} - \frac{(\rho_j-\rho_{j-1})^2}{(\rho_j+\rho_{j-1}+2\varepsilon)^2}\right].$$

It can also be proved that $\tilde{E}_{h,\varepsilon}^{\mathrm{FD}}(\rho)$ *is convex in* ρ, *and therefore we changed the original problem to be a convex optimization problem. The details are omitted here for brevity.*

4.3.3 Convergence analysis

In this section, we aim to study the convergence of the ground state $\rho_g^{h,\varepsilon}$ of the discrete regularized energy (4.3.10) to the ground state ρ_g of the MGPE, which is defined in (2.4.7). The results in this subsection can be summarized in the following diagram,

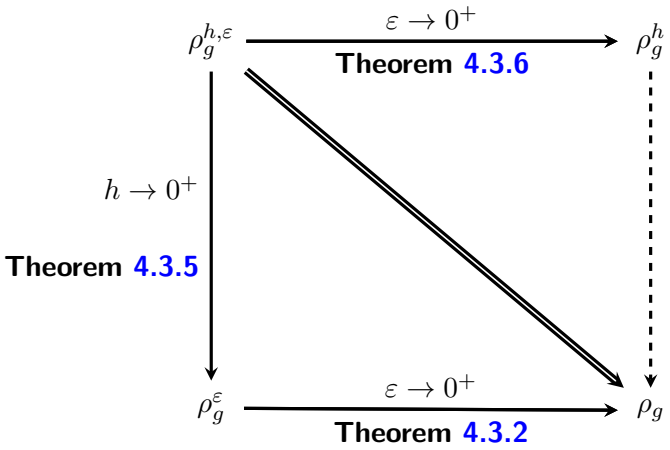

where ρ_g^h is the ground state of the discrete energy without regularization, i.e.

$$\rho_g^h = \arg\min_{\rho\in S} E_h^{\mathrm{FD}}(\rho), \tag{4.3.16}$$

where S is the feasible set defined as

$$S = \{\rho \in \mathbb{R}^{N+1} \,|\, \rho_j \geq 0, h\sum_{j=0}^{N} \rho_j = 1, \rho_0 = \rho_N = 0\}. \tag{4.3.17}$$

We begin with the results showing the convergence of the ground state of the regularized energy, i.e. ρ_g^ε, as $\varepsilon \to 0^+$. First, we can observe the following lemma, which provides one side limit for the energy.

Lemma 4.3.1. *For ρ_g and ρ_g^ε defined in (4.3.4) with $\beta \geq 0$ and $\delta > 0$, we have*

$$E^\varepsilon(\rho_g^\varepsilon) \leq E(\rho_g), \text{ for any } \varepsilon \geq 0. \tag{4.3.18}$$

Proof. Due to the fact $|\nabla\sqrt{\rho+\varepsilon}|^2 \leq |\nabla\sqrt{\rho}|^2$ where $\varepsilon \geq 0$ and ρ is an arbitrary function satisfying $\rho \geq 0$, it's obvious that

$$E^\varepsilon(\rho) \leq E(\rho), \tag{4.3.19}$$

holds for all $\varepsilon \geq 0$ and $\rho \geq 0$. Now take $\rho = \rho_g$ and recall the definition of ρ_g^ε (4.3.4), we have $E^\varepsilon(\rho_g^\varepsilon) \leq E^\varepsilon(\rho_g) \leq E(\rho_g)$. □

Now we want to show $\lim_{\varepsilon\to 0} E^\varepsilon(\rho_g^\varepsilon) = E(\rho_g)$. In fact, we can prove a stronger conclusion, which actually considers the convergence of ρ_g^ε to ρ_g and is stated as follows.

Theorem 4.3.2. *For ρ_g and ρ_g^ε defined in (4.3.3) and (4.3.4) with $\beta \geq 0$ and $\delta > 0$, we have*

$$\rho_g^\varepsilon \to \rho_g \text{ in } H^1 \text{ and } \nabla\sqrt{\rho_g^\varepsilon+\varepsilon} \to \nabla\sqrt{\rho_g} \text{ in } L^2, \tag{4.3.20}$$

which immediately implies

$$\lim_{\varepsilon\to 0^+} E^\varepsilon(\rho_g^\varepsilon) = E(\rho_g). \tag{4.3.21}$$

Proof. First, as shown in Lemma 4.3.1, $E^\varepsilon(\rho_g^\varepsilon) \leq E(\rho_g)$, which means that $E^\varepsilon(\rho_g^\varepsilon)$ is uniformly bounded above by the constant $E(\rho_g)$ with respect to ε. Further we get the boundedness for each term in the energy functional $E^\varepsilon(\cdot)$ (4.3.2). The

boundedness for last two terms implies $\rho_g^\varepsilon \xrightarrow{H^1} \rho_g^0$ for some $\rho_g^0 \in H^1$. In fact, the weak convergence we get is for a subsequence, but, for simplicity, we still denote it as ρ_g^ε. By a similar argument for the first two terms in the functional E^ε (4.3.2), we have $\nabla\sqrt{\rho_g^\varepsilon + \varepsilon} \xrightarrow{L^2} f$ for some $f \in L^2$ and the uniform boundedness of the external potential term, i.e. $\int_{\mathbb{R}^d} V(\mathbf{x})\rho_g^\varepsilon \, d\mathbf{x} \leq C$ for some constant C with respect to all $\varepsilon \geq 0$.

Next, we want to show $f = \nabla\sqrt{\rho_g^0}$ and ρ_g^0 is indeed a minimizer of $E(\rho)$, i.e. $\rho_g^0 \geq 0$, $\int_{\mathbb{R}^d} \rho_g^0 \, d\mathbf{x} = 1$ and $E(\rho_g^0) \leq E(\rho_g)$.

(1) To show $\int_{\mathbb{R}^d} \rho_g^0 \, d\mathbf{x} = 1$ and $\rho_g^0 \geq 0$:

For any $\eta > 0$, by using the confinement of $V(\mathbf{x})$, we can choose R large enough such that $V(\mathbf{x}) \geq \frac{C}{\eta}$ for all $\mathbf{x} \in \Omega_R^c$, where $\Omega_R = \{x \,|\, |x| < R\}$. Then $C \geq \int_{\Omega_R^c} V\rho_g^\varepsilon \, d\mathbf{x} \geq \frac{C}{\eta}\int_{\Omega_R^c} \rho_g^\varepsilon \, dx$, i.e. $\int_{\Omega_R^c} \rho_g^\varepsilon \, d\mathbf{x} \leq \eta$.

In the bounded domain Ω_R, the weak convergence in H^1 implies the strong convergence in L^2 by the Sobolev embedding theorem, and therefore $\rho_g^\varepsilon \xrightarrow{L^2} \rho_g^0$ in Ω_R. Furthermore, we get $\rho_g^\varepsilon \xrightarrow{L^1} \rho_g^0$ in Ω_R by the Hölder's inequality, and $\int_{\mathbb{R}^d} \rho_g^0 \, d\mathbf{x} \in [1-\eta, 1]$ as a consequence. Because η is arbitrary, we get $\int_{\mathbb{R}^d} \rho_g^0 \, d\mathbf{x} = 1$. In fact, we can further extend the strong L^1 convergence from Ω_R to the whole space by combing the confining condition of the external potential and the current convergence result in Ω_R for arbitrary R.

Besides, the strong convergence in L_2 in Ω_R suggests that we can choose a subsequence that will converge pointwisely to ρ_g^0. Then $\rho_g^0 \geq 0$ in Ω_R is a direct result of the fact that $\rho_g^\varepsilon \geq 0$ for any $\varepsilon > 0$. And further we get $\rho_g^0 \geq 0$ in $\mathbb{R}^d$ since R can be chosen arbitrarily large.

(2) To show $f = \nabla\sqrt{\rho_g^0}$:

Suppose the test function ϕ is a smooth function with compact support in Ω_R. Then on one hand, by definition,

$$\lim_{\varepsilon \to 0^+} \int_{\mathbb{R}^d} \nabla\sqrt{\rho_g^\varepsilon + \varepsilon}\phi \, d\mathbf{x} = \int_{\mathbb{R}^d} f\phi \, d\mathbf{x}. \tag{4.3.22}$$

On the other hand, we will show that

$$\lim_{\varepsilon \to 0^+} \int_{\mathbb{R}^d} \nabla\sqrt{\rho_g^\varepsilon + \varepsilon}\phi \, d\mathbf{x} = \int_{\mathbb{R}^d} \nabla\sqrt{\rho_g^0}\phi \, d\mathbf{x}. \tag{4.3.23}$$

This can be reasoned in the following way. Firstly, it's obvious that

$$\left|\int_{\mathbb{R}^d}\left(\nabla\sqrt{\rho_g^\varepsilon+\varepsilon}-\nabla\sqrt{\rho_g^0}\right)\phi\,d\mathbf{x}\right| = \left|\int_{\Omega_R}\left(\sqrt{\rho_g^\varepsilon+\varepsilon}-\sqrt{\rho_g^0}\right)\nabla\phi\,d\mathbf{x}\right|$$
$$\leq \int_{\Omega_R}|\sqrt{\rho_g^\varepsilon+\varepsilon}-\sqrt{\rho_g^0}||\nabla\phi|\,d\mathbf{x} \leq C\int_{\Omega_R}|\sqrt{\rho_g^\varepsilon+\varepsilon}-\sqrt{\rho_g^0}|\,d\mathbf{x}$$

for some constant C depending on ϕ. Therefore, it's sufficient to prove

$$\lim_{\varepsilon\to 0^+}\int_{\Omega_R}|\sqrt{\rho_g^\varepsilon+\varepsilon}-\sqrt{\rho_g^0}|\,d\mathbf{x}=0. \tag{4.3.24}$$

To show (4.3.24), defining $D_\eta=\{\mathbf{x}:\rho_g^0>\eta\}$ for arbitrarily chosen $\eta>0$, we can see that $\int_{\Omega_R\cap D_\eta}|\sqrt{\rho_g^\varepsilon+\varepsilon}-\sqrt{\rho_g^0}|\,dx\leq\frac{1}{\sqrt{\eta}}\int_{\Omega_R}|\rho_g^\varepsilon+\varepsilon-\rho_g^0|\,dx\to 0$, where the last step is because $\rho_g^\varepsilon\xrightarrow{L^1}\rho_g^0$. For the remained part $\Omega_R\cap D_\eta^c$, we have

$$\limsup_{\varepsilon\to 0^+}\int_{\Omega_R\cap D_\eta^c}|\sqrt{\rho_g^\varepsilon+\varepsilon}-\sqrt{\rho_g^0}|\,d\mathbf{x}\leq\limsup_{\varepsilon\to 0^+}\left[\sqrt{\eta}|\Omega_R|+\int_{\Omega_R\cap D_\eta^c}\sqrt{\rho_g^\varepsilon+\varepsilon}\,d\mathbf{x}\right]$$
$$\leq\limsup_{\varepsilon\to 0^+}\left[\sqrt{\eta}|\Omega_R|+\sqrt{|\Omega_R|}\sqrt{\int_{\Omega_R\cap D_\eta^c}(\rho_g^\varepsilon+\varepsilon)\,d\mathbf{x}}\right]=\sqrt{\eta}|\Omega_R|+\sqrt{|\Omega_R|}\sqrt{\int_{\Omega_R\cap D_\eta^c}\rho_g^0\,d\mathbf{x}}$$
$$\leq\sqrt{\eta}|\Omega_R|+\sqrt{|\Omega_R|}\sqrt{\eta|\Omega_R|}=2\sqrt{\eta}|\Omega_R|$$

Because η can be chosen arbitrarily small, we get (4.3.24) and consequently (4.3.23). Then the uniqueness of the weak limit implies that $f=\nabla\sqrt{\rho_g^0}$ in L^2.

(3) To show $E(\rho_g^0)\leq E(\rho_g)$:

The strong convergence in L^1 enables us to choose a subsequence, while still denoted as ρ_g^ε for simplicity, such that $\rho_g^\varepsilon\to\rho_g^0$ almost everywhere. By Fatou's lemma, we get

$$\liminf_{\varepsilon\to 0^+}\int_{\mathbb{R}^d}V\rho_g^\varepsilon\,d\mathbf{x}\geq\int_{\mathbb{R}^d}V\rho_g^0\,d\mathbf{x}. \tag{4.3.25}$$

Besides, by the weak convergence, it's easy to see that

$$\liminf_{\varepsilon\to 0^+}\int_{\mathbb{R}^d}|\rho_g^\varepsilon|^2\,d\mathbf{x}\geq\int_{\mathbb{R}^d}|\rho_g^0|^2\,d\mathbf{x},\ \liminf_{\varepsilon\to 0^+}\int_{\mathbb{R}^d}|\nabla\rho_g^\varepsilon|^2\,d\mathbf{x}\geq\int_{\mathbb{R}^d}|\nabla\rho_g^0|^2\,d\mathbf{x} \tag{4.3.26}$$

and

$$\liminf_{\varepsilon\to 0^+}\int_{\mathbb{R}^d}|\nabla\sqrt{\rho_g^\varepsilon+\varepsilon}|^2\,d\mathbf{x}\geq\int_{\mathbb{R}}|\nabla\sqrt{\rho_g^0}|^2\,d\mathbf{x}. \tag{4.3.27}$$

Thus $E(\rho_g^0) \leq E^\varepsilon(\rho_g^\varepsilon) \leq E(\rho_g)$. But, by definition, ρ_g is the ground state of $E(\cdot)$, which means $E(\rho_g^0) \geq E(\rho_g)$. Therefore, $E(\rho_g^0) = E(\rho_g) = \lim_{\varepsilon\to 0^+} E^\varepsilon(\rho_g^\varepsilon)$ and $\rho_g = \rho_g^0$ by the uniqueness of the minimizer. What's more, all the inequalities in the proof become equalities, which implies all weak convergence proved is actually strong convergence.

Note that the above proof is true for arbitrary sequence of $\varepsilon \to 0^+$. Thus we get the conclusion. □

We're interested in the convergence rate of the ground state. In fact, the convergence rate is related to the order of convergence of the corresponding energy. The result can be formulated in the following theorem.

Theorem 4.3.3. *For ρ_g and ρ_g^ε defined in (4.3.3) and (4.3.4) with $\beta \geq 0$ and $\delta > 0$, we have*

$$\beta\|\rho_g - \rho_g^\varepsilon\|^2 + \delta\|\nabla(\rho_g - \rho_g^\varepsilon)\|^2 \leq 2(E(\rho_g) - E^\varepsilon(\rho_g^\varepsilon)). \tag{4.3.28}$$

Proof. The proof follows from a direct computation. But we need to show the following lemma first which is essential in the proof of the Theorem 4.3.3.

Lemma 4.3.2.

$$R(\rho_g, \rho_g^\varepsilon) \geq \int_{\mathbb{R}^d} \left[-\frac{\nabla\rho_g^\varepsilon \cdot \nabla(\rho_g - \rho_g^\varepsilon)}{4(\rho_g^\varepsilon + \varepsilon)} + \frac{|\nabla\rho_g^\varepsilon|^2(\rho_g - \rho_g^\varepsilon)}{8(\rho_g^\varepsilon + \varepsilon)^2} \right] d\mathbf{x}, \tag{4.3.29}$$

where $R(\rho_g, \rho_g^\varepsilon)$ is defined as

$$R(\rho_g, \rho_g^\varepsilon) = \int_{\mathbb{R}^d} \left[V(\mathbf{x})(\rho_g - \rho_g^\varepsilon) + \beta\rho_g^\varepsilon(\rho_g - \rho_g^\varepsilon) + \delta\nabla\rho_g^\varepsilon \cdot \nabla(\rho_g - \rho_g^\varepsilon) \right] d\mathbf{x}. \tag{4.3.30}$$

Proof of Lemma 4.3.2. Define $f(t) = E^\varepsilon(\rho_g^\varepsilon + t(\rho_g - \rho_g^\varepsilon))$. It's easy to check that $\rho_g^\varepsilon + t(\rho_g - \rho_g^\varepsilon)$ satisfies the constraints $\|\rho\|_1 = 1, \rho \geq 0$ for $t \in [0, 1]$. Therefore, $f(t)$ takes its minimum value at $t = 0$ because ρ_g^ε minimizes $E^\varepsilon(\rho)$ among all ρ satisfying the constraint $\|\rho\|_1 = 1, \rho \geq 0$, which indicates $f'(0) \geq 0$. A direct computation will lead to the inequality (4.3.29). The details of the computation are omitted here for simplicity.

□

Now we can prove the Theorem 4.3.3. A direct computation implies that

$$
\begin{aligned}
&E(\rho_g) - E^\varepsilon(\rho_g^\varepsilon) \\
&= \int_{\mathbb{R}^d} \left[\frac{1}{2}|\nabla\sqrt{\rho_g}|^2 - \frac{1}{2}|\nabla\sqrt{\rho_g^\varepsilon+\varepsilon}|^2\right] d\mathbf{x} + R(\rho_g,\rho_g^\varepsilon) + \frac{\beta}{2}\|\rho_g-\rho_g^\varepsilon\|^2 + \frac{\delta}{2}\|\nabla(\rho_g-\rho_g^\varepsilon)\|^2 \\
&\geq \int_{\mathbb{R}^d} \left[\frac{1}{2}|\nabla\sqrt{\rho_g}|^2 - \frac{1}{2}|\nabla\sqrt{\rho_g^\varepsilon+\varepsilon}|^2 - \frac{\nabla\rho_g^\varepsilon\cdot\nabla(\rho_g-\rho_g^\varepsilon)}{4(\rho_g^\varepsilon+\varepsilon)} + \frac{|\nabla\rho_g^\varepsilon|^2(\rho_g-\rho_g^\varepsilon)}{8(\rho_g^\varepsilon+\varepsilon)^2}\right] d\mathbf{x} \\
&\quad + \frac{\beta}{2}\|\rho_g-\rho_g^\varepsilon\|^2 + \frac{\delta}{2}\|\nabla(\rho_g-\rho_g^\varepsilon)\|^2 \\
&= \int_{\mathbb{R}^d} \left[\frac{|\nabla\rho_g|^2}{8\rho_g} - \frac{\nabla\rho_g^\varepsilon\cdot\nabla\rho_g}{4(\rho_g^\varepsilon+\varepsilon)} + \frac{|\nabla\rho_g^\varepsilon|^2(\rho_g+\varepsilon)}{8(\rho_g^\varepsilon+\varepsilon)^2}\right] d\mathbf{x} + \frac{\beta}{2}\|\rho_g-\rho_g^\varepsilon\|^2 + \frac{\delta}{2}\|\nabla(\rho_g-\rho_g^\varepsilon)\|^2 \\
&\geq \int_{\mathbb{R}^d} \left[\frac{|\nabla\rho_g||\nabla\rho_g^\varepsilon|}{4(\rho_g^\varepsilon+\varepsilon)} - \frac{\nabla\rho_g^\varepsilon\cdot\nabla\rho_g}{4(\rho_g^\varepsilon+\varepsilon)}\right] d\mathbf{x} + \frac{\beta}{2}\|\rho_g-\rho_g^\varepsilon\|^2 + \frac{\delta}{2}\|\nabla(\rho_g-\rho_g^\varepsilon)\|^2 \\
&\geq \frac{\beta}{2}\|\rho_g-\rho_g^\varepsilon\|^2 + \frac{\delta}{2}\|\nabla(\rho_g-\rho_g^\varepsilon)\|^2, \qquad (4.3.31)
\end{aligned}
$$

where Lemma 4.3.2 is applied in the first inequality. □

Next we aim to study the convergence of the ground state of the discrete regularized energy, i.e. $\rho_g^{h,\varepsilon}$, as $h \to 0^+$. Only the 1D case is considered here for simplicity. Extension to 2D and 3D is similar. First, the following lemma, which will used later in the study of the convergence, can be observed.

Lemma 4.3.3. *For any nonnegative vectors $f, g \in \mathbb{R}^{N-1}$ and matrix A (4.2.4), we have $f^T A f \geq (f^2/g)^T A g$.*

Proof. The matrix A (4.2.4) can be decomposed as $A = \frac{1}{h^2}I + B$, where I is the identity matrix and B is a symmetric matrix with $B_{i,j} \leq 0$ and $B_{i,i} = 0$. Then

$$
\begin{aligned}
f^T A f - (f^2/g)^T A g = f^T B f - (f^2/g)^T B g &= \sum_{i,j}[f_i B_{i,j} f_j - f_i^2/g_i B_{i,j} g_j] \\
&= \sum_{i\neq j} B_{i,j}(f_i f_j - \frac{1}{2}f_i^2 g_j/g_i - \frac{1}{2}f_j^2 g_i/g_j) \geq 0
\end{aligned}
$$

□

Then we have the following theorem, which tells us that the disctere l_2 and h_1 norm can be bounded by the difference of the energy if $\beta > 0$ and $\delta > 0$.

Theorem 4.3.4. *For the ground states* $\rho_g^{h,\varepsilon} = (\rho_{g,1}^{h,\varepsilon}, \rho_{g,2}^{h,\varepsilon}, \dots, \rho_{g,N-1}^{h,\varepsilon})^T \in \mathbb{R}^{N-1}$ (4.3.10) *and an arbitrary density vector* $\rho^h = (\rho_1^h, \rho_2^h, \dots, \rho_{N-1}^h)^T \in \mathbb{R}^{N-1}$ *satisfying* $\rho^h \geq 0$, $\rho_0 = \rho_N = 0$ *and* $\|\rho^h\|_{h_1} = 1$, *we have*

$$h\sum_{j=0}^{N-1}\left[\frac{\beta}{2}|\rho_{g,j}^{h,\varepsilon} - \rho_j^h|^2 + \frac{\delta}{2}\left|\delta_+\rho_j^h - \delta_+\rho_{g,j}^{h,\varepsilon}\right|^2\right] \leq E_{h,\varepsilon}^{\mathrm{FD}}(\rho^h) - E_{h,\varepsilon}^{\mathrm{FD}}(\rho_g^{h,\varepsilon}). \tag{4.3.32}$$

Proof. For simplicity, we rewrite the discrete energy (4.3.7) by using the matrix (4.2.4). Noticing that

$$\sum_{j=0}^{N-1}|\frac{f_{j+1}-f_j}{h}|^2 = 2f^TAf, \tag{4.3.33}$$

for aritrary $f = (f_1, f_2, \dots, f_{N-1})^T$ with $f_0 = f_N = 0$, we have

$$\begin{aligned} E_{h,\varepsilon}^{\mathrm{FD}}(\rho) &= h\sum_{j=0}^{N-1}\left[\frac{1}{2}|\frac{\sqrt{\rho_{j+1}+\varepsilon}-\sqrt{\rho_j+\varepsilon}}{h}|^2 + V_j\rho_j + \frac{\beta}{2}\rho_j^2 + \frac{\delta}{2}|\frac{\rho_{j+1}-\rho_j}{h}|^2\right] \\ &= h\sum_{j=0}^{N-1}\left[V_j\rho_j + \frac{\beta}{2}\rho_j^2\right] + hg^TAg + h\delta\rho^TA\rho, \end{aligned}$$

where $g = \sqrt{\rho+\varepsilon} - \sqrt{\varepsilon}$.

Define $f(t) = E_{h,\varepsilon}^{\mathrm{FD}}(\rho_g^{h,\varepsilon} + t(\rho^h - \rho_g^{h,\varepsilon}))$, then we have $f'(0) \geq 0$. A direct computation implies the following the inequality

$$h(V + \beta\rho_g^{h,\varepsilon} + 2\delta A\rho_g^{h,\varepsilon})^T(\rho^h - \rho_g^{h,\varepsilon}) + h\left(\sqrt{\rho_g^{h,\varepsilon}+\varepsilon} - \sqrt{\varepsilon}\right)^T A\frac{\rho^h - \rho_g^{h,\varepsilon}}{\sqrt{\rho_g^{h,\varepsilon}+\varepsilon} - \sqrt{\varepsilon}} \geq 0. \tag{4.3.34}$$

Now we compute the difference of the energies:

$$
\begin{aligned}
&E^{\mathrm{FD}}_{h,\varepsilon}(\rho^h) - E^{\mathrm{FD}}_{h,\varepsilon}(\rho_g^{h,\varepsilon}) = f(1) - f(0)\\
&= h(V + \frac{\beta}{2}(\rho^h + \rho_g^{h,\varepsilon}) + \delta A(\rho^h + \rho_g^{h,\varepsilon}))^T(\rho^h - \rho_g^{h,\varepsilon})\\
&\quad + h(\sqrt{\rho^h + \varepsilon} - \sqrt{\varepsilon})^T A(\sqrt{\rho^h + \varepsilon} - \sqrt{\varepsilon}) - h(\sqrt{\rho_g^{h,\varepsilon} + \varepsilon} - \sqrt{\varepsilon})^T A(\sqrt{\rho_g^{h,\varepsilon} + \varepsilon} - \sqrt{\varepsilon}),\\
&= h(V + \beta\rho_g^{h,\varepsilon} + 2\delta A\rho_g^{h,\varepsilon})^T(\rho^h - \rho_g^{h,\varepsilon}) + \frac{\beta}{2}\|\rho^h - \rho_g^{h,\varepsilon}\|^2 + h\delta(\rho^h - \rho_g^{h,\varepsilon})^T A(\rho^h - \rho_g^{h,\varepsilon})\\
&\quad + h(\sqrt{\rho^h + \varepsilon} - \sqrt{\varepsilon})^T A(\sqrt{\rho^h + \varepsilon} - \sqrt{\varepsilon}) - h(\sqrt{\rho_g^{h,\varepsilon} + \varepsilon} - \sqrt{\varepsilon})^T A(\sqrt{\rho_g^{h,\varepsilon} + \varepsilon} - \sqrt{\varepsilon}),\\
&\geq -h(\sqrt{\rho_g^{h,\varepsilon} + \varepsilon} - \sqrt{\varepsilon})^T A\frac{\rho^h - \rho_g^{h,\varepsilon}}{\sqrt{\rho_g^{h,\varepsilon} + \varepsilon} - \sqrt{\varepsilon}} + \frac{\beta}{2}\|\rho^h - \rho_g^{h,\varepsilon}\|^2 + h\delta(\rho^h - \rho_g^{h,\varepsilon})^T A(\rho^h - \rho_g^{h,\varepsilon})\\
&\quad + h(\sqrt{\rho^h + \varepsilon} - \sqrt{\varepsilon})^T A(\sqrt{\rho^h + \varepsilon} - \sqrt{\varepsilon}) - h(\sqrt{\rho_g^{h,\varepsilon} + \varepsilon} - \sqrt{\varepsilon})^T A(\sqrt{\rho_g^{h,\varepsilon} + \varepsilon} - \sqrt{\varepsilon}),\\
&= -h(\sqrt{\rho_g^{h,\varepsilon} + \varepsilon} - \sqrt{\varepsilon})^T A\frac{(\sqrt{\rho^h + \varepsilon} - \sqrt{\varepsilon})^2}{\sqrt{\rho_g^{h,\varepsilon} + \varepsilon} - \sqrt{\varepsilon}} + \frac{\beta}{2}\|\rho^h - \rho_g^{h,\varepsilon}\|^2 + h\delta(\rho^h - \rho_g^{h,\varepsilon})^T A(\rho^h - \rho_g^{h,\varepsilon})\\
&\quad + h(\sqrt{\rho^h + \varepsilon} - \sqrt{\varepsilon})^T A(\sqrt{\rho^h + \varepsilon} - \sqrt{\varepsilon}),\\
&\geq \frac{\beta}{2}\|\rho^h - \rho_g^{h,\varepsilon}\|^2 + h\delta(\rho^h - \rho_g^{h,\varepsilon})^T A(\rho^h - \rho_g^{h,\varepsilon})\\
&= \frac{\beta}{2}\|\rho^h - \rho_g^{h,\varepsilon}\|^2 + \frac{\delta}{2}\|\delta_+\rho^h - \delta_+\rho_g^{h,\varepsilon}\|^2,
\end{aligned}
$$

where we applies Lemma 4.3.3 in the last inequality by letting $f = \sqrt{\rho^h + \varepsilon} - \sqrt{\varepsilon}$ and $g = \sqrt{\rho_g^{h,\varepsilon} + \varepsilon} - \sqrt{\varepsilon}$. □

Based on Theorem 4.3.4, we can study the discrete l_2 and h_1 error estimates. For simplicity, we use the notation $\tilde{\rho}_g^{\varepsilon}$ to be the interpolation of the ground state ρ_g^{ε} (4.3.4) on the grid points, i.e.

$$
\tilde{\rho}_g^{\varepsilon} = (\rho_g^{\varepsilon}(x_1), \rho_g^{\varepsilon}(x_2), \ldots, \rho_g^{\varepsilon}(x_{N-1}))^T. \tag{4.3.35}
$$

Then we have the following results considering the limit $h \to 0^+$.

Theorem 4.3.5. *Fix ε and denote the error to be $e^{\varepsilon} = \tilde{\rho}_g^{\varepsilon} - \rho_g^{h,\varepsilon}$. If $\beta > 0$ and $\delta > 0$ and $|\rho_g^{\varepsilon}|_{H^2}$ is bounded, then we have*

$$
|e^{\varepsilon}|_{H^1} := \|\delta_+ e^{\varepsilon}\|_{l^2} = \mathcal{O}(h), \quad \|e^{\varepsilon}\|_{l^2} = \mathcal{O}(h^2). \tag{4.3.36}
$$

Proof. Since $\tilde{\rho}_g^{\varepsilon}$ is the interpolation of the ground states on the grid points, it's easy to check that $E^{\varepsilon}(\rho_g^{\varepsilon}) = E^{\mathrm{FD}}_{h,\varepsilon}(\tilde{\rho}_g^{\varepsilon}) + \mathcal{O}(h^2)$. Besides, if we consider the piecewise linear

function $\tilde{\rho}_g^{h,\varepsilon}$ in the domain such that $\tilde{\rho}_g^{h,\varepsilon}(x_j) = \rho_{g,j}^{h,\varepsilon}$, i.e. $\tilde{\rho}_g^{h,\varepsilon}$ is the piecewise linear interpolation of ρ_g^{ε}, a similar procedure implies that $E^{\varepsilon}(\tilde{\rho}_g^{h,\varepsilon}) = E_{h,\varepsilon}^{\mathrm{FD}}(\rho_g^{h,\varepsilon}) + \mathcal{O}(h^2)$. Then recalling Theorem 4.3.4, we have

$$\begin{aligned}\frac{\beta}{2}\|e^{\varepsilon}\|_{l_2}^2 + \frac{\delta}{2}\|\delta_+ e^{\varepsilon}\|_{l_2}^2 &\leq E_{h,\varepsilon}^{\mathrm{FD}}(\tilde{\rho}_g^{\varepsilon}) - E_{h,\varepsilon}^{\mathrm{FD}}(\rho_g^{h,\varepsilon}) \\ &= E^{\varepsilon}(\rho_g^{\varepsilon}) - E^{\varepsilon}(\tilde{\rho}_g^{h,\varepsilon}) + \mathcal{O}(h^2) \\ &\leq \mathcal{O}(h^2).\end{aligned}$$

The fact that $E^{\varepsilon}(\rho_g^{\varepsilon}) \leq E^{\varepsilon}(\rho_g^{h,\varepsilon})$ is applied in the last step. Therefore, if we assume $\beta > 0$ and $\delta > 0$, we can get $|e^{\varepsilon}|_{H^1} < C(\varepsilon)h$, which will further implies $\|e^{\varepsilon}\|_{L^2} < C(\varepsilon)h^2$ by Bramble-Hilbert lemma and a standard scaling argument. □

Remark 4.3.3. *The above theorem is only true for a fixed ε. It's not clear yet whether there is a uniform bound for $C(\varepsilon)$ with respect to ε.*

In the last part of this subsection, we study the convergence of $\rho_g^{h,\varepsilon}$ as $\varepsilon \to 0^+$. Obviously for $\beta > 0$ and $\delta > 0$, $E_{h,\varepsilon}^{\mathrm{FD}}$ is bounded from below and convex. Therefore ρ_g^h exists and is unique. In this case, we can show the convergence of $\rho_g^{h,\varepsilon}$ to ρ_g^h as $\varepsilon \to 0^+$.

Theorem 4.3.6. *If $\beta > 0$ and $\delta > 0$, then ρ_g^h exists and is unique and we have*

$$\rho_g^{h,0} = \lim_{\varepsilon \to 0^+} \rho_g^{h,\varepsilon} = \rho_g^h. \tag{4.3.37}$$

Proof. Existence and uniqueness are obvious. Only (4.3.37) is proven here. Because of the boundedness and compactness of the feasible set S (4.3.17), for any sequence $\varepsilon_n \to 0$, there exists a subsequence ε_{n_k} such that $\rho_g^{h,\varepsilon_{n_k}} \to \tilde{\rho}$ for some $\tilde{\rho} \in S$. A term by term convergence implies that $E_{h,\varepsilon_{n_k}}^{\mathrm{FD}}(\rho_g^{h,\varepsilon_{n_k}}) \to E_{h,0}^{\mathrm{FD}}(\tilde{\rho})$.

On the other hand, for any ε, we have $E_{h,\varepsilon}^{\mathrm{FD}}(\rho_g^{h,\varepsilon}) \leq E_{h,\varepsilon}^{\mathrm{FD}}(\rho_g^h) \leq E_{h,0}^{\mathrm{FD}}(\rho_g^h)$, which indicates that $E_{h,0}^{\mathrm{FD}}(\tilde{\rho}) \leq E_{h,0}^{\mathrm{FD}}(\rho_g^h)$. Therefore, we must have $\tilde{\rho} = \rho_g^h$ due to the uniqueness of the minimizer of $E_{h,0}^{\mathrm{FD}}$. Noticing that the above argument is true for any sequence $\varepsilon_n \to 0$, we get the conclusion. □

4.3.4 Fast iterative shrinkage-thresholding algorithm

In this section, we will describe explicitly the algorithm and introduce briefly the method used for solving (4.3.10), which is the key step in updating. The stopping criteria in Algorithm 2 and Algorithm 3 can be chosen as $\|\rho^{(n,m)} - \rho^{(n,m-1)}\|_\infty < \eta_0$ for a given $0 < \eta_0 \ll 1$.

Algorithm 2 Main procedure

Set $n = 1$, $\beta \geq 0$ and $\delta \geq 0$.
Set a sequence $\{\varepsilon_k\} \geq 0$ satisfying $\lim_{k\to\infty} \varepsilon_k = 0$. Set $\varepsilon = \varepsilon_1$.
INITIALIZATION: construct $\rho^{(1,0)}$ which is suitable for given β, δ.
while ε not small enough **do** ▷ Stop at a small ε
    $m \leftarrow 0$
    while stopping conditions are not met **do** ▷ Stop when converge
        $m \leftarrow m + 1$
        UPDATE: solve (4.3.10) update $\rho^{(n,m)}$ from $\rho^{(n,m-1)}$
    end while
    $\varepsilon \leftarrow \varepsilon_{n+1}$ and $\rho^{(n+1,0)} \leftarrow \rho^{(n,m)}$
    $n \leftarrow n + 1$
end while

For the updating from $\rho^{(n,m-1)}$ to $\rho^{(n,m)}$, the Fast Iterative Shrinkage-Thresholding Algorithm (FISTA) proposed by Amir Beck and Marc Teboulle [35], which is a gradient based method generalized from [89], can be applied. FISTA, a kind of the accelerated proximal gradient (APG) method, has been widely used since proposed due to its simplicity and fast convergence. We will introduce briefly FISTA here for self-consistency. Consider the problem

$$\rho_g^{h,\varepsilon} = \arg\min_{\rho\in\Delta} E_{h,\varepsilon}(\rho), \tag{4.3.38}$$

where $E_{h,\varepsilon}$ can be $E_{h,\varepsilon}^{\mathrm{FD}}$ or discrete energy via other spatial discretization,

$$\Delta = \{\rho \in \mathbb{R}^{N+1} : \|\rho\|_{h_1} = 1, \rho \geq 0, \rho_0 = \rho_N = 0\} \tag{4.3.39}$$

is the feasible set. Denote $\rho^{(k)}$ to be the solution after k-th step from the given initial value $\rho^{(0)}$. It can be proved that $E_{h,\varepsilon}(\rho^{(k)}) - E_{h,\varepsilon}(\rho_g^{h,\varepsilon}) = \mathcal{O}(1/k^2)$, i.e. we will have a convergence rate $\mathcal{O}(1/k^2)$ [35, 89].

FISTA originates from the projected gradient method, which combines a proximal step with a gradient step. Instead of considering the problem (4.3.38) directly, we study the following equivalent problem,

$$\rho_g^{h,\varepsilon} = \arg\min_{\rho\in\mathbb{R}^{N+1}} \quad E_{h,\varepsilon}(\rho) + \mathbb{I}_\Delta(\rho), \tag{4.3.40}$$

where $\mathbb{I}_\Delta$ is the indicator function defined as

$$\mathbb{I}_\Delta(\rho) = \begin{cases} 0, & \text{if } \rho \in \Delta, \\ \infty, & \text{otherwise.} \end{cases} \tag{4.3.41}$$

Notice that by rewriting the problem (4.3.38) as (4.3.40), we get a nonsmooth optimization problem with no constraints. The objective function can be viewed as a combination of a convex function that is continuously differentiable with Lipschitz continuous gradient and another convex extended-valued function which is possibly nonsmooth. Then the popular ISTA method can be applied as proposed in [35, 46, 56, 62, 109] and so on. FISTA is quite similar to ISTA, but unlike ISTA which uses data in the current step only, FISTA uses a very special linear combination of the current data and the data in the previous step. Surprisingly, this trick enables us to improve the convergence rate from sublinear to $\mathcal{O}(1/k^2)$.

For simplicity, we introduce the following notations. For given $L > 0$, denote the quadratic approximation of $E_{h,\varepsilon}(\rho) + \mathbb{I}_\Delta(\rho)$ at a given point $\rho = y$ as

$$Q_L(x, y) := E_{h,\varepsilon}(y) + < x - y, \nabla E_{h,\varepsilon}(y) > + \frac{L}{2}\|x - y\|_2 + \mathbb{I}_\Delta(x), \tag{4.3.42}$$

which admits a unique minimizer

$$p_L(y) := \arg\min\{Q_L(x, y) : x \in \mathbb{R}^{N+1}\}. \tag{4.3.43}$$

Simple algebra implies that (ignoring constant terms in y)

$$p_L(y) = \arg\min_{x\in\mathbb{R}^{N+1}} \left\{ \mathbb{I}_\Delta(x) + \frac{L}{2}\|x - \left(y - \frac{1}{L}\nabla E_{h,\varepsilon}(y)\right)\|^2 \right\}, \tag{4.3.44}$$

$$= \arg\min_{x\in\Delta} \|x - \left(y - \frac{1}{L}\nabla E_{h,\varepsilon}(y)\right)\|^2. \tag{4.3.45}$$

Obviously for our problem, to compute $p_L(y)$ is equivalent to find the projection of $y - \frac{1}{L}\nabla E_{h,\varepsilon}(y)$ onto the feasible set Δ (4.3.39). Due to the special structure of Δ, which is a simplex, we may apply efficient existing routines for this step [73, 75, 83]. Finally, the update step in Algorithm 2 where FISTA is applied is summarized as Algorithm 3.

Algorithm 3 Update with backtracking

Given the current solution $\rho^{(0)}$ and ε.
Set $k = 1$, $L_0 > 0$, $\eta > 1$, $y_1 = \rho^{(0)}$ and $t_1 = 1$.
Set $\bar{L} = L_0$, $\tilde{\rho} = P_{\bar{L}}(y_k)$.
while stopping conditions are not met or $k = 0$ **do**
    while $E_{h,\varepsilon}(\tilde{\rho}) > Q_{\bar{L}}(\tilde{\rho}, y_k)$ **do**
        $\bar{L} \leftarrow \eta\bar{L}$
        $\tilde{\rho} \leftarrow P_{\bar{L}}(y_k)$
    end while
    $\rho^{(k)} \leftarrow \tilde{\rho}$, $t_{k+1} \leftarrow \frac{1+\sqrt{1+4t_k^2}}{2}$
    $L_k \leftarrow \bar{L}$, $y_{k+1} \leftarrow \tilde{\rho} + \left(\frac{t_k - 1}{t_{k+1}}\right)(\tilde{\rho} - \rho^{(k-1)})$
    $k \leftarrow k + 1$
end while

4.3.5 Accuracy test

In this section, we perform numerical tests to check the accuracy of our methods proposed in Section 4.3.

Firstly, the impact of the mesh size h will be tested. We fix $\varepsilon = 0.1$. The setup of the numerical is chosen to be the one in Example 4.1.1, and the 'exact' solution is

Error	$h = 1/8$	$h/2$	$h/2^2$	$h/2^3$	$h/2^4$
$\lvert E^\varepsilon(\rho_{g,h}^{\varepsilon,\mathrm{FD}}) - E^\varepsilon(\rho_g^\varepsilon)\rvert$	1.34E-5	2.85E-6	5.86E-7	1.33E-7	3.28E-8
rate	-	2.23	2.28	2.14	2.02
$\lVert\rho_{g,h}^{\varepsilon,\mathrm{FD}} - \rho_g^\varepsilon\rVert_{l_2}$	8.51E-5	1.92E-5	3.13E-6	9.70E-7	2.40E-7
rate	-	2.15	2.62	1.69	2.02
$\lVert\rho_{g,h}^{\varepsilon,\mathrm{FD}} - \rho_g^\varepsilon\rVert_{h_1}$	2.09E-3	1.16E-3	6.52E-4	3.39E-4	1.66E-4
rate	-	0.85	0.83	0.94	1.03
$\lVert\rho_{g,h}^{\varepsilon,\mathrm{FD}} - \rho_g^\varepsilon\rVert_{\infty}$	2.15E-4	6.25E-5	2.28E-5	6.01E-6	1.40E-6
rate	-	1.78	1.45	1.92	2.10

Table 4.7: Spatial resolution of the ground state for Case I in Example 4.1.1.

chosen to be the one computed by Algorithm 2 using the discretized energy (4.3.7) with a sufficiently small mesh size $h = 1/1024$. We denote the numerical ground state using the energy (4.3.7) to be $\rho_{g,h}^{\varepsilon,\mathrm{FD}}$, then Table 4.7 listed the errors for Case I and Table 4.8 listed the errors for Case II. From Table 4.7 and Table 4.8, we can see that the the numerical ground state computed using (4.3.7) is second order accurate in L_2 norm.

It's remarkable that the numerical test for Case II implies the convergence order proposed in Theorem 4.3.5 is true. Note that the results in Theorem 4.3.5 is valid only for $\beta \geq 0$ and $\delta > 0$. For $\beta > 0$ with $\delta = 0$, a similar procedure only guarantee the first order accuracy in L_2 norm and there will be no results for the accuracy in H_1 norm. However, the numerical test for Case I shows that, though not perfect, we still have roughly second order accuracy in L_2 norm and first order accuracy in H_1 norm.

Next, we study the convergence as $\varepsilon \to 0^+$. In this case, for each fixed $\varepsilon > 0$, a sufficiently small mesh size is chosen to avoid the spatial discretization error. In practice, the finite difference method (4.3.7) with a sufficiently small mesh size is used to guarantee the spatial error negligible. A small ε usually requires fine mesh as numerically tested. The exact solution for $\varepsilon = 0$ is chosen to be the one computed

Error	$h = 1/8$	$h/2$	$h/2^2$	$h/2^3$	$h/2^4$
$\lvert E^\varepsilon(\rho_{g,h}^{\varepsilon,\mathrm{FD}}) - E^\varepsilon(\rho_g^\varepsilon)\rvert$	6.21E-4	1.60E-4	3.97E-5	9.91E-6	2.45E-6
rate	-	1.96	2.01	2.00	2.02
$\lVert\rho_{g,h}^{\varepsilon,\mathrm{FD}} - \rho_g^\varepsilon\rVert_{l_2}$	8.19E-5	2.04E-5	4.88E-6	9.81E-7	2.42E-7
rate	-	2.00	2.06	2.31	2.02
$\lVert\rho_{g,h}^{\varepsilon,\mathrm{FD}} - \rho_g^\varepsilon\rVert_{h_1}$	3.54E-3	1.77E-3	8.85E-4	4.42E-4	2.20E-4
rate	-	1.00	1.00	1.00	1.01
$\lVert\rho_{g,h}^{\varepsilon,\mathrm{FD}} - \rho_g^\varepsilon\rVert_\infty$	9.77E-5	3.12E-5	8.17E-6	1.92E-6	4.01E-7
rate	-	1.65	1.94	2.09	2.26

Table 4.8: Spatial resolution of the ground state for Case II in Example 4.1.1.

with a sufficiently small ε and a sufficiently small mesh size h depending on ε. Table 4.9 and Table 4.10 list the results of convergence as $\varepsilon \to 0^+$. As seen from the table, we will have the order of convergence approaching 1 as $\varepsilon \to 0^+$ though the exact order is not quite clear.

4.4 Numerical results

In this section, we'll apply the methods proposed before for 1D and 2D problems. We will perform numerical experiments to show that our methods does work for general problems. Since all the three methods will lead to similar numerical results, we will not state explicitly which method is used for computing the ground state for the rest of this section and will mainly focus on the effects of the parameters β, δ and the phenomenons we get.

The effect of the HOI term for the 1D case under a box or a harmonic potential is shown in Fig. 4.2. As shown in Fig. 4.2, the increase of δ will drive the two sides of the ground state solution away from center.

For 2D problems, we first compute the ground states of the MGPE (2.4.1) under a box potential (2.4.3). To be more specific, we consider the MGPE in $\Omega = (0, 1) \times$

Error	$\varepsilon = \frac{1}{40}$	$\varepsilon/2^2$	$\varepsilon/2^4$	$\varepsilon/2^6$	$\varepsilon/2^8$	$\varepsilon/2^{10}$
$\lvert E^\varepsilon(\rho_g^\varepsilon) - E(\rho_g)\rvert$	1.29E-2	8.15E-3	4.14E-3	1.76E-3	6.64E-4	2.30E-4
rate	-	0.33	0.49	0.62	0.70	0.76
$\lvert E(\rho_g^\varepsilon) - E(\rho_g)\rvert$	6.56E-3	3.71E-3	1.41E-3	5.20E-4	1.52E-4	4.56E-5
rate	-	0.41	0.70	0.72	0.89	0.87
$\lVert\rho_g^\varepsilon - \rho_g\rVert_{l_2}$	1.09E-3	6.68E-4	3.03E-4	1.06E-4	3.19E-5	8.47E-6
rate	-	0.35	0.57	0.75	0.87	0.96
$\lVert\rho_g^\varepsilon - \rho_g\rVert_{h_1}$	4.59E-3	2.64E-3	1.13E-3	3.77E-4	1.07E-4	2.76E-5
rate	-	0.40	0.62	0.79	0.90	0.98
$\lVert\rho_g^\varepsilon - \rho_g\rVert_{\infty}$	1.23E-3	7.02E-4	2.98E-4	1.02E-4	3.06E-5	8.44E-6
rate	-	0.41	0.62	0.77	0.87	0.92

Table 4.9: Convergence test for Case I in Example 4.1.1 as $\varepsilon \to 0^+$.

Error	$\varepsilon = \frac{1}{80}$	$\varepsilon/2$	$\varepsilon/2^2$	$\varepsilon/2^3$	$\varepsilon/2^4$	$\varepsilon/2^5$
$\lvert E^\varepsilon(\rho_g^\varepsilon) - E(\rho_g)\rvert$	1.88E-2	1.36E-2	9.46E-3	6.30E-3	4.05E-3	2.52E-3
rate	-	0.47	0.53	0.59	0.64	0.69
$\lvert E(\rho_g^\varepsilon) - E(\rho_g)\rvert$	3.71E-3	3.08E-3	2.37E-3	1.64E-3	1.04E-3	6.12E-4
rate	-	0.27	0.38	0.54	0.65	0.77
$\lVert\rho_g^\varepsilon - \rho_g\rVert_{l_2}$	7.75E-4	5.82E-4	4.20E-4	2.91E-4	1.98E-4	1.38E-4
rate	-	0.41	0.47	0.53	0.55	0.53
$\lVert\rho_g^\varepsilon - \rho_g\rVert_{h_1}$	2.26E-3	1.83E-3	1.37E-3	9.46E-4	5.97E-4	3.54E-4
rate	-	0.30	0.41	0.54	0.66	0.75
$\lVert\rho_g^\varepsilon - \rho_g\rVert_{\infty}$	7.76E-4	6.13E-4	4.52E-4	3.10E-4	1.98E-4	1.18E-4
rate	-	0.34	0.44	0.54	0.65	0.75

Table 4.10: Convergence test for Case II in Example 4.1.1 as $\varepsilon \to 0^+$.

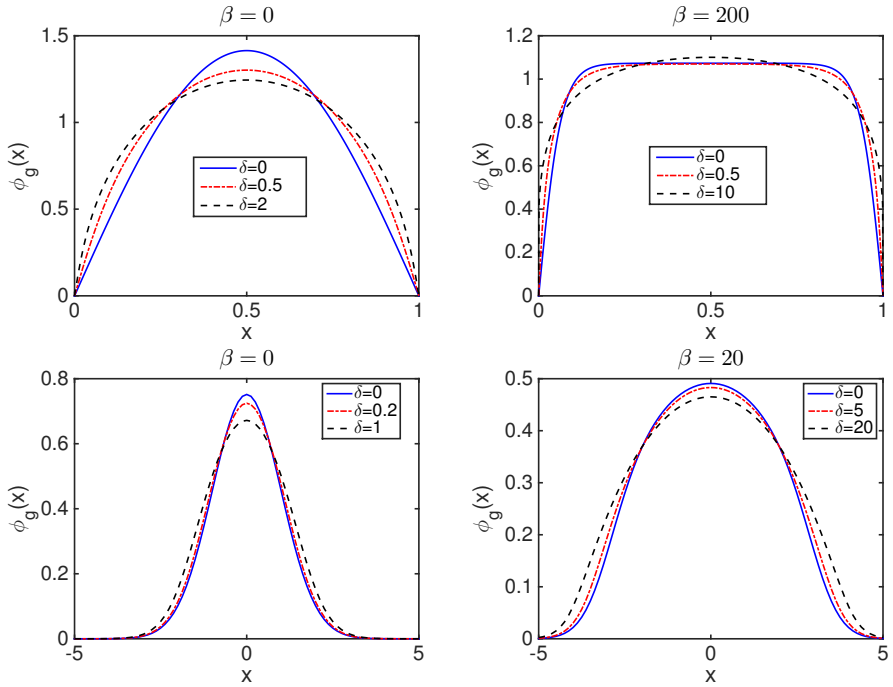

Figure 4.2: Graph for ground states $\phi_g(\mathbf{x})$ under the box potential in $(0,1)$ (top) or the harmonic potential $V(x) = x^2/2$ (bottom).

$(0,1)$ with $V(x,y) = 0$ where $(x,y) \in \Omega$ and $\phi|_{\partial\Omega} = 0$. We will test for different pairs of $\beta \geq 0$ and $\delta \geq 0$. The initial values are properly chosen according to the values of β and δ, where the complete guidance can be found in Section 3.4. Fig. 4.3 shows the numerical results of ground states with box potential with different β's and δ's.

Next, we will compute the ground states of the MGPE (2.4.1) under the harmonic potential $V(x,y) = (x^2 + 4y^2)/2$, and the computational domain is chosen as $\Omega = (-6,6) \times (-6,6)$. Again, different pairs of $\beta \geq 0$ and $\delta \geq 0$ will be tested and the initial values will be properly chosen according to the values of β and δ according to the results in Section 3.3. Fig. 4.4 shows the numerical results of ground states with harmonic potential with different β's and δ's.

Finally, we will consider the ground states under a harmonic potential combined with an optical potential, i.e. $V(x,y) = (x^2 + y^2)/2 + 20(\sin(\pi x/4)^2 + \sin(\pi y/4)^2)$, and choose the computational domain to be $\Omega = (-6,6) \times (-6,6)$. For tests with

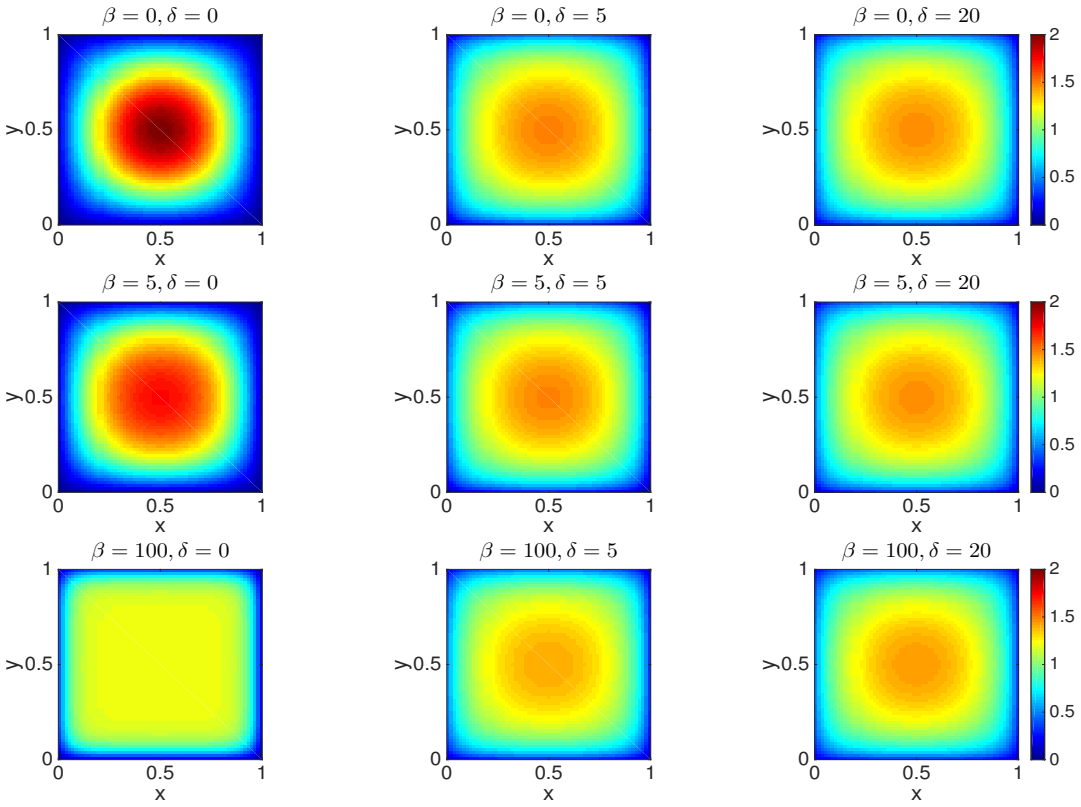

Figure 4.3: Graph for ground states $\phi_g(\mathbf{x})$ with $\beta = 0, 5, 100$ (from top to bottom) and $\delta = 0, 5, 20$ (from left to right) under the box potential in $(0, 1) \times (0, 1)$.

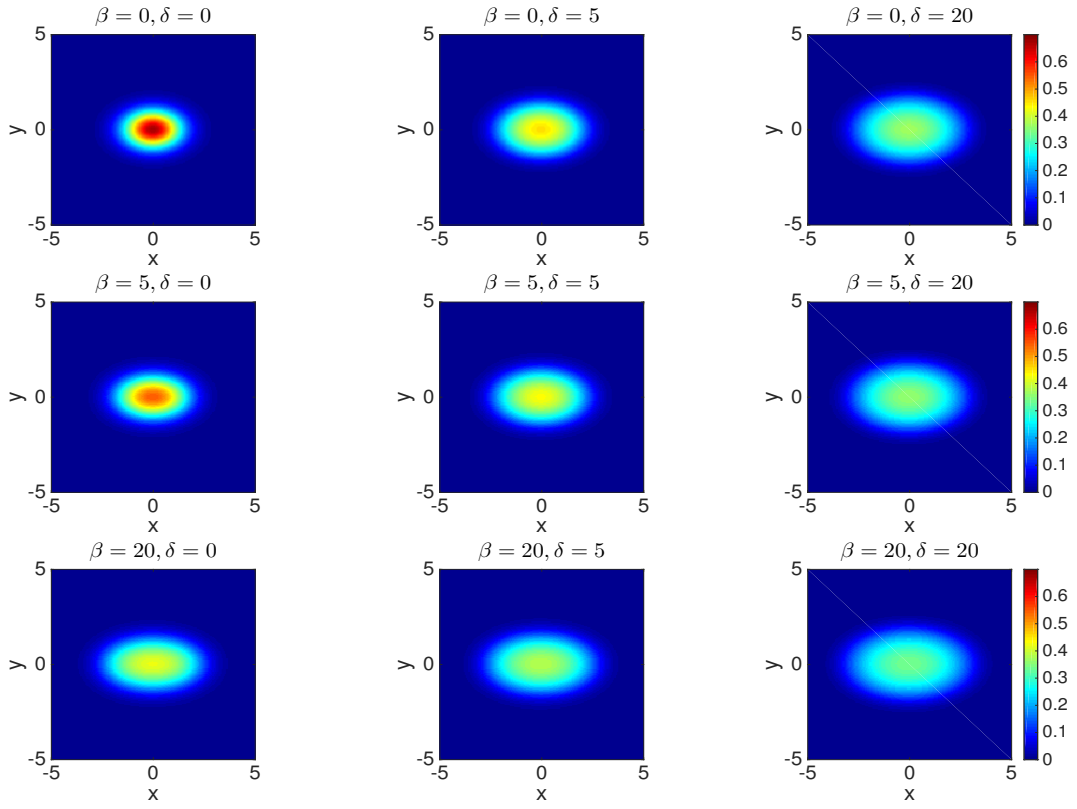

Figure 4.4: Graph for ground states $\phi_g(\mathbf{x})$ with $\beta = 0, 5, 20$ (from top to bottom) and $\delta = 0, 5, 20$ (from left to right) under the harmonic potential $V(x, y) = (x^2 + 4y^2)/2$.

a general external potential, we may just choose the initial data to be of Gaussian type. Fig. 4.5 shows the numerical results of ground states with this new potential with different β's and δ's.

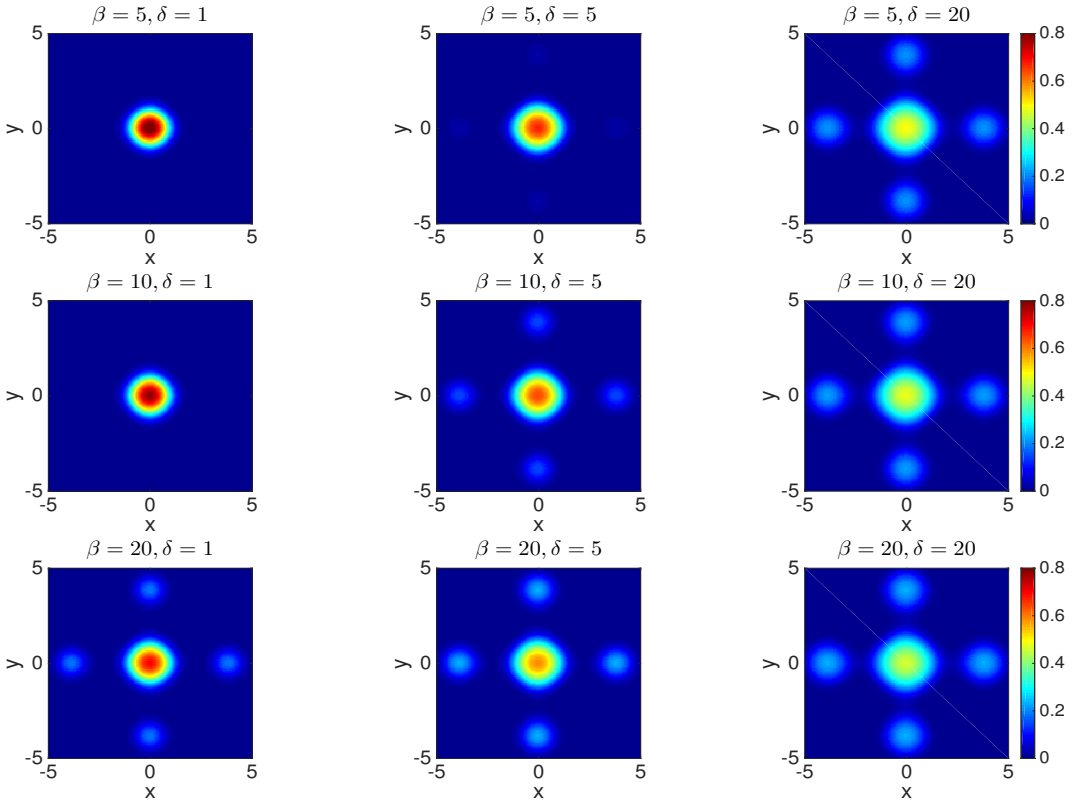

Figure 4.5: Graph for ground states $\phi_g(\mathbf{x})$ with $\beta = 5, 10, 20$ (from top to bottom) and $\delta = 1, 5, 20$ (from left to right) under the potential $V(x, y) = (x^2 + y^2)/2 + 20(\sin(\pi x/4)^2 + \sin(\pi y/4)^2)$.

It can be seen from Fig. 4.3, Fig. 4.4 and Fig. 4.5 that both the increase of β and δ will lead to stronger repulsive interaction and the solution will become more flat.

Chapter 5

Dynamics and its Computation

In this chapter, we investigate the dynamics of BEC with HOI governed by the MGPE (2.4.1). In particular, we would like to see how the δ term affects the dynamics. It is worth pointing out that the local well-posedness of the MGPE (2.4.1) with the initial data

$$\psi(\mathbf{x}, 0) = \psi_0(\mathbf{x}), \qquad \mathbf{x} \in \mathbb{R}^d, \tag{5.0.1}$$

has been established [87,94]. Accordingly, we will assume the MGPE (2.4.1) admits a smooth solution $\psi(\mathbf{x}, t)$ in the subsequent discussion.

5.1 Dynamical properties

In this part, we will show the behavior of important quantities, namely the mass, energy, momentum, the center of mass and angular momentum expectation, that measure the dynamical properties of the MGPE.

First, let's consider the mass (L2-norm) (2.4.5) and the energy (2.4.6).

Lemma 5.1.1. *Assume $\psi(\mathbf{x}, t)$ is the solution of (2.4.1) with $E(\psi(\mathbf{x}, 0)) < \infty$ and $\lim_{|\mathbf{x}|\to\infty} V(\mathbf{x}) = \infty$, then we have*

$$N(t) := \|\psi(\cdot, t)\|_2^2 \equiv N(0) = 1, \quad t \geq 0, \tag{5.1.1}$$

and

$$E(\psi(\mathbf{x},t)) \equiv E(\psi(\mathbf{x},0)), \tag{5.1.2}$$

i.e. the mass and energy of the BEC with HOI will be preserved.

Proof. The confining condition of the external potential $V(\mathbf{x})$ implies that $\lim_{|\mathbf{x}|\to\infty} \psi(\mathbf{x},t) \to 0$. For simplicity, define

$$H\psi = -\frac{1}{2}\Delta\psi + V\psi + \beta|\psi|^2\psi - \delta\Delta(|\psi|^2)\psi, \tag{5.1.3}$$

and then the MGPE (2.4.1) is equivalent of $i\partial_t\psi = H\psi$. For the mass, we have

$$\begin{aligned}\dot{N}(t) &= \int_{\mathbb{R}^d} \left[\psi_t\bar{\psi} + \psi\bar{\psi}_t\right] d\mathbf{x} = \int_{\mathbb{R}^d} \left[-i(H\psi)\bar{\psi} + i(H\bar{\psi})\psi\right] d\mathbf{x} \\ &= \frac{i}{2}\int_{\mathbb{R}^d} \left[\bar{\psi}\Delta\psi - \psi\Delta\bar{\psi}\right] d\mathbf{x} = 0.\end{aligned}$$

For the energy, multiplying $\bar{\psi}_t$ on both sides of the MGPE (2.4.1) and doing integration, we will get

$$i\int_{\mathbb{R}^d} |\partial_t\psi|^2\, d\mathbf{x} = \int_{\mathbb{R}^d} \left[\frac{1}{2}\nabla\psi\nabla\bar{\psi}_t + V(\mathbf{x})\psi\bar{\psi}_t + \beta|\psi|^2\psi\bar{\psi}_t - \delta\Delta(|\psi|^2)\psi\bar{\psi}_t\right] d\mathbf{x}. \tag{5.1.4}$$

Taking the complex conjugate of (5.1.4) on both sides will lead to

$$-i\int_{\mathbb{R}^d} |\partial_t\psi|^2\, d\mathbf{x} = \int_{\mathbb{R}^d} \left[\frac{1}{2}\nabla\bar{\psi}\nabla\psi_t + V(\mathbf{x})\bar{\psi}\psi_t + \beta|\psi|^2\bar{\psi}\psi_t - \delta\Delta(|\psi|^2)\bar{\psi}\psi_t\right] d\mathbf{x}. \tag{5.1.5}$$

Combing (5.1.4) and (5.1.5) together, we will get

$$0 = \partial_t \int_{\mathbb{R}^d} \left[\frac{1}{2}|\nabla\psi|^2 + V(\mathbf{x})|\psi|^2 + \frac{\beta}{2}|\psi|^4 + \frac{\delta}{2}|\nabla(|\psi|^2)|^2\right] d\mathbf{x} = \dot{E}(t), \tag{5.1.6}$$

which is true for all $t \geq 0$ and thus we proved $E(t) \equiv E(0)$. □

Next, consider the momentum defined as

$$\mathbf{P}(t) = \int_{\mathbb{R}^d} \mathrm{Im}(\bar{\psi}(\mathbf{x},t)\nabla\psi(\mathbf{x},t))\, d\mathbf{x}, \quad t \geq 0, \tag{5.1.7}$$

where $\mathrm{Im}(f)$ and $\bar{f}$ denote the imaginary part and complex conjugate of f, respectively. Then we have the following result.

Lemma 5.1.2. *Assume $\psi(\mathbf{x},t)$ is a sufficiently smooth solution of (2.4.1) with (5.0.1) and $|\nabla V(\mathbf{x})| \le C(V(\mathbf{x})+1)$ for $\mathbf{x}\in\mathbb{R}^d$, then we have*

$$\dot{\mathbf{P}}(t) = -\int_{\mathbb{R}^d} |\psi(\mathbf{x},t)|^2 \nabla V(\mathbf{x})\, d\mathbf{x}, \qquad t \ge 0. \tag{5.1.8}$$

In particular, the momentum is conserved if $V(\mathbf{x}) \equiv C_0$ with C_0 a constant.

Proof. The proof is a slight generalization of the one shown in [14, 33]. To be more specific, differentiating (5.1.7) with respect to t, recalling (2.4.1) and integrating by parts using the result that ψ decays to 0 exponentially as $|\mathbf{x}| \to \infty$, we have

$$\begin{aligned}\dot{\mathbf{P}}(t) &= -i\int_{\mathbb{R}^d} \left[\bar{\psi}_t \nabla\psi - \psi_t \nabla\bar{\psi}\right] d\mathbf{x} = \int_{\mathbb{R}^d} \left[(-i\bar{\psi}_t)\nabla\psi + i\psi_t\nabla\bar{\psi}\right] d\mathbf{x} \\ &= \int_{\mathbb{R}^d} \left[(-\frac{1}{2}\nabla^2\bar{\psi} + V(\mathbf{x})\bar{\psi} + \beta|\psi|^2\bar{\psi} - \delta\nabla^2|\psi|^2\bar{\psi})\nabla\psi + c.c.\right] d\mathbf{x},\end{aligned}$$

where *c.c.* denotes the complex conjugate of the first part in the integral. A simple computation implies that

$$\int_{\mathbb{R}^d} \left[-\delta\nabla^2|\psi|^2\bar{\psi}\nabla\psi - \delta\nabla^2|\psi|^2\psi\nabla\bar{\psi}\right] d\mathbf{x} = \frac{\delta}{2}\int_{\mathbb{R}^d} \nabla(|\nabla|\psi|^2|^2) d\mathbf{x} = 0,$$

while the integral of the remained terms is shown in [14] to be

$$\int_{\mathbb{R}^d} \left[(-\frac{1}{2}\nabla^2\bar{\psi} + V(\mathbf{x})\bar{\psi} + \beta|\psi|^2\bar{\psi})\nabla\psi + c.c.\right] d\mathbf{x} = -\int_{\mathbb{R}^d} |\psi(\mathbf{x},t)|^2\nabla V(\mathbf{x})\, d\mathbf{x},$$

and thus we complete the proof. □

The center of mass is another important quantity to describe the dynamics and is defined as

$$\mathbf{x}_c(t) = \int_{\mathbb{R}^d} \mathbf{x}|\psi(\mathbf{x},t)|^2 d\mathbf{x}, \quad t \ge 0, \tag{5.1.9}$$

and we can get the following lemma describing the motion of $\mathbf{x}_c$,

Lemma 5.1.3. *Assume $\psi(\mathbf{x},t)$ is a sufficiently smooth solution of (2.4.1) with (5.0.1), then we have*

$$\dot{\mathbf{x}}_c(t) = \frac{i}{2}\int_{\mathbb{R}^d} \left[\psi\nabla\bar{\psi} - \bar{\psi}\nabla\psi\right] d\mathbf{x}, \quad \ddot{\mathbf{x}}_c(t) = -\int_{\mathbb{R}^d} |\psi(\mathbf{x},t)|^2\nabla V(\mathbf{x}) d\mathbf{x}. \tag{5.1.10}$$

Proof. Analogous to calculation in Lemma 5.1.2, we get

$$\dot{\mathbf{x}}_c(t) = \frac{i}{2}\int_{\mathbb{R}^d} \left[\psi\nabla\bar{\psi} - \bar{\psi}\nabla\psi\right] d\mathbf{x} = \mathbf{P}(t),$$

and then $\ddot{\mathbf{x}}_c(t)$ follows the result in Lemma 5.1.2. □

Next, we consider the angular momentum expectation defined as

$$\langle L_z\rangle = \int_{\mathbb{R}^d} \bar{\psi} L_z \psi d\mathbf{x} = i\int_{\mathbb{R}^d} \bar{\psi}(y\partial_x - x\partial_y)\psi d\mathbf{x}, \tag{5.1.11}$$

and we have the following lemma on the dynamical law of the angular momentum expectation with a harmonic potential.

Lemma 5.1.4. *Assume $\psi(\mathbf{x},t)$ is a sufficiently smooth solution of (2.4.1) with (5.0.1) and $d \geq 2$ and $V(\mathbf{x})$ is a harmonic potential (2.4.2), then we have*

$$\frac{d\langle L_z\rangle}{dt} = \int_{\mathbb{R}^d} (\gamma_x^2 - \gamma_y^2) xy |\psi(\mathbf{x},t)|^2 d\mathbf{x}, \qquad t \geq 0. \tag{5.1.12}$$

Consequently, the angular momentum expectation is conserved if $\gamma_x = \gamma_y$.

Proof. The proof is a generalization of the proof for $\delta = 0$ case shown in [14, 19, 33]. For simplicity, we consider the case $d = 2$. The case $d = 3$ can be derived in a similar way. Differentiate $\langle L_z\rangle$ with respect to t, we get

$$\begin{aligned}\frac{d\langle L_z\rangle}{dt} &= i\int_{\mathbb{R}^d} \left[\bar{\psi}_t(y\partial_x - x\partial_y)\psi + \bar{\psi}(y\partial_x - x\partial_y)\psi_t\right] d\mathbf{x} \\ &= \int_{\mathbb{R}^d} \left[\left(-\frac{1}{2}\nabla^2\bar{\psi} + V(\mathbf{x})\bar{\psi} + \beta|\psi|^2\bar{\psi} - \delta\nabla^2|\psi|^2\bar{\psi}\right)(x\partial_y\psi - y\partial_x\psi) + c.c.\right] d\mathbf{x}.\end{aligned}$$

From results in [14, 19, 33], for the part without δ, we have

$$\begin{aligned}&\int_{\mathbb{R}^d} \left[\left(-\frac{1}{2}\nabla^2\bar{\psi} + V(\mathbf{x})\bar{\psi} + \beta|\psi|^2\bar{\psi}\right)(x\partial_y\psi - y\partial_x\psi) + c.c.\right] d\mathbf{x} \\ &= \int_{\mathbb{R}^d} (\gamma_x^2 - \gamma_y^2) xy|\psi|^2 d\mathbf{x}.\end{aligned}$$

For the remained term, i.e. terms containing δ, we have

$$\begin{aligned}
&\int_{\mathbb{R}^d} \left[-\delta\nabla^2|\psi|^2\bar{\psi}(x\partial_y\psi - y\partial_x\psi) - \delta\nabla^2|\psi|^2\psi(x\partial_y\bar{\psi} - y\partial_x\bar{\psi})\right] d\mathbf{x} \\
&= \delta \int_{\mathbb{R}^d} \nabla|\psi|^2 \cdot \nabla(x\partial_y|\psi|^2 - y\partial_x|\psi|^2)\, d\mathbf{x} \\
&= \delta \int_{\mathbb{R}^d} \left[\frac{1}{2}\partial_y(x|\nabla|\psi|^2|^2) - \frac{1}{2}\partial_x(y|\nabla|\psi|^2|^2) + \nabla|\psi|^2 \cdot \begin{pmatrix} \partial_y|\psi|^2 \\ -\partial_x|\psi|^2 \end{pmatrix}\right] d\mathbf{x} \\
&= 0.
\end{aligned}$$

The conclusion follows directly from the above results. □

Comparing with $\delta = 0$ case [14, 33], we find the δ term does not affect the dynamical laws of momentum, center-of-mass and the angular momentum expectation. But the fact that the dynamical laws is unaffected does not mean that the dynamics of the quantities is unaffected since the wave function ψ depends on the value of δ.

5.2 An analytical solution under a harmonic potential

In this section, we construct an exact solution of the MGPE (2.4.1) with the external potential to be the harmonic potential (2.4.2) and the initial data to be a stationary state with its center shifted. This kind of analytical solution is useful in practice, especially for the validation of numerical schemes. To be more specific, let $\phi_s(\mathbf{x})$ be a stationary state of the MGPE (2.4.1) with chemical potential μ_s, i.e.

$$\mu_s\phi_s(\mathbf{x}) = -\frac{1}{2}\nabla^2\phi_s + V(\mathbf{x})\phi_s + \beta|\phi_s|^2\phi_s - \delta\nabla^2|\phi_s|^2\phi_s, \quad \|\phi_s\| = 1. \tag{5.2.1}$$

Then we have the following lemma.

Lemma 5.2.1. *Suppose $V(\mathbf{x})$ is given by (2.4.2) and the initial data (5.0.1) is chosen as*

$$\psi_0(\mathbf{x}) = \phi_s(\mathbf{x} - \mathbf{x}_0)e^{i(\mathbf{k}_0\cdot\mathbf{x}+\omega_0)}, \quad \mathbf{x} \in \mathbb{R}^d, \tag{5.2.2}$$

where $\mathbf{x}_0 \in \mathbb{R}^d$, $\mathbf{k}_0 \in \mathbb{R}^d$ *and* $\omega_0 \in \mathbb{R}$ *are given. Then the solution of* (2.4.1) *with* (5.2.2) *can be expressed as*

$$\psi(\mathbf{x}, t) = \phi_s(\mathbf{x} - \mathbf{x}_c(t))e^{-i\mu_s t}e^{i(\mathbf{k}(t)\cdot\mathbf{x}+\omega(t))}, \quad \mathbf{x} \in \mathbb{R}^d, \quad t \geq 0, \tag{5.2.3}$$

where $\mathbf{x}_c(t)$ *satisfies the second order ODE*

$$\ddot{\mathbf{x}}_c(t) + A\mathbf{x}_c(t) = 0, \qquad t > 0, \tag{5.2.4}$$

with the initial data

$$\mathbf{x}_c(0) = \mathbf{x}_0, \quad \dot{\mathbf{x}}_c(0) = \mathbf{k}_0, \tag{5.2.5}$$

and A *is a* $d \times d$ *matrix defined as* $A = (\gamma_x^2)$ *when* $d = 1$, $A = \mathrm{diag}(\gamma_x^2, \gamma_y^2)$ *when* $d = 2$ *and* $A = \mathrm{diag}(\gamma_x^2, \gamma_y^2, \gamma_z^2)$ *when* $d = 3$. *The equations governing* $\mathbf{k}(t)$ *and* $\omega(t)$ *can also be derived as*

$$\dot{\mathbf{k}}(t) = -A\mathbf{x}_c(t), \quad \dot{\omega}(t) = -\frac{|\mathbf{k}|^2}{2} - \frac{1}{2}\mathbf{x}_c^T A\mathbf{x}_c, \qquad t > 0, \tag{5.2.6}$$

respectively, with the initial data

$$\mathbf{k}(0) = \mathbf{k}_0, \quad \omega(0) = \omega_0. \tag{5.2.7}$$

Proof. An analogous reasoning for $\delta = 0$ case in [14,19,33] is applied here. Differentiating (5.2.3) with respect to t and $\mathbf{x}$ respectively, plugging in the MGPE (2.4.1), changing the variable $\mathbf{x} - \mathbf{x}_c(t) \to \mathbf{x}$, and using the fact that ϕ_s is a stationary state, we get

$$\begin{aligned} &- i\partial_t\mathbf{x}_c \cdot \nabla\phi_s(\mathbf{x}) - (\partial_t\mathbf{k} \cdot \mathbf{x} + \partial_t\omega(t))\phi_s(\mathbf{x}) \\ &= -i\mathbf{k} \cdot \nabla\phi_s(\mathbf{x}) + \frac{|\mathbf{k}|^2}{2}\phi_s + (V(\mathbf{x} + \mathbf{x}_c) - V(\mathbf{x}))\phi_s(\mathbf{x}). \end{aligned}$$

We can see that the δ term does not introduce new terms in this procedure compared to the traditional GPE, i.e. $\delta = 0$ case [14,19,33]. As a result, we will get the same result. The details are omitted here for brevity. □

5.3 Finite time blow-up

By the local well-posedness [87, 94], we expect a local smooth solution of the MGPE (2.4.1) for smooth initial data. Below, we show a criteria when a smooth solution of (2.4.1) develops finite time singularity. We will need the following lemma on the time evolution of the variance defined as

$$\delta_\alpha(t) = \int_{\mathbb{R}^d} \alpha^2 |\psi(\mathbf{x},t)|^2 d\mathbf{x}, \quad t \geq 0, \tag{5.3.1}$$

with α being either x, y or z. We have the following lemma regarding the dynamic of the quantity.

Lemma 5.3.1. *Assume $\psi(\mathbf{x},t)$ is a sufficiently smooth solution of (2.4.1) with (5.0.1), then we have with $\rho = |\psi|^2$*

$$\dot{\delta}_\alpha(t) = i\int_{\mathbb{R}^d} \alpha(\psi\partial_\alpha\bar{\psi} - \bar{\psi}\partial_\alpha\psi)d\mathbf{x}, \qquad t \geq 0, \tag{5.3.2}$$

$$\ddot{\delta}_\alpha(t) = \int_{\mathbb{R}^d} \left[2|\partial_\alpha\psi|^2 + (\beta\rho - 2\alpha\,\partial_\alpha V(\mathbf{x}))\rho + 2\delta|\partial_\alpha\rho|^2 + \delta|\nabla\rho|^2\right] d\mathbf{x}. \tag{5.3.3}$$

Proof. Differentiating (5.3.1) with respect to t, applying (2.4.1) and integrating by parts, we get (5.3.2). (5.3.3) is obtained similarly. □

Theorem 5.3.1. *Assume $V(\mathbf{x})$ is smooth and satisfies $V(\mathbf{x})d + \mathbf{x}\cdot\nabla V(\mathbf{x}) \geq 0$ for $\mathbf{x} \in \mathbb{R}^d$. For any smooth solution $\psi(\mathbf{x},t)$ of the MGPE (2.4.1) with (5.0.1), if $\int_{\mathbb{R}^d} |\mathbf{x}|^2|\psi_0|^2 d\mathbf{x} < \infty$, $\delta < 0$ and $d = 2, 3$, there exists finite time blow-up if one of the following holds:*

(i) $E(\psi_0) < 0$,

(ii) $E(\psi_0) = 0$ and $i\int_{\mathbb{R}^d}\left[\mathbf{x}\cdot(\psi_0\nabla\bar{\psi}_0 - \bar{\psi}_0\nabla\psi_0)\right]d\mathbf{x} < 0$,

(iii) $E(\psi_0) > 0$ and $i\int_{\mathbb{R}^d}\left[\mathbf{x}\cdot(\psi_0\nabla\bar{\psi}_0 - \bar{\psi}_0\nabla\psi_0)\right]d\mathbf{x} < -2\sqrt{E(\psi_0)d}\,\|\mathbf{x}\psi_0\|_2$.

Proof. Lemma 5.3.1 shows that for the variance $\delta_{\mathbf{x}}(t) = \int_{\mathbb{R}^d}|\mathbf{x}|^2|\psi(\mathbf{x},t)|^2 d\mathbf{x}$, $\dot{\delta}_{\mathbf{x}}(t) = i\int_{\mathbb{R}^d}\left[\mathbf{x}\cdot(\psi\nabla\bar{\psi} - \bar{\psi}\nabla\psi)\right]d\mathbf{x}$ and

$$\begin{aligned}
\ddot{\delta}_{\mathbf{x}}(t) =& \int_{\mathbb{R}^d}\left[2|\nabla\psi|^2 - 2|\psi|^2\mathbf{x}\cdot\nabla V(\mathbf{x}) + \beta|\psi|^4 d + (d+2)\delta|\nabla|\psi|^2|^2\right]d\mathbf{x}\\
=& 2E(\psi)d - (d-2)\|\nabla\psi\|^2 + 2\delta\|\nabla|\psi|^2\|^2 - 2\int_{\mathbb{R}^d}|\psi|^2(\mathbf{x}\cdot\nabla V(\mathbf{x}) + V(\mathbf{x})d)d\mathbf{x}\\
<& 2E(\psi_0)d, \qquad t > 0.
\end{aligned}$$

Therefore, we get

$$\delta_{\mathbf{x}}(t) \leq E(\psi_0)t^2 d + \dot{\delta}_{\mathbf{x}}(0)t + \delta_{\mathbf{x}}(0), \qquad t \geq 0. \tag{5.3.4}$$

There exists a finite time $0 < T < +\infty$ such that $\delta_{\mathbf{x}}(T) < 0$ if one of (i), (ii) and (iii) is satisfied. It means there exists a singularity at or before $t = T$. □

It is interesting to see that for $\delta < 0$, there exists smooth ψ_0 such that $E(\psi_0) < 0$ even if $\beta > 0$, while the MGPE (2.4.1) with $\beta > 0$ and $\delta = 0$ is globally well-posed [14]. As a consequence, a HOI term with $\delta < 0$ will cause the dynamical instability of the underlying BEC system.

5.4 A time-splitting pseudospectral method

In this section, I will briefly introduce a numerical method which can be used for computing the dynamics of the MGPE (2.4.1).

5.4.1 The method

The time splitting procedure was originally proposed for differential equations in [102] and applied to Schrödinger equations in [69, 104]. And recently the method was studied in [85] for a problem which is slightly more general than the MGPE. Therefore, there are not many things new in this section. Here, we will just apply the method in [85] for the specific MGPE problem and do some numerical tests.

For self-consistency of the thesis, an introduction of the time splitting method will be included here. Consider an abstract initial value problem $u : [0, T] \to \mathcal{B}$, where $\mathcal{B}$ is a Banach space, and the dynamics of $u(t)$ is governed by the following equation,

$$\frac{du(t)}{dt} = (A + B)u(t), \quad u(0) \in \mathcal{B}, \tag{5.4.1}$$

where A and B are two operators, i.e. the simplest two-step case is considered here.

Then the solution can be written in the abstract form as

$$u(t) = e^{t(A+B)}u(0). \tag{5.4.2}$$

We aim to get approximations of the solution at $t_n = n\tau$, where $\tau > 0$ is the time step, and denote it as u^n. The time-splitting approximation of (5.4.2) is usually given as [102, 114]

$$u^{n+1} = e^{\tau A}e^{\tau B}u^n, \quad \text{Lie-Trotter splitting,} \tag{5.4.3}$$

or

$$u^{n+1} = e^{\tau A/2}e^{\tau B}e^{\tau A/2}u^n, \quad \text{Strang splitting.} \tag{5.4.4}$$

It is easy to see that the approximation error of Lie-Trotter splitting is of first order $\mathcal{O}(\tau)$, and the error of Strang splitting is of second order $\mathcal{O}(\tau^2)$ by using the Taylor expansion. It's remarkable that the time-splitting method with higher order accuracy is possible [28, 114], but the scheme will be much more complicated. Therefore, we will choose the Strang splitting for the MGPE problem (2.4.1) due to its simplicity and relatively high accuracy.

Now we construct a numerical scheme for the MGPE (2.4.1) by using the Strang splitting method. We may view the MGPE (2.4.1) as a composition of two differential equations,

$$i\partial_t\psi = -\frac{1}{2}\nabla^2\psi, \tag{5.4.5}$$

$$i\partial_t\psi = \left[V(\mathbf{x}) + \beta|\psi|^2 - \delta\nabla^2(|\psi|^2)\right]\psi. \tag{5.4.6}$$

Similar to the GPE case [14, 85], a simple computation implies that (5.4.6) preserves the density function $\rho(\mathbf{x}, t) = |\psi(\mathbf{x}, t)|^2$ unchanged. Therefore for $t \in [t_n, t_{n+1}]$, we can replace $|\psi(\mathbf{x}, t)|$ by $|\psi(\mathbf{x}, t_n)|$, which will make (5.4.6) to be a linear equation and thus can be solved exactly and explicitly. Consider the equation from $t = t_n$ to t_{n+1}, the splitting of the operators is then clear as follows.

$$i\partial_t\phi = (A + B)\psi, \tag{5.4.7}$$

where $A = -\frac{1}{2}\nabla^2$ and $B = V(\mathbf{x}) + \beta|\psi(\mathbf{x}, t_n)|^2 - \delta\nabla^2(|\psi(\mathbf{x}, t_n)|^2)$.

In space, we may use the sine pseudospectral method because of the Dirichlet BC we applied to the MGPE (2.4.1). And then (5.4.5) can be solved in a standard way and we can write out the time splitting sine pseudospectral scheme (TSSP) in details. For simplicity, only 1D case is considered here. The extension to 2D and 3D is straightforward and omitted here. Here we choose $\tau > 0$ to be the time step, $a = x_0 < x_1 < \cdots < x_N = b$ are the grid points and $\psi^n = (\psi_1^n, \psi_2^n, \ldots, \psi_{N-1}^n)^T$ is the numerical solution at $t = t_n$ with $\psi_0^n = \psi_N^n = 0$ and ψ_j^n to be the numerical approximation of $\psi(x_j, t_n)$. The Strang type time splitting scheme from time $t = t_n$ to $t = t_{n+1}$ can be written as

$$\psi_j^{(1)} = \frac{2}{N}\sum_{l=1}^{N-1} e^{-i\tau\mu_l^2/4}\tilde{\psi}_l^n \sin(\mu_l(x_j - a)), \quad j = 0, 1, \ldots, N \tag{5.4.8}$$

$$\psi_j^{(2)} = e^{-i(V(x_j)+\beta|\psi_j^{(1)}|^2 - \delta\partial_{xx}^s(|\psi_j^{(1)}|^2))\tau}\psi_j^{(1)}, \tag{5.4.9}$$

$$\psi_j^{n+1} = \frac{2}{N}\sum_{l=1}^{N-1} e^{-i\tau\mu_l^2/4}\tilde{\psi}_l^{(2)} \sin(\mu_l(x_j - a)), \tag{5.4.10}$$

where $\mu_l = l\pi/(b-a)$ for $l = 1, 2, \ldots, N-1$, $\tilde{\psi}_l^n$ and $\tilde{\psi}_l^{(2)}$ are coefficients of the discrete sine transform of ψ^n and $\psi^{(2)}$ respectively, and ∂_{xx}^s is the pseudospectral differential operator approximating ∂_{xx}. One can also exchange the order of the two operators in the TSSP scheme and will get the results that are almost the same.

5.4.2 Numerical results

In this section, we report numerical results of the TSSP. To test the numerical errors, we consider the problem in Section 5.2, where an exact solution is applicable. We will test the second order accuracy in time. To set up the problem, we choose $d = 1$ and consider the MGPE (2.4.1) with $\beta = 10$, $\delta = 1$ and the external potential to be $V(x) = x^2/2$ for $x \in (-16, 16)$. Then the problem have the unique positive ground state ϕ_s. Take the initial data

$$\psi(x, 0) = \phi_s(x - x_0)e^{i(k_0 x + \omega_0)}, \tag{5.4.11}$$

Error	$h=1$	$h/2$	$h/2^2$	$h/2^3$
$\|\rho_{h,\tau}(1)-\rho(1)\|_{l_2}$	1.61E-2	2.43E-4	3.33E-8	<1E-10
$\|\rho_{h,\tau}(1)-\rho(1)\|_{\infty}$	1.27E-2	1.69E-4	2.47E-8	<1E-10

Table 5.1: Spatial resolution of the solution at $T=1$ with τ =1E-5.

with $x_0=1$, $k_0=1$ and $\omega_0=0$. Then Lemma 5.2.1 describes the exact solution we have.

We solve this problem on $[-16,16]$ with homogenous Dirichlet BCs. Fig. 5.1 depicts the dynamics from $t=0$ to 20, and also the dynamics of the mass (2.4.5), energy (2.4.6), momentum (5.1.7) and center of mass (5.1.9). From Fig. 5.1, we can easily see the conservation of the mass and energy. Let $\psi(x,t)$ be the exact solution, which is obtained via fine mesh and small time step, and $\psi_{h,\tau}(x,t)$ be the numerical solution by TSSP with mesh size h and time step τ. We denote $\rho_{h,\tau}(\mathbf{x},t)=|\psi_{h,\tau}(\mathbf{x},t)|^2$ and $\rho(\mathbf{x},t)=|\psi(\mathbf{x},t)|^2$.

Firstly, we test the discretization error in space. A sufficiently small time step $\tau=0.0000125$ is chosen to make the error in time negligible. Table 5.1 lists the numerical errors $\|\psi(\cdot,t)-\psi_{h,\tau}(\cdot,t)\|$ at $t=1$ for various spatial mesh sizes h. Secondly, we test the discretization error in time. Now we choose mesh size to be as small as possible while keeping the scheme to be stable at the same time. The numerical errors $\|\psi(\cdot,t)-\psi_{h,\tau}(\cdot,t)\|$ at $t=1$ for different time steps τ are listed in Table 5.2.

From the table, we can observe that the TSSP method we introduced here is second order accurate in time and spectral accurate in space. It's worth mentioning that the numerical scheme proposed here is far from satisfactory because the scheme is not stable and can easily blow up. In practice, we can't choose h too small and Δt too large, which restricts us from getting accurate solutions and increases computational cost significantly. A study of the stability of the scheme can be referred to [85].

Now we apply the scheme to compute the dynamics of the density function starting from $\psi_0(x)=\left(\frac{1}{\pi}\right)^{\frac{1}{4}}e^{-\frac{(x-1)^2}{2}}$ under the potential $V(x)=\frac{x^2}{2}+20\sin^2\left(\frac{\pi x}{4}\right)$.

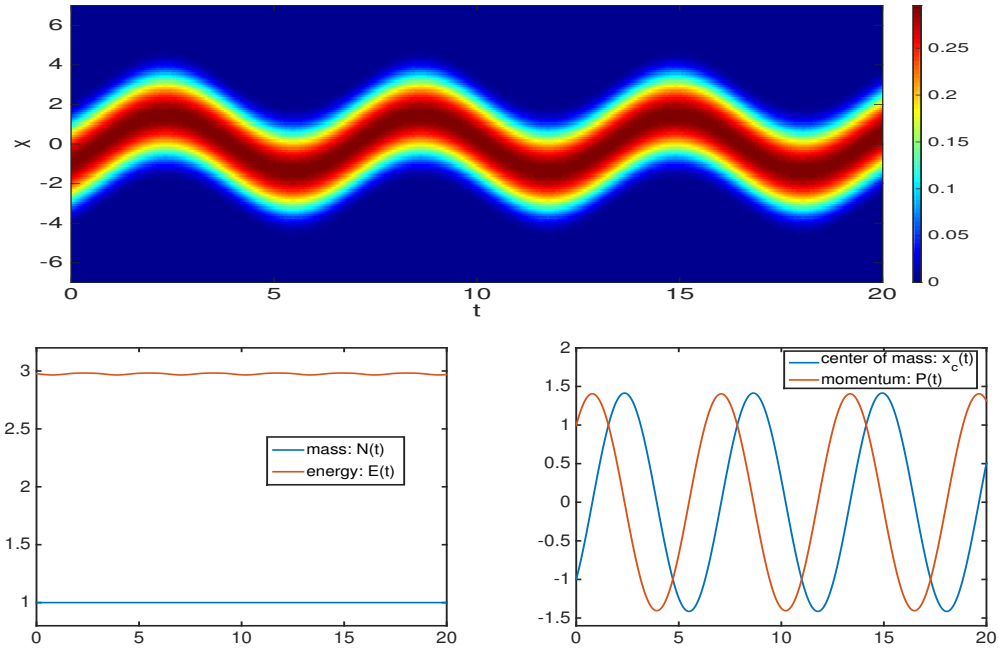

Figure 5.1: Dynamics of the density (top) and some quantities (bottom), i.e. the mass (2.4.5), energy (2.4.6), momentum (5.1.7) and center of mass (5.1.9), starting from $\psi(x,0) = \phi_s(x-1)e^{ix}$ under the harmonic potential $V(x) = x^2/2$ with $\beta = 10$ and $\delta = 1$. In this case, $\dot{P}(t) = -x_c(t)$.

Error	τ =5E-3	$\tau/2$	$\tau/2^2$	$\tau/2^3$
$\|\rho_{h,\tau}(1) - \rho(1)\|_{l_2}$	6.47E-7	1.62E-7	4.05E-8	1.01e-8
rate	-	2.00	2.00	2.00
$\|\rho_{h,\tau}(1) - \rho(1)\|_{\infty}$	5.50E-7	1.38E-7	3.44E-8	8.59E-9
rate	-	2.00	2.00	2.00

Table 5.2: Time discretization error of the solution at $T = 1$ with $h = 1/8$.

We aim to find how the HOI term affects the solution by fixing $\beta = 10$ and choosing $\delta = 0,\ 0.2,\ 1$, respectively. The numerical results are shown in Fig. 5.2. As shown in Fig. 5.2, the increase of δ will flatten the solution.

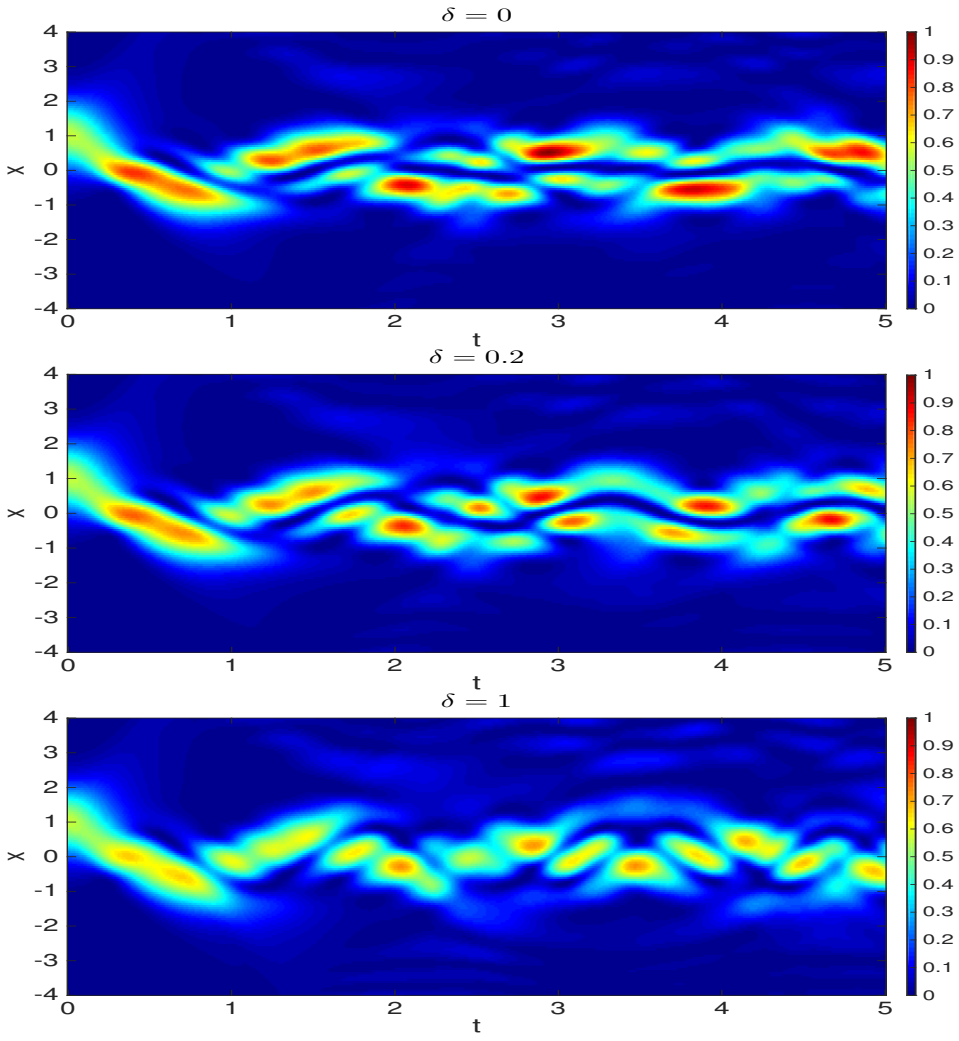

Figure 5.2: Dynamics of the density starting from $\psi(x,0) = \phi_0(x)$ under the harmonic potential $V(x) = x^2/2 + 20\sin^2(\pi x/4)$ with $\beta = 10$ and $\delta = 0, 0.2, 1$.

Chapter 6

Fundamental Gaps of the GPE

In this Chapter, we consider the fundamental gap of the GPE as stated in section 1.3. The fundamental gap problem originates from the problem of finding a sharp lower bound to the gap between the first two eigenvalues of a Laplacian operator [37], and later extended to the Schrödinger operator [100] based on the fundamental work by Brascamp and Lieb [40, 41] proving log-concavity of the ground state. A so-called gap conjecture for the Schrödinger operator was formulated in the literature [7,8,100] as follows. Assuming that U is a bounded convex domain and the potential $V(\mathbf{x}) \in C(U)$, then

$$\delta_E(0) = E_1 - E_g \geq \frac{3\pi^2}{2D_U^2}, \qquad \text{with} \quad D_U := \sup_{\mathbf{y},\mathbf{z}\in U} |\mathbf{y}-\mathbf{z}|. \tag{6.0.1}$$

Recently, by the use of the gradient flow and geometric analysis and assuming that $V(\mathbf{x}) \in C(U)$ is convex, Andrews and Clutterbuck proved the gap conjecture [5]. In addition, they showed that if $U = \mathbb{R}^d$ and the potential $V(\mathbf{x})$ satisfies $D^2V(\mathbf{x}) \geq \gamma^2 I_d$ for $\mathbf{x} \in \mathbb{R}^d$ with $\gamma > 0$, where I_d is the identity matrix in d-dimensions, the fundamental gap satisfies $\delta_E(0) := E_1 - E_g \geq \gamma$ [5]. In this chapter, we generalize the problem to the nonlinear Schrödinger equation and study the impact of the interaction strength on the fundamental gaps under a fixed external potential.

For the GPE (1.2.5), the ground state has been obtained asymptotically in weakly and strongly interaction regimes, i.e. $0 \leq \beta \ll 1$ and $\beta \gg 1$, respectively, for several different trapping potentials [26]. Numerical computations are then performed via

efficient and accurate numerical methods such as the normalized gradient flow via backward Euler finite difference/Fourier pseudo-spectral discretization [14, 16–18]. One thing worth noticing is that it is possible that the first excited state for the linear problem, i.e. when $\beta = 0$, is not unique. We call such case to be the **degenerate case**. Otherwise, we call it the **nondegenerate case**. For simplicity, we define the following eigenspace

$$W_1 = \left\{ \phi \;\middle|\; -\frac{1}{2}\Delta\phi + V(\mathbf{x})\phi = E_1\phi \right\}, \tag{6.0.2}$$

where E_1 is the second smallest eigenvalue of $-\frac{1}{2}\Delta + V(\mathbf{x})$. We denote the dimension of W_1 as $\dim(W_1)$. Then the degenerate case is equivalent saying that $\dim(W_1) > 1$, and the nondegenerate case corresponds to $\dim(W_1) = 1$. As turned out later, whether $\dim(W_1) > 1$ or not will affect the fundamental gap for the nonlinear problem significantly, and therefore we shall be careful and discuss the two cases separately.

6.1 On bounded domains

Consider the time-independent GPE

$$\left[-\frac{1}{2}\Delta + V(\mathbf{x}) + \beta|\phi(\mathbf{x})|^2 \right] \phi(\mathbf{x}) = \mu\phi(\mathbf{x}), \quad \mathbf{x} \in \Omega, \qquad \phi(\mathbf{x})|_{\partial\Omega} = 0, \tag{6.1.1}$$

where $\Omega \subset \mathbb{R}^d$ $(d = 1, 2, 3)$ is a bounded domain, $V(\mathbf{x})$ is a given weakly convex real function and the wave function ϕ is normalized via (1.2.6).

6.1.1 Asymptotic results under a box potential

A special problem is studied in this section. Here we take $\Omega = \prod_{j=1}^{d}(0, L_j)$ satisfying $L_1 \geq L_2 \geq \cdots \geq L_d > 0$ and $V(\mathbf{x}) \equiv 0$ for $\mathbf{x} \in \Omega$ in (6.1.1), i.e. we choose the box potential as the external potential. It is trivial that an equivalent way to describe the problem is to consider the whole space problem with the external potential to be the box potential (2.4.3)

For simplicity, we provide the summarized asymptotic results for the fundamental gaps here and then show the proof of the statement.

Proposition 6.1.1 (for GPE with a box potential via asymptotic and numerical methods). *When $\Omega = \prod_{j=1}^{d}(0, L_j)$ satisfying $L_1 \geq L_2 \geq \cdots \geq L_d$ ($d = 1, 2, 3$) and $V(\mathbf{x}) \equiv 0$ for $\mathbf{x} \in \Omega$ in (6.1.1), we have the following asymptotics for the fundamental gaps $\delta_E(\beta)$ and $\delta_\mu(\beta)$.*

(1) If $d = 1$ or $d \geq 2$ with $L_1 > L_2$,

$$\delta_E(\beta) = \begin{cases} \frac{3\pi^2}{2L_1^2} + o(\beta), \\ \frac{4A_0}{3L_1}\beta^{\frac{1}{2}} + A_1 + o(1), \end{cases} \quad \delta_\mu(\beta) = \begin{cases} \frac{3\pi^2}{2L_1^2} + o(\beta), & 0 \leq \beta \ll 1, \\ \frac{2A_0}{L_1}\beta^{\frac{1}{2}} + \frac{6}{L_1^2} + o(1), & \beta \gg 1, \end{cases} \tag{6.1.2}$$

where

$$A_0 = \frac{1}{\sqrt{\prod_{j=1}^{d} L_j}}, \quad A_1 = \frac{2}{L_1}\left(\frac{25}{9L_1} + \frac{2}{9}\sum_{j=1}^{d}\frac{1}{L_j}\right), \quad A_2 = \frac{\pi^2}{2}\sum_{j=1}^{d}\frac{1}{L_j^2}. \tag{6.1.3}$$

(2) If $d = 2$ or 3 with $L_1 = L_2$. When $0 < \beta \ll 1$,

$$\delta_E(\beta) = \frac{3\pi^2}{2L^2} - \frac{5dA_0^2}{32}\beta + o(\beta), \quad \delta_\mu(\beta) = \frac{3\pi^2}{2L^2} - \frac{5dA_0^2}{16}\beta + o(\beta). \tag{6.1.4}$$

(3) If $d = 2$ with $L_1 = L_2$. When $\beta \gg 1$, we have

$$\delta_E(\beta) = \frac{\pi}{2L^2}\ln(\beta) + \mathcal{O}(1), \quad \delta_\mu(\beta) = \frac{\pi}{2L^2}\ln(\beta) + \mathcal{O}(1). \tag{6.1.5}$$

Now we show the proof of the statement. As said before, we need to consider the degenerate and nondegenerate case separately.

(I) Nondegenerate case, i.e. $L_1 > L_2$:

In this scenario, when $\beta = 0$, all the eigenfunctions can be obtained via the sine series [25, 26] and $\dim(W_1) = 1$. Thus the ground state $\phi_g^0(\mathbf{x})$ and the first excited state $\phi_1^0(\mathbf{x})$ can be given explicitly as [25, 26] for $\mathbf{x} \in \bar{\Omega}$

$$\phi_g^0(\mathbf{x}) = 2^{\frac{d}{2}} A_0 \prod_{j=1}^{d} \sin\left(\frac{\pi x_j}{L_j}\right), \quad \phi_1^0(\mathbf{x}) = 2^{\frac{d}{2}} A_0 \sin\left(\frac{2\pi x_1}{L_1}\right) \prod_{j=2}^{d} \sin\left(\frac{\pi x_j}{L_j}\right). \tag{6.1.6}$$

Fig. 6.1 indicates how the interaction strength affect the ground state and the first excited state. Fig. 6.2 shows the energies of the ground state and the excited states excited in $x-$ or $y-$direction.

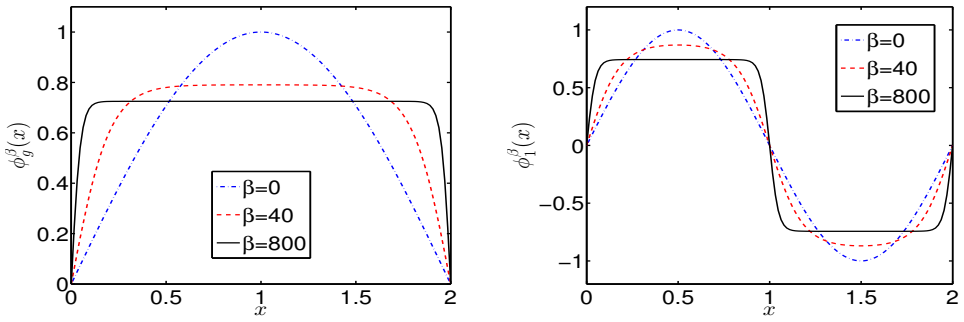

Figure 6.1: Ground states (left) and first excited states (right) of the GPE in 1D with a box potential for different β.

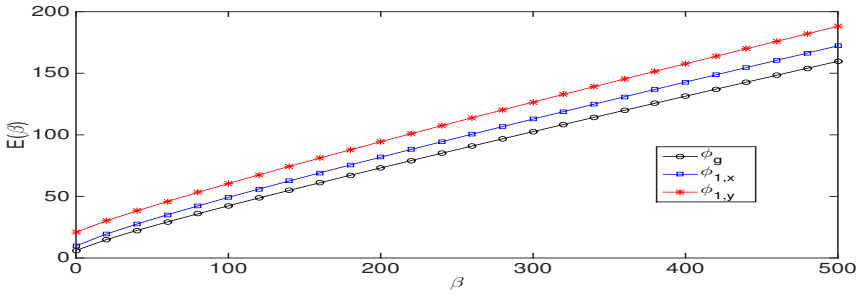

Figure 6.2: Energy for ϕ_g^β, $\phi_{1,x}^\beta$ and $\phi_{1,y}^\beta$ in 2D with $\Omega = (0,2) \times (0,1)$. The graph for $L_1 \neq L_2$ case is totally different from that for $L_1 = L_2$ case, which is shown in Fig. 6.5.

Lemma 6.1.1. *In the weakly repulsive interaction regime, i.e.* $0 < \beta \ll 1$, *we have*

$$E_g(\beta) = A_2 + \frac{3^d A_0^2}{2^{d+1}}\beta + o(\beta), \quad \mu_g(\beta) = A_2 + \frac{3^d A_0^2}{2^d}\beta + o(\beta), \tag{6.1.7}$$

$$E_1(\beta) = \frac{3\pi^2}{2L_1^2} + A_2 + \frac{3^d A_0^2}{2^{d+1}}\beta + o(\beta), \quad \mu_1(\beta) = \frac{3\pi^2}{2L_1^2} + A_2 + \frac{3^d A_0^2}{2^d}\beta + o(\beta). \tag{6.1.8}$$

Proof. When $0 < \beta \ll 1$, we can approximate the ground state $\phi_g^\beta(\mathbf{x})$ and the first excited state $\phi_1^\beta(\mathbf{x})$ by $\phi_g^0(\mathbf{x})$ and $\phi_1^0(\mathbf{x})$, respectively. Thus we have

$$\phi_g^\beta(\mathbf{x}) \approx \phi_g^0(\mathbf{x}), \qquad \phi_1^\beta(\mathbf{x}) \approx \phi_1^0(\mathbf{x}), \qquad \mathbf{x} \in \bar{\Omega}. \tag{6.1.9}$$

Plugging (6.1.9) into (1.2.11) and (1.2.7), after a detailed computation which is omitted here for brevity, we can obtain (6.1.7)-(6.1.8) immediately. □

Lemma 6.1.2. *In the strongly repulsive interaction regime, i.e. $\beta \gg 1$, we have*

$$E_g(\beta) = \frac{A_0^2}{2}\beta + \frac{4A_0A_3}{3}\beta^{\frac{1}{2}} + 2A_3^2 - \frac{8A_4}{9} + o(1), \tag{6.1.10}$$

$$\mu_g(\beta) = A_0^2\beta + 2A_0A_3\beta^{\frac{1}{2}} + 2A_3^2 - A_4 + o(1), \qquad \beta \gg 1, \tag{6.1.11}$$

$$E_1(\beta) = \frac{A_0^2}{2}\beta + \frac{4A_0(A_3L_1+1)}{3L_1}\beta^{\frac{1}{2}} + \frac{2(A_3L_1+1)^2}{L_1^2} - \frac{8A_5}{9} + o(1), \tag{6.1.12}$$

$$\mu_1(\beta) = A_0^2\beta + \frac{2A_0(A_3L_1+1)}{L_1}\beta^{\frac{1}{2}} + \frac{2(A_3L_1+1)^2}{L_1^2} - A_5 + o(1), \tag{6.1.13}$$

where

$$A_3 = \sum_{j=1}^{d}\frac{1}{L_j}, \quad A_4 = 4\sum_{1\le j<k\le d}\frac{1_{\{d\ge 2\}}}{L_jL_k}, \quad A_5 = A_4 + 4\sum_{1<j\le d}\frac{1_{\{d\ge 2\}}}{L_1L_j}, \tag{6.1.14}$$

with $1_{\{d\ge 2\}}$ the standard set function, which takes 1 when $d \ge 2$ and 0 otherwise.

Proof. When $\beta \gg 1$, the ground and the first excited states can be approximated by the Thomas-Fermi (TF) approximations and/or uniformly accurate matched approximations. For $d = 1$ and $\Omega = (0, L)$, these approximations have been given explicitly and verified numerically in the literature [18, 20, 25, 26] as

$$\phi_g(x) \approx \sqrt{\frac{\mu_g}{\beta}}\,\phi^{(1)}_{L,\mu_g}(x), \qquad \phi_1(x) \approx \sqrt{\frac{\mu_1}{\beta}}\,\phi^{(2)}_{L,\mu_1}(x), \qquad 0 \le x \le L, \tag{6.1.15}$$

where

$$\begin{aligned}\phi^{(1)}_{L,\mu}(x) &= \tanh\left(\sqrt{\mu}x\right) + \tanh\left(\sqrt{\mu}(L-x)\right) - \tanh\left(\sqrt{\mu}L\right), \ 0 \le x \le L,\\ \phi^{(2)}_{L,\mu}(x) &= \tanh\left(\sqrt{\mu}x\right) - \tanh\left(\sqrt{\mu}(L-x)\right) + \tanh\left(\sqrt{\mu}\left(L/2-x\right)\right),\end{aligned} \tag{6.1.16}$$

with μ_g and μ_1 determined from the normalization condition (1.2.6) and $\tanh\left(\sqrt{\mu}L\right) \approx 1$. These results in 1D can be extended to d-dimensions ($d = 1, 2, 3$) for the approximations of the ground and the first excited states as

$$\phi_g^\beta(\mathbf{x}) \approx \phi_g^{\mathrm{MA}}(\mathbf{x}) = \sqrt{\frac{\mu_g(\beta)}{\beta}}\prod_{j=1}^{d}\phi^{(1)}_{L_j,\mu_g}(x_j), \qquad \mathbf{x} \in \bar{\Omega}, \tag{6.1.17}$$

$$\phi_1^\beta(\mathbf{x}) \approx \phi_1^{\mathrm{MA}}(\mathbf{x}) = \sqrt{\frac{\mu_1(\beta)}{\beta}}\,\phi^{(2)}_{L_1,\mu_1}(x_1)\prod_{j=2}^{d}\phi^{(1)}_{L_j,\mu_1}(x_j), \tag{6.1.18}$$

where $\mu_g(\beta)$ and $\mu_1(\beta)$ are determined from the normalization condition (1.2.6). Inserting (6.1.17) and (6.1.18) into (1.3.5) and (1.3.6), after a detailed computation which is omitted here for brevity, we can obtain (6.1.10)-(6.1.13) immediately. □

Proof of Proposition 6.1.1 When $0 \le \beta \ll 1$, subtracting (6.1.7) from (6.1.8), noting (1.3.2), we obtain (6.1.2) in this parameter regime. Similarly, when $\beta \gg 1$, subtracting (6.1.10) and (6.1.11) from (6.1.12) and (6.1.13), respectively, we get (6.1.2) in this parameter regime. □

Lemma 6.1.1 implies that $\delta_E(\beta) = E_1(\beta) - E_g(\beta) \approx \frac{3\pi^2}{2L_1^2}$ and $\delta_\mu(\beta) = \mu_1(\beta) - \mu_g(\beta) \approx \frac{3\pi^2}{2L_1^2}$ for $0 \le \beta \ll 1$, which are independent of β. In order to get the dependence on β, we need to find more accurate approximations of the ground state ϕ_g^β and ϕ_1^β and obtain the following asymptotic of the fundamental gaps. The details can be referred to [27] and is omitted here for simplicity.

Lemma 6.1.3. *When $0 \le \beta \ll 1$, we have*

$$\delta_E(\beta) = \frac{3\pi^2}{2L_1^2} + G_d^{(1)}\beta^2 + o(\beta^2), \qquad \delta_\mu(\beta) = \frac{3\pi^2}{2L_1^2} + G_d^{(2)}\beta^2 + o(\beta^2), \tag{6.1.19}$$

where

$$G_d^{(1)} = \begin{cases} \frac{3}{64\pi^2}, \\ \frac{A_0^4}{64\pi^2}\left(\frac{27}{4}L_1^2 + \frac{3}{A_6(A_6L_1^2+3)}\right), \\ \frac{1}{256\pi^2}(C_{1,1,1} - C_{2,1,1}), \end{cases} \quad G_d^{(2)} = \begin{cases} \frac{9}{64\pi^2}, & d=1, \\ \frac{3A_0^4}{64\pi^2}\left(\frac{27}{4}L_1^2 + \frac{3}{A_6(A_6L_1^2+3)}\right), & d=2, \\ \frac{3}{256\pi^2}(C_{1,1,1} - C_{2,1,1}), & d=3, \end{cases}$$

with

$$A_6 = \sum_{j=1}^{d} \frac{1}{L_j^2}, \quad C_{k_1,k_2,k_3} = A_0^4\left(81\sum_{j=1}^{3}\frac{L_j^2}{k_j^2} + 9\sum_{i<j}\frac{1}{\frac{k_i^2}{L_i^2}+\frac{k_j^2}{L_j^2}} + \frac{1}{\sum_{j=1}^{3}\frac{k_j^2}{L_j^2}}\right). \tag{6.1.20}$$

(II) Degenerate case, i.e. $L_1 = L_2$:

In this part, we consider the case $d \ge 2$ with $L_1 = L_2 = L$. Noticing that the first excited state for the linear problem, i.e. $\beta = 0$, is not unique, we need to be careful to determine the correct form of the first excited state for $\beta > 0$. One special type of the excited state, i.e. the vortex-type solution as shown in Fig. 6.3 in 2D and Fig. 6.4 in 3D, will appear, which makes the scenario for the degenerate case totally different. Unlike the nondegenerate case, there is a crossing for the energy of different excited states at $\beta = 0$ as shown in Fig. 6.5.

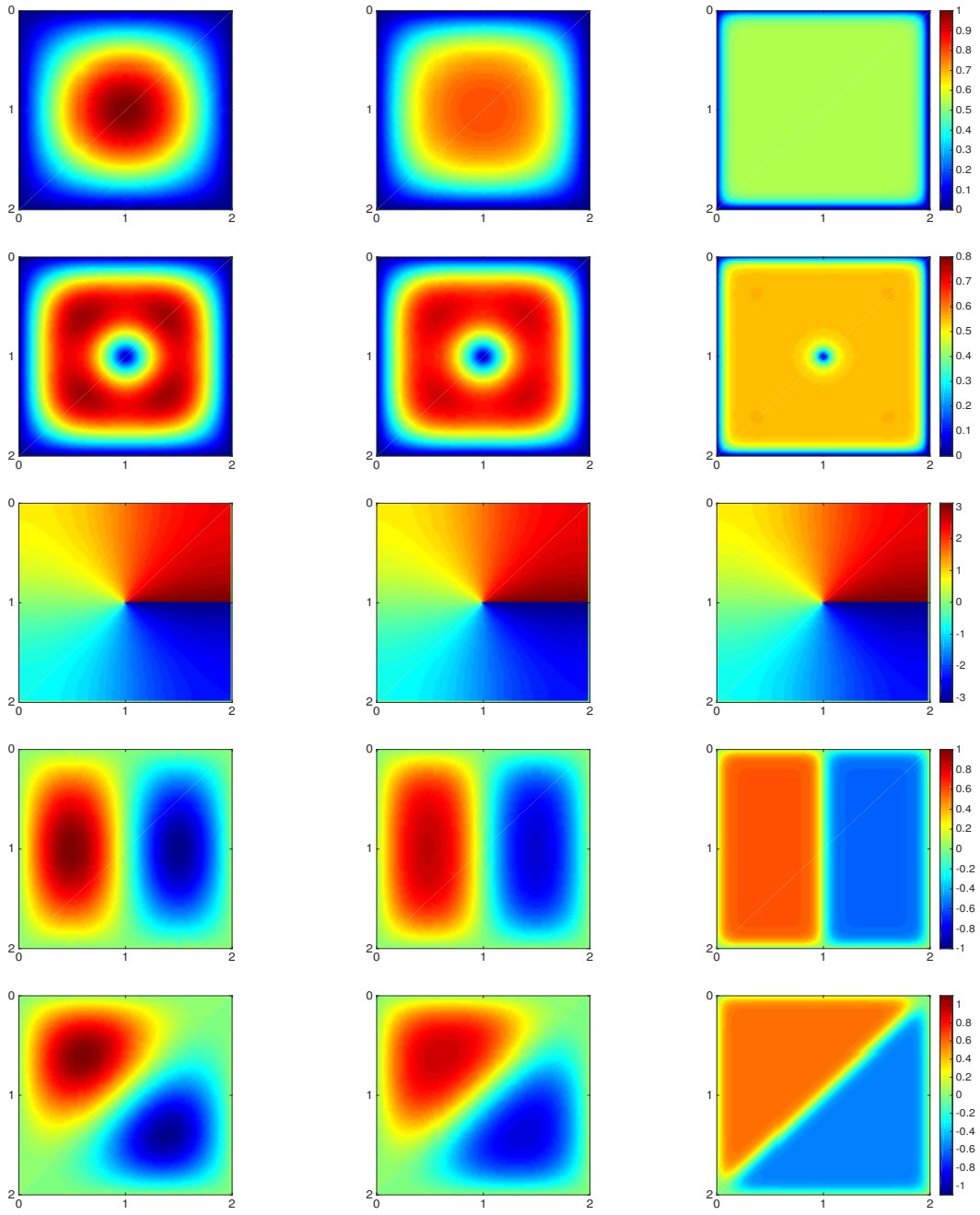

Figure 6.3: Graph for ground state $\phi_g(\mathbf{x})$ (top), vortex solution $|\phi_{1,v}(\mathbf{x})|$(2nd), x-excited state $\phi_{1,x}(\mathbf{x})$(4th) and diagonal-excited state $\phi_{1,c}(\mathbf{x})$ (bottom). The 3rd row is the phase angle graph of the vortex solution.

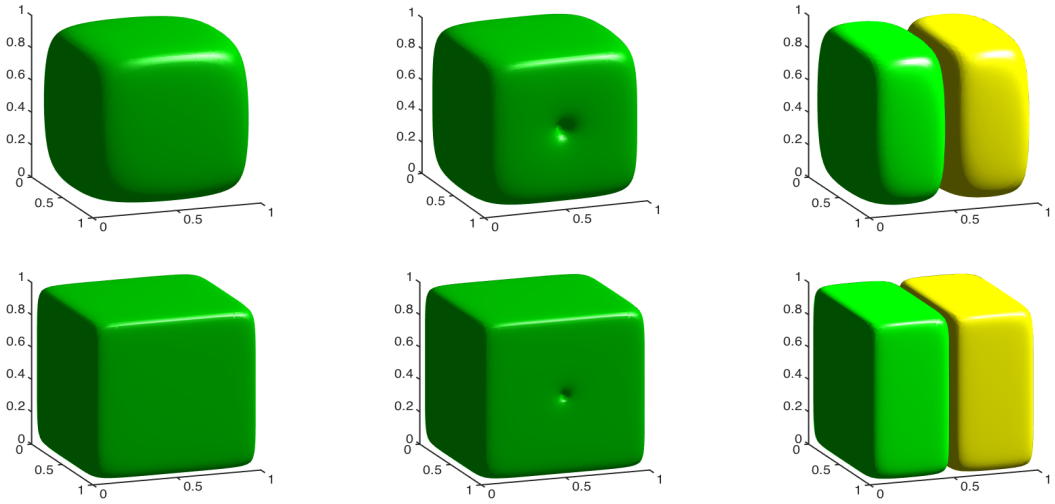

Figure 6.4: Isosurface(value=0.1) of solution for ground state $\phi_g(\mathbf{x})$ (left), vortex solution $|\phi_{1,v}(\mathbf{x})|$ (middle) and x-excitation solution $\phi_{1,x}(\mathbf{x})$ (right) with $\beta = 0$ (top) and $\beta = 100$(bottom).

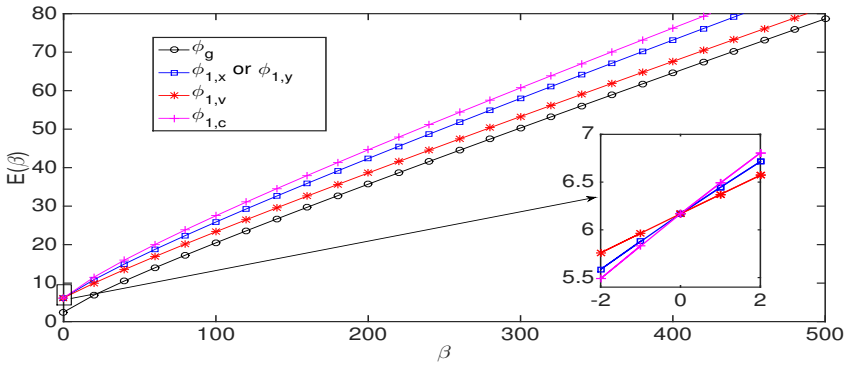

Figure 6.5: Plot for the ground state energy and different excited states with box potential in $\Omega = (0, 2)^2$.

Lemma 6.1.4. *For weakly repulsive interaction, i.e.* $0 < \beta \ll 1$, *we have*

$$E_1(\beta) = \frac{3\pi^2}{2L^2} + A_2 + \frac{13d}{32}A_0^2\beta + o(\beta),\ \mu_1(\beta) = \frac{3\pi^2}{2L^2} + A_2 + \frac{13d}{16}A_0^2\beta + o(\beta), \tag{6.1.21}$$

where $d = 2$ *or* 3.

Proof. For simplicity, we only present the 2D case and the extension to 3D is

straightforward. Denote

$$\phi_g^0(x) = \sqrt{\frac{2}{L}} \sin\left(\frac{\pi x}{L}\right), \qquad \phi_1^0(x) = \sqrt{\frac{2}{L}} \sin\left(\frac{2\pi x}{L}\right), \qquad 0 \le x \le L. \quad (6.1.22)$$

When $d = 2$ and $\beta = 0$, it is easy to see that $\varphi_1(\mathbf{x}) := \phi_1^0(x_1)\phi_g^0(x_2)$ and $\varphi_2(\mathbf{x}) := \phi_g^0(x_1)\phi_1^0(x_2)$ are two linearly independent first excited states. In order to find an appropriate approximation of the first excited state when $0 < \beta \ll 1$, we take an ansatz

$$\varphi_{a,b}(\mathbf{x}) = a\phi_1^0(x_1)\phi_g^0(x_2) + b\phi_g^0(x_1)\phi_1^0(x_2), \qquad \mathbf{x} = (x_1, x_2) \in \bar{\Omega}, \quad (6.1.23)$$

where $a, b \in \mathbb{C}$ satisfying $|a|^2 + |b|^2 = 1$ which implies $\|\varphi_{a,b}\|_2 = 1$. Then a and b will be determined by minimizing $E(\varphi_{a,b})$. Plugging (6.1.23) into (1.3.6), a simple direct computation implies that

$$\begin{aligned} E(\varphi_{a,b}) &= \frac{3\pi^2}{2L^2} + A_2 + \frac{8\beta}{L^4} \iint_{[0,L]^2} \left| a \sin(\frac{2\pi x_1}{L}) \sin(\frac{\pi x_2}{L}) + b \sin(\frac{\pi x_1}{L}) \sin(\frac{2\pi x_2}{L}) \right|^4 d\mathbf{x} \\ &= \frac{3\pi^2}{2L^2} + A_2 + \frac{9\beta}{8L^2}(|a|^4 + |b|^4) + \frac{\beta}{2L^2}(4|a|^2|b|^2 + a^2\bar{b}^2 + \bar{a}^2 b^2) \\ &= \frac{3\pi^2}{2L^2} + A_2 + \frac{9\beta}{8L^2} + \frac{\beta}{4L^2}(2a^2\bar{b}^2 + 2\bar{a}^2 b^2 - |a|^2|b|^2). \end{aligned}$$

To minimize $E(\varphi_{a,b})$, we may take $a = e^{i\xi}\cos(\theta)$ and $b = e^{i\eta}\sin(\theta)$, which guarantees $|a|^2 + |b|^2 = 1$ automatically, and then

$$E(\varphi_{a,b}) = \frac{3\pi^2}{2L^2} + A_2 + \frac{9\beta}{8L^2} - \frac{\beta}{16L^2}\sin^2(2\theta)(1 - 4\cos(2(\xi - \eta))),$$

which is minimized when $\theta = \pm\pi/4$ and $\xi - \eta = \pm\pi/2$, i.e. $a = \pm ib$. By taking $a = 1/\sqrt{2}$ and $b = i/\sqrt{2}$, we obtain an approximation of the first excited state when $0 < \beta \ll 1$ as

$$\phi_1^\beta(\mathbf{x}) \approx \frac{\sqrt{2}}{2}(\phi_1^0(x_1)\phi_g^0(x_2) + i\phi_g^0(x_1)\phi_1^0(x_2)), \qquad \mathbf{x} \in \bar{\Omega}. \quad (6.1.24)$$

Substituting (6.1.24) into (1.3.6) and (1.3.5), we get (6.1.21). □

Remark 6.1.1. *The degenerate case in 3D in weak interaction regime can be computed similarly. If $L_1 = L_2 > L_3$, since $\dim(W_1) = 2$, the first excited state*

should be vortex type solution, similar to the 2D case but rotating along a line. If $L_1 = L_2 = L_3$, the problem would be more complicated. But it can be shown that the first excited state in weak interaction regime is of form

$$\phi_1^\beta(\mathbf{x}) \approx a\phi_g^0(x_1)\phi_g^0(x_2)\phi_1^0(x_3) + b\phi_g^0(x_1)\phi_1^0(x_2)\phi_g^0(x_3) + c\phi_1^0(x_1)\phi_g^0(x_2)\phi_g^0(x_3),$$

where $\mathbf{x} = (x_1, x_2, x_3) \in \bar{\Omega}$, $a, b, c \in \mathbb{C}$ satisfying $|a|^2 + |b|^2 + |c|^2 = 1, a^2 + b^2 + c^2 = 0$ and $abc = 0$. It implies that the first excited state in this case is also a vortex type solution rotating along a line. The details are omitted here for brevity.

Lemma 6.1.5. *For the 2D case with strongly repulsive interaction, i.e. $d = 2$ and $\beta \gg 1$, we have*

$$E_1(\beta) = \frac{\beta}{2L^2} + \frac{8\sqrt{\beta}}{3L^2} + \frac{\pi}{2L^2}\ln(\beta) + o(\ln(\beta)), \tag{6.1.25}$$

$$\mu_1(\beta) = \frac{\beta}{L^2} + \frac{4\sqrt{\beta}}{L^2} + \frac{\pi}{2L^2}\ln(\beta) + o(\ln(\beta)). \tag{6.1.26}$$

Proof. The whole proof is based on the assumption that the first excited state can be well approximated by the vortex-type solution as suggested in the proof of Lemma 6.1.4, and the vortex should appear in the middle of the domain and should be small and radially symmetric. In the region away from the middle of the domain, i.e. the outer region, the first excited state can be approximated by the uniformly accurate matched approximations,

$$\phi^{\text{out}}(\mathbf{x}) \approx \sqrt{\frac{\mu_1}{\beta}}\phi_{L,\mu_1}^{(1)}(x_1)\phi_{L,\mu_1}^{(1)}(x_2).$$

where $\phi_{L,\mu}^{(1)}(x)$ is defined in (6.1.16), μ_1 is the chemical potential of the first excited state. While in the middle of the domain, i.e. the inner region, we take the following ansatz for the vortex

$$\phi^{\text{in}}(\mathbf{x}) = f(r)e^{i\theta}, \tag{6.1.27}$$

where r and θ are the modulus and argument of $(x_1 - L/2) + i(x_2 - L/2)$, respectively. Substituting (6.1.27) into (7.1.1), we get the equation for $f(r)$

$$-\frac{1}{2}f''(r) - \frac{1}{2r}f'(r) + \frac{1}{2r^2}f(r) + \beta f^3(r) = \mu_1 f(r). \tag{6.1.28}$$

The density follows by the standard matched asymptotic approximation which combines the solution in the outer region and inner region

$$|\phi_1^\beta(\mathbf{x})| \approx \sqrt{\frac{\mu_1}{\beta}} \left(f(r) + \phi^{(1)}_{L,\mu_1}(x_1)\phi^{(1)}_{L,\mu_1}(x_2) - 1 \right). \tag{6.1.29}$$

To get the approximations to the corresponding energy and chemical potential, we need to have an explicit form of $f(r)$ in (6.1.29). Unfortunately, the equation (6.1.28) is difficult to solve analytically. But if we drop the term f'' in (6.1.28), the equation (6.1.28) admits solution

$$f(r) = \sqrt{\frac{\mu_1}{\beta}} \sqrt{\frac{2\mu_1 r^2}{1 + 2\mu_1 r^2}}. \tag{6.1.30}$$

The chemical potential (6.1.26) is then computed by the normalization condition and the energy (6.1.25) is computed by substituting (6.1.29) and (6.1.30) into (1.3.6). Though the approximation to $f(r)$ in (6.1.30) introduces some error, a more careful analysis which considers the error in energy and chemical potential caused by this inaccuracy via the definitions (1.3.6) and (1.3.5) indicates it is of order $o(\ln(\beta))$. Therefore, the leading order approximations in (6.1.25), (6.1.26) still hold true. □

Lemma 6.1.4 and Lemma 6.1.5 implies the results for the degenerate case in Proposition 6.1.1.

6.1.2 Numerical results on bounded domains

In this chapter, we will first show the accuracy tests of our asymptotic results in Proposition 6.1.1. And then we will do numerical tests for problems with a general domain and a general external potential.

(I) Accuracy tests for the nondegenerate case:

Fig 6.6 checks the accuracy of the asymptotic approximations of fundamental gaps for $L_1 > L_2$ in 1D, 2D and 3D proposed in Proposition 6.1.1. Our numerical results suggest that $\delta_E(\beta)$ and $\delta_\mu(\beta)$ are increasing functions for $\beta \geq 0$, which immediately

imply that

$$\delta_E^\infty := \inf_{\beta\geq 0} \delta_E(\beta) \geq \delta_E(0) = \frac{3\pi^2}{2L_1^2}, \qquad \delta_\mu^\infty := \inf_{\beta\geq 0} \delta_\mu(\beta) \geq \delta_\mu(0) = \frac{3\pi^2}{2L_1^2}. \quad (6.1.31)$$

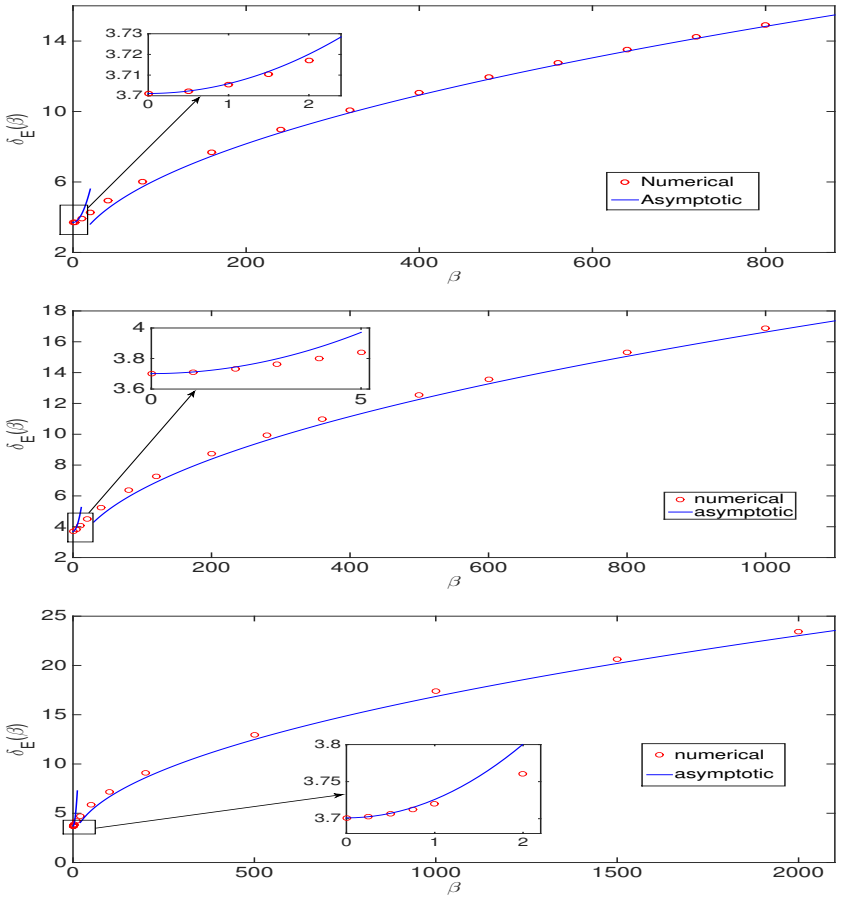

Figure 6.6: Gaps between the ground state and the x_1-direction excited state in energy of the GPE with a box potential in 1D with $\Omega = (0, 2)$ (top), in 2D with $\Omega = (0, 2) \times (0, 1)$ (middle), and in 3D with $\Omega = (0, 2) \times (0, 1) \times (0, 1)$ (bottom).

(II) Accuracy tests for the degenerate case:

Fig 6.7 checks the accuracy of the asymptotic approximations of fundamental gaps for $L_1 = L_2$ in 2D and 3D proposed in Proposition 6.1.1. Our numerical results suggest that the approximations (6.1.4) provide a lower bound of the exact result

for the 2D problem, and thus combining the approximations will give us a uniform lower bound as follows,

$$\delta_E^{\infty} := \inf_{\beta\geq 0} \delta_E(\beta) \geq \frac{\pi^2}{2L_1^2}, \qquad \delta_\mu^{\infty} := \inf_{\beta\geq 0} \delta_\mu(\beta) \geq \frac{3\pi^2}{8L_1^2}. \tag{6.1.32}$$

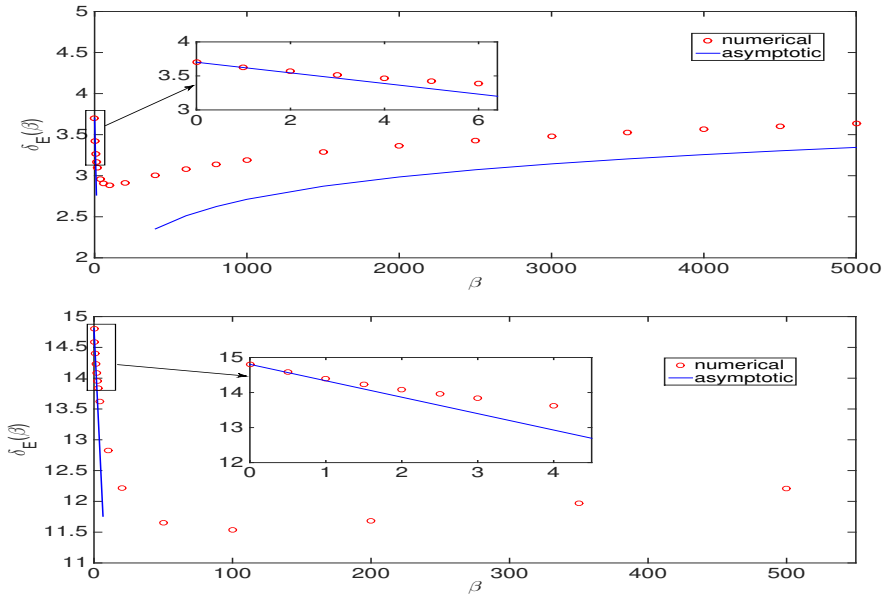

Figure 6.7: Plot for the fundamental gap under a box potential in 2D with $\Omega = (0, 2)^2$ and in 3D with $\Omega = (0, 1)^3$.

(III) Numerical tests for general cases:

We remark that for a general bounded domain Ω and/or $V(\mathbf{x}) \neq 0$, we cannot get asymptotic results on the fundamental gaps, but can always find the fundamental gaps numerically. If Ω and $V(\mathbf{x})$ are symmetric with respect to the axis, then we compute numerically the ground and first excited states and their corresponding energy and chemical potential as well as the fundamental gaps by using the normalized gradient flow via backward Euler finite difference discretization [14, 16–18]. Discretization in space can be performed using the finite element method instead of finite difference or spectral method for the normalized gradient flow to compute the

ground and first excited states [29]. For external potentials which are arbitrarily chosen, we do not have any symmetric property of the first excited state. It implies that the normalized gradient flow method is not applicable in this case for computing the first excited state. One way to compute the first excited state is to directly find the critical point of the energy functional with a proper initial guess with the help of the continuity technique [29], i.e. using the first excited state for a small β as an initial guess for computing the first excited state for a larger β.

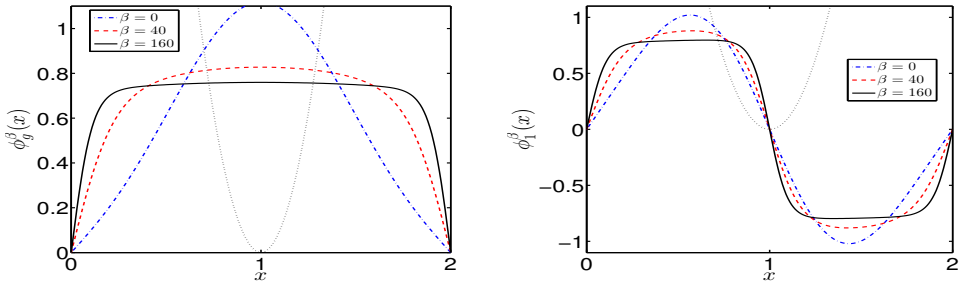

Figure 6.8: Ground states (left) and first excited states (right) of the GPE in 1D with $V(x) = 10(x-1)^2$ (dot line) and $\Omega = (0, 2)$ for different β.

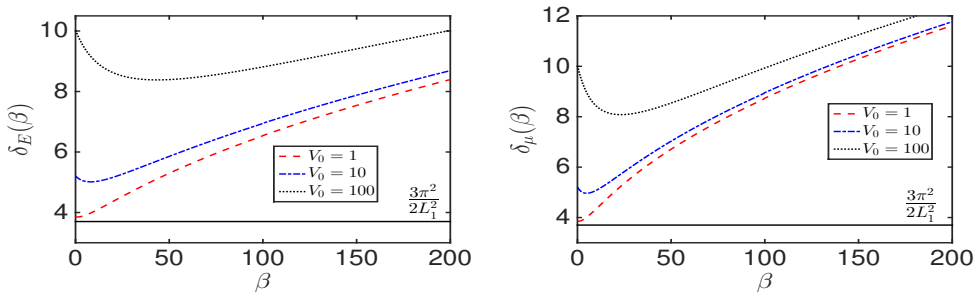

Figure 6.9: Fundamental gaps in energy (left) and chemical potential (right) of the GPE in 1D with $V(x) = V_0(x-1)^2$ for different V_0 and β.

We first report numerical results of the GPE in 1D, i.e. $d = 1$ and $\Omega = (0, 2)$. Figure 6.8 plots ground states and first excited states with $V(x) = 10(x-1)^2$ for different β's, and Figure 6.9 depicts fundamental gaps in energy and chemical potential with $V(x) = V_0(x-1)^2$ for different V_0 and β. Figure 6.10 shows ground

states and first excited states with $\beta = 40$ for different convex trapping potentials, and Figure 6.11 lists fundamental gaps in energy and chemical potential for different β's and different convex trapping potentials.

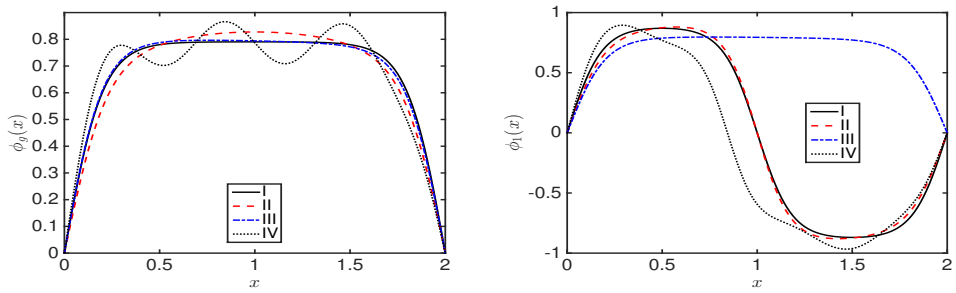

Figure 6.10: Ground states (left) and first excited states (right) of the GPE on $(0, 2)$ with $\beta = 40$ for different convex potentials: (I) $V(x) = 0$, (II) $V(x) = 10(x-1)^2$, (III) $V(x) = (x-1)^2 + \sin(x-1)$, (IV) $V(x) = 10\sin(10(x-1))$.

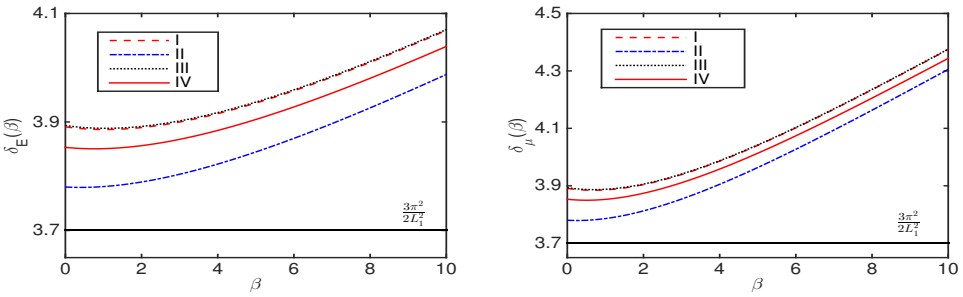

Figure 6.11: Fundamental gaps in energy (left) and chemical potential (right) of the GPE on $(0, 2)$ for different β and different convex potentials: (I) $V(x) = (x-1)^2 + \sin(x-1)$, (II) $V(x) = (x-1)^2 + \cos(x-1)$, (III) $V(x) = (x-1)^2 - x + 1$, (IV) $V(x) = (x-1)^2 - (x-1)^3/3$.

Next, we report fundamental gaps of the GPE in 1D with non-convex trapping potentials. Figure 6.12 plots fundamental gaps in energy and chemical of the GPE with $d = 1$, $\Omega = (0, 2)$ for different β's and non-convex trapping potentials.

Based on the above numerical results and additional extensive numerical results not shown here for brevity as well as our asymptotic results in Proposition 6.1.1, we

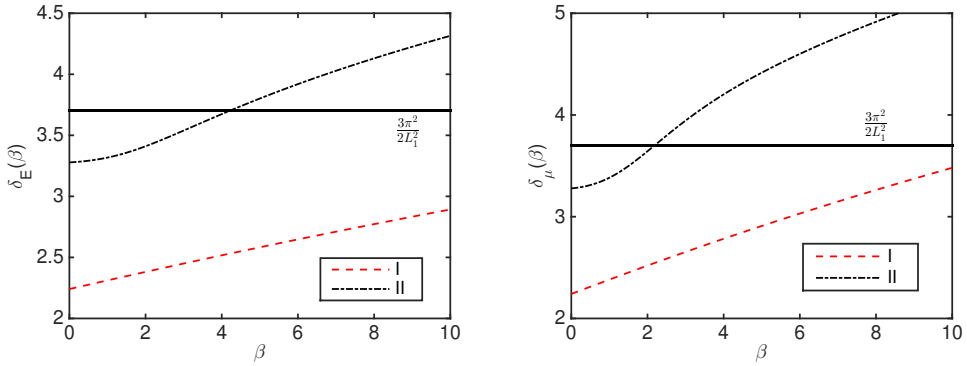

Figure 6.12: Fundamental gaps in energy (left) and chemical potential (right) of the GPE in 1D with $\Omega = (0, 2)$ for different β and non-convex trapping potentials: (I) $V(x) = -10x^2$, and (II) $V(x) = 10\sin(10(x-1))$.

speculate the Gap Conjecture which will be stated later in Section 6.1.3. In fact, our numerical results suggest a stronger conjecture for the nondegenerate case as

$$\delta_E(\beta) \geq \max\{\frac{3\pi^2}{2D^2}, \frac{4\beta^{1/2}}{3D|\Omega|^{1/2}}\}, \quad \delta_\mu(\beta) \geq \max\{\frac{3\pi^2}{2D^2}, \frac{2\beta^{1/2}}{D|\Omega|^{1/2}}\}. \tag{6.1.33}$$

where $|\Omega|$ is the volume of Ω. On the other hand, Figure 6.12 suggests that the gap conjecture (6.1.34) is not true for arbitrary external potentials, e.g. non-convex trapping potentials.

Finally, we show one numerical test for the degenerate case. We choose $V(\mathbf{x})$ to be a box potential defined in a disk $\Omega = D(0, 1) = \{(x, y) \,|\, x^2 + y^2 < 1\}$ and check the fundamental gaps in this case. It is obvious from Fig 6.13 that the fundamental gap is larger than the lower bound proposed in Gap Conjecture as (6.1.35), which is $\frac{\pi^2}{2D^2} \approx 1.234$

6.1.3 A gap conjecture

As indicated from the numerical tests, the asymptotic results proposed in Proposition 6.1.1 are indeed lower bounds of the fundamental gaps in both weak and strong interaction regimes. Based on the asymptotic results for the special problem considered in Section 6.1.1, we propose the following gap conjecture.

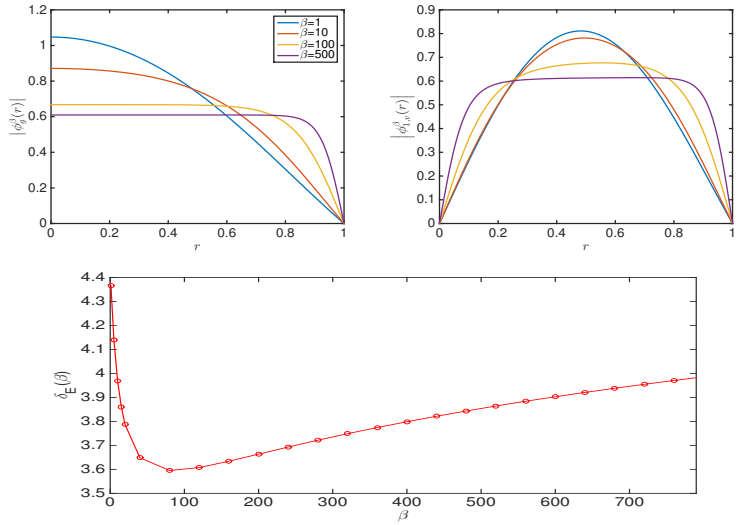

Figure 6.13: Plots in the top show $\phi_g^\beta(r)$ (left) and $|\phi_{1,v}^\beta(r)|$ (right) under a box potential defined in $\Omega = D(0,1) = \{(x,y)\,|\,x^2+y^2<1\}$ but with different β's. Plot in the bottom describes the energy gap $\delta_E(\beta) = E(\phi_{1,v}^\beta) - E(\phi_g^\beta)$.

Gap Conjecture (for GPE on a bounded domain with homogeneous Dirichlet BC)**.** *Suppose Ω is a convex bounded domain and the external potential $V(\mathbf{x})$ is convex, we have the following conjectures.*

(1) If the first excited state for the linear problem is nondegenerate,

$$\delta_E^\infty := \inf_{\beta\geq 0}\delta_E(\beta) \geq \frac{3\pi^2}{2D^2}, \qquad \delta_\mu^\infty := \inf_{\beta\geq 0}\delta_\mu(\beta) \geq \frac{3\pi^2}{2D^2}, \tag{6.1.34}$$

where $D := \sup_{\mathbf{x},\mathbf{z}\in\Omega}|\mathbf{x}-\mathbf{z}|$ is the diameter of Ω.

(2) If $d = 2$ and the first excited state for the linear problem is degenerate, we have a non-sharp lower bound as

$$\delta_E^\infty := \inf_{\beta\geq 0}\delta_E(\beta) \geq \frac{\pi^2}{2D^2}, \qquad \delta_\mu^\infty := \inf_{\beta\geq 0}\delta_\mu(\beta) \geq \frac{3\pi^2}{8D^2}, \tag{6.1.35}$$

where D is defined as before.

6.2 In the whole space

Consider the time-independent GPE in the whole space

$$\left[-\frac{1}{2}\Delta + V(\mathbf{x}) + \beta|\phi(\mathbf{x})|^2\right]\phi(\mathbf{x}) = \mu\phi(\mathbf{x}), \quad \mathbf{x} \in \mathbb{R}^d, \tag{6.2.1}$$

where $V(\mathbf{x})$ is a given function satisfying $D^2V(\mathbf{x}) \geq \gamma_v^2 I_d$ with $\gamma_v > 0$ a constant and the wave function ϕ is normalized via (1.2.6).

6.2.1 Asymptotic results under a harmonic potential

In this section, we take a harmonic potential (2.4.2) with $\gamma_j > 0$ $(j = 1, \ldots, d)$ satisfying $\gamma_1 < \gamma_2 \leq \cdots \leq \gamma_d$. The asymptotic results for the harmonic potential can be summarized in the following statement.

Proposition 6.2.1 (for GPE with a harmonic potential via asymptotic and numerical methods)**.** *When $\Omega = \mathbb{R}^d$ $(d = 1, 2, 3)$ and $V(\mathbf{x}) = (\sum_{j=1}^d \gamma_j^2 x_j^2)/2$ for $\mathbf{x} \in \mathbb{R}^d$ satisfying $0 < \gamma_1 \leq \gamma_2 \leq \cdots \leq \gamma_d$, we have the following asymptotics for the fundamental gaps*

(1) If $d = 1$ or $d \geq 2$ and $\gamma_1 < \gamma_2$,

$$\delta_E(\beta) = \begin{cases} \gamma_1 - \frac{B_0}{8}\beta + o(\beta), \\ \frac{\sqrt{2}}{2}\gamma_1 + o(1), \end{cases} \quad \delta_\mu(\beta) = \begin{cases} \gamma_1 - \frac{B_0}{4}\beta + o(\beta), & 0 \leq \beta \ll 1, \\ \frac{\sqrt{2}}{2}\gamma_1 + o(1), & \beta \gg 1, \end{cases} \tag{6.2.2}$$

where

$$B_0 = \prod_{j=1}^d \sqrt{\frac{\gamma_j}{2\pi}}, \qquad B_1 = \frac{1}{2}\sum_{j=1}^d \gamma_j, \qquad B_2 = \prod_{j=1}^d \gamma_j. \tag{6.2.3}$$

(2) If $d = 2$ or 3 with $\gamma_1 = \gamma_2$. When $0 < \beta \ll 1$,

$$\delta_E(\beta) = \gamma - \frac{(4-d)B_0}{8}\beta + o(\beta), \quad \delta_\mu(\beta) = \gamma - \frac{(4-d)B_0}{4}\beta + o(\beta). \tag{6.2.4}$$

(3) If $d = 2$ with $\gamma_1 = \gamma_2$. When $\beta \gg 1$,

$$\delta_E(\beta) = \frac{\gamma_1}{2}\sqrt{\frac{\pi}{\beta}}\ln(\beta) + o(\frac{\ln(\beta)}{\sqrt{\beta}}), \quad \delta_\mu(\beta) = \frac{\gamma_1}{4}\sqrt{\frac{\pi}{\beta}}\ln(\beta) + o(\frac{\ln(\beta)}{\sqrt{\beta}}), \tag{6.2.5}$$

which implies $\delta_E(\beta) \to 0$ and $\delta_\mu(\beta) \to 0$ as $\beta \to \infty$.

Now we show the proof of the statement. As said before, we need to consider the degenerate and nondegenerate case separately.

(I) Nondegenerate case, i.e. $\gamma_1 < \gamma_2$:

In this scenario, when $\beta = 0$, all the eigenfunctions can be obtained via the Hermite functions [25, 26]. Thus the ground state $\phi_g^0(\mathbf{x})$ and the first excited state $\phi_1^0(\mathbf{x})$ can be given explicitly as [25, 26]

$$\phi_g^0(\mathbf{x}) = \prod_{j=1}^{d} \left(\frac{\gamma_j}{\pi}\right)^{\frac{1}{4}} e^{-\frac{\gamma_j x_j^2}{2}}, \quad \phi_1^0(\mathbf{x}) = \sqrt{2\gamma_1} x_1 \prod_{j=1}^{d} \left(\frac{\gamma_j}{\pi}\right)^{\frac{1}{4}} e^{-\frac{\gamma_j x_j^2}{2}}, \quad \mathbf{x} \in \mathbb{R}^d. \tag{6.2.6}$$

Fig. 6.14 indicates how the interaction strength affect the ground state and the first excited state. Fig. 6.15 shows the energies of the ground state and the excited states excited in $x-$ or $y-$direction.

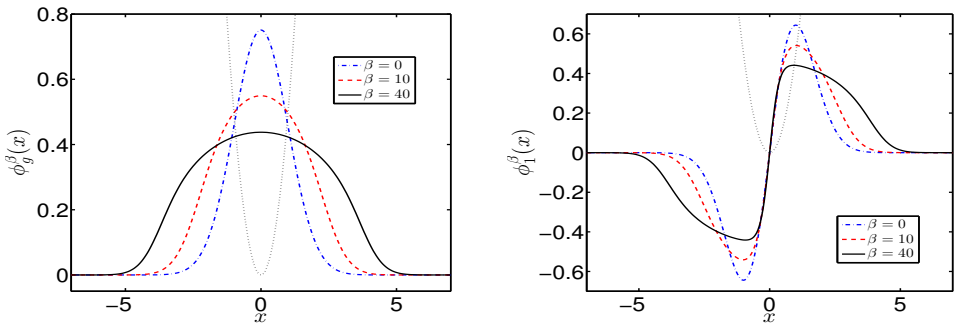

Figure 6.14: Ground states (left) and first excited states (right) of the GPE in 1D with a harmonic potential $V(x) = x^2/2$ (dot line) for different β.

Lemma 6.2.1. *In the weakly repulsive interaction regime, i.e.* $0 < \beta \ll 1$, *we have*

$$E_g(\beta) = B_1 + \frac{B_0}{2}\beta + o(\beta), \quad \mu_g(\beta) = B_1 + B_0\beta + o(\beta), \tag{6.2.7}$$

$$E_1(\beta) = \gamma_1 + B_1 + \frac{3B_0}{8}\beta + o(\beta), \quad \mu_1(\beta) = \gamma_1 + B_1 + \frac{3B_0}{4}\beta + o(\beta). \tag{6.2.8}$$

Proof. When $0 < \beta \ll 1$, we can approximate the ground state $\phi_g^\beta(\mathbf{x})$ and the first excited state $\phi_1^\beta(\mathbf{x})$ by $\phi_g^0(\mathbf{x})$ and $\phi_1^0(\mathbf{x})$, respectively. Thus we have

$$\phi_g^\beta(\mathbf{x}) \approx \phi_g^0(\mathbf{x}), \qquad \phi_1^\beta(\mathbf{x}) \approx \phi_1^0(\mathbf{x}), \qquad \mathbf{x} \in \mathbb{R}^d. \tag{6.2.9}$$

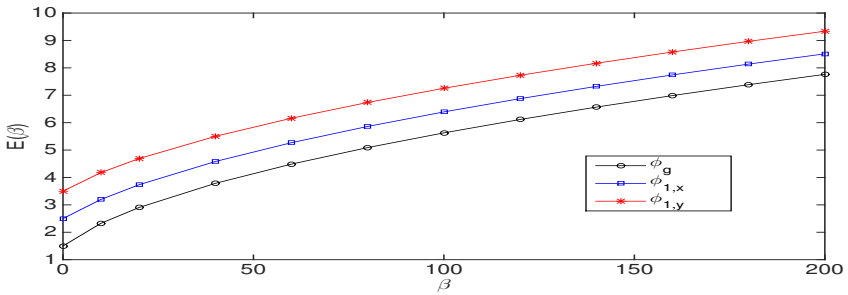

Figure 6.15: Energy for ϕ_g^β, $\phi_{1,x}^\beta$ and $\phi_{1,y}^\beta$ in 2D with $\gamma_1 = 1, \gamma_2 = 2$. The graph for $\gamma_1 \neq \gamma_2$ case is totally different from that for $\gamma_1 = \gamma_2$ case, which is shown in Fig. 6.18.

Plugging (6.2.9) into (1.3.5) and (1.3.6), after a detailed computation which is omitted here for brevity, we can obtain (6.2.7) and (6.2.8). □

Lemma 6.2.2. *In the strongly repulsive interaction regime, i.e. $\beta \gg 1$, we have*

$$\mu_g(\beta) \approx \mu_g^{\mathrm{TF}} = \frac{1}{2}\left(\frac{(d+2)B_2\beta}{C_d}\right)^{\frac{2}{d+2}}, \quad E_g(\beta) = \frac{2+d}{4+d}\mu_g^{\mathrm{TF}} + o(1), \tag{6.2.10}$$

$$\mu_1(\beta) \approx \mu_1^{\mathrm{MA}} = \mu_g^{\mathrm{TF}} + \frac{\sqrt{2}}{2}\gamma_1 + o(1),\ E_1(\beta) = E_g(\beta) + \frac{\sqrt{2}}{2}\gamma_1 + o(1), \tag{6.2.11}$$

where

$$C_d = \int_{\{\mathbf{x}\,||\mathbf{x}|\le 1\}} 1\,d\mathbf{x} = \begin{cases} 2, & d=1, \\ \pi, & d=2, \\ \frac{4\pi}{3}, & d=3. \end{cases} \tag{6.2.12}$$

Proof. When $\beta \gg 1$, the ground and first excited states can be approximated by the TF approximations and/or uniformly accurate matched asymptotic approximations. For $d = 1$ and $V(x) = \frac{\gamma^2 x^2}{2}$, these approximations have been given explicitly and verified numerically in the literature [18, 20, 25, 26], and the results can be extended to d dimensions ($d = 1, 2, 3$) as

$$\phi_g^\beta(\mathbf{x}) \approx \phi_g^{\mathrm{TF}}(\mathbf{x}) = \sqrt{\frac{(\mu_g^{\mathrm{TF}} - V(\mathbf{x}))_+}{\beta}}, \qquad \mathbf{x} \in \mathbb{R}^d, \tag{6.2.13}$$

$$\phi_1^{\beta}(\mathbf{x}) \approx \phi_1^{\mathrm{MA}}(\mathbf{x}) = \begin{cases} \sqrt{\frac{g_1(\mathbf{x})}{\beta}} + \sqrt{\frac{g_2(\mathbf{x})}{\beta}} \left[\tanh(x_1\sqrt{g_2(\mathbf{x})}) - 1\right], & g_1(\mathbf{x}) \geq 0 \& x_1 \geq 0, \\ -\sqrt{\frac{g_1(\mathbf{x})}{\beta}} + \sqrt{\frac{g_2(\mathbf{x})}{\beta}} \left[1 + \tanh(x_1\sqrt{g_2(\mathbf{x})})\right], & g_1(\mathbf{x}) \geq 0 \& x_1 < 0, \\ 0, & \text{otherwise}, \end{cases} \tag{6.2.14}$$

where $(f)_+ := \max\{f, 0\}$, $g_1(\mathbf{x}) = \mu_1^{\mathrm{MA}} - \frac{1}{2}\sum_{j=1}^{d} \gamma_j^2 x_j^2$ and $g_2(\mathbf{x}) = \mu_1^{\mathrm{MA}} - \frac{1}{2}\sum_{j=2}^{d} \gamma_j^2 x_j^2$, and μ_g^{TF} and μ_1^{MA} can be obtained via the normalization condition (1.2.6). Inserting (6.2.13) and (6.2.14) into (1.3.5), after a detailed computation which is omitted here for brevity, we get approximations of $E_g(\beta)$ and $E_1(\beta)$, respectively. □

Proof of Proposition 6.2.1. Subtracting (6.2.7) from (6.2.8) and subtracting (6.2.10) from (6.2.11), we obtain (6.2.2) in the weak and strong interaction regimes, respectively.

Remark 6.2.1. *When $\beta \gg 1$, by performing asymptotic expansion of μ_1^{MA} to the next order, we can obtain the following asymptotics of the fundamental gaps (details are omitted here for brevity)*

$$\delta_E(\beta) = \frac{\sqrt{2}}{2}\gamma_1 + \frac{\gamma_1^2(d+2)^{\frac{d}{d+2}}}{4}\left(\frac{C_d}{B_2\beta}\right)^{\frac{2}{d+2}} + o(\beta^{-\frac{2}{d+2}}), \qquad \beta \gg 1, \tag{6.2.15}$$

$$\delta_\mu(\beta) = \frac{\sqrt{2}}{2}\gamma_1 + \frac{\gamma_1^2 d(d+2)^{-\frac{2}{d+2}}}{4}\left(\frac{C_d}{B_2\beta}\right)^{\frac{2}{d+2}} + o(\beta^{-\frac{2}{d+2}}), \qquad \beta \gg 1. \tag{6.2.16}$$

(II) Degenerate case, i.e. $\gamma_1 = \gamma_2$:

In this section, we consider the case $d \geq 2$ with $\gamma_1 = \gamma_2 = \gamma$. Again due to the non-uniqueness of the first excited states for the linear problem, we need to be careful to determine the correct form of the first excited state for $\beta > 0$. The vortex-type solution as shown in Fig. 6.16 in 2D and Fig. 6.17 in 3D, will appear, which makes the scenario for the degenerate case totally different. Like the box potential case, a crossing for the energy of different excited states at $\beta = 0$ occurs as shown in Fig. 6.18. For simplicity, only the proof for the 2-dimensional problem is shown in this section.

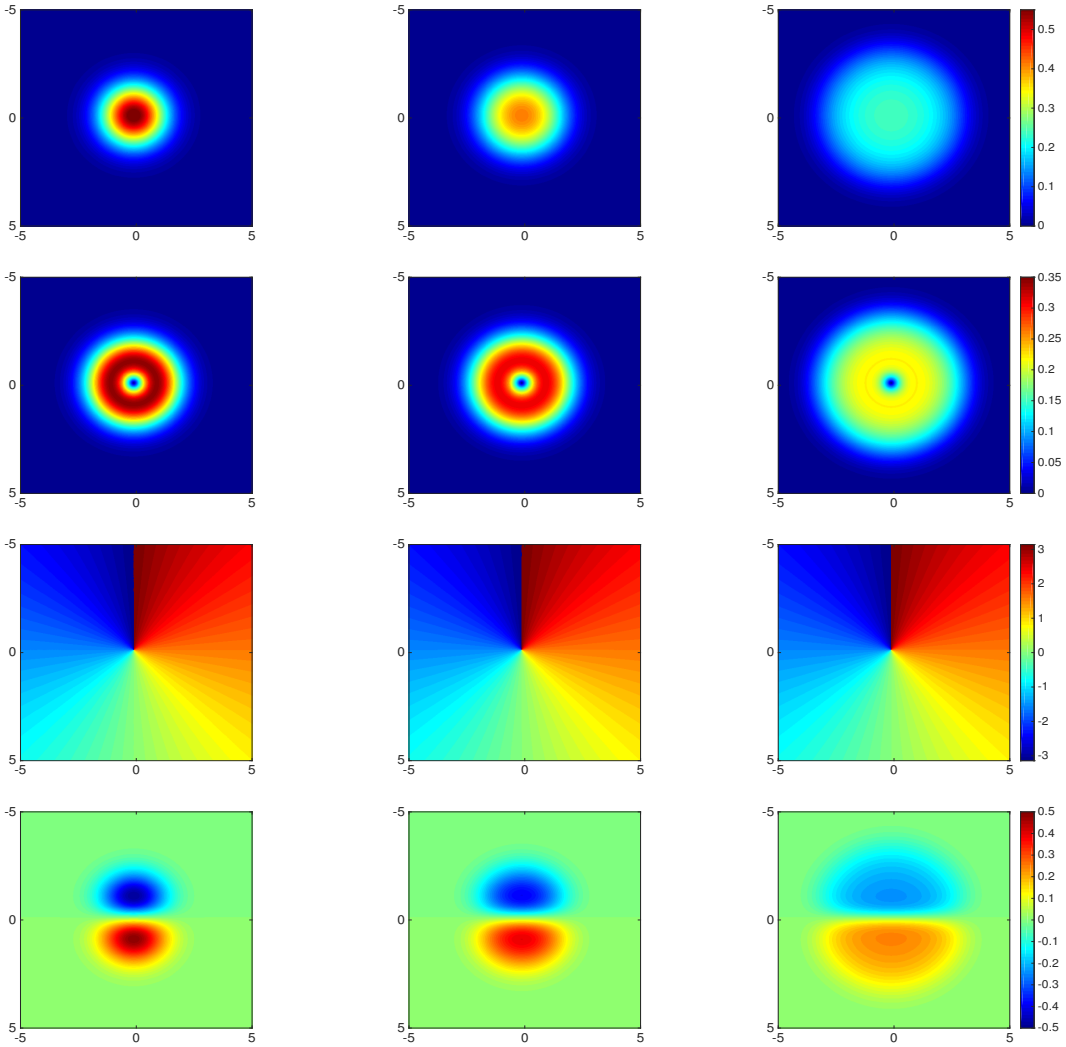

Figure 6.16: Solution for ground state $\phi_g(\mathbf{x})$ (top), vortex solution $|\phi_{1,v}(\mathbf{x})|$(2nd) and x-excitation solution $\phi_{1,x}(\mathbf{x})$(bottom). The 3rd row is the phase angle graph of the vortex solution.

Lemma 6.2.3. *For weakly interaction regime, i.e.* $0 < \beta \ll 1$, *we have for* $d \geq 2$

$$E_1(\beta) = \frac{3\gamma}{2} + \frac{B_0 d}{8}\beta + o(\beta), \quad \mu_1(\beta) = \frac{3\gamma}{2} + \frac{B_0 d}{4}\beta + o(\beta). \tag{6.2.17}$$

Proof. For simplicity, we only present the 2D case and extension to 3D is straightforward. Denote

$$\phi_g^0(x) = \left(\frac{\gamma}{\pi}\right)^{\frac{1}{4}} e^{-\frac{\gamma x^2}{2}}, \qquad \phi_1^0(x) = \sqrt{2\gamma}\left(\frac{\gamma}{\pi}\right)^{\frac{1}{4}} x e^{-\frac{\gamma x^2}{2}}. \tag{6.2.18}$$

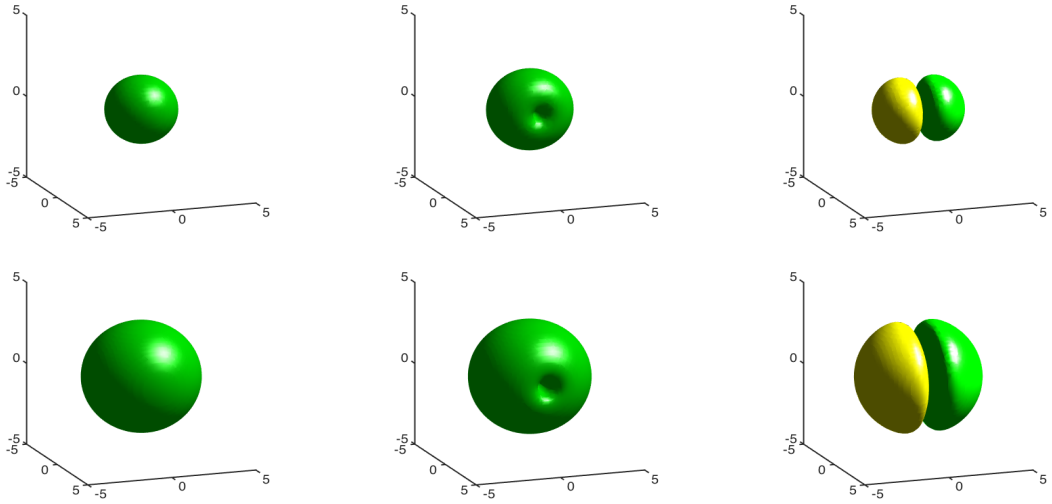

Figure 6.17: Isosurface(value=0.05) of solution for ground state(left), vortex solution(middle) and x-excitation solution(right) with $\beta = 0$(top) and 1000(bottom).

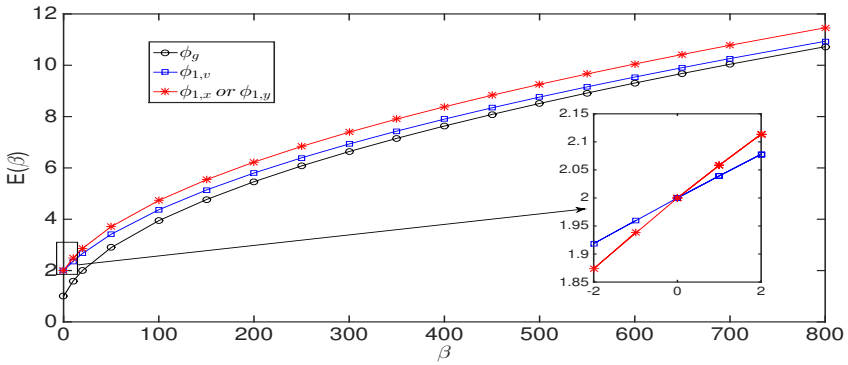

Figure 6.18: Plot for the ground state energy and different excited states with harmonic potential $V(x_1, x_2) = \frac{x_1^2+x_2^2}{2}$.

When $d = 2$ and $\beta = 0$, it is easy to see that $\varphi_1(\mathbf{x}) := \phi_1^0(x_1)\phi_g^0(x_2)$ and $\varphi_2(\mathbf{x}) := \phi_g^0(x_1)\phi_1^0(x_2)$ are two linearly independent orthonormal first excited states. In fact, $W_1 = \text{span}\{\varphi_1, \varphi_2\}$. In order to find an appropriate approximation of the first excited state when $0 < \beta \ll 1$, we take an ansatz

$$\varphi_{a,b}(\mathbf{x}) = a\varphi_1(\mathbf{x}) + b\varphi_2(\mathbf{x}), \qquad \mathbf{x} \in \mathbb{R}^2, \tag{6.2.19}$$

where $a, b \in \mathbb{C}$ satisfying $|a|^2 + |b|^2 = 1$ implies $\|\varphi_{a,b}\|_2 = 1$. Then a and b can be

determined by minimizing $E(\varphi_{a,b})$. Plugging (6.2.19) into (1.3.6), we have for $\beta \geq 0$

$$E(\varphi_{a,b}) = 3\gamma + \frac{\gamma\beta}{16\pi}[|a^2+b^2|^2 + 2(|a|^2+|b|^2)^2] \geq 3\gamma + \frac{\gamma\beta}{8\pi}, \tag{6.2.20}$$

which is minimized when $a^2+b^2=0$, i.e. $a=\pm ib$. By taking $a=1/\sqrt{2}$ and $b=i/\sqrt{2}$, we get an approximation of the first excited state as

$$\phi_1^\beta(\mathbf{x}) \approx \phi_{1,v}(\mathbf{x}) = \frac{\gamma}{\sqrt{\pi}}(x_1+ix_2)e^{-\frac{\gamma(x_1^2+x_2^2)}{2}} = \frac{\gamma}{\sqrt{\pi}} r e^{-\frac{\gamma r^2}{2}} e^{i\theta}, \tag{6.2.21}$$

where (r,θ) is the polar coordinate. Substituting (6.2.21) into (1.3.6) and (1.3.5), we get (6.2.17). □

Remark 6.2.2. *The degenerate case in 3D in weak interaction regime can be computed in a similar, but much more complicated way. If $\gamma_1=\gamma_2=\gamma<\gamma_3$, then the problem shares the same property as the 2D degenerate case as the $\dim(W_1)=2$, where W_1 is defined in (6.0.2). If $\gamma_1=\gamma_2=\gamma_3=\gamma$, then $\dim(W_1)=3$. It can be shown that, in this case, the first excited state in weak interaction regime is of form*

$$\phi_1^\beta(\mathbf{x}) \approx a\phi_g^0(x_1)\phi_g^0(x_2)\phi_1^0(x_3) + b\phi_g^0(x_1)\phi_1^0(x_2)\phi_g^0(x_3) + c\phi_1^0(x_1)\phi_g^0(x_2)\phi_g^0(x_3),$$

where $\mathbf{x}=(x_1,x_2,x_3)\in\bar{\Omega}$, $a,b,c\in\mathbb{C}$ satisfying $|a|^2+|b|^2+|c|^2=1, a^2+b^2+c^2=0$. Therefore, one choice of the first excited state is

$$\frac{1}{\sqrt{\pi}}\gamma(x_1+ix_2)e^{-\frac{\gamma(x_1^2+x_2^2+x_3^2)}{2}}, \qquad \mathbf{x}=(x_1,x_2,x_3)\in\mathbb{R}^3.$$

Lemma 6.2.4. *For the 2D case with strongly repulsive interaction, i.e. $d=2$ and $\beta\gg 1$, we have*

$$E_1(\beta) = E_g^{\mathrm{TF}} + \frac{\gamma}{2}\sqrt{\frac{\pi}{\beta}}\ln(\beta) + \mathcal{O}(\frac{1}{\sqrt{\beta}}), \mu_1(\beta) = \mu_g^{\mathrm{TF}} + \frac{\gamma}{4}\sqrt{\frac{\pi}{\beta}}\ln(\beta) + \mathcal{O}(\frac{1}{\sqrt{\beta}}), \tag{6.2.22}$$

where μ_g^{TF} is given in (6.2.10) and $E_g^{TF}=\frac{2+d}{4+d}\mu_g^{TF}$.

Proof. From Lemma 6.2.3, when $0<\beta\ll 1$, the first excited state needs to be taken as a vortex-type solution. By assuming that there is no band crossing when $\beta>0$, the first excited state can be well approximated by the vortex-type solution when

$\beta \gg 1$ too. Thus when $\beta \gg 1$, we approximate the first excited state via a matched asymptotic approximation.

(i) In the outer region, i.e. $|\mathbf{x}| > o(1)$, it is approximated by the TF approximation as

$$\phi_1^\beta(\mathbf{x}) \approx \phi^{\text{out}}(\mathbf{x}) \approx \sqrt{\frac{(2\mu_1 - \gamma^2 r^2)_+}{2\beta}}, \qquad r > o(1), \tag{6.2.23}$$

where $\mu = \mu_1(\beta)$ is the chemical potential of the first excited state.

(ii) In the inner region near the origin, i.e. $|\mathbf{x}| \ll 1$, it is approximated by a vortex solution with winding number $m = 1$ as

$$\phi_1^\beta(\mathbf{x}) \approx \phi^{\text{in}}(\mathbf{x}) = \sqrt{\frac{\mu_1}{\beta}} f(r) e^{i\theta}, \qquad |\mathbf{x}| \ll 1, \tag{6.2.24}$$

Substituting (6.1.27) into (7.1.1), we get the equation for $f(r)$

$$-\frac{1}{2}f''(r) - \frac{1}{2r}f'(r) + \frac{1}{2r^2}f(r) + \frac{\gamma^2 r^2}{2}f(r) + \mu_1 f^3(r) = \mu_1 f(r), \qquad r > 0, \tag{6.2.25}$$

with boundary conditions $f(0) = 0$. When $\beta \gg 1$, by dropping the terms $-\frac{1}{2}f''(r)$ and $\frac{\gamma^2 r^2}{2}f(r)$ in (6.2.25) and then solving it analytically with the far field limit $\lim_{r\to+\infty} f(r) = 1$, we get (6.1.30). Combining the outer and inner approximations via the matched asymptotic technique, we obtain an asymptotic approximation of the density of the first excited state as

$$|\phi_1^\beta(\mathbf{x})|^2 \approx \frac{2\mu_1 r^2}{1 + 2\mu_1 r^2} \frac{(2\mu_1 - \gamma^2 r^2)_+}{2\beta}, \qquad r \geq 0. \tag{6.2.26}$$

Substituting (6.2.26) into the normalization condition $\|\phi_1^\beta\|_2 = 1$ and (1.3.5), a detailed computation gives the approximation of the chemical potential and energy in (6.2.22). The details of the computation are omitted here for brevity. □

Lemma 6.2.3 and Lemma 6.2.4 implies the results for the degenerate case in Proposition 6.2.1.

6.2.2 Numerical results in the whole space

In this chapter, we will first show the accuracy tests of our asymptotic results in Proposition 6.2.1. And then we will do numerical tests for problems with a general domain and a general external potential.

(I) Accuracy tests for the nondegenerate case:

Fig 6.19 checks the accuracy of the asymptotic approximations of fundamental gaps for $L_1 > L_2$ in 1D, 2D and 3D proposed in Proposition 6.2.1. From Figure 6.19, we can see that the asymptotic results in Proposition 6.2.1 are very accurate in both weakly interaction regime, i.e. $0 \leq \beta \ll 1$, and strongly repulsive interaction regime, i.e. $\beta \gg 1$. In addition, our numerical results suggest that both $\delta_E(\beta)$ and $\delta_\mu(\beta)$ are decreasing functions for $\beta \geq 0$, which immediately imply that

$$\delta_E^\infty := \inf_{\beta\geq 0} \delta_E(\beta) \geq \delta_E(\infty) \geq \frac{\sqrt{2}}{2}\gamma_1, \qquad \delta_\mu^\infty := \inf_{\beta\geq 0} \delta_\mu(\beta) \geq \delta_\mu(\infty) \geq \frac{\sqrt{2}}{2}\gamma_1. \quad (6.2.27)$$

(II) Accuracy tests for the degenerate case:

Fig 6.20 checks the accuracy of the asymptotic approximations of fundamental gaps for $\gamma_1 = \gamma_2$ in 2D and 3D proposed in Proposition 6.2.1. Our numerical results suggest approximation (6.2.4) gives a lower bound of $\delta_E(\beta)$ and $\delta_\mu(\beta)$.

(III) Numerical tests for general cases:

Ground and first excited states as well as their corresponding energy and chemical potentials can be computed numerically for different external potentials. The ground state can be computed by the normalized gradient flow method [14, 16–18]. For problems with a symmetric convex external potential, the first excited state can be also obtained numerically by the normalized gradient flow method [14, 16–18]; while for other cases, the first excited state is obtained numerically by finding the critical point of the energy functional with a proper initial guess with the help of the continuity technique [29], i.e. using the first excited state for a small β as an initial guess for computing the first excited state for a larger β.

Again, we first report numerical results of the GPE in 1D, i.e. $d = 1$. Figure 6.21 plots ground states and first excited states with $V(x) = \frac{x^2}{2} + 0.5\cos(x)$ for different β's, and Figure 6.22 depicts fundamental gaps in energy and chemical potential with

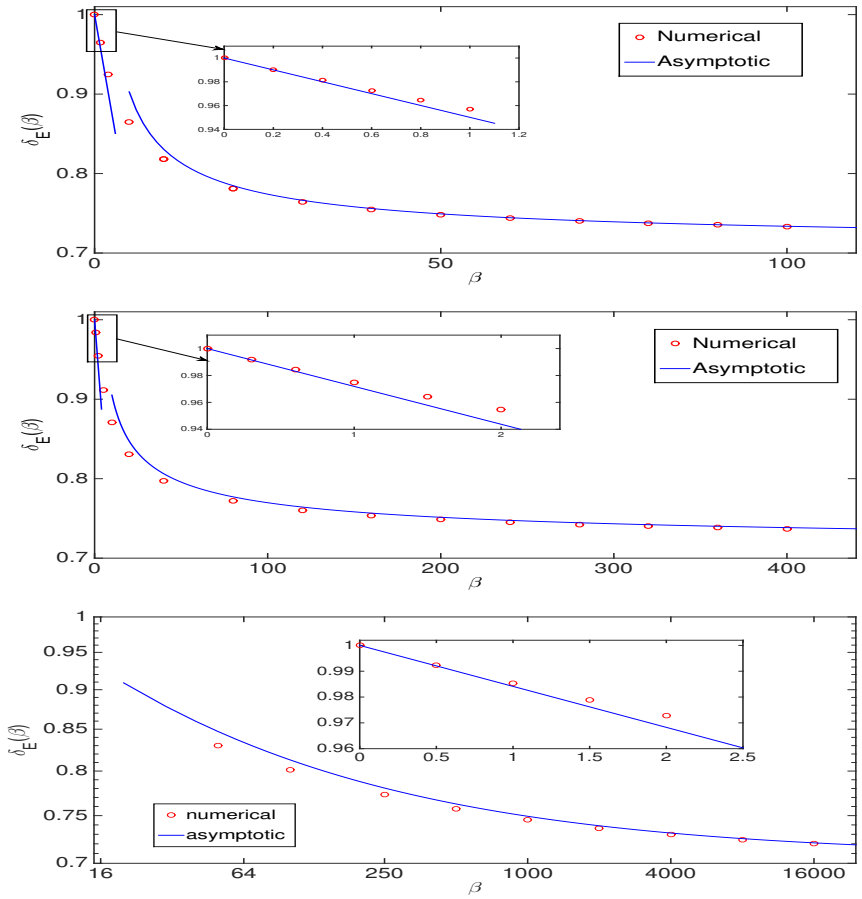

Figure 6.19: Fundamental gaps in energy for the GPE with a harmonic potential in 1D with $\gamma_1 = 1$ (top), in 2D with $\gamma_1 = 1$ and $\gamma_2 = 2$ (middle), and in 3D with $\gamma_1 = 1$ and $\gamma_2 = \gamma_3 = 2$ (bottom).

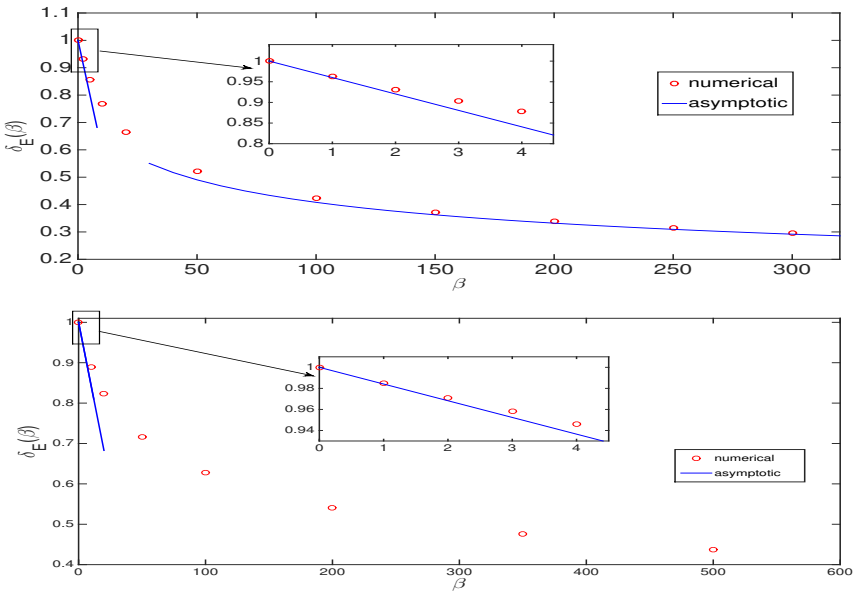

Figure 6.20: Plot for the fundamental gap with harmonic potential $V(x_1, x_2) = (x_1^2 + x_2^2)/2$ in 2D (top) and $V(x_1, x_2, x_3) = (x_1^2 + x_2^2 + x_3^2)/2$ in 3D (bottom).

$V(x) = \frac{x^2}{2} + V_0 \cos(kx)$ for different V_0, k and β. Figure 6.23 shows ground states and first excited states with $\beta = 50$ for different trapping potentials, and Figure 6.24 lists fundamental gaps in energy and chemical potential for different β and different trapping potentials.

Based on the above numerical results and additional extensive numerical results not shown here for brevity as well as our asymptotic results in Proposition 6.2.1, we speculate the Gap Conjecture which will be stated later in Section 6.2.3.

6.2.3 A gap conjecture

As indicated from the numerical tests, the asymptotic results proposed in Proposition 6.2.1 are indeed lower bounds of the fundamental gaps in both weak and strong interaction regimes. Based on the asymptotic results for the special problem considered in Section 6.2.1, we propose the following gap conjecture.

Gap Conjecture (for GPE in $\mathbb{R}^d$). *Suppose $\Omega = \mathbb{R}^d$ and the external potential $V(\mathbf{x})$ satisfies $D^2V(\mathbf{x}) \geq \gamma_v^2 I_d$ for $\mathbf{x} \in \mathbb{R}^d$ with $\gamma_v > 0$ a constant, we have the following*

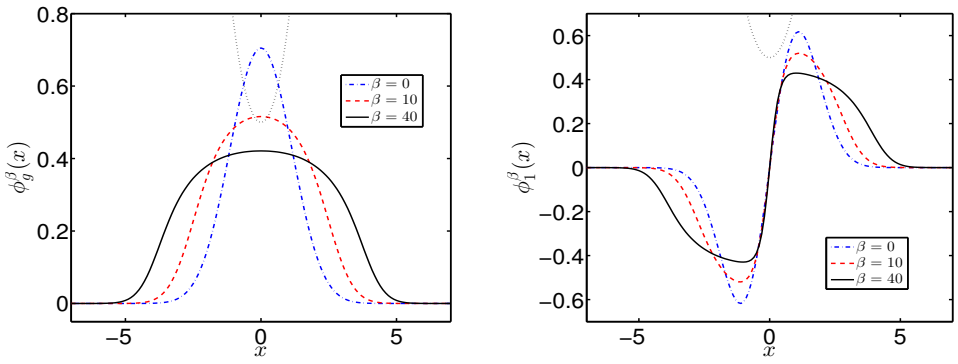

Figure 6.21: Ground states (left) and first excited states (right) of the GPE in 1D with $V(x) = \frac{x^2}{2} + 0.5\cos(x)$ (dot line) for different β.

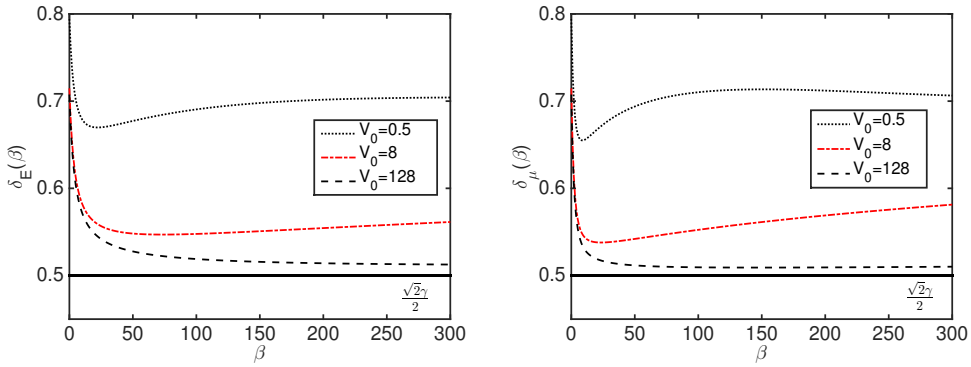

Figure 6.22: Fundamental gaps in energy (left) and chemical potential (right) of the GPE in 1D with $V(x) = \frac{x^2}{2} + V_0\cos(kx)$ satisfying $V_0k^2 = 0.5$ for different β, V_0 and k.

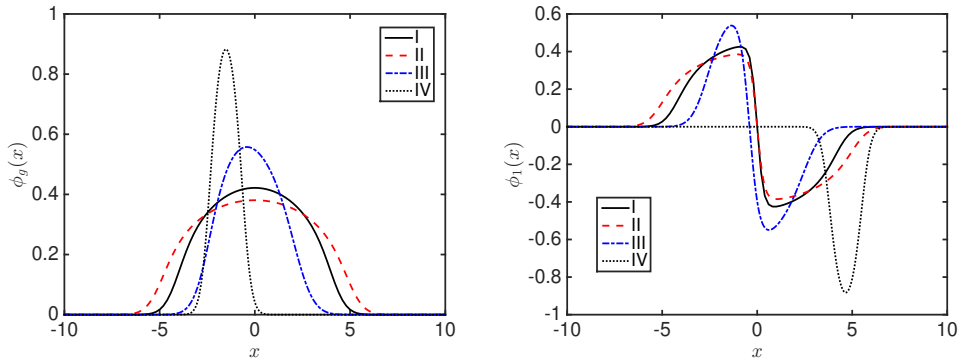

Figure 6.23: Ground states (left) and first excited states (right) of the GPE in 1D with $\beta = 50$ and (I) $V(x) = \frac{x^2}{2}$, (II) $V(x) = \frac{x^2}{2} + 8\cos(0.25x)$, (III) $V(x) = \frac{x^2}{2} + 0.5\sin(x)$, (IV) $V(x) = |x| + 20\sin(x)$.

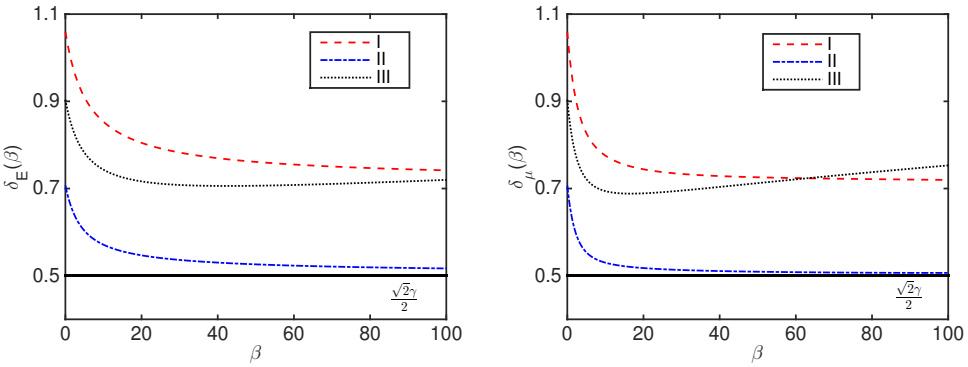

Figure 6.24: Fundamental gaps in energy (left) and chemical potential (right) of the GPE in 1D with (I) $V(x) = \frac{x^2}{2} + 0.5\sin(x)$, (II) $V(x) = \frac{x^2}{4} - x$, (III) $V(x) = \frac{x^2}{4} + \frac{x^4}{100} + x$.

conjectures.

(1) If the first excited state for the linear problem is nondegenerate,

$$\delta_E^\infty := \inf_{\beta\geq 0}\delta_E(\beta) \geq \frac{\sqrt{2}}{2}\gamma_v, \qquad \delta_\mu^\infty := \inf_{\beta\geq 0}\delta_\mu(\beta) \geq \frac{\sqrt{2}}{2}\gamma_v. \tag{6.2.28}$$

(2) If $d = 2$ and the first excited state for the linear problem is degenerate,

$$\delta_E^\infty := \inf_{\beta\geq 0}\delta_E(\beta) = 0, \qquad \delta_\mu^\infty := \inf_{\beta\geq 0}\delta_\mu(\beta) = 0. \tag{6.2.29}$$

6.3 With periodic boundary conditions

Consider the time-independent GPE

$$\left[-\frac{1}{2}\Delta + V(\mathbf{x}) + \beta|\phi(\mathbf{x})|^2\right]\phi(\mathbf{x}) = \mu\phi(\mathbf{x}), \quad \mathbf{x}\in\Omega, \tag{6.3.1}$$

where $\Omega = \prod_{j=1}^d(0, L_j) \subset \mathbb{R}^d$ $(d = 1, 2, 3)$ is a bounded domain satisfying $L_1 = \max\{L_1, \ldots, L_d\} > 0$, $V(\mathbf{x}) \equiv 0$ for $\mathbf{x} \in \Omega$ is a given convex real function and the wave function ϕ satisfies the periodic BC and is normalized via (1.2.6). When $d = 1$, it corresponds to a BEC on a ring [14]; and when $d = 2$, it corresponds to a BEC on a torus. In this case, the ground state ϕ_g^β is defined the same as before provided that the set S is replaced by $S = \{\phi \,|\, \|\phi\|_2^2 := \int_\Omega |\phi(\mathbf{x})|^2 d\mathbf{x} = 1,\ E(\phi) < \infty,\ \phi \text{ is periodic on } \partial\Omega\}$, and the first excited state ϕ_1^β is defined similarly.

In this scenario, when $\beta = 0$, all the eigenfunctions can be obtained via the Fourier series [25, 26]. Similar to the case when $d = 1$, we have the following results for the ground state [25, 26].

Lemma 6.3.1. *Assume $V(\mathbf{x}) \equiv 0$, for all $\beta \geq 0$ and $d = 1, 2, 3$, we have*

$$\phi_g^\beta(\mathbf{x}) = \phi_g^0(\mathbf{x}) \equiv A_0 = \frac{1}{\sqrt{\prod_{j=1}^d L_j}}, \qquad \mathbf{x}\in\bar{\Omega}, \tag{6.3.2}$$

$$E_g(\beta) = \frac{A_0^2}{2}\beta, \qquad \mu_g(\beta) = A_0^2\beta, \qquad \beta \geq 0. \tag{6.3.3}$$

Proof. It is easy to see that $\phi_g^\beta \in S$. For any $\phi \in S$, we obtain

$$1 = \|\phi\|^2 = \left(\int_\Omega |\phi|^2 d\mathbf{x}\right)^2 \leq \int_\Omega |\phi|^4 d\mathbf{x}\int_\Omega 1 d\mathbf{x} = \frac{1}{A_0^2}\int_\Omega |\phi|^4 d\mathbf{x}. \tag{6.3.4}$$

Thus we have

$$\int_\Omega |\phi|^4 d\mathbf{x} \geq A_0^2 = \int_\Omega A_0^4 d\mathbf{x} = \int_\Omega |\phi_g^\beta(\mathbf{x})|^4 d\mathbf{x}. \tag{6.3.5}$$

When $\beta \geq 0$, we get

$$E(\phi) = \int \left[\frac{1}{2}|\nabla\phi|^2 + \frac{\beta}{2}|\phi|^4\right] d\mathbf{x} \geq \frac{\beta}{2}\int |\phi_g^\beta(\mathbf{x})|^4 d\mathbf{x} = E(\phi_g^\beta), \qquad \phi \in S. \tag{6.3.6}$$

Therefore, ϕ_g^0 is the ground state when $\beta \geq 0$. Plugging (6.3.2) into (1.2.7) and (1.2.11) with $V(\mathbf{x}) \equiv 0$, we obtain (6.3.3). □

Lemma 6.3.2. *Assume $V(\mathbf{x}) \equiv 0$, for all $\beta \geq 0$ and $d = 1, 2, 3$, we have*

$$E_1(\beta) = \frac{2\pi^2}{L_1^2} + \frac{A_0^2}{2}\beta, \quad \mu_1(\beta) = \frac{2\pi^2}{L_1^2} + A_0^2\beta. \tag{6.3.7}$$

Proof. for simplicity, we only present 1D case and extensions to 2D and 3D are straightforward. When $d = 1$ and $\beta = 0$, it is easy to see that $\varphi_1(x) := \sqrt{2}A_0 \cos(2\pi x/L_1)$ and $\varphi_2(x) := \sqrt{2}A_0 \sin(2\pi x/L_1)$ are two linearly independent orthonormal first excited states. In fact, in this case, $W_1 = \text{span}\{\varphi_1, \varphi_2\}$. In order to find an appropriate approximation of the first excited state when $0 < \beta \ll 1$, we take an ansatz

$$\varphi_{a,b}(\mathbf{x}) = a\varphi_1(x) + b\varphi_2(x), \qquad 0 \leq x \leq L_1, \tag{6.3.8}$$

where $a, b \in \mathbb{C}$ satisfying $|a|^2 + |b|^2 = 1$ implies $\|\varphi_{a,b}\|_2 = 1$. Then a and b can be determined by minimizing $E(\varphi_{a,b})$. Plugging (6.3.8) into (1.3.6), we have for $\beta \geq 0$

$$E(\varphi_{a,b}) = \frac{2\pi^2}{L_1^2} + \frac{\beta}{4L_1}\left[2(|a|^2 + |b|^2)^2 + |a^2 + b^2|^2\right] \geq \frac{2\pi^2}{L_1^2} + \frac{\beta}{2L_1}, \tag{6.3.9}$$

which is minimized when $a^2 + b^2 = 0$, i.e. $a = \pm ib$. By taking $a = 1/\sqrt{2}$ and $b = i/\sqrt{2}$, we get an approximation of the first excited state as

$$\phi_1^\beta(x) \approx \phi_1^0(x) := A_0 e^{i2\pi x/L_1}, \qquad 0 \leq x \leq L_1. \tag{6.3.10}$$

In fact, noticing $\int_\Omega |\phi_1^0(x)|^4 dx = A_0^2$ and (6.3.5), we can prove rigorously that

$$\phi_1^\beta(x) \equiv \phi_1^0(x) := A_0 e^{i2\pi x/L_1}, \qquad 0 \leq x \leq L_1, \tag{6.3.11}$$

for all $\beta \geq 0$. Plugging (6.3.11) into (1.3.6) and (1.3.5), we obtain (6.3.7). □

Remark 6.3.1. *The choice of the first excited state may not be unique in the degenerate case. It is trivial to see that when $d = 2$ and $L_1 = L_2 = L$, we can choose the first excited state to be $\phi_1^\beta(x, y) = A_0 e^{i2\pi x/L}$ or $\phi_1^\beta(x, y) = A_0 e^{i2\pi y/L}$.*

To obtain the asymptotics of the fundamental gaps, we subtract (6.3.3) from (6.3.7) and get the following statement.

Proposition 6.3.1. *When $\Omega = \prod_{j=1}^d (0, L_j)$ $(d = 1, 2, 3)$ satisfying $L_1 = \max\{L_1, \ldots, L_d\}$ and $V(\mathbf{x}) \equiv 0$ for $\mathbf{x} \in \Omega$ in (6.3.1), i.e. GPE with the periodic boundary condition, we have*

$$\delta_E(\beta) = \delta_\mu(\beta) = \frac{2\pi^2}{L_1^2} \tag{6.3.12}$$

Based on above asymptotic results and numerical results, a conjecture for the general case is proposed as follows.

Gap Conjecture (for GPE on a bounded domain with periodic BC)**.** *Suppose the domain $\Omega = \prod_{j=1}^d (0, L_j)$ $(d = 1, 2, 3)$ satisfies $L_1 = \max\{L_1, \ldots, L_d\}$ and the external potential $V(\mathbf{x})$ is convex, we speculate the following gap conjecture for the fundamental gaps of the GPE with periodic BC,*

$$\delta_E^\infty := \inf_{\beta \geq 0} \delta_E(\beta) \geq \frac{2\pi^2}{D^2}, \qquad \delta_\mu^\infty := \inf_{\beta \geq 0} \delta_\mu(\beta) \geq \frac{2\pi^2}{D^2}, \tag{6.3.13}$$

where D is the diameter of Ω.

6.4 With Neumann boundary conditions

Again we consider the time-independent GPE (6.3.1) where $\Omega = \prod_{j=1}^d (0, L_j)$ satisfying $L_1 = \max\{L_1, \ldots, L_d\} > 0$, $V(\mathbf{x}) \equiv 0$ for $\mathbf{x} \in \Omega$ and assume that ϕ satisfies the homogeneous Neumann BC, i.e. $\partial_{\mathbf{n}} \phi|_{\partial\Omega} = 0$ with $\mathbf{n}$ the unit outward normal vector. In this case, the ground state ϕ_g^β is defined the same as before provided that the set S is replaced by $S = \{\phi \,|\, \|\phi\|_2^2 := \int_\Omega |\phi(\mathbf{x})|^2 d\mathbf{x} = 1,\ E(\phi) < \infty,\ \partial_{\mathbf{n}} \phi|_{\partial\Omega} = 0\}$, and the first excited state ϕ_1^β is defined similarly.

6.4.1 Asymptotic results

In this scenario, when $\beta = 0$, all the eigenfunctions can be obtained via the cosine series [25, 26]. Similar to Lemma 6.3.1, we have the following results for the ground state and its corresponding energy and chemical potential.

Lemma 6.4.1. *For all $\beta \geq 0$, we have*

$$\phi_g^\beta(\mathbf{x}) = \phi_g^0(\mathbf{x}) \equiv A_0 = \frac{1}{\sqrt{\prod_{j=1}^d L_j}}, \qquad \mathbf{x} \in \bar{\Omega}, \tag{6.4.1}$$

$$E_g(\beta) = \frac{A_0^2}{2}\beta, \qquad \mu_g(\beta) = A_0^2\beta, \qquad \beta \geq 0. \tag{6.4.2}$$

However, for the first excited state, we first consider a special case by taking $\Omega = \Omega_0$ and distinguish two different cases: (i) nondegenerate case $L_1 > L_2$ ($\Leftrightarrow \dim(W_1) = 1$); and (ii) degenerate case $L_1 = L_2$ and $d \geq 2$ ($\Leftrightarrow \dim(W_1) \geq 2$).

Lemma 6.4.2. *(nondegenerate case) Assume $d = 1$ or $d \geq 2$ with $L_1 > L_2$, we have*

(i) in the weakly repulsive interaction regime, i.e. $0 < \beta \ll 1$,

$$E_1(\beta) = \frac{\pi^2}{2L_1^2} + \frac{3A_0^2}{4}\beta + o(\beta), \quad \mu_1(\beta) = \frac{\pi^2}{2L_1^2} + \frac{3A_0^2}{2}\beta + o(\beta); \tag{6.4.3}$$

(ii) in the strongly repulsive interaction regime, i.e. $\beta \gg 1$,

$$E_1(\beta) = \frac{A_0^2}{2}\beta + \frac{4A_0}{3L_1}\beta^{1/2} + \frac{2}{L_1^2} + o(1), \ \mu_1(\beta) = A_0^2\beta + \frac{2A_0}{L_1}\beta^{1/2} + \frac{2}{L_1^2} + o(1). \tag{6.4.4}$$

Proof. Here we only present the proof in 1D case and extension to high dimensions is similar to that in Lemma 6.1.2. When $d = 1$ and $\beta = 0$, the first excited state can be taken as $\phi_1^0(x) = \sqrt{2}A_0 \cos(\pi x/L_1)$ for $x \in [0, L_1]$. When $0 < \beta \ll 1$, we can approximate $\phi_1^\beta(x)$ by $\phi_1^0(x)$, i.e.

$$\phi_1^\beta(x) \approx \phi_1^0(x) = \sqrt{2}A_0 \cos\left(\pi x/L_1\right), \qquad 0 \leq x \leq L_1. \tag{6.4.5}$$

Plugging (6.4.5) into (1.3.6) and (1.3.5) with $V(\mathbf{x}) \equiv 0$, we obtain (6.4.3). When $\beta \gg 1$, i.e. in strongly repulsive interaction regime, the first excited state can be approximated via the matched asymptotic method shown in [25, 26] as

$$\phi_1^\beta(x) \approx \phi_1^{MA}(x) = \sqrt{\frac{\mu_1^{MA}}{\beta}} \tanh\left(\sqrt{\mu_1^{MA}}\left(\frac{L_1}{2} - x\right)\right), \qquad 0 \leq x \leq L_1. \tag{6.4.6}$$

Substituting (6.4.6) into the normalization condition (1.2.6) and (1.3.5), we obtain (6.4.4). □

Lemma 6.4.3. *(degenerate case) Assume $d \geq 2$ and $L_1 = L_2 := L$, we have*

(i) in the weakly repulsive interaction regime, i.e. $0 \leq \beta \ll 1$,

$$E_1(\beta) = \frac{\pi^2}{2L^2} + \frac{5A_0^2}{8}\beta + o(\beta), \quad \mu_1(\beta) = \frac{\pi^2}{2L^2} + \frac{5A_0^2}{4}\beta + o(\beta); \tag{6.4.7}$$

(ii) in the strongly repulsive interaction regime, i.e. $\beta \gg 1$, and $d = 2$,

$$E_1(\beta) = \frac{\beta}{2L^2} + \frac{\pi}{2L^2}\ln(\beta) + o(\ln(\beta)),\ \mu_1(\beta) = \frac{\beta}{L^2} + \frac{\pi}{2L^2}\ln(\beta) + o(\ln(\beta)). \tag{6.4.8}$$

Proof. The proof is similar to that for Lemmas 6.1.4&6.1.5 in the box potential case and thus it is omitted here for brevity. □

Lemmas 6.4.2&6.4.3 implies the following proposition about the fundamental gaps.

Proposition 6.4.1. *When $\Omega = \prod_{j=1}^{d}(0, L_j)$ $(d = 1, 2, 3)$ satisfying $L_1 \geq L_2 \geq \cdots \geq L_d$ and $V(\mathbf{x}) \equiv 0$ for $\mathbf{x} \in \Omega$ in (6.3.1), i.e. GPE with the homogeneous Neumann BC, we have the following asymptotics for the fundamental gaps $\delta_E(\beta)$ and $\delta_\mu(\beta)$.*
(i) if $d = 1$ or $L_1 > L_2$ when $d \geq 2$, i.e. nondegenerate case,

$$\delta_E(\beta) = \begin{cases} \frac{\pi^2}{2L_1^2} + \frac{A_0^2}{4}\beta + o(\beta), \\ \frac{4A_0}{3L_1}\beta^{1/2} + \frac{2}{L_1^2} + o(1), \end{cases} \quad \delta_\mu(\beta) = \begin{cases} \frac{\pi^2}{2L_1^2} + \frac{A_0^2}{2}\beta + o(\beta), & 0 \leq \beta \ll 1, \\ \frac{2A_0}{L_1}\beta^{1/2} + \frac{2}{L_1^2} + o(1), & \beta \gg 1; \end{cases} \tag{6.4.9}$$

(ii) if $L_1 = L_2 := L$, i.e. degenerate case, with $0 < \beta \ll 1$ and $d \geq 2$,

$$\delta_E(\beta) = \frac{\pi^2}{2L^2} + \frac{A_0^2}{8}\beta + o(\beta), \quad \delta_\mu(\beta) = \frac{\pi^2}{2L^2} + \frac{A_0^2}{4}\beta + o(\beta). \tag{6.4.10}$$

For the degenerate case with $\beta \gg 1$ and $d = 2$,

$$\delta_E(\beta) = \frac{\pi}{2L^2}\ln(\beta) + o(\ln(\beta)),\ \delta_\mu(\beta) = \frac{\pi}{2L^2}\ln(\beta) + o(\ln(\beta)). \tag{6.4.11}$$

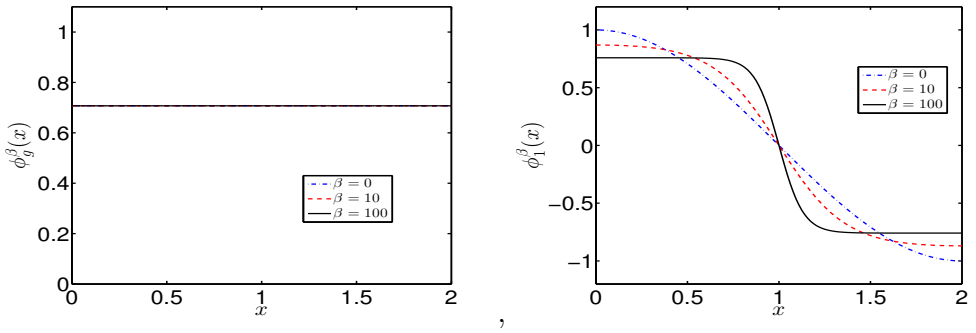

Figure 6.25: Ground states (left) and first excited states (right) of the GPE in 1D with homogeneous Neumann BC for different β.

6.4.2 Numerical results

In order to verify the asymptotic results on the fundamental gaps in Proposition 6.4.1, we solve the time-independent GPE (6.3.1) numerically by using the normalized gradient flow via backward Euler finite difference discretization [14, 16–18] to find the ground and first excited states and their corresponding energy and chemical potentials. Figure 6.25 shows the ground and first excited states for different β in 1D, while Figure 6.26 depicts fundamental gaps in energy obtained numerically and asymptotically in 1D and 2D.

From Figure 6.26, we can see that the asymptotic results in Proposition 6.4.1 for nondegenerate case are very accurate in both weakly interaction regime, i.e. $0 \leq \beta \ll 1$, and strongly repulsive interaction regime, i.e. $\beta \gg 1$, while the asymptotic results roughly captures the leading order behavior for the degenerate case. In addition, our numerical results suggest that both $\delta_E(\beta)$ and $\delta_\mu(\beta)$ are increasing functions for $\beta \geq 0$, which immediately imply that

$$\delta_E^\infty := \inf_{\beta \geq 0} \delta_E(\beta) \geq \frac{\pi^2}{2L_1^2}, \qquad \delta_\mu^\infty := \inf_{\beta \geq 0} \delta_\mu(\beta) \geq \frac{\pi^2}{2L_1^2}. \tag{6.4.12}$$

Based on above asymptotic results and numerical results, a conjecture for the general case is proposed as follows.

Gap Conjecture (for GPE on a bounded domain with homogeneous Neumann BC)**.** *Suppose the domain Ω is a convex bounded domain and the external potential*

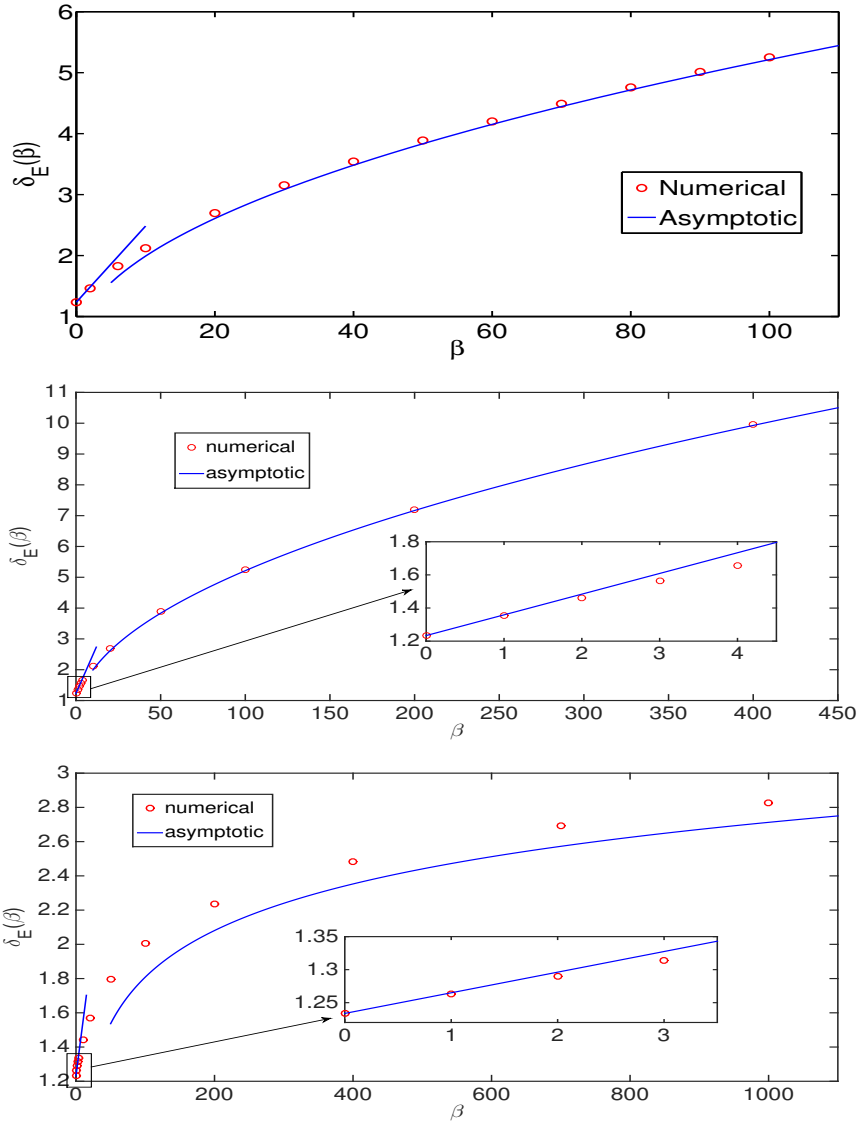

Figure 6.26: Fundamental gaps in energy of the GPE for different β's in 1D with $\Omega = (0, 2)$ (top), in 2D with $\Omega = (0, 2) \times (0, 1)$ (middle) or $\Omega = (0, 2) \times (0, 2)$ (bottom). The homogeneous Neumann boundary condition is applied.

$V(\mathbf{x})$ is weakly convex, we speculate the following gap conjecture for the fundamental gaps of the GPE with homogeneous Neumann BC,

$$\delta_E^{\infty} := \inf_{\beta \geq 0} \delta_E(\beta) \geq \frac{\pi^2}{2D^2}, \qquad \delta_{\mu}^{\infty} := \inf_{\beta \geq 0} \delta_{\mu}(\beta) \geq \frac{\pi^2}{2D^2}. \tag{6.4.13}$$

Chapter 7

Energy Asymptotics of the NLSE

7.1 The nonlinear Schrödinger equation (NLSE)

In this chapter, we will consider the dimensionless time-independent nonlinear Schrödinger equation (NLSE) in d-dimensions ($d = 3, 2, 1$) [10, 14, 21, 54, 93, 103]

$$\left[-\frac{1}{2}\Delta + V(\mathbf{x}) + \beta|\phi(\mathbf{x})|^{2\sigma}\right]\phi(\mathbf{x}) = \mu\phi(\mathbf{x}), \qquad \mathbf{x} \in \Omega \subseteq \mathbb{R}^d, \tag{7.1.1}$$

where $\phi := \phi(\mathbf{x})$ is the wave function (or eigenfunction) normalized via $\|\phi\|_2 = 1$, $V(\mathbf{x})$ is a given real-valued potential, $\beta \geq 0$ is a dimensionless constant describing the repulsive (defocussing) interaction strength, $\sigma \geq 0$ represents different nonlinearities, and the eigenvalue (or chemical potential in physics literature) $\mu := \mu(\phi)$ is defined as [10, 14, 54, 93]

$$\mu(\phi) = E(\phi) + \frac{\sigma\beta}{\sigma+1}\int_\Omega |\phi(\mathbf{x})|^{2\sigma+2} d\mathbf{x}, \tag{7.1.2}$$

with the energy $E := E(\phi)$ defined as [14, 103]

$$E(\phi) = \int_\Omega \left[\frac{1}{2}|\nabla\phi(\mathbf{x})|^2 + V(\mathbf{x})|\phi(\mathbf{x})|^2 + \frac{\beta}{\sigma+1}|\phi(\mathbf{x})|^{2\sigma+2}\right] d\mathbf{x}. \tag{7.1.3}$$

Again, if Ω is bounded, the homogeneous Dirichlet BC, i.e. $\phi(\mathbf{x})|_{\partial\Omega} = 0$, needs to be imposed. Thus, the time-independent NLSE (7.1.1) is a nonlinear eigenvalue problem under the constraint $\|\phi\|_2 = 1$. It is a mean field model arising from Bose-Einstein condensates (BECs) [4, 10, 54, 76], nonlinear optics [50], and some other

applications [1, 93, 103] that can be obtained from the Schrödinger equation (1.1.3) via the Hartree ansatz and mean field approximation [14, 45, 79, 93]. When $\beta = 0$ or $\sigma = 0$, it collapses to the time-independent linear Schrödinger equation. When $\sigma = 1$, the nonlinearity is cubic and it is usually known as the Gross-Pitaevskii equation (GPE) [10, 54, 55, 93]. When $\sigma = 2$, the nonlinearity is quintic and it is used to model the Tonks-Girardeau (TG) gas in BEC [65, 77, 79, 107].

The ground state of the NLSE (7.1.1) is usually defined as the minimizer of the non-convex minimization problem (or constrained minimization problem) [10, 14, 54, 76]

$$\phi_g = \arg\min_{\phi \in S} E(\phi), \tag{7.1.4}$$

where $S = \{\phi \,|\, \|\phi\|_2^2 := \int_\Omega |\phi(\mathbf{x})|^2 d\mathbf{x} = 1,\ E(\phi) < \infty,\ \phi|_{\partial\Omega} = 0 \text{ if } \Omega \text{ is bounded}\}$. Similar to the case when $\sigma = 1$ [14, 80, 112], we have the following theorem concerning the existence and uniqueness of the ground state [97].

Theorem 7.1.1. *(Existence and uniqueness) Suppose $V(\mathbf{x}) \geq 0$ satisfies the confining condition, i.e. $\lim_{|\mathbf{x}|\to\infty} V(\mathbf{x}) = +\infty$, where $\mathbf{x} \in \mathbb{R}^d$, then there exists a minimizer $\phi_g \in S$ if one of the following conditions holds*
(i) $\beta \in \mathbb{R}$ for $0 < d\sigma < 2$,
(ii) $\beta > -\frac{(\sigma+1)}{2} C_b(d,\sigma)$ when $d\sigma = 2$,
(iii) $\beta \geq 0$ for $d\sigma > 2$,
where $C_b(d,\sigma) := \inf_{0 \neq f \in H^1(\mathbb{R}^d)} \frac{\|\nabla f\|^{d\sigma} \|f\|^{2+(2-d)\sigma}}{\|f\|_{2\sigma+2}^{2\sigma+2}}$. Furthermore, when $\beta \geq 0$, $\sigma \geq 0$, the ground state can be chosen as nonnegative $|\phi_g|$, and $\phi_g = e^{i\theta}|\phi_g|$ for some constant $\theta \in \mathbb{R}$. For $\sigma > 0$ and $\beta \geq 0$, the nonnegative ground state is unique.
In contrast, there exists no ground state if one of the following conditions holds
(i') $\beta < -\frac{(\sigma+1)}{2} C_b(d,\sigma)$ when $d\sigma = 2$;
(ii') $\beta < 0$ for $d\sigma > 2$.

Thus, from now on, we consider $\beta \geq 0$ and $\sigma \geq 0$ and refer to the ground state as the nonnegative one. It is easy to see that the ground state ϕ_g satisfies the

time-independent NLSE (7.1.1) and the normalization constraint. Hence it is an eigenfunction (or stationary state) of (7.1.1) with the least energy.

7.2 Asymptotic results under a box potential

In this section, we take $\Omega = \prod_{j=1}^{d}(0, L_j)$ with $L_j > 0$ for $j = 1, \ldots, d$, $V(\mathbf{x}) \equiv 0$ for $\mathbf{x} \in \Omega$ in the NLSE (7.1.1) with the homogeneous Dirichlet BC, i.e. the NLSE with a box potential. We denote the ground state as $\phi_g^{\beta,\sigma}(\mathbf{x})$, obtained from (7.1.4), for any given $\beta \geq 0$ and $\sigma \geq 0$, and the corresponding energy and chemical potential are denoted as $E_g(\beta, \sigma) = E(\phi_g^{\beta,\sigma})$ and $\mu_g(\beta, \sigma) = \mu(\phi_g^{\beta,\sigma})$, respectively. For $\sigma = 0$, it collapses to the linear Schrödinger equation and the ground state $\phi_g^{\beta,0}(\mathbf{x}) = \phi_g^0(\mathbf{x})$ with $\phi_g^0(\mathbf{x})$ given in (6.1.6). Thus from now on, we assume $\sigma > 0$.

7.2.1 Approximations with a fixed nonlinearity σ

When $0 \leq \beta \ll 1$, i.e. weakly repulsive interaction regime, we can approximate the ground state $\phi_g^{\beta,\sigma}(\mathbf{x})$ by $\phi_g^0(\mathbf{x})$ given in (6.1.6). Thus we have,

Lemma 7.2.1. *When $0 \leq \beta \ll 1$, i.e. weakly repulsive interaction regime, the ground state $\phi_g^{\beta,\sigma}$ can be approximated as*

$$\phi_g^{\beta,\sigma}(\mathbf{x}) \approx \phi_g^0(\mathbf{x}) = 2^{\frac{d}{2}} A_0 \prod_{j=1}^{d} \sin\left(\frac{\pi x_j}{L_j}\right), \qquad \mathbf{x} \in \bar{\Omega}, \tag{7.2.1}$$

and the corresponding energy and chemical potential can be approximated as

$$E_g(\beta, \sigma) = A_2 + \frac{2^{d(\sigma+1)} A_0^{2\sigma} \beta}{(\sigma+1)\pi^d} \left[\frac{\Gamma(\sigma + \frac{3}{2})\Gamma(\frac{1}{2})}{\Gamma(\sigma+2)}\right]^d + o(\beta), \tag{7.2.2}$$

$$\mu_g(\beta, \sigma) = A_2 + \frac{2^{d(\sigma+1)} A_0^{2\sigma} \beta}{\pi^d} \left[\frac{\Gamma(\sigma + \frac{3}{2})\Gamma(\frac{1}{2})}{\Gamma(\sigma+2)}\right]^d + o(\beta), \qquad 0 \leq \beta \ll 1. \tag{7.2.3}$$

Proof. Plugging (7.2.1) into (1.3.6) with $V(\mathbf{x}) \equiv 0$, we get

$$E_g(\beta, \sigma) = E(\phi_g^{\beta,\sigma}) \approx E(\phi_g^0) = \int_\Omega \left[\frac{1}{2}|\nabla \phi_g^0(\mathbf{x})|^2 + \frac{\beta}{\sigma+1}|\phi_g^0(\mathbf{x})|^{2\sigma+2}\right] d\mathbf{x}. \tag{7.2.4}$$

Substituting (7.2.1) into (7.2.4) and noting (6.1.3), we can obtain (7.2.2) after performing a detailed computation, which is omitted here for brevity. Similarly, we can obtain (7.2.2) via (1.3.5) and (7.2.1). □

When $\beta \gg 1$, i.e. strongly repulsive interaction regime, the simplest approximation of the ground state is via the Thomas-Fermi (TF) approximation. Then we have,

Lemma 7.2.2. *When $\beta \gg 1$, i.e. strongly repulsive interaction regime, the TF approximation of the ground state can be given as*

$$\phi_g^{\beta,\sigma}(\mathbf{x}) \approx \phi_g^{TF}(\mathbf{x}) = A_0, \qquad \mathbf{x} \in \Omega, \tag{7.2.5}$$

and the corresponding energy and chemical potential can be approximated as

$$E_g(\beta,\sigma) \approx E_g^{TF} = \frac{A_0^{2\sigma}}{\sigma+1}\beta, \quad \mu_g(\beta,\sigma) \approx \mu_g^{TF} = A_0^{2\sigma}\beta, \quad \beta \gg 1. \tag{7.2.6}$$

Proof. Dropping the diffusion term in (7.1.1) with $V(\mathbf{x}) \equiv 0$, we get

$$\mu_g^{TF}\phi_g^{\mathrm{TF}}(\mathbf{x}) = \beta|\phi_g^{\mathrm{TF}}(\mathbf{x})|^{2\sigma}\phi_g^{\mathrm{TF}}(\mathbf{x}), \qquad \mathbf{x} \in \Omega. \tag{7.2.7}$$

Solving the above equation, we get

$$\phi_g^{TF}(\mathbf{x}) = \left(\frac{\mu_g^{TF}}{\beta}\right)^{\frac{1}{2\sigma}}, \qquad \mathbf{x} \in \Omega. \tag{7.2.8}$$

Plugging it into the normalization condition, we get the second equation in (7.2.6) and thus, we can obtain the TF approximation (7.2.5). Inserting (7.2.5) into (1.3.6) with $V(\mathbf{x}) \equiv 0$, we obtain the first equation in (7.2.6). □

Note that the TF approximation (7.2.5) does not satisfy the homogeneous Dirichlet BC. Therefore, the approximation is not uniformly accurate. In fact, there exists a boundary layer along $\partial\Omega$ in the ground state when $\beta \gg 1$. Similar to the case of $\sigma = 1$ [25, 26], by using the matched asymptotic expansion method, we can obtain an approximate ground state which is uniformly accurate when $\beta \gg 1$.

Lemma 7.2.3. *When $\beta \gg 1$, i.e. strongly repulsive interaction regime, a uniformly accurate ground state approximation can be given as*

$$\begin{aligned}\phi_g^{\beta,\sigma}(\mathbf{x}) &\approx \phi_g^{MA}(\mathbf{x}) \\ &= \left(\frac{\mu_g^{MA}}{\beta}\right)^{\frac{1}{2\sigma}} \prod_{j=1}^{d} \left[\varphi_\sigma\left(x_j\sqrt{\mu_g^{MA}}\right) + \varphi_\sigma\left((L_j - x_j)\sqrt{\mu_g^{MA}}\right)\right. \\ &\quad \left. -\varphi_\sigma\left(L_j\sqrt{\mu_g^{MA}}\right)\right], \end{aligned} \tag{7.2.9}$$

where $\varphi_\sigma\left(L_j\sqrt{\mu_g^{MA}}\right) \approx 1$ and $\mu_g^{MA} \approx \mu_g(\beta,\sigma) = O(\beta)$ is the approximate chemical potential determined by the normalization condition $\|\phi\|_2 = 1$ and $\varphi_\sigma(x)$ satisfies the problem

$$\begin{cases} \varphi_\sigma(x) = -\frac{1}{2}\varphi_\sigma''(x) + \varphi_\sigma^{2\sigma+1}(x), & 0 < x < +\infty, \\ \varphi_\sigma(0) = 0, \qquad \lim\limits_{x\to+\infty} \varphi_\sigma(x) = 1. \end{cases} \tag{7.2.10}$$

Proof. For the simplicity of notation, we only prove it in 1D here. Extension to higher dimensions can be done via dimension-by-dimension. When $d = 1$, there are two boundary layers in the ground state at $x_1 = 0$ and $x_1 = L_1$, respectively. Near $x_1 = 0$, we introduce the new variables

$$\tilde{x} = x_1\sqrt{\mu_g(\beta,\sigma)}, \quad \varphi_\sigma(\tilde{x}) = \left(\frac{\beta}{\mu_g(\beta,\sigma)}\right)^{\frac{1}{2\sigma}} \phi(x_1), \quad x_1 \geq 0. \tag{7.2.11}$$

Substituting (7.2.11) into (7.1.1) with $d = 1$, $\Omega = (0, L_1)$ and $V(\mathbf{x}) \equiv 0$ and then removing all $\tilde{}$, we get (7.2.10). After obtaining the solution of (7.2.10), an inner approximation of the ground state near $x_1 = 0$ is given as

$$\phi_g^{\beta,\sigma}(x_1) \approx \left(\frac{\mu_g(\beta,\sigma)}{\beta}\right)^{\frac{1}{2\sigma}} \varphi_\sigma\left(x_1\sqrt{\mu_g(\beta,\sigma)}\right), \qquad 0 \leq x_1 \ll 1. \tag{7.2.12}$$

Similarly, we can get the inner approximation of the ground state near $x_1 = L_1$ as

$$\phi_g^{\beta,\sigma}(s) \approx \left(\frac{\mu_g(\beta,\sigma)}{\beta}\right)^{\frac{1}{2\sigma}} \varphi_\sigma\left(s\sqrt{\mu_g(\beta,\sigma)}\right), \quad 0 \leq s := L_1 - x_1 \ll 1. \tag{7.2.13}$$

Combining (7.2.12), (7.2.13) and the outer TF approximation (7.2.5), using the matched asymptotic expansion method via denoting μ_g^{TF} and $\mu_g(\beta,\sigma)$ by μ_g^{MA}, we can obtain (7.2.9). □

When $\sigma = 1$, i.e. GPE, the solution of (7.2.10) is given as $\varphi_1(x) = \tanh(x)$ for $x \geq 0$ [25, 26]. For $0 < \sigma \neq 1$, in general, the problem (7.2.10) cannot be solved explicitly. But a mathematical analysis of $\varphi_\sigma(x)$ can be done as follows to get some properties of it. Multiplying (7.2.10) by $\varphi'_\sigma(x)$, we get

$$\frac{1}{2}\left(\varphi_\sigma^2(x)\right)' = -\frac{1}{4}\left((\varphi'_\sigma(x))^2\right)' + \frac{1}{2\sigma+2}\left(\varphi_\sigma^{2\sigma+2}(x)\right)', \qquad x > 0. \tag{7.2.14}$$

Therefore, we have

$$\varphi_\sigma^2(x) = -\frac{1}{2}\left(\varphi'_\sigma(x)\right)^2 + \frac{1}{\sigma+1}\varphi_\sigma^{2\sigma+2}(x) + C, \qquad x \geq 0, \tag{7.2.15}$$

where C is the integrating constant. When $x \to +\infty$, we have $\varphi_\sigma(x) \to 1$ and $\varphi'_\sigma(x) \to 0$. So we get $C = \frac{\sigma}{1+\sigma}$. Letting $x = 0$ in (7.2.15), we get

$$\varphi'_\sigma(0) = \sqrt{\frac{2\sigma}{\sigma+1}}, \qquad \sigma > 0. \tag{7.2.16}$$

For $\sigma > 0$, by using the maximum principle, we have $0 \leq \varphi_\sigma(x) < 1$ for $x \geq 0$. When $\sigma \to \infty$, we have $\varphi_\sigma^{2\sigma+1}(x) \to 0$ for $x \geq 0$. Therefore, when $\sigma \to \infty$, noting (7.2.16), the problem (7.2.10) converges to the following linear problem:

$$\begin{cases} \varphi_\infty(x) = -\frac{1}{2}\varphi''_\infty(x), & x > 0, \\ \varphi_\infty(0) = 0, \qquad \varphi'_\infty(0) = \sqrt{2}. \end{cases} \tag{7.2.17}$$

Solving this problem, we obtain (7.2.18) immediately. □

To illustrate the solution $\varphi_\sigma(x)$ of (7.2.10), Figure 7.1 plots $\varphi_\sigma(x)$ obtained numerically for different σ. From this figure, we can see that: (i) For any $\sigma > 0$, $\varphi_\sigma(x)$ is a monotonically increasing function. (ii) When $\sigma \to +\infty$, $\varphi_\sigma(x)$ converges to $\varphi_\infty(x)$ uniformly for $x \geq 0$ (cf. Figure 7.1).

The results for $\varphi_\sigma(x)$ can be formulated as the following lemma.

Lemma 7.2.4. *For any $\sigma > 0$, the solution $\varphi_\sigma(x)$ of (7.2.10) is a strictly increasing function for $x \geq 0$ and satisfies $\varphi'_\sigma(0) = \sqrt{\frac{2\sigma}{\sigma+1}}$. In addition, when $\sigma \to +\infty$, we have*

$$\varphi_\sigma(x) \to \varphi_\infty(x) = \begin{cases} \sin(\sqrt{2}x), & 0 \leq x < \frac{\sqrt{2}\pi}{4}, \\ 1, & x \geq \frac{\sqrt{2}\pi}{4}. \end{cases} \tag{7.2.18}$$

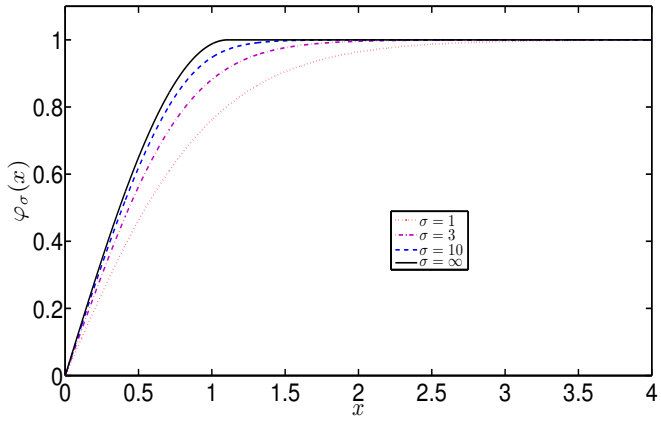

Figure 7.1: Plots of the solution $\varphi_\sigma(x)$ of the problem (7.2.10) for $\sigma = 1, 3, 10, \infty$ (with the order from right to left).

Combining Lemmas 7.2.3 and 7.2.4, we get the width of the boundary layers in the ground state of the NLSE in strongly repulsive interaction regime, i.e. $\beta \gg 1$, is of order $O\left(\frac{1}{\sqrt{\beta}}\right)$ for any $\sigma > 0$, which is the same as in the GPE case [25, 26].

Figure 7.2 shows the relative error of the energy approximation of the ground state, i.e. $e(\beta) := \frac{|E_g(\beta,2) - E_g^{\rm app}|}{E_g(\beta,2)}$ when $\sigma = 2$ for different $\beta \geq 0$ in both weak and strong interaction regimes.

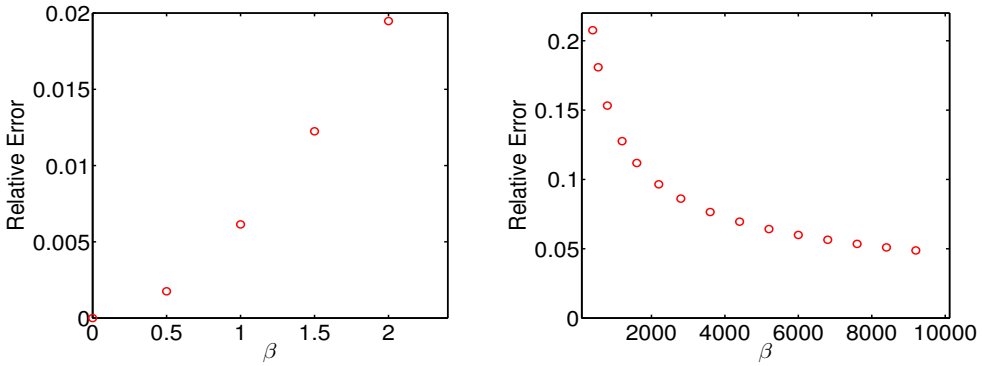

Figure 7.2: Relative errors of the energy approximation of the ground state for the NLSE with $L = 1$ and $\sigma = 2$ in 1D with the box potential in the weak (left) and strong (right) interaction regimes.

7.2.2 Approximations when $\sigma \to \infty$

Here we assume $\beta > 0$ is a given constant and we shall study the limit of the ground state $\phi_g^{\beta,\sigma}$ when $\sigma \to \infty$. For the simplicity of notation, we will only consider the NLSE in 1D, i.e. $d = 1$ on a bounded domain $\Omega = (0, L)$ with $L > 0$ a fixed constant. Then we have

Lemma 7.2.5. *For any given $\beta > 0$, when $\sigma \to \infty$, we have*

(i) if $0 < L < 1$, the ground state converges to the TF approximation

$$\phi_g^{\beta,\sigma}(x) \to \phi_g^{TF}(x) = \frac{1}{\sqrt{L}}, \qquad 0 < x < L, \tag{7.2.19}$$

$$\mu_g(\beta,\sigma) \approx \frac{\beta}{L^{\sigma+1}} \to \infty, \quad E_g(\beta,\sigma) \approx \frac{\beta}{(\sigma+1)L^{\sigma+1}} \to \infty. \tag{7.2.20}$$

(ii) if $L \geq 2$, the ground state converges to the linear approximation

$$\phi_g^{\beta,\sigma}(x) \approx \phi_g^0(x) = \sqrt{\frac{2}{L}} \sin\Big(\frac{\pi x}{L}\Big), \qquad 0 \leq x \leq L, \tag{7.2.21}$$

$$\mu_g(\beta,\sigma) \approx \frac{\pi^2}{2L^2} + \frac{2\beta}{\pi}\left(\frac{2}{L}\right)^{\sigma}\left[\frac{\Gamma(\sigma+\frac{3}{2})\Gamma(\frac{1}{2})}{\Gamma(\sigma+2)}\right] \to \frac{\pi^2}{2L^2}, \tag{7.2.22}$$

$$E_g(\beta,\sigma) \approx \frac{\pi^2}{2L^2} + \frac{2\beta}{(\sigma+1)\pi}\left(\frac{2}{L}\right)^{\sigma}\left[\frac{\Gamma(\sigma+\frac{3}{2})\Gamma(\frac{1}{2})}{\Gamma(\sigma+2)}\right] \to \frac{\pi^2}{2L^2}; \tag{7.2.23}$$

(iii) if $1 < L < 2$, the ground state converges to

$$\phi_g^{\beta,\sigma}(x) \to \phi_g^{\infty}(x) = \begin{cases} \sin(\frac{\pi x}{2(L-1)}), & 0 \leq x < L-1, \\ 1, & L-1 \leq x \leq 1, \\ \sin(\frac{\pi(L+x-2)}{2(L-1)}), & 1 < x \leq L, \end{cases} \tag{7.2.24}$$

$$\mu_g(\beta,\sigma) \to \frac{\pi^2}{8(L-1)^2}, \quad E_g(\beta,\sigma) \to \frac{\pi^2}{8(L-1)}. \tag{7.2.25}$$

Proof. For any given $\beta > 0$, when $\sigma \gg 1$, note that

$$a^{2\sigma} \to \begin{cases} 0, & |a| < 1, \\ 1, & a = 1, \\ +\infty, & a > 1. \end{cases} \tag{7.2.26}$$

Thus, to find the limit of $\phi_g^{\beta,\sigma}(x)$ when $\sigma \to \infty$, the main idea is to determine which term on the left hand side of (7.1.1) is negligible when $\sigma >> 1$. In the region where $|\phi(x)| < 1$, the nonlinear term can be dropped and we get the linear approximation, whose solution is the sine function. In the region where $|\phi(x)| > 1$, the diffusion term can be dropped and we get the TF approximation, whose solution is a constant. Therefore, there are three possible cases concerning the limit $\phi_g^{\beta,\sigma}(x) \to \phi^{\text{app}}(x)$ for $0 < x < L$ when $\sigma \to +\infty$: (i) $|\phi^{\text{app}}(x)| \geq 1$ for all $x \in (0, L)$, (ii) $|\phi^{\text{app}}(x)| \leq 1$ for all $x \in (0, L)$, and (iii) there exists $0 < x_c < L/2$ such that $|\phi^{\text{app}}(x)| \geq 1$ for $x \in [x_c, L - x_c]$ and $|\phi^{\text{app}}(x)| < 1$ otherwise.

(i) When $0 < L \leq 1$, the TF approximation suggests that $\phi^{\text{app}}(x) = \sqrt{1/L} \geq 1$ for $0 < x < L$. Note that the requirement that $\inf_{0<x<L} \phi^{\text{app}}(x) \geq 1$ implies that $L \leq 1$. Therefore, we get the necessary and sufficient condition about L for (7.2.19) to be true.

(ii) When $L \geq 2$, the linear approximation suggests that $\phi^{\text{app}}(x) = \frac{2}{L} \sin\left(\frac{\pi x}{L}\right) \leq 1$ for $0 < x < L$. Note that the requirement that $\sup_{0<x<L} \phi^{\text{app}}(x) \leq 1$ implies that $L \geq 2$. Therefore, we get the necessary and sufficient condition about L for (7.2.21) to be true.

(iii) When $1 < L < 2$, we may expect neither the linear approximation nor the TF approximation is valid for $0 < x < L$. Instead, a combination of the linear approximation and TF approximation should be used. To be more specific, for any fixed $\sigma > 0$, when $\beta >> 1$, there exists a constant x_c^σ such that when $x \in (0, x_c^\sigma)$ or $x \in [L - x_c^\sigma, L]$, the linear approximation is used; and when $x \in [x_c^\sigma, L - x_c^\sigma]$, the TF approximation which is a constant, should be used. For $x \in [x_c^\sigma, L - x_c^\sigma]$, assuming that $\phi_g^\sigma(x) = A_\sigma$ with $A_\sigma > 0$ is a constant to be determined, the approximate solution in $(0, x_c^\sigma)$ must be $\phi_g^\sigma(x) = A_\sigma \sin\left(\frac{\pi x}{2x_c^\sigma}\right)$ in order to make the combined solution to be C^1 continuous. Now we need to determine the value of A_σ and x_c^σ. By the normalization condition, we get

$$\frac{1}{2} = \int_0^{\frac{L}{2}} |\phi_g^\sigma(x)|^2 dx = \int_0^{x_c^\sigma} |\phi_g^\sigma(x)|^2 dx + \int_{x_c^\sigma}^{\frac{L}{2}} |\phi_g^\sigma(x)|^2 dx = A_\sigma^2 \left(\frac{L}{2} - \frac{x_c^\sigma}{2}\right) \quad (7.2.27)$$

Thus, we have

$$A_\sigma = \frac{1}{\sqrt{L - x_c^\sigma}}. \tag{7.2.28}$$

In $[0, x_c^\sigma)$, dropping the nonlinear term in (7.1.1) and substituting the approximate solution into it, we get

$$\mu_g = \frac{\pi^2}{8(x_c^\sigma)^2}. \tag{7.2.29}$$

In $[x_c^\sigma, L - x_c^\sigma]$, dropping the diffusion term in (7.1.1), we get

$$\mu_g = \beta A_\sigma^{2\sigma}. \tag{7.2.30}$$

Combining (7.2.29) and (7.2.30), we obtain

$$A_\sigma^2 = \left(\frac{\pi^2}{8\beta(x_c^\sigma)^2}\right)^{1/\sigma}. \tag{7.2.31}$$

Inserting (7.2.28) into (7.2.31), we have

$$\left(\frac{\pi^2}{8\beta(x_c^\sigma)^2}\right)^{\frac{1}{\sigma}} = \frac{1}{L - x_c^\sigma}. \tag{7.2.32}$$

Letting $\sigma \to \infty$ and assuming $x_c^\sigma \to x_c$ and $A_\sigma \to A$, we have $1 = \frac{1}{L - x_c}$, which implies that $x_c = L - 1$ and we get $A = 1$ via (7.2.28) when $\sigma \to \infty$. Thus we get (7.2.24) when $\sigma \to \infty$. $\mu_g(\beta, \infty)$ can be computed from (7.2.29) and $E_g(\beta, \infty)$ is from definition (1.3.6),

$$E_g(\beta, \infty) = \lim_{\sigma \to \infty} \int_0^L \left[\frac{1}{2}|\nabla \phi_g^{\beta,\sigma}|^2 + \frac{\beta}{\sigma + 1}|\phi_g^{\beta,\sigma}|^{2\sigma+2}\right] dx.$$

However, direct computation by using (7.2.24) may be unreasonable because we cannot get the limit of $\int_{L-1}^1 |\phi_g^{\beta,\sigma}|^{2\sigma+2} dx$. In fact, to get $E_g(\beta, \infty)$, we only need the upper limit of $\int_{L-1}^1 |\phi_g^{\beta,\sigma}|^{2\sigma+2} dx$ is bounded, which is true because

$$0 \le \limsup_{\sigma \to \infty} \beta \int_{L-1}^1 |\phi_g^{\beta,\sigma}|^{2\sigma+2} dx \le \lim_{\sigma \to \infty} \mu_g(\beta, \sigma) = \frac{\pi^2}{8(L-1)^2}.$$

It follows that $\lim_{\sigma \to \infty} \int_0^L \frac{\beta}{\sigma+1} |\phi_g^{\beta,\sigma}|^{2\sigma+2} dx = 0$ and

$$E_g(\beta, \infty) = \lim_{\sigma \to \infty} \int_0^L \frac{1}{2} |\nabla \phi_g^{\beta,\sigma}|^2 dx \approx \int_0^L \frac{1}{2} |\nabla \phi_g^{\beta,\infty}|^2 dx = \frac{\pi^2}{8(L-1)}.$$

□

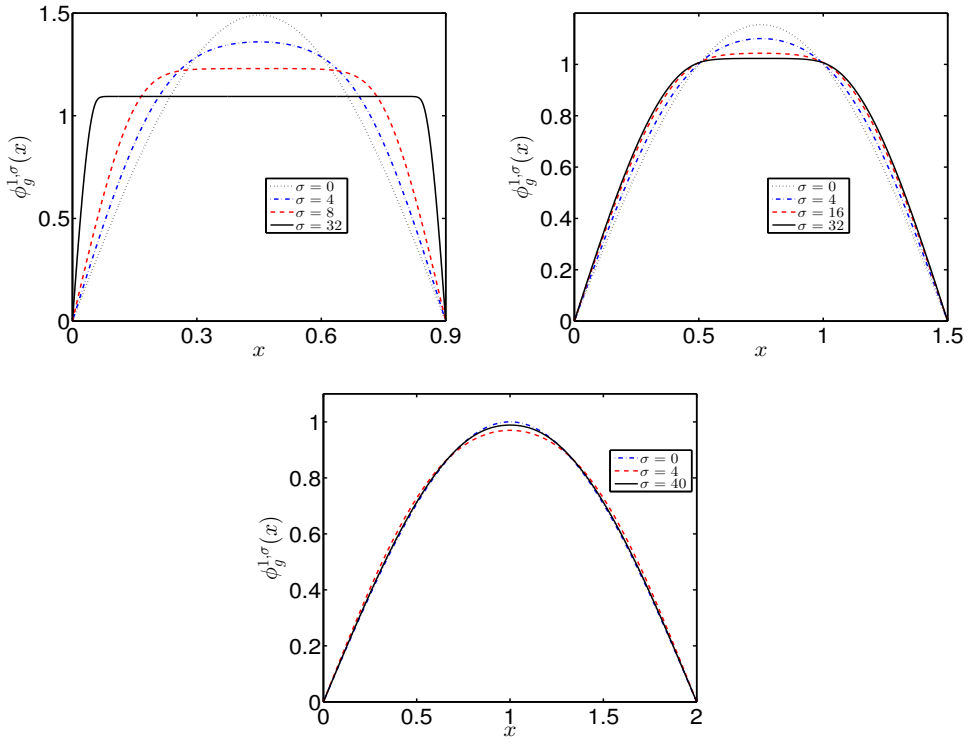

Figure 7.3: Ground states of the NLSE in 1D with $\beta = 1$ and the box potential for different σ and $L = 0.9 < 1$ (upper left), $1 < L = 1.5 < 2$ (upper right) and $L = 2.0$ (bottom).

In order to check our asymptotic results in Lemma 7.2.5, we solve the time-independent NLSE (7.1.1) numerically by using the normalized gradient flow via backward Euler finite difference discretization [14, 16–18] to find the ground states and their corresponding energy and chemical potentials. Figure 7.3 plots the ground states with $\beta = 1$ for different σ and L, and Figure 7.4 depicts the ground state energy with $\beta = 1$ and $L = 1.2$ for different σ.

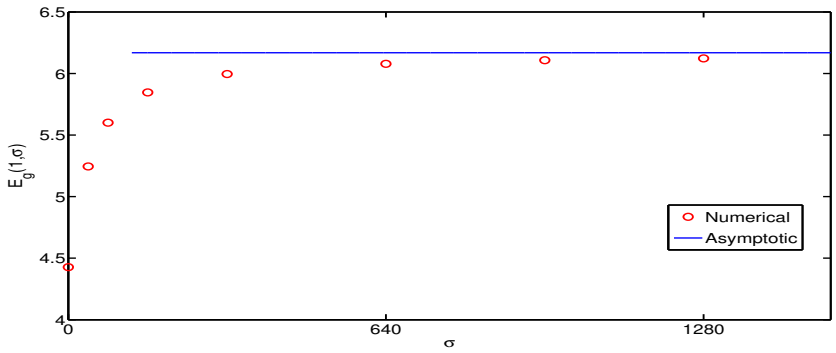

Figure 7.4: Ground state energy of the NLSE in 1D with $\beta = 1$, $L = 1.2$ and the box potential.

7.3 Asymptotic results under a harmonic potential

In this section, we take $\Omega = \mathbb{R}^d$ and $V(\mathbf{x}) = \frac{\gamma^2|\mathbf{x}|^2}{2}$ with $\gamma > 0$ a constant in the NLSE (7.1.1), i.e. the NLSE with a harmonic potential. We denote the ground state as $\phi_g^{\beta,\sigma}(\mathbf{x})$, obtained from (7.1.4), for any given $\beta \geq 0$ and $\sigma \geq 0$, and the corresponding energy and chemical potential are denoted as $E_g(\beta, \sigma) = E(\phi_g^{\beta,\sigma})$ and $\mu_g(\beta, \sigma) = \mu(\phi_g^{\beta,\sigma})$, respectively. For $\sigma = 0$, it collapses to the linear Schrödinger equation with the ground state given by $\phi_g^{\beta,0}(\mathbf{x}) = \phi_g^0(\mathbf{x})$, where $\phi_g^0(\mathbf{x})$ is given in (6.2.6). Thus from now on, we assume $\sigma > 0$.

7.3.1 Approximations with a fixed nonlinearity σ

When $0 \leq \beta \ll 1$, i.e. weakly repulsive interaction regime, we can approximate the ground state $\phi_g^{\beta,\sigma}(\mathbf{x})$ by $\phi_g^0(\mathbf{x})$ given in (6.2.6). Thus we have,

Lemma 7.3.1. *When $0 \leq \beta \ll 1$, i.e. weakly repulsive interaction regime, the ground state $\phi_g^{\beta,\sigma}$ can be approximated as*

$$\phi_g^{\beta,\sigma}(\mathbf{x}) \approx \phi_g^0(\mathbf{x}) = \prod_{j=1}^{d} \left(\frac{\gamma}{\pi}\right)^{\frac{1}{4}} e^{-\frac{\gamma x_j^2}{2}}, \qquad \mathbf{x} \in \mathbb{R}^d, \tag{7.3.1}$$

and the corresponding energy and chemical potential can be approximated as

$$E_g(\beta,\sigma) = \frac{d\gamma}{2} + \frac{\beta}{(\sigma+1)^{\frac{d+2}{2}}} \left(\frac{\gamma}{\pi}\right)^{\frac{d\sigma}{2}} + o(\beta), \tag{7.3.2}$$

$$\mu_g(\beta,\sigma) = \frac{d\gamma}{2} + \frac{\beta}{(\sigma+1)^{\frac{d}{2}}} \left(\frac{\gamma}{\pi}\right)^{\frac{d\sigma}{2}} + o(\beta), \qquad 0 \leq \beta \ll 1. \tag{7.3.3}$$

Proof. Plugging (7.3.1) into (1.3.6) with $V(\mathbf{x}) = \frac{\gamma^2|\mathbf{x}|^2}{2}$, we get

$$\begin{aligned} E_g(\beta,\sigma) &= E(\phi_g^{\beta,\sigma}) \approx E(\phi_g^0) \\ &= \int_{\mathbb{R}^d} \left[\frac{1}{2}|\nabla\phi_g^0(\mathbf{x})|^2 + V(\mathbf{x})|\phi_g^0(\mathbf{x})|^2 + \frac{\beta}{\sigma+1}|\phi_g^0(\mathbf{x})|^{2\sigma+2}\right] d\mathbf{x}. \end{aligned} \tag{7.3.4}$$

Substituting (7.3.1) into (7.3.4), after a detailed computation which is omitted here for brevity, we can obtain (7.3.2). Similarly, we can obtain (7.3.3) via (1.3.5) and (7.3.1). □

When $\beta \gg 1$, i.e. strongly repulsive interaction regime, the simplest approximation of the ground state is via the TF approximation. Then we have,

Lemma 7.3.2. *When $\beta \gg 1$, i.e. strongly repulsive interaction regime, the TF approximation of the ground state can be given as*

$$\phi_g^{\beta,\sigma}(\mathbf{x}) \approx \phi_g^{TF}(\mathbf{x}) = \begin{cases} \left(\frac{\mu_g^{\mathrm{TF}} - \gamma^2|\mathbf{x}|^2/2}{\beta}\right)^{\frac{1}{2\sigma}}, & \gamma^2|\mathbf{x}|^2 \leq 2\mu_g^{\mathrm{TF}}, \\ 0, & \text{otherwise}, \end{cases} \tag{7.3.5}$$

and the corresponding energy and chemical potential can be approximated as

$$\mu_g(\beta,\sigma) \approx \mu_g^{\mathrm{TF}} = \left(\frac{\beta^{\frac{1}{\sigma}}\gamma^d}{2^{\frac{d}{2}-1}dC_dB(\frac{d}{2},1+\frac{1}{\sigma})}\right)^{\frac{1}{\frac{d}{2}+\frac{1}{\sigma}}}, \tag{7.3.6}$$

$$E_g(\beta,\sigma) \approx E_g^{\mathrm{TF}} = \frac{2+d\sigma}{2\sigma+2+d\sigma}\mu_g^{\mathrm{TF}}, \qquad \beta \gg 1. \tag{7.3.7}$$

where $B(a,b)$ is the standard beta function and C_d is defined in (6.2.12).

Proof. When $\beta \gg 1$, we drop the diffusion term in (7.1.1) and obtain

$$\frac{\gamma^2|\mathbf{x}|^2}{2}\phi_g^{\mathrm{TF}}(\mathbf{x}) + \beta|\phi_g^{\mathrm{TF}}(\mathbf{x})|^{2\sigma}\phi_g^{\mathrm{TF}}(\mathbf{x}) = \mu_g^{\mathrm{TF}}\phi_g^{\mathrm{TF}}(\mathbf{x}), \qquad \mathbf{x}\in\mathbb{R}^d. \tag{7.3.8}$$

Solving the above equation, we get (7.3.5). Substituting (7.3.5) into the normalization condition, we get (7.3.6) after performing a detailed computation. Plugging (7.3.5) into (1.3.6), we get

$$\begin{aligned} E_g(\beta,\sigma) = E(\phi_g^{\beta,\sigma}) &= \mu(\phi_g^{\beta,\sigma}) - \frac{\sigma\beta}{1+\sigma}\int_{\mathbb{R}^d}|\phi_g^{\beta,\sigma}(\mathbf{x})|^{2\sigma+2}d\mathbf{x} \\ &\approx \mu_g^{\mathrm{TF}} - \frac{\sigma\beta}{1+\sigma}\int_{\mathbb{R}^d}|\phi_g^{\beta,\sigma}(\mathbf{x})|^{2\sigma+2}d\mathbf{x}. \end{aligned} \tag{7.3.9}$$

Inserting (7.3.5) and (7.3.6) into (7.3.9), we obtain (7.3.7). □

Figure 7.5 depicts the energy asymptotics with $\sigma = 2$ and $\gamma = 3$ for different β's.

7.3.2 Approximations when $\sigma \to \infty$

Here we assume $\beta > 0$ is a given constant and we shall study the limit of the ground state $\phi_g^{\beta,\sigma}$ when $\sigma \to \infty$. For the simplicity of notation, we will only consider the NLSE in 1D, i.e. $d = 1$ with a harmonic potential $V(x) = \frac{\gamma^2x^2}{2}$ for $\gamma > 0$ a constant. Then we have

Lemma 7.3.3. *For any given $\beta > 0$, when $\sigma \to \infty$, we have*

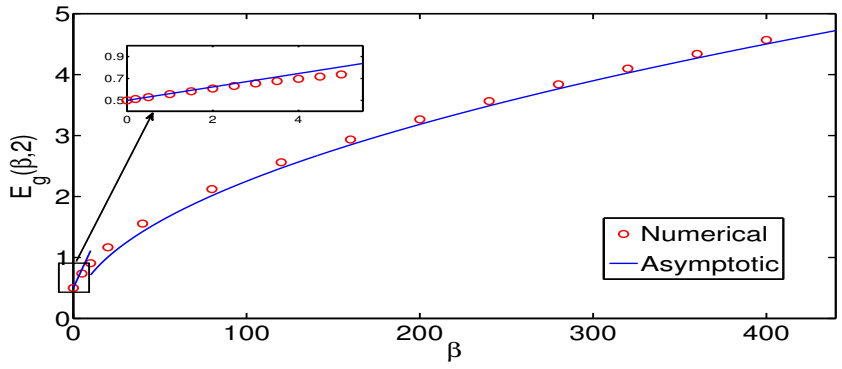

Figure 7.5: Plots of the ground state energy of the NLSE (7.1.1) in 1D under a harmonic potential with $\gamma = 3$ and $\sigma = 2$ (quintic nonlinearity for TG gas) for different β's.

(i) if $0 < \gamma \leq \pi$, *the ground state converges to the linear approximation*

$$\phi_g^{\beta,\sigma}(x) \approx \phi_g^0(x) = \left(\frac{\gamma}{\pi}\right)^{\frac{1}{4}} e^{-\frac{\gamma x^2}{2}}, \qquad x \in \mathbb{R}, \tag{7.3.10}$$

$$E_g(\beta,\sigma) \approx \frac{\gamma}{2} + \frac{\beta}{(\sigma+1)^{\frac{3}{2}}}\left(\frac{\gamma}{\pi}\right)^{\frac{\sigma}{2}} \to \frac{\gamma}{2}, \quad \mu_g(\beta,\sigma) \approx \frac{\gamma}{2} + \frac{\beta}{(\sigma+1)^{\frac{1}{2}}}\left(\frac{\gamma}{\pi}\right)^{\frac{\sigma}{2}} \to \frac{\gamma}{2}; \tag{7.3.11}$$

(ii) if $\gamma > \pi$, *the ground state converges to*

$$\phi_g^{\beta,\sigma}(x) \to \phi_g^{\gamma}(x) = \begin{cases} \varphi(-x), & x < -x_\gamma, \\ 1, & -x_\gamma \leq x \leq x_\gamma, \\ \varphi(x), & x > x_\gamma, \end{cases} \tag{7.3.12}$$

where $\varphi(x)$ *is the unique positive ground state of the following linear eigenvalue problem with* μ *the corresponding eigenvalue*

$$\begin{cases} \mu\varphi(x) = -\frac{1}{2}\varphi''(x) + \frac{\gamma^2 x^2}{2}\varphi(s), & x > x_\gamma, \\ \varphi(x_\gamma) = 1, \qquad \varphi'(x_\gamma) = 0, \qquad \lim\limits_{x\to+\infty}\varphi(x) = 0, \end{cases} \tag{7.3.13}$$

with the constant $x_\gamma \geq 0$ *determined by*

$$x_\gamma + \int_{x_\gamma}^{\infty} |\varphi(x)|^2 dx = \frac{1}{2}. \tag{7.3.14}$$

Proof. Similar to the proof of Lemma 7.2.5, in order to find the limit of $\phi_g^{\beta,\sigma}(x)$ when $\sigma \to \infty$, the main idea is to determine which term on the left hand side of (7.1.1) is negligible when $\sigma >> 1$. In the region where $|\phi(x)| < 1$, the nonlinear term can be dropped and we get the linear approximation, whose solution is the Gaussian function. In the region where $|\phi(x)| > 1$, the diffusion term can be dropped and we get the TF approximation. Therefore, there are two possible cases about the limit $\phi_g^{\beta,\sigma}(x) \to \phi^{\text{app}}(x)$ for $x \in \mathbb{R}$ when $\sigma \to +\infty$: (i) $|\phi^{\text{app}}(x)| \leq 1$ for all $x \in \mathbb{R}$, (ii) there exists a $x_c \geq 0$ such that $|\phi^{\text{app}}(x)| > 1$ for $x \in [-x_c, x_c]$ and $|\phi^{\text{app}}(x)| < 1$ otherwise.

(i) When $0 < \gamma \leq \pi$, the linear approximation suggests that $\phi^{\text{app}}(x) = \left(\frac{\gamma}{\pi}\right)^{\frac{1}{4}} e^{-\frac{\gamma x^2}{2}} \leq 1$ for $x \in \mathbb{R}$. Note that the requirement that $\sup_{x\in\mathbb{R}} \phi^{\text{app}}(x) \leq 1$ implies that $0 < \gamma \geq \pi$. Therefore, we get the necessary and sufficient condition about γ for (7.3.10) to be true.

(ii) When $\gamma > \pi$, we may expect neither the linear approximation nor the TF approximation is valid for $x \in \mathbb{R}$. Instead, a combination of the linear approximation and TF approximation should be used. To be more specific, for any fixed $\sigma > 0$, when $\beta >> 1$, there exists a constant $x_c^\sigma \geq 0$ such that when $x \in (-\infty, x_c^\sigma) \cup (x_c^\sigma, \infty)$, the linear approximation is used; and when $x \in [-x_c^\sigma, x_c^\sigma]$, the TF approximation $\phi(x) = \left(\frac{\mu_g - \gamma^2 x^2/2}{\beta}\right)^{\frac{1}{2\sigma}}$ which goes to the constant 1 as $\sigma \to \infty$. Therefore, we can simply use the constant function 1 in the case. The constant x_c^σ can be determined by the normalization condition. Letting $\sigma \to \infty$ and assuming $x_c^\sigma \to x_\gamma$, we get (7.3.12) when $\sigma \to \infty$. Plugging (7.3.12) into the normalization condition, we obtain (7.3.14). □

In order to check our asymptotic results in Lemma 7.3.3, we solve the time-independent NLSE (7.1.1) numerically by using the normalized gradient flow via backward Euler finite difference discretization [14, 16–18] to find the ground states and the corresponding energy. Figure 7.6 plots the ground states with $\beta = 1$ for different σ and γ, Figure 7.7 shows the numerical solution of (7.3.13) while Figure 7.8 depicts the energy asymptotics with $\beta = 1$ and $\gamma = 3$ for different σ's. One thing

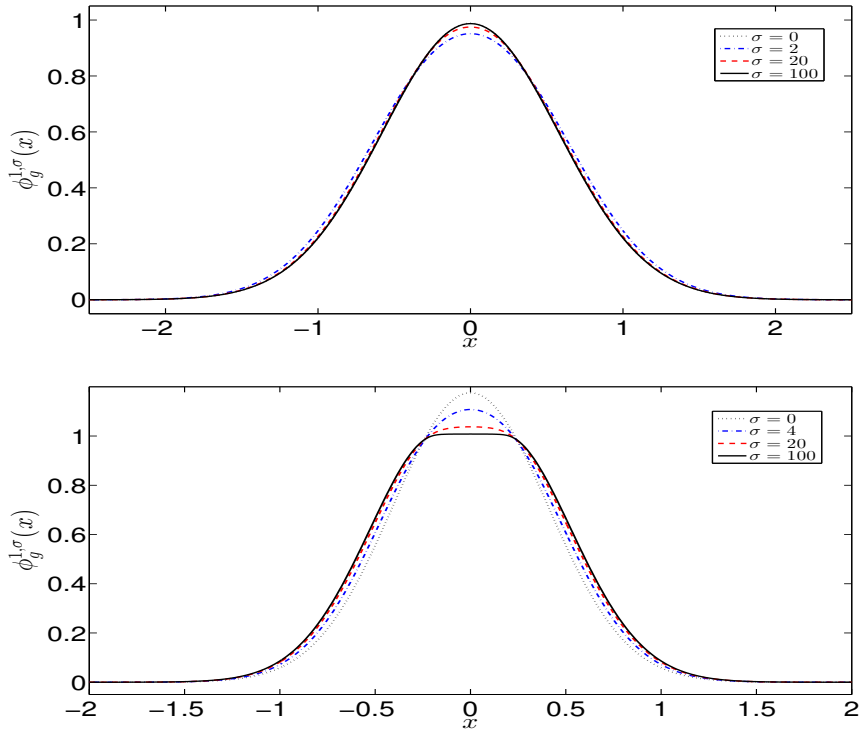

Figure 7.6: Ground states of the NLSE in 1D with $\beta = 1$ and $\gamma = 3 < \pi$ (top) and $\gamma = 6 > \pi$ (bottom) for different nonlinearities, i.e. σ.

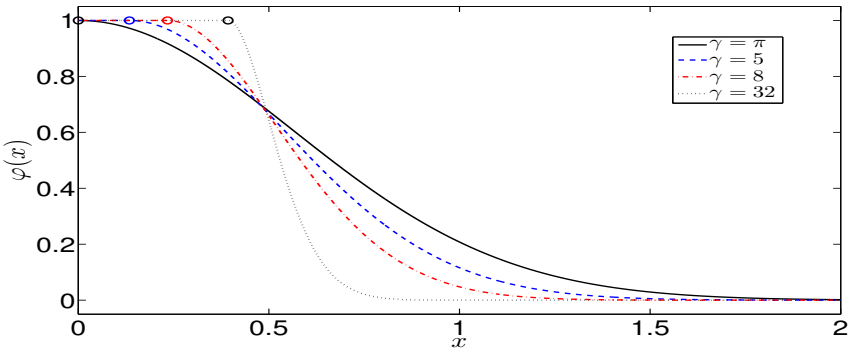

Figure 7.7: Numerical solution of (7.3.13). The circles denote the points $(x_\gamma, 1)$ corresponding to the different γ's.

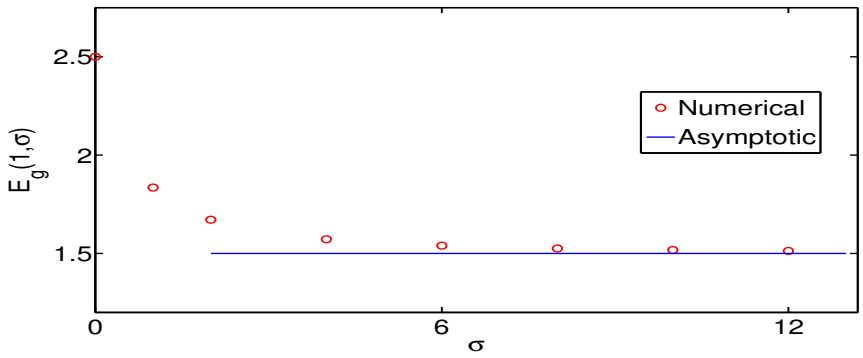

Figure 7.8: Plots of the ground state energy of the NLSE (7.1.1) in 1D under a harmonic potential with $\gamma = 3$ and $\beta = 1$ for different nonlinearities, i.e. σ's.

that needs to be pointed out is that we can speculate the solution to (7.3.13) to have the following properties from Figure 7.7:

(i) $x_\gamma \to 0$, and $\phi_g^\gamma(x) \to \phi_g^\pi(x) = e^{-\frac{\pi x^2}{2}}$ when $\gamma \to \pi$,

(ii) $x_\gamma \to 0.5$ and $\phi_g^\gamma(x) \to \phi_g^\infty(x) = 1 - 1_{\{|x| \geq 0.5\}}$ when $\gamma \to \infty$.

Chapter 8

Conclusions and Future Works

The thesis focuses on the mathematical analysis and numerical simulation for the modified Gross-Pitaevskii equation (MGPE), as well as the the fundamental gap problems for the GPE and the ground state asymptotics for the NLSE. The main work in my thesis is summarized here and my contributions are highlighted as well.

1. Mathematical theory and numerical computation of the MGPE

Most efforts are devoted to the theory and efficient computation of ground states. We not only establish the existence, uniqueness and non-existence results of the MGPE, but also provide a detailed characterization of the ground states under the box potential or harmonic potential. It is worth noticing that due to the extra nonlinear HOI term, we need to compare the effects of both nonlinear terms in the MGPE and therefore the Thomas-Fermi (TF) approximations become more complicated. The complete and detailed characterizations of the TF approximations are listed.

For the strongly anisotropic harmonic potential case, we studied the dimension reduction problem. A significantly different scenario for the 3D to 1D case is discovered, which tells us the HOI term in the MGPE does introduce something nontrivial. Effective one-(1D) and two-dimensional (2D) models are derived rigourously.

For computing the ground state, we firstly generalized the methods for the GPE

case to the MGPE case and numerical accuracy tests are performed. And then, we propose a new method, which minimizes the discrete energy formulated via the density function. Due to the possible singularity problems, a regularized energy needs to be considered instead. The convergence of the regularized energy to the original one is considered and accuracy tests are performed as well. Finally, some simple dynamical properties of the MGPE are studied.

In future, the MGPE combined with other terms, such as the dipolar term and the rotation term, may be considered both theoretically and numerically. It is not clear now whether the HOI term will result in new phenomenons in such cases. I will also try to improve the performance of the current numerical methods, especially the scheme for the dynamics. More stable schemes with higher order convergence and easy implementation need to be designed.

2. Fundamental gap for the GPE

We provide explicitly the asymptotic expressions for the fundamental gaps in energy and chemical potential of the GPE with repulsive interaction under some specially chosen box potentials and harmonic potentials. And gap conjectures concerning the effect of the interaction strength on the fundamental gaps are proposed.

One future work is to make the results more rigorously in mathematics since currently only asymptotic results are shown here while the analytical results are left far behind. Other future works include studying the fundamental gap problem for other equations, for example the MGPE and the fractional Schrödinger operator. Besides, designing efficient, accurate and stable numerical schemes for the ground state and the first excited state is also a topic to be studied in future.

3. Ground state asymptotics for the NLSE

We study the ground state approximations for the NLSE with box or harmonic potential for several limiting processes: $\beta \to 0$ or ∞ with $\sigma > 0$ fixed, OR $\sigma \to \infty$ with $\beta > 0$ fixed. The limit process when the power of the nonlinearity goes to ∞ is of particular interest, where a bifurcation in the ground states is observed.

One possible future work is to consider the fundamental gap problems for the

NLSE, which requires me to find more accurate approximations for the ground state energy and the first excited state energy. Efficient and stable computation for the ground state and the first excited state is needed as well.

Bibliography

[1] M. J. Ablowitz, *Nonlinear Dispersive Waves, Asymptotic Analysis and Solitons*, Cambridge University Press, 2011.

[2] S. Adhikari and B. A. Malomed, *Gap solitons in a model of a superfluid fermion gas in optical lattices*, Physica D, 238 (2009), 1402-1412.

[3] J. O. Andersen, *Theory of the weakly interacting Bose gas*, Rev. Mod. Phys., 76 (2004), 599-639.

[4] M. H. Anderson, J. R. Ensher, M. R. Matthews, C. E. Wieman and E. A. Cornell, *Observation of Bose-Einstein condensation in a dilute atomic vapor*, Science, 269 (1995), 198–201.

[5] B. Andrews and J. Clutterbuck, *Proof of the fundamental gap conjecture*, J. Amer. Math. Soc., 24 (2011), 899–916.

[6] X. Antoine, W. Bao and C. Besse, *Computational methods for the dynamics of the nonlinear Schrödinger/Gross-Pitaevskii equations*, Comput. Phys. Commun., 184 (2013), 2621–2633.

[7] M. Ashbaugh, *The Fundamental Gap*, Workshop on Low Eigenvalues of Laplace and Schrödinger Operators, American Institute of Mathematics, Palo Alto, California, 2006.

[8] M. S. Ashbaugh and R. Benguria, *Optimal lower bound for the gap between the first two eigenvalues of one-dimensional schrdinger operators with symmetric single-well potentials*, Proc. Amer. Math. Soc., 105 (1989), 419–424.

[9] W. Bao, *Ground states and dynamics of multicomponent Bose-Einstein condensates*, Multiscale Model. Simul., 2 (2004), 210–236.

[10] W. Bao, *Mathematical models and numerical methods for Bose-Einstein condensation*, Proceedings of the International Congress of Mathematicians (Seoul 20140), IV (2014), 971–996.

[11] W. Bao, N. Ben Abdallah and Y. Cai, *Gross-Pitaevskii-Poisson equations for dipolar Bose-Einstein condensate with anisotropic confinement*, SIAM J. Math. Anal., 44 (2012), 1713–1741.

[12] W. Bao and Y. Cai, *Uniform error estimates of finite difference methods for the nonlinear Schrödinger equation with wave operator*, SIAM J Numer. Anal., 50 (2012), 492–521.

[13] W. Bao and Y. Cai, *Optimal error estimates of finite difference methods for the Gross-Pitaevskii equation with angular momentum rotation*, Math. Comp., 82 (2013), 99–128.

[14] W. Bao and Y. Cai, *Mathematical theory and numerical methods for Bose-Einstein condensation*, Kinet. Relat. Mod., 6 (2013), 1–135.

[15] W. Bao, Y. Cai and X. Ruan, *Ground states and dynamics of Bose-Einstein condensates with higher order interactions*, arXiv:1701.01245.

[16] W. Bao and M.-H. Chai, *A uniformly convergent numerical method for singularly perturbed nonlinear eigenvalue problems*, Commun. Comput. Phys., 4 (2008), 135-160.

[17] W. Bao, I.-L. Chern and F. Y. Lim, *Efficient and spectrally accurate numerical methods for computing ground and first excited states in Bose-Einstein condensates*, J. Comput. Phys., 219 (2006), 836–854.

[18] W. Bao and Q. Du, *Computing the ground state solution of Bose-Einstein condensates by a normalized gradient flow*, SIAM J. Sci. Comput., 25 (2004), 1674–1697.

[19] W. Bao, Q. Du and Y. Zhang, *Dynamics of rotating Bose-Einstein condensates and their efficient and accurate numerical computation*, SIAM J. Appl. Math., 66 (2006), 758–786.

[20] W. Bao, Y. Ge, D. Jaksch, P. A. Markowich and R. M. Weishaeupl, *Convergence rate of dimension reduction in Bose-Einstein condensates*, Comput. Phys. Commun., 177 (2007), 832–850.

[21] W. Bao, D. Jaksch and P. A. Markowich, *Numerical solution of the Gross-Pitaevskii equation for Bose-Einstein condensation*, J. Comput. Phys., 187 (2003), 318–342.

[22] W. Bao, S. Jin and P. A. Markowich, *On time-splitting spectral approximation for the Schrödinger equation in the semiclassical regime*, J. Comput. Phys., 175 (2002), 487–524.

[23] W. Bao, S. Jin and P. A. Markowich, *Numerical study of time-splitting spectral discretizations of nonlinear Schrödinger equations in the semiclassical regimes*, SIAM J. Sci. Comput., 25 (2003), 27–64.

[24] W. Bao, L. Le Treust and F. Mehats, *Dimension reduction for anisotropic Bose-Einstein condensates in the strong interaction regime*, Nonlinearity, 28 (2015), 755-772.

[25] W. Bao and F. Y. Lim, *Analysis and computation for the semiclassical limits of the ground and excited states of the Gross-Pitaevskii equation*, Proc. Sympos. Appl. Math., Amer. Math. Soc., 67 (2009), 195–215.

[26] W. Bao, F. Y. Lim and Y. Zhang, *Energy and chemical potential asymptotics for the ground state of Bose-Einstein condensates in the semiclassical regime*, Bull. Inst. Math. Acad. Sin. (N.S.), 2 (2007), 495–532.

[27] W. Bao and X. Ruan, *Fundamental gaps of the Gross-Pitaevskii equation with repulsive interaction*, arXiv:1512.07123.

[28] W. Bao and J. Shen, *A fourth-order time-splitting Laguerre-Hermite pseudospectral method for Bose-Einstein condensates*, SIAM J. Sci. Comput., 26 (2005), 2020–2028.

[29] W. Bao, W. Tang, *Ground state solution of Bose-Einstein condensate by directly minimizing the energy functional*, J. Comput. Phys., 187 (2003), 230–254.

[30] W. Bao, Q. Tang and Z. Xu, *Numerical methods and comparison for computing dark and bright solitons in the nonlinear Schrödinger equation*, J. Comput. Phys., 235 (2013), 423–445.

[31] W. Bao and H. Wang, *An efficient and spectrally accurate numerical method for computing dynamics of rotating Bose-Einstein condensates*, J. Comput. Phys., 217 (2006), 612–626.

[32] W. Bao, Z. Wen and X. Wu, *A regularized Newton method for computing ground states of Bose-Einstein condensates*, arXiv:1504.02891.

[33] W. Bao and Y. Zhang, *Dynamics of the ground state and central vortex states in Bose-Einstein condensation*, Math. Mod. Meth. Appl. Sci., 15 (2005), 1863–1896.

[34] J. Barzilai and J.M. Borwein, *Two-point step size gradient methods*, IMA J. Numer. Anal., 8 (1988), 141–148.

[35] A. Beck and M. Teboulle, *A fast iterative shrinkage-thresholding algorithm for linear inverse problems*, SIAM J. Imaging Sci. (2009), 2(1), 183–202.

[36] N. Ben Abdallah, F. Méhats, C. Schmeiser and R. M. Weishäupl, *The nonlinear Schrödinger equation with a strongly anisotropic harmonic potential*, SIAM J. Math. Anal., 47 (2005), pp. 189–199.

[37] M. van den Berg, *On condensation in the free-boson gas and the spectrum of the Laplacian*, J. Stat. Phys., 31 (1983), 623–637.

[38] S. N. Bose, *Plancks gesetz und lichtquantenhypothese*, Zeitschrift fr Physik, 3 (1924), 178–181.

[39] C. C. Bradley, C. A. Sackett, J. J. Tollett and R. G. Hulet, *Evidence of Bose-Einstein condensation in an atomic gas with attractive interaction*, Phys. Rev. Lett., 75 (1995), 1687–1690.

[40] H. J. Brascamp and E. H. Lieb, *Some inequalities for Gaussian measures, Functional Integration and Its Applications*, A. M. Arthurs, editor, Oxford University Press, London, 1975, 1–14.

[41] H. J. Brascamp and E. H. Lieb, *On extensions of the Brunn-Minkowski and Prékopa-Leindler theorems, including inequalities for log concave functions, and with an application to the diffusion equation*, J. Funct. Anal. 22 (1976), 366–389.

[42] Y. Cai, M. Rosenkranz, Z. Lei and W. Bao, *Mean-field regime of trapped dipolar Bose-Einstein condensates in one and two dimensions*, Phys. Rev. A, 82 (2010), 043623.

[43] E. Cancès, R. Chakir and Y. Maday, *Numerical analysis of nonlinear eigenvalue problems*, J. Sci. Comput., 45 (2010), 90–117.

[44] T. Cazenave, *Semilinear Schrödinger Equations*, Courant Lect. Notes Math., 10, Amer. Math. Soc., Providence, R.I., 2003.

[45] P. M. Chaikin and T. C. Lubensky, *Principles of condensed matter physics*, Cambridge University Press, Cambridge, 1995.

[46] A. Chambolle, R. A. DeVore, N. Y. Lee, and B. J. Lucier, *Nonlinear wavelet image processing: Variational problems, compression, and noise removal through wavelet shrinkage*, IEEE Trans. Image Process., 7 (1998), 319–335.

[47] Q. Chang, B. Guo and H. Jiang, *Finite difference method for generalized Zakharov equations*, Math. Comp., 64 (1995), 537–553.

[48] Q. Chang, E. Jia and W. Sun, *Difference schemes for solving the generalized nonlinear Schrödinger equation*, J. Comput. Phys., 148 (1999), 397–415.

[49] S. M. Chang, W. W. Lin and S. F., Shieh, *Gauss-Seidel-type methods for energy states of a multi-component Bose-Einstein condensate*, J. Comput. Phys., 202 (2005), pp. 367–390.

[50] R. Y. Chiao, T. K. Gustafson, and P. L. Kelley. *Self-focusing: Past and Present Fundamentals and Prospects (Topics in Applied Physics Series Volume 114)*, Springer New York, New York, 2009.

[51] M. L. Chiofalo, S. Succi and M. P. Tosi, *Ground state of trapped interacting Bose- Einstein condensates by an explicit imaginary-time algorithm*, Phys. Rev. E, 62 (2000), 7438–7444.

[52] M. Colin, L. Jeanjean and M. Squassina, *Stability and instability results for standing waves of quasi-linear Schrödinger equations*, Nonlinearity, 23 (2010), 1353–1385.

[53] A. Collin, P. Massignan and C. J. Pethick, *Energy-dependent effective interactions for dilute many-body systems*, Phys. Rev. A, 75 (2007), 013615.

[54] F. Dalfovo, S. Giorgini, L. P. Pitaevskii and S. Stringari, *Theory of Bose-Einstein condensation in trapped gases*, Rev. Mod. Phys., 71 (1999), 463.

[55] F. Dalfovo and S. Stringari, *Bosons in anisotropic traps: Ground state and vortices*, Phys. Rev. A, 53 (1996), 2477–2485.

[56] I. Daubechies, M. Defrise, and C. D. Mol, *An iterative thresholding algorithm for linear inverse problems with a sparsity constraint*, Comm. Pure Appl. Math., 57 (2004), 1413–1457.

[57] K. B. Davis, M. O. Mewes, M. R. Andrews, N. J. van Druten, D. S. Durfee, D. M. Kurn and W. Ketterle, *Bose-Einstein condensation in a gas of sodium atoms*, Phys. Rev. Lett., 75 (1995), 3969–3973.

[58] A. Einstein, *Quantentheorie des einatomigen idealen gases*, Sitzungsberichte der Preussischen Akademie der Wissenschaften, 22 (1924), 261–267.

[59] A. Einstein, *Quantentheorie des einatomigen idealen gases, zweite abhandlung*, Sitzungsberichte der Preussischen Akademie der Wissenschaften, 1 (1925), 3–14.

[60] B. D. Esry and C. H. Greene, *Validity of the shape-independent approximation for Bose-Einstein condensates*, Phys. Rev. A, 60 (1999), 1451–1462.

[61] L. C. Evans, *Partial Differential Equations*, Amer. Math. Soc., Providence, RI, 1998.

[62] M. A. T. Figueiredo and R. D. Nowak, *An EM algorithm for wavelet-based image restoration*, IEEE Trans. Image Process., 12 (2003), 906–916.

[63] H. Fu, Y. Wang, and B. Gao, *Beyond the Fermi pseudopotential: A modified Gross-Pitaevskii equation*, Phys. Rev. A, 67 (2003), 053612.

[64] J. J. Garcia-Ripoll, V. V. Konotop, B. A. Malomed and V. M. Perez-Garcia, *A quasi-local Gross-Pitaevskii equation for attractive Bose-Einstein condensates*, Math. Comput. Simul., 62 (2003), 21-30.

[65] M. Girardeau, *Relationship between systems of impenetrable bosons and fermions in one dimension*, J. Math. Phys., 1 (1960), 516–523.

[66] A. Görlitz *et al.*, *Realization of Bose-Einstein condensates in lower dimensions*, Phys. Rev. Lett., 87 (2001), 130402.

[67] E. P. Gross, *Structure of a quantized vortex in boson systems*, Nuovo. Cimento., 20 (1961), 454–457.

[68] Y. Guo, X. Zeng and H. Zhou, *Energy estimates and symmetry breaking in attractive Bose-Einstein condensates with ring-shaped potentials*, Ann. I. H. Poincare' C, 33 (2016), 809–828.

[69] R. H. Hardin and F. D. Tappert, *Applications of the split-step Fourier method to the numerical solution of nonlinear and variable coefficient wave equations*, SIAM Rev. Chronicle, 15 (1973), 423.

[70] L. V. Hau, B. D. Busch, C. Liu, Z. Dutton, M. M. Burns, and J. A. Golovchenko, *Near-resonant spatial images of confined Bose-Einstein condensates in a 4-Dee magnetic bottle*, Phys. Rev. A, 58 (1998), R54.

[71] M. J. Holland, D. Jin, M. L. Chiofalo, and J. Cooper, *Emergence of interaction effects in Bose-Einstein condensation*, Phys. Rev. Lett., 78 (1997), 3801.

[72] B. Jiang and Y. Dai, *A framework of constraint preserving update schemes for optimization on Stiefel manifold*, Math. Program., 153 (2015), 535–575.

[73] D. John, S. Shai, S. Yoram and C. Tushar, *Efficient projections onto the l_1-ball for learning in high dimensions*, Proceedings of the 25th International Conference on Machine Learning (2008), 272-279.

[74] P. Kapitza, *Viscocity of liquid helium below the λ-point*, Nature, 141 (1938), 74–74.

[75] C. Laurent , *Fast projection onto the simplex and the l_1 ball*, Math. Prog., 158 (2016), 575-585.

[76] A. J. Leggett, *Bose-Einstein condensation in the alkali gases: Some fundamental concepts*, Rev. Modern Phys., 73 (2001), 307–356.

[77] E. H. Lieb and W. Liniger, *Exact analysis of an interacting bose gas. i. the general solution and the ground state*, Phys. Rev., 130 (1963), 1605–1616.

[78] E. H. Lieb and M. Loss, *Analysis, Graduate Studies in Mathematics*, Amer. Math. Soc., 2nd ed., 2001.

[79] E. H. Lieb, R. Seiringer, J. P. Solovej and J. Yngvason, *The Mathematics of the Bose Gas and its Condensation*, Oberwolfach seminars 34, Birkhäuser, Basel, 2005.

[80] E. H. Lieb, R. Seiringer and J. Yngvason, *Bosons in a trap: a rigorous derivation of the Gross-Pitaevskii energy functional*, Phy. Rev. A, 61 (2000), 043602.

[81] J.Q. Liu, Y.Q. Wang and Z.Q. Wang, *Soliton solutions for quasi-linear Schrödinger equations II*, J. Differ. Equat., 187 (2003), 473–493.

[82] J.Q. Liu, Y.Q. Wang and Z.Q. Wang, *Solutions for quasilinear Schrödinger equations via the Nehari method*, Comm. Part. Differ. Equat., 29 (2004), 879–901.

[83] J. Liu, S. Ji and J. Ye, *Slep: Sparse Learning with Efficient Projections*, 2009.

[84] F. London, *The λ-phenomenon of liquid helium and the Bose-Einstein degeneracy*, Nature, 141 (1938), 643–644.

[85] J. Lu and J. L. Marzuola, *Strang splitting methods for a quasilinear Schrödinger equation - convergence, instability and dynamics*, Commun. Math. Sci, 13(2015), 1051–1074.

[86] P. A. Markowich, P. Pietra and C. Pohl, *Numerical approximation of quadratic observables of Schrödinger-type equations in the semi-classical limit*, Numer. Math., 81 (1999), 595–630.

[87] J. Marzuola, J. Metcalfe and D. Tataru, *Quasilinear Schrödinger equations II: Small data and cubic nonlinearities*, Kyoto J. Math., 54 (2014), 529–546.

[88] P. Muruganandam and S. K. Adhikari, *Bose-Einstein condensation dynamics in three dimensions by the pseudospectral and finite-difference methods*, J. Phys. B, 36 (2003), 2501–2513.

[89] Y. E. Nesterov, *A method for solving the convex programming problem with convergence rate $O(1/k^2)$*, Dokl. Akad. Nauk SSSR, 269 (1983), 543–547 (in Russian).

[90] C. J. Pethick and H. Smith, *Bose-Einstein Condensation in Dilute Gases*, Cambridge University Press, London, 2002.

[91] A. Petrosyan, H. Shahgholian, and N. N. Uraltseva, *Regularity of Free Boundaries in Obstacle-Type Problems*, AMS, 2012.

[92] L. P. Pitaevskii, *Vortex lines in an imperfect Bose gas*, Soviet Phys. JETP, 13 (1961), 451–454.

[93] L. P. Pitaevskii and S. Stringari, *Bose-Einstein Condensation*, Clarendon Press, Oxford, 2003.

[94] M. Poppenberg, *On the local well posedness of quasi-linear Schrödinger equations in arbitrary space dimension*, J. Differ. Equat., 172 (2001), 83–115.

[95] W. Qi, Z. Liang and Z. Zhang, *The stability condition and collective excitation of a trapped Bose-Einstein condensate with higher-order interactions*, J. Phys. B: At. Mol. Opt. Phys., 46 (2013), 175301.

[96] X. Qi and X. Zhang, *Modulational instability of a modified Gross-Pitaevskii equation with higher-order nonlinearity*, Phys. Rev. E, 86 (2012), 017601.

[97] X. Ruan, *Ground states and energy asymptotics of the nonlinear Schrödinger equation*, arXiv:1703.01901.

[98] X. Ruan, Y. Cai and W. Bao, *Mean-field regime and Thomas-Fermi approximations of trapped Bose-Einstein condensates with higher order interactions in one and two dimensions*, J. Phys. B: At. Mol. Opt. Phys., 49 (2016), 125304.

[99] L. Salasnich, *Generalized nonpolynomial Schrodinger equations for matter waves under anisotropic transverse confinement*, J. Phys. A: Math. Theor., 42 (2009), 335205.

[100] I. Singer, B. Wong, S.-T. Yau and S. S.-T. Yau, *An estimate of the gap of the first two eigenvalues in the Schrödinger operator.*, Ann. Sc. Norm. Super. Pisa Cl. Sci. (4), 12 (1985), 319–333.

[101] D. M. Stamper-Kurn,, M. R. Andrews, A. P. Chikkatur, S. Inouye, H.-J. Miesner, J. Stenger, and W. Ketterle, *Optical confinement of a Bose-Einstein condensate*, Phys. Rev. Lett., 80 (1998), 2027.

[102] G. Strang, *On the construction and comparison of difference schemes*, SIAM J. Numer. Anal., 5 (1968), 506–517.

[103] C. Sulem and P. L. Sulem, *The Nonlinear Schrödinger Equation, Self-focusing and Wave Collapse*, Springer-Verlag, New York, 1999.

[104] T. R. Taha and M. J. Ablowitz, *Analytical and numerical aspects of certain nonlinear evolution equations, II. Numerical, nonlinear Schrödinger equation*, J. Comput. Phys., 55 (1984), 203–230.

[105] M. Thalhammer, M. Caliari and C. Neuhauser, *High-order time-splitting Hermite and Fourier spectral methods*, J. Comput. Phys., 228 (2009), 822–832.

[106] M. Thøgersen, N. T. Zinner and A. S. Jensen, *Thomas-Fermi approximation for a condensate with higher-order interactions*, Phys. Rev. A , 80 (2009), 043625.

[107] L. Tonks, *The complete equation of state of one, two and three-dimensional gases of hard elastic spheres*, Phys. Rev., 50 (1936), 955–963.

[108] H. Veksler, S. Fishman and W. Ketterle, *Simple model for interactions and corrections to the Gross-Pitaevskii equation*, Phys. Rev. A, 90 (2014), 023620.

[109] C. Vonesch and M. Unser, *Fast iterative thresholding algorithm for wavelet-regularized deconvolution*, in Proceedings of the SPIE Optics and Photonics 2007 Conference on Mathematical Methods: Wavelet XII, Vol. 6701, San Diego, CA, 2007, 1–5.

[110] E. Wamba, S. Sabari, K. Porsezian, A. Mohamadou, and T. C. Kofané, *Dynamical instability of a Bose-Einstein condensate with higher-order interactions in an optical potential through a variational approach*, Phys. Rev. E, 89 (2014), 052917.

[111] H. Wang, *A time-splitting spectral method for coupled Gross-Pitaevskii equations with applications to rotating Bose-Einstein condensates*, J. Comput. Appl. Math., 205 (2007), 88–104.

[112] M. I. Weinstein, *Nonlinear Schrödinger equations and sharp interpolation estimates*, Comm. Math. Phys, 87 (1982), 567–576.

[113] Z. Wen and W. Yin, *A feasible method for optimization with orthogonality constraints*, Math. Program. Ser. A., 142 (2013), 397–434.

[114] H. Yoshida, *Construction of higher order symplectic integrators*, Phys. Lett. A, 150 (1990), 262–268.

[115] L. E. Young S., L. Salasnich and S. K. Adhikari, *Dimensional reduction of a binary Bose-Einstein condensate in mixed dimensions*, Phys. Rev. A, 82 (2010), 053601.

List of Publications

[1] *Mean-field regime and Thomas-Fermi approximations of trapped Bose-Einstein condensates with higher order interactions in one and two dimensions* (with Yongyong Cai and Weizhu Bao), J. Phys. B: At. Mol. Opt. Phys., 49 (2016), 125304.

[2] *Fundamental gaps of the Gross-Pitaevskii equation with repulsive interaction* (with Weizhu Bao), arXiv:1512.07123.

[3] *Effects of the non-parabolic kinetic energy on non-equilibrium polariton condensates* (with Florian Pinsker and Tristram J. Alexander), arXiv:1606.02130v3, accepted, Sci. Rep..

[4] *Ground states and dynamics of Bose-Einstein condensates with higher order interactions* (with Weizhu Bao and Yongyong Cai), arXiv:1701.01245.

[5] *Ground states and energy asymptotics of the nonlinear Schrödinger equation*, arXiv:1703.01901.